Wave-Induced Motions on High Froude Number Slender Twin-Hull Vessels

by

Nigel L.Watson, B.E. (Naval Architecture) (Hons.)

School of Engineering

Submitted in fulfilment of the requirements
for the degree of
Doctor of Philosophy

University of Tasmania

May 2004

Thesis Confidentiality

This thesis contains data originating from a collaborative research program between INCAT Tasmania and the University of Tasmania and is submitted under the terms of the agreement between the Department of Civil and Mechanical Engineering, University of Tasmania and INCAT Australia Pty for an INCAT Tasmania Award for research on Ship Technology.

The thesis contents should not be made available to or divulged in any form to any person other than the thesis examiners, supervisor, Professor M. R. Davis and appropriate INCAT staff.

Statement of Originality

This thesis contains no material, which has been accepted for a degree or diploma by the university or any tertiary institution, except by way of background information and duly acknowledged in the thesis. To the best of my knowledge and belief, this thesis contains no material previously published or written by another person, except when due acknowledgment is made in the text.

Nigel L. Watson

Abstract

A study of the wave-induced motions experienced by slender twin-hull vessels was conducted through experimental measurements and numerical computation. Particular attention was required in the analysis of measured data for comparison with the predicted motions. The difficulties of analysing measured data from a vessel that had encountered sea waves of a random nature were addressed by grouping the data into subsets based on primary wave direction, vessel speed, and hull configuration. The primary wave direction was determined by considering the motions of the vessel as for a directional wave buoy. The data acquisition system consisted of hardware and software that was developed and assembled on two twin-hull full-scale vessels for periods of up to 12 months each. Designed to operate mostly unsupervised whilst collecting data in remote locations, a data recording sequence was initiated through a preset trigger level from a motion sensor. In the subsequent analysis, transfer functions were obtained from the measured data based on the sorted data subsets.

Numerical modelling of the vessels in head sea waves used an existing strip theory code that defined the hull as sectional boundary elements that contributed to solving a Green function problem for the free surface and sectional motion in the time domain. A modification to the code allowed the effects of motion control surfaces on the motion transfer functions to be determined through selection of appropriate gain setting that minimised the average vertical hull accelerations. With the damping effect of control surfaces not scaling linearly with wave height, the controls were modelled to minimise the hull average vertical acceleration in a 2.5 metre Bretschneider wave spectrum of 7 second average period. The inclusion of control surfaces in the motion computation combined with non-linear wave height effects in some instances greatly improved the correlation between the numerical and measured motion transfer functions by reducing the frequency of maximum response.

The accelerations and motion sickness incidence (MSI) distributions derived through computations on an 86 metre vessel indicate the presence of high accelerations that are not fully counteracted by a motion control system of practicable size.

Future advances in numerical prediction codes may require verification with detailed full-scale measurements to ensure the scale effects are adequately considered. Full-scale measurements should therefore constitute part of a complete testing and analysis program for motions, but due to the high cost of these trials the measurements required for analysis may best be obtained from data supplied from on board monitoring systems during regular service operations.

Acknowledgments

This research could not have been accomplished without the assistance of a number of people and organisations at various stages.

My supervisor for the duration of this project was Professor Michael Davis whom contributed much support, direction and editorial assistance.

I am grateful to fellow postgraduate students Damien Holloway and Jason Roberts for their willingness to share their time and experience on various research related topics. Damien's assistance in the initial implementation of the computational solutions was gratefully appreciated.

Financial assistance was provided by an Australian Postgraduate Award scholarship through the University of Tasmania with a supplementary contribution from an industry participant Incat Tasmania.

I would like to thank the engineering services of Incat Tasmania for their cooperation and assistance in the preparation of the vessels for full-scale measurements. The electrical contractors of Incat Tasmania also provided valuable assistance with interconnections between the instrumentation equipment, ship systems and the monitoring equipment.

Maritime Dynamics Inc. now part of Vosper Thornicroft in some instances kindly permitted the use of the ship motion signals that could be incorporated into the data recording system. Their trials representative, Mr Bob Chandler provided useful on board assistance and went out of his way on many occasions to provide assistance.

The vessels owner at the time of this work was Holymans whom permitted their vessels to be instrumented and without their cooperation both during the delivery voyages and service operations on the commercial routes no information about the vessels could have been gathered. I also acknowledge the assistance of the operators Condor Marine Services throughout the duration of the ships commercial operations, for providing feedback on the data acquisition system and in the eventual retrieval of the data and equipment.

I would like to extend my gratitude to Mr Glenn Mayhew, an electronics engineer with the University of Tasmania for his contribution of expertise and personal hours in the development and improvement of the instrumentation. These included accelerometers, ultrasonic measurement devices and electronic hardware. His contribution proved considerably valuable in improving the quality of the measurements.

Finally, and most importantly I would like to thank my wife Debra who exhibited great patience and support throughout the duration of this research and in many unseen ways contributed enormously to its completion.

Contents

List of Figures

List of Tables

Nomenclature

(a) Roman Symbols

a	Vector projection variable for wave direction determination
A_i	Plan area of i^{th} lifting surface
$\overline{c}$	Foil mean chord length [m]
b	Vector projection variable for wave direction determination
B	Hull beam [m]
c	Vector projection variable for wave direction determination
C_l	Lift coefficient
$C_{l\infty}$	Lift coefficient without free surface effects
C_m	Moment coefficient at quarter chord point
f_s	Data sampling frequency [Hz]
F_n	Froude number
F_L	Lift force of ride control surface [N]
F_{fwd}	Component of lifting surface force transferred to the forward adjacent section
F_{aft}	Component of lifting surface force transferred to the aft adjacent section
g	Gravitational acceleration constant $= 9.81 m/s^2$
h	Depth below mean free surface [m]
$H_{\frac{1}{3}}$	Significant wave height [m]
H_s	Significant wave height by definition $= 4\sqrt{m_0}$ [m]
H_i	Transfer function of the i^{th} degree of freedom
H_w	Height of regular waves [m]
k	Wave number $(= \frac{2\pi}{\lambda})$
k_{44}	Roll mass radius of gyration [m]
k_{55}	Pitch mass radius of gyration [m]
k_{66}	Yaw mass radius of gyration [m]
k_{46}	Roll-yaw mass radius of gyration $= k_{64}$ [m]
$K_{\dot{\eta}_3 i}$	Velocity based heave gain for the $i^t h$ control surface
$K_{\dot{\eta}_5 i}$	Velocity based pitch gain for the $i^t h$ control surface
L	Length parameter (typically equivalent to waterline length or length between perpendiculars) [m]
Lpp	Length between perpendiculars [m]
Lwl	Length of waterline [m]
m	Vector projection variable for wave direction determination
m_0	Zeroth moment of reponse or wave spectrum
m_1	First moment of reponse or wave spectrum
m_2	Second moment of reponse or wave spectrum
m_k	k^{th} moment of reponse or wave spectrum
n	Number of data samples
n_s	Number of numerical hull sections or strips

N_1	factor for calculating the appropriate number of time steps
N_2	factor for calculating the appropriate number of time steps
p_0	Total static pressure ($p_a + \rho gh$) [Pa]
p_v	Fluid vapour pressure [Pa]
q	Dynamic pressure ($0.5\rho V_0^2$)
S_j	Response spectrum of the i^{th} degree of freedom
$S_\zeta(\omega)$	Wave spectrum ordinate
$S_\zeta(\omega_e)$	Wave encounter spectrum ordinate
t	Time [s]
T	Hull draft [m]
T_1	Wave average period (or $\overline{T}$)
T_2	Wave zero crossing period (or T_z)
u	horizontal wave particle velocity in time and space due to a regular long crested wave [m/s]
U	Constant vessel forward speed $[m/s^2]$
V_0	Fluid free stream velocity (=U) $[m/s^2]$
w	vertical wave particle velocity in time and space due to a regular long crested wave [m/s]
x	x axis of vessel coordinates (from LCG to bow)
$x_{1/4c}$	longitudinal distance between the hull centre of gravity and the centre of control surface force application
x_{5w}	Deck slope direction angle [radians or degrees]
x_a	Longitudinal distance from lifting surface position to the aft adjacent section
x_f	Longitudinal distance from lifting surface position to the forward adjacent section
x_s	Deck slope magnitude [radians or degrees]
$x_{\dot{\eta}_3(+)}$	Primary wave direction [deg or rad]
$x_{\dot{\eta}_3(-)}$	Wave encounter direction [deg or rad]
X_{a_i}	Variable for calculating gains of i^{th} control surface for local acceleration feedback control
X_i	Variable of gains finding routine for i^{th} surface deflection control
Y_m	Variable for calculating position of minimum vertical motion
X_{v_i}	Variable for calculating gains of i^{th} control surface for local velocity feedback control
y	y axis of vessel coordinates (from LCG to port)
Y_{a_i}	Variable for calculating gains of i^{th} control surface for local acceleration feedback control
Y_i	Variable of gains finding routine for i^{th} surface deflection control
Y_m	Variable for calculating position of minimum vertical motion
Y_{v_i}	Variable for calculating gains of i^{th} control surface for local velocity feedback control
z	z axis of vessel coordinates (from LCG vertically upwards)
z_{cs}	Vertical distance of the control surface to the mean water level [m]
z_B	z axis of hull fix trihedron coordinates from LCG perpendicular to deck

(*b*) Greek Symbols

α	Incident angle of the free stream velocity on the main body of the lifting surface
α_0	Angle of incidence of the forward fixed part of T-foil relative to the hull baseline
α_w	Incident angle created by the presence of waves ignoring the presence of hull
β	Variable for solving the position of vertical motion
δ_i	Flap angle of i^{th} control surface proportional to heave and pitch [rad]
$\overline{\delta_i}$	Flap angle amplitude of i^{th} control surface [rad]
δf	Spectral resolution [Hz]
δx	Length of hull section element [m]
ε_3	Heave phase [radians]
ε_5	Pitch phase [radians]
ε_{3v}	Heave velocity phase [radians]
ε_{5v}	Pitch velocity phase [radians]
ε_{3a}	Heave acceleration phase [radians]
ε_{5a}	Pitch acceleration phase [radians]
η_3	Heave displacement in time [m]
η_{3f}	Heave response to T-foil sinudoidal flap oscillation [m]
η_{3t}	Heave response to transom tab sinudoidal oscillation [m]
η_{3tf}	Heave response to transom tab sinudoidal oscillation, T-foil fixed [m]
η_4	Roll displacement in time [radians]
η_5	Pitch displacement in time [radians]
η_{5f}	Pitch response to T-foil sinudoidal flap oscillation [radians]
η_{5t}	Pitch response to transom tab sinudoidal oscillation [radians]
η_{5tf}	Pitch response to transom tab sinudoidal oscillation, T-foil fixed [radians]
η_6	Yaw displacement in time [radians]
η_{6w}	Direction of downward deck slope in time [radians]
$\overline{\eta}_3$	Heave displacement amplitude [m]
$\overline{\eta}_5$	Pitch displacement amplitude [rad]
$\dot{\eta}_3$	Heave velocity in time [m]
$\dot{\eta}_5$	Pitch velocity in time [rad]
$\ddot{\eta}_3$	Heave acceleration in time [m]
$\ddot{\eta}_5$	Pitch acceleration in time [rad]
$\theta_{\dot{h}}$	Angle of free stream flow due to heave velocity and forward speed
$\theta_{\dot{p}}$	Angle of free stream flow due to pitch velocity and forward speed
λ	Wave length [m]
μ	Wave direction or primary wave direction [rad or deg]
$\overline{\mu}$	Mean primary wave direction [rad or deg]
μ_e	Wave encounter direction [rad or deg]
ζ	Free surface displacement from still water level [m]
$\overline{\zeta}$	Wave amplitude [m]
ρ	Sea water density = 1025 $[kg/m^3]$
σ	Cavitation number $(= (p_0 - p_v)/(0.5\rho V_0^2))$ or standard deviation
ϕ	Motion control surface optimum phase at selected regular wave frequency [radians]
ϕ_v	Motion control surface phase at selected regular wave frequency (based on local velocity feedback) [radians]
ϕ_a	Motion control surface phase at selected regular wave frequency (based on local acceleration feedback) [radians]
ξ_3	Vertical displacement at some longitudinal position [m]

$\overline{\xi_3}$	Amplitude of vertical displacement at some longitudinal position [m]
ω	Wave frequency $[rad/s]$
ω_e	Wave encounter (also flap oscillation) frequency $[rad/s]$
ω^*	Non-dimensional wave frequency $= \omega\sqrt{\frac{Lpp}{g}}$
ω_e^*	Non-dimensional wave encounter frequency $= \omega_e\sqrt{\frac{Lpp}{g}}$

(*c*) Subscripts

1	Surge
2	Sway
3	Heave
4	Roll
5	Pitch
6	Yaw

(*d*) Acronyms

AP	Aft perpendicular
FFT	Fast fourier transform
FIR	Finite impulse response
FP	Forward perpendicular
GPS	Global positioning system
INA	Institution of Naval Architects
ITTC	International Towing Tank Conference
MCS	Motion control system or motion control surface
MSI	Motion sickness incidence
RINA	Royal Institution of Naval Architects
SNAME	Society of Naval Architects and Marine Engineers
UCL	University College London
UTAS	University of Tasmania

Chapter 1

Introduction

1.1 Development of High Speed Vessels and Emergence of Motion Problems

High-speed vessels have been operating for many decades and in development since the advent of the steam reciprocating engine in the early nineteenth century but high Froude number hull forms are of more recent design. With the ability to move directly into the wind also came the necessity to move directly into the waves, which increased the motions, loads and slamming type phenomenon (see Lewis (1988a)).

During the nineteenth century an 83ft vessel built in 1873 achieved 21 knots whilst a 147ft torpedo boat built in 1887 reached 26 knots. Speeds over 30 knots first appeared in 1896 with a 200ft torpedo boat called the Turbinia, a 100ft craft of 43-ton displacement, which achieved approximately 32 knots (see Dorey (1990)). In comparison, hydrofoils developed from 1897 to 1905 achieved speeds up to 50 knots in sheltered waters (see Coggeshall (1985)).

Navigation between continents remained the domain of slower sailing ships up until 1819 when the paddle steamer MV Savannah crossed the North Atlantic from the Savannah River to Liverpool in 27 days. From that time, passenger numbers began to increase as their reliability improved. When the steam turbine and multiple propellers replaced the steam reciprocating engine and paddle wheel, cruising speeds increased from 9 knots in 1838 with the Great Western to 29 knots in 1936 with the liners Normandy and Queen Mary where they remained for the next few decades. Most of the existing liners had excellent seakeeping characteristics because of their length, large displacement and low metacentric height, a combination of hull parameters that are impossible to duplicate on smaller vessels (see Lloyd (1989)). At their high cruising speeds, these vessels were able to maintain acceptable seakeeping standards as their length based Froude numbers generally remained low, in a range below 0.3 (see Othfors and Ljungström (2003)). Maintaining acceptable roll motions was achieved with the provision of bilge keels and active roll damping mechanisms such as the roll fin introduced in 1890 (see Saul (1946)) or the gyroscopic roll stabilizer (see Scarborough (1958)), which was effective at reducing roll right down to zero forward speed.

With the advent of airline travel between continents, long distant travel by ship decreased and the liner was eventually replaced by the slower more economic cruise ship designed for the leisure market and generally slow short distance voyages.

Achieving higher speeds with displacement hull forms, required compact high-powered engines combined with a slender, lightweight hull constructed of aluminium alloy (see Callahan (1991)). The medium speed diesel engine or gas turbines combined with lighter construction methods of the large aluminium displacement vessels in the

1980s (see Hercus (1988)) made not only higher speeds possible but also higher Froude numbers. Compared with the traditional liner, cruise ship or conventional passenger ferry, these vessels were much shorter in length, had a shallow draft and in favourable wave conditions could achieve speeds of over 40 knots. As these designs matured, approval was obtained for these vessels to operate in open water routes but the limited ability of the lighter structural design to withstand the loadings of larger wave heights, which were a high probability in open waters, meant that restrictions had to be imposed. These included limiting the operational wave height and the provision that the route allowed the vessel to seek a sheltered harbour in the case of adverse wave conditions within a certain amount of time. Restricted wave height operations also existed because the adopted novel evacuation systems required as part of their effective operation, a relatively quick transition of personnel to the life rafts tethered along side in the event of a major fire outbreak or catastrophic structural failure due to for example, collision or grounding.

Shortly after the recruitment of high Froude number passenger vessels into service, large resonant heave motions were reported that caused severe discomfort and even emesis to a large proportion of the passenger population. This problem improved with the installation of motion control devices (see Hercus et al. (1991) and Adams (1996)), which were an existing technology but still in development for this type of application. Despite the improvement these devices made, it was common for the vessel's speed to be reduced in combination with a course change in the event of adverse wave conditions with the expectation this would improve passenger comfort and reduce the severity of wave impacts on the hull (see Dogliani and Bondini (1999)). Under the circumstances where a reduction in speed was sought, the high Froude number, operationally limited vessel would often find that its cruising speed would end up below 28 knots and thus no better than the cruising speed of the modern unrestricted steel Ro-Ro mono-hull ferries. Wave-induced motions and structural loads on these vessels therefore remain an important consideration if their operational limitations are to be improved.

Maintenance and versatility of recent motion control systems have improved to the point where hydraulic actuators are controlled from computer software through a digital network, but their force capability essentially remains a device size issue that must be considered in relation to the magnitude of wave forces on the hull. Unfortunately, the sizing of a motion control device is often a compromise with other hull design constraints such as hydrodynamic resistance and structural weight.

Seakeeping in general involves more than just subtle changes in hull shape or delicate optimizations (see Holloway (1998)) to achieve major performance benefits (see Gaillarde (2002)). However, the cost of ignoring the seakeeping aspects of a hull design are often misunderstood, so there remains much scope for seakeeping to be defined in terms of economic cost to the owner, operator and ultimately the manufacturer. Such benefits however may not by readily apparent when placed into the context of the many other demanding economic issues that an operator must deal with. For example, a passenger ferry purchased for operation without an understanding of its seakeeping characteristics may end up proving that it was entirely an unsuitable combination with the encountered wave conditions. In these circumstances low passenger numbers and reduced onboard sales of merchandise may be one outcome brought on simply because of passenger discomfort. It is likely that a prior understanding of both the wave environment and hull motion characteristics will avoid these problems and the operator will thus be better assured of an acceptable outcome for both the business operations and passengers. Alternatively, the operator of a successful vessel may not recognize that the seakeeping performance and compatibility with the wave environment contributed

enormously to that outcome.

For many, the complexity of a seakeeping analysis and the difficulty of extracting information that can make a useful contribution to the design process remains the largest obstacle for seakeeping prediction methods or model tests to be fully utilized (see Hearn (1991)). This problem is set to improve as some consensus and accuracy of numerical prediction methods improves and the presentation of useful results to the designer are standardized.

The prediction of motions and loads are some of the most heavily regulated and time consuming areas in ship design and these regulations are increasing as practical tools become more available. Higher hull speeds have increased the complexity of hull motions and loads so the scope and dimension of some long-standing problems in seakeeping remain. In particular, the magnitude of response at resonant frequencies is much more pronounced and coupling between degrees of freedom is more important, particularly for high Froude number vessels.

Motion and load prediction methods have steadily improved since the introduction of strip theory by Korvin-Kroukovsky and Jacobs (1957), with validation predominantly coming from experimental model tests. Whilst these tests form an invaluable part of the verification process, the complete solution may not be immediately clear until verified with full-scale experiments, particularly as numerical prediction methods overcome their inherent shortcomings and improve both their accuracy and reliability.

Saunders (Second printing 1982) in 1960 stated, "In a seaway, the ship is moved involuntarily in all its six degrees of freedom, by forces over which man has as yet only a rather feeble and certainly an inadequate control. Until this control is achieved, he should at least know what motions may be expected under any given set of conditions. At the time of writing he knows relatively little."

Seakeeping is one of the most important aspects of ship design as it relates to the on-board comfort and enjoyment of personnel while at anchor, vessel integrity and safety while at sea or the feel-good impression and perception of being on board a safe and seaworthy vessel (see Gaillarde (2002)). Non-linear motions exhibited by the high speed light craft (see Zhao and Aarsnes (1995)) make full scale tests more important if prediction methods are to be improved whilst maintaining an adequate check on the reality of the problem.

1.2 Vessel Motion in Waves

1.2.1 Experimental Model Studies

Formal seakeeping studies that preceded present day thinking commenced with the pioneering work of William Froude and his son Robert Edmund in the 1860s shortly before their first tank work in 1871. The first tanks in Europe appeared shortly after, but experimental model scale investigation of ship motions in waves did not begin until the first installation of wave makers in model basins in 1887 in Great Britain, 1894 in the Soviet Union and 1916 in the United States. Full-scale experimental testing and observations occurred later on a more organized basis in the early 1900s.

A general overview of the subject material has been provided by standard texts such as Saunders (Second printing 1982), Korvin-Kroukovsky (1961) and Lewis (1989).

Towing tanks have been used on numerous occasions to test and validate numerical models and theories. To the operator of a high Froude number vessel the seakeeping is of great importance to ensure structural integrity and motion levels are appropriate for its intended use. It is more common therefore for seakeeping criteria and motion

guarantees to be confirmed. This can occur through validated numerical predictions, but usually sea trials or a model-testing program is required for verification (see Dussert-Vidalet et al. (1995) provides an example of this for a Corsaire 11000 mono-hull). Other validations made through tank tests are too numerous to list but by way of example, Gong et al. (1994) conducted model-tests specifically to validate a 2D strip theory method on an 80 metre catamaran at Froude numbers up to 0.67. Hudson et al. (1995) conducted model tests on a displacement catamaran with various hull separations for comparison with three potential flow prediction methods that included a three dimensional panel source distribution and simple strip theory. In the results it was observed that in some cases an unexplained lower frequency of response in the measured heave and pitch resonance peaks occurred compared with the predicted solutions.

Wellicome et al. (1995) conducted some generic model tests on a "series 60" hull and produced transfer functions and phases in heave, roll and pitch providing researchers with a reference on this hull type for numerical comparisons.

1.2.2 Analytical Predictions

Formal analytical methods for the prediction of hull motions commenced with the work of Froude (1861), Kriloff (1896), Kriloff (1898) and the more recent work by St Denis and Pierson (1953) for his contribution on the application of the principle of superposition. Korvin-Kroukovsky (1955) introduced a "strip" method which allowed the hydrodynamic load distribution along the length of the hull to be determined. Further comparison with experimental data showed that improvements and corrections could be made to the bending moment calculations which lead to the subsequent work of Korvin-Kroukovsky and Jacobs (1957) (also contained in the text Korvin-Kroukovsky (1961)). This was the first method considered suitable for numerical computations and was enhanced by Jacobs (1958) to include regular wave induced vertical shear forces. A reasonable review of the progress of this era was given by Ogilvie (1964) and was shortly followed by slender ship theory to improve the forward speed effects not accounted for in simple strip theory. The original strip theory of Korvin-Kroukovsky and Jacobs (1957) was recognized by Salvesen et al. (1970) to be one of the most significant contributions in seakeeping but the theory published by Salvesen et al. (1970) is now a more recent standard. Nordenstrøm et al. (1971) applied this theory to a catamaran at zero forward speed. Since that time, numerous two- and three-dimensional methods have evolved to improve on the generally acknowledge shortcoming of strip theory which is its theoretical validity being limited to low speeds and high frequencies (see for example Newman (1978), Yeung and Kim (1984), Faltinsen and Zhao (1991)). Outside these boundaries, the results clearly become less acceptable (Holloway and Davis (2001a)), particularly for less conventional hull forms. Furthermore, these numerical methods are unable to deal with the non-linear responses evident at high Froude numbers and high wave heights. This problem was partly addressed with developments such as the rational strip theory of Ogilvie and Tuck (1969), which was a higher order theory in a moving reference frame, the unified theory of Newman (1978), Newman and Sclavounos (1980), Yeung and Kim (1981) and Yeung and Kim (1984). Some of these have also been reviewed by Kashiwagi (1997) and a more general overview of the analytical seakeeping methods given by Hutchison (1990). Holloway and Davis (2001a) reviewed some notable strip, strip like and 3D theories since 1970 and proposed the hypothesis that dissipative damping had a significant effect on hull motions. This implies that the merit of highly complex potential theories have been brought into question as a useful engineering tool as they are unable to account for these effects whilst also possessing a

long computation time to obtain a solution that cannot not fully achieve validation by experiment, particularly at high Froude numbers.

1.2.2.1 Motion Control

For prediction codes to be useful to the designer, they must also have the capacity to deal with the non-linear effects introduced by a motion control system. Since the early 1990s as the high Froude number passenger vessel developed, such systems are considered a necessity (see Adams (1994), Adams (1996), Akers (1999)) to reduce the large heave excitations observed, to reduce fuel consumption through improved hull resistance in waves (see Burns (1990)) and to improve passenger comfort through reduced accelerations.

Any numerical ship motion prediction method can utilize motion control devices in the computation and numerous publications have reported such attempts in both the frequency and time domain. However, without a common method of control, appendage size and type, results will remain unique to a particular hull form and motion control appendage configuration.

Kvalsvold et al. (1999) investigated the operability of a high speed mono-hull fitted with a motion control system and experimented with a range of control coefficients to determine the operability against a range of motion criteria. Improving the operability depended on the selection of devices combined with an appropriate selection of control coefficients.

Kang and Gong (1995) modelled the effect of motion control fins on a catamaran with a time domain solution formulated to solve the wave exciting force with a 3D transient Green function (see Wehausen and Laitone (1960)). Using transient hydrodynamic theory of Newman (1977), the force reduction and change in the force phase due to the sinusoidal change in fin angle of attack and sinusoidal wave particle velocity were accounted for using the Wagner and Kussner functions respectively. The flap angle was limited to the assumed stall angle of 35 degrees at approximately 20 knots (Fn=0.548) vessel speed but did not address the possible effects of cavitation.

Ohtsubo and Kubota (1991) modelled a hydrofoil with a time domain strip theory that included a steady lift component, an unsteady component due to the orbital wave motion using gust theory, an unsteady component due to the ship motions and finally, the lift reduction due to the proximity of the free surface. The lift due to the proximity of the free surface was based on experimental results, which increased exponentially from approximately zero at the free surface to a maximum at some depth below five chord lengths. Their definition had the advantage that it accounted for the angle of attack of the foil at a given depth by decreasing the foil lift as the angle of attack[1] increased. Wadlin and Christopher (1958) produced a theoretical derivation to account for foil depth effects but their formulation was much less influenced by the foil angle of attack. At moderate attack angles (say 6°), their formulation began to resemble that of Ohtsubo and Kubota (1991) where the lift reduction with depth occurred at approximately the same rate, but this quickly changed with only a few degrees change in foil angle of attack. Wadlin and Christopher (1958) also determined the lift generated by a planning surface, such as a foil as it rides over the free surface and changes from a submerged lifting device to a planning surface, which for shallow draft high Froude number hull forms is a distinct possibility. Fossen (1994, p 383) also accounted for a reduction in lift due to foil depth that changed linearly from a factor of 0.5 at the

[1]Increased foil camber also had an effect but the foils discussed in this work are symmetrical, thus have zero camber.

free surface to a factor of one at a depth equivalent to one chord. (see figure 1.1 for a comparison in the lift reduction factor at an angle of attack of 8 degrees) Theoretical and experimental work conducted by Lee et al. (1997) on fins mounted on a strut showed that the free surface influenced the foil lift for submergence depths less than three chord lengths.

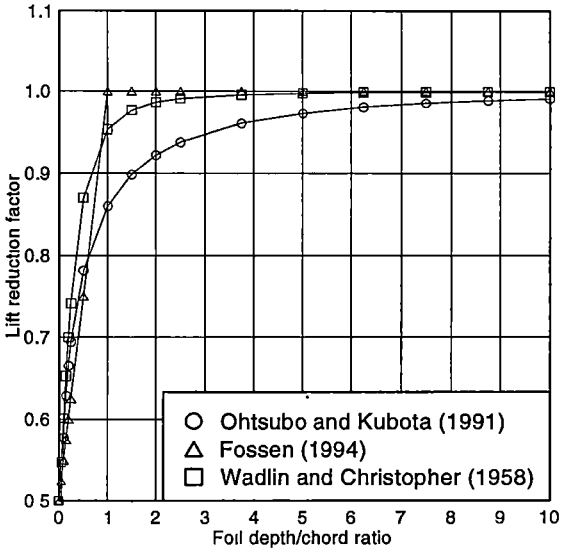

Figure 1.1: Lift reduction factor with depth/chord ratio. (foil angle of attack $\alpha = 8°$, chord $= 2$ metres)

Schellin and Rathje (1995) developed a 3D potential theory for predicting hull motions using pulsating sources and included the lift generated by cantilevered motion control fins. The lift calculation based at the fin centre of pressure included the influence of incident waves made up of the wave particle velocities, the translation and rotation due to the ship's motion and forward speed. Neglected are the effect of radiated and diffracted waves, down wash between fins, free surface influence and blockage of the other hull. Included is the body-fin interaction using the procedure given by Lee and Curphey (1977) (see also the original source Pitts et al. (1959)). This empirical formula considered the lift generated on the hull due to the cantilevered fin and the lift on the cantilevered fin due to the hull. The modelling in detail of further effects was considered to be a difficult task to accomplish satisfactorily. Each fin was located on the inboard side of the SWATH demi-hulls.

Other work has moved to create more complex numerical models for predicting the forces on hydrofoils. For example, Walree (1997) developed a computational method for evaluating the hydrodynamic performance of arbitrary hydrofoil configurations performing arbitrary motions in six degrees of freedom, based on an unsteady vortex lattice time domain panel method. However, Savitsky and Brown (1976) remains the most relevant work for lift generated by a transom flap/tab.

1.3 Development of Full-Scale Motion Measurements

Full-scale measurements and the collection of data from ships at sea were a need that had existed for a long time before Kent (1924) (see also Kent (1927)) commenced some work by making six ocean voyages on three passenger liners. The observations reported the environmental conditions and the ship response to these conditions (see Korvin-Kroukovsky (1961, pp. 183-184)) generally using only the standard ship equipment. The only specialized equipment was for measuring roll and pitch angles with a flywheel type device and pen recorder. During this period, J. L. Kent presented only a small part of the collected material in numerous papers, which was related in no small part to the difficulty in post processing the information.

The measurement of heave, roll and pitch simultaneously over long time periods was possible after the development of the accelerometer and gyro-type sensor combined with a simultaneous pen recorder. Korvin-Kroukovsky (1961) noted that prior to 1955, no comparison of calculated and measured ship model motions had been made, despite the existence of full-scale measurements and mathematical methods. The first comparison was conducted by Korvin-Kroukovsky and Lewis (1955). Research methods improved with the introduction of the portable computer, so large amounts of data could be collected over long periods and processed simultaneously or stored for later analysis.

The study of motion and loads potentially involves complex motion and vibration problems that can include any number of degrees of freedom. Experimentation at model scale remains the prime means of comparison as wave conditions can be prescribed and it can be the most efficient means to obtain a result. However, scale effects can often reduce the accuracy and reliability of the results when they are not fully understood so full-scale experimentation remains a valuable option in the numerical validation process.

1.3.1 Motion Measurement

Full-scale measurements have often been undertaken in conjunction with hull monitoring programs in which data was recorded during routine vessel operations and in some cases over an extended period of time, such as those conducted by Vulovich et al. (1989), Beaumont and Robinson (1991), Brown et al. (1991), Witmer and Lewis (1994), Witmer and Lewis (1995) and Cannon and Mutton (1997). In some instances the measured data was not only stored for post-analysis, but was used to present the crew with real time hull motions, loads and wave conditions, thus providing an additional resource that could contribute to the ship operations decision-making process. Dogliani and Bondini (1999) made long term measurements on a high speed mono-hull whilst in operational service but had to rely on visual estimations and hind cast data to determine the dominant wave direction for each data record.

Most full-scale measurements reported by numerous authors have been for confirming the seakeeping performance of a new vessel, to evaluate a numerical prediction method or to verify model test results. Some are for the express purpose of improving or developing a new measurement technique. These include work by Klaka and Webb (1992) who conducted full-scale measurements to verify a shallow water motions prediction method through the derivation of transfer functions and responses from full scale measurements. However, they were unable to detect changes in hull response with changes in water depth. There was also difficulty in resolving the approach of the transfer functions to unity at low frequencies. Kohlmoos and Schellin (2002) conducted specific full-scale measurements to derive transfer functions and a motion sickness prediction according to the method described by the International Organisation for Stan-

dardisation, ISO 2631/3 (1985) and motion sickness incidence according to O'Hanlon and McCauley (1974) for a 52 metre catamaran fitted with a motion control system. Yum et al. (1995) conducted full-scale measurements on an actively controlled foil catamaran and made comparisons with a simple strip theory and 3D panel method by deriving root mean square responses for comparisons of heave, roll and pitch. Boulton (1999) used full-scale measurement data from a new vessel to verify its seakeeping and for comparison with previous vessels. Rantanen et al. (1995) used full-scale measurements to confirm the seakeeping performance of a new vessel and to evaluate numerical predictions and model tests, as did Schellin and Papanikolaou (1991) for a SWATH hull form in which comparative transfer functions were presented. Wang et al. (1999) used full-scale measurements on a mono-hull to evaluate both linear and non-linear numerical methods. Thompson (1979) conducted extensive full-scale measurements on an Attack Class Patrol Boat and was able to derive response spectra and transfer functions for roll and pitch using a wave rider buoy and analogue instrumentation techniques. Haywood and Duncan (1997) used full-scale measurements on high-speed ferries to tune a motion control system using a system identification techniques. Aksu et al. (2002) performed full-scale trials on a twin hull 86 metre vessel, which was a similar type to the 86 metre vessel used for the present study. They conducted motion measurements at various wave headings and speeds for comparison with a numerical three-dimensional panel method. Finally, as part of the program of extensive ship monitoring and data recording conducted by Witmer and Lewis (1994) and Witmer and Lewis (1995), it was important to provide feedback of the measurements to the crew by means of a display monitor mounted on the bridge during the monitoring period so they could make appropriate decisions and take action to maintain the ship operation within the defined loading limits. This required almost real time data post processing and data storage.

1.3.2 Wave Measurement

Wave measurement instruments broadly fall into two categories that include point measurement or spatial averaging devices. Wave rider buoys containing instrumentation or pressure sensors generally fall under the former description and can provide either omni- or uni-directional wave statistics (see Clauss et al. (1999)). Satellites fall into the description of spatial averaging devices that require calibration with a wave rider buoy but are generally unsuitable for providing local wave statistics in real time for a vessel at sea.

The Darbyshire wave spectrum was developed with a ship borne wave recorder (see Tucker (1952)) that consisted of a pressure gauge mounted on the hull approximately 10ft below the free surface on both the port and starboard side. Combined with each gauge was an integrating accelerometer that recorded the stationary ship's heave motion over 7 to 10 minutes (see also Tucker (1956), Tucker (1991)).

Cartwright (1956) tried to measure the directional distribution of waves in the open sea using a ship mounted wave recorder that could be analysed to obtain a scalar spectrum. By steering the ship around a regular dodecagonal circuit (12 sided) at 7 knots, the directional sensitivity was determined through calculating the "Doppler shift". Theoretically it was possible to determine the directional spectrum from this procedure but the variability in the spectral estimates were too great due to the short sample duration of 12 minutes to make the evaluation practical (see Korvin-Kroukovsky (1961)).

In another method proposed by St. Denis (1957), several probes were arranged along a straight line and orientated alternately in several directions but this was not tried

experimentally. In other work Barber (1954) used a row of detectors mounted on wharf piles, each consisting of a pair of parallel vertical copper strips partly immersed in the water, but this was not demonstrated for use as a ship borne system. Similarly, Dipper (1987) evaluated various methods to accurately estimate the directional components of ocean and basin waves to assist with requirements for manoeuvring and seakeeping tests. He went on to examine a method to estimate the directional wave spectra through an application of the Maximum Likelihood Method (MLM). This method was capable of such estimates provided the spacing of the fixed wave probe arrays were tuned spatially with respect to the frequency content of the waves for which a directional spectrum is to be estimated. He had better success with closely spaced wire capacitance transducers than a broadly spaced ultrasonic transducers. This problem was related to the poor tuning of the sonic transducers to the analysed wave conditions. The procedure was well equipped to determine the directional wave spectra for presentation and analysis at both full and model scale, but the method implies that the transducer mounting must be fixed in space.

Investigations using full-scale ship motions alone to estimate the wave spectra were undertaken by Marks (1967). Hua and Palmquist (1995) determined the wave spectra from hull response measurements, which they called the *variation method.* These proved to be successful in bow waves but following wave directions gave unsatisfactory results.

Bachman et al. (1987) investigated the use of a surface following wave buoy for application to full-scale measurement and analysis. They noted that there were differences between the frequency of ship encountered waves and buoy encountered waves, which could be increased if the buoy was free to move with a current moving in the opposite direction to the vessel. Furthermore, it could not be guaranteed that the wave data recorded would correspond to those encountered by the vessel as the trials course would often take the vessel some distance from the buoy location.

Recent developments make use of ultrasonic, laser, infrared or microwave transducer (more details in sections 1.3.2.1 to 1.3.2.4 respectively) techniques for making uni-directional relative distance measurement from a vessel to the sea surface. More sophisticated radar systems are better described as a far field devices that provide directional wave spectra to a base of either wave or encounter frequency. These transducers have the ability to scan the sea surface that surrounds the vessel, from which the statistical surface heights may be determined as a function of wave height and wave direction.

1.3.2.1 Ultrasonic Transducers

For particular applications the ultrasonic transducer makes a relatively low cost distance ranging device. They can only operate at the speed of sound so their maximum sample rate is a function of the time taken for a sound pulse to be transmitted and received over the range being measured. These units are also subject to ambient temperature variations that can be allowed for with temperature compensation. High sample rate is thus associated with short range measurement whilst long range measurement must suffer a reduction in sample rate. (section 2.2.1 discusses sample rate issues).

To operate effectively, an ultrasonic transducer must have an orthogonal surface to reflect the acoustic pulse so it is possible from time to time for a return signal to be lost or received through secondary reflections causing erroneous readings. With the relatively short range of ultrasonic transducers it is often necessary to mount the unit as close to the free surface as possible. In the event of extreme seas, this increases the likelihood of erroneous readings with the possibility of the transducer unit becoming submerged below the free surface or enveloped by spray.

1.3.2.2 Laser Transducers

Whilst laser units are expensive and their delicate construction make them prone to breakage, they can make excellent ranging devices for wave measurement (see Slotwinski et al. (1989)). Experience with these units showed that a return signal is possible whilst operating at low grazing angles [2] to the free surface. In principle, the laser units required a relatively high number of returns in order to determine the range measurement with an acceptable order of accuracy. For example, over a range of 10 metres to achieve an accuracy of 0.1 metres the maximum sample rate is limited to 1 Hertz.

1.3.2.3 Infrared Transducers

Infrared transducers have been used with success for wave height measurement on fixed platforms and was used with success for wave measurement from a moving vessel for deriving wave encounter spectra by Steinmann et al. (1999). They have a range of up to 50 metres and have been used primarily for fixed position wave height measurement.

1.3.2.4 Microwave Transducers

The microwave transducer has been used successfully in previous studies such as those by Yasuda et al. (1985) and Rantanen et al. (1995) that produced a ship borne type microwave Doppler radar for full-scale measurements. The work of the former subsequently became the microwave unit of Tsurumi Seiki Co. Ltd. (TSK) (see TSK (2003)). Dipper (1997) attempted to measure the waves with a TSK ship borne radar, which on occasion was compared with a wave rider buoy by holding the vessel stationary. Good agreement was obtained between the two measurement systems except at very low frequencies (approximately 0.06 Hz) where the TSK results appeared to be slightly attenuated. Steinmann et al. (1999) concluded from experiments with a TSK microwave radar and a Thorn infrared meter, that there was little difference between the two apart from erroneous low frequency results in the wave spectra of the TSK unit. Korvin-Kroukovsky (1961, pp. 67-68) suggested that such effects may be the result of d-c drift in the recording electronics where the wave record drifts away from the preset zero of the recorder. This is manifest in the spectrum as a spike at or near the zero frequency and corresponds to the apparent infinite wave period generated by the drift. This can be a particular problem for ship mounted wave sensors that move with the speed of the ship as there is difficulty in measuring low frequency components, particularly if there are wave components travelling in the same direction as the vessel. This proposition contributes to the likelihood of not detecting any following wave patterns moving in the direction of vessel travel, which may exclude waves whose headings are aft of the beam from forming part of a seakeeping analysis when a fixed ship mounted sea surface sensor is used. Generally the linear drift is not a serious problem if the measurement application is planned with appropriate filters.

It was a similar TSK microwave transducer device that was installed on vessels for wave measurements in the present analysis.

1.3.3 Spectral Derivation

There are various accounts given on the analysis procedure adopted for full-scale analysis. A general overview has been given by Bendat and Piersol (1980), Beauchamp and Yuen (1979) and more particular application to sea spectrum derivation by Korvin-Kroukovsky (1961).

[2] 35 degrees was quite achievable for these units.

Tucker (1991) suggested that response spectra should be produced from a data record that contained a minimum of 100 motion cycles (Run time = $100T_p$, where T_p = mean period of motion peaks) to obtain reasonable confidence in the spectral estimates.

Dipper (1997) recorded data for 30 minutes at 8 Hertz with a ship mounted TSK microwave Doppler wave radar whose operation is described by Yasuda et al. (1985) with the assumption that the amplitude data followed a Raleigh distribution. According to Pierce (1992) high run lengths are required to achieve at least a 90 percent accuracy in resolving the power spectral density (PSD) for the ship motions in beam sea waves. Higher encounter frequencies in head sea wave measurements increase the statistical reliability for a given recording period, whilst a lower encounter frequency in following waves lowers the statistical reliability unless the record length is extended. Comparisons made by Dipper (1997) between wave spectra developed from forward speed and zero forward speed wave spectra showed good agreement. PSD analyses was conducted by first removing extraneous frequencies above the Nyquist frequency using a linear phase filter with a cut off frequency of 2.0 Hz., then applying a 50% data segment overlap with a full cosine data window. The 50% overlap is also an approach to FFT analysis presented by Welch (1967).

Wang et al. (1999) used full-scale measurements on a mono-hull to evaluate both linear and non-linear numerical methods. Derived power spectra came from an average of 36 data record segments of equal length taken from a one-hour sample period. This resulted in a spectrum derived from a 100 second FFT to give a spectral resolution of 0.01 Hz.

Rodriguez et al. (1999) investigated different numerical methods of spectral estimation and considered the uncertainty associated with the spectral parameters for measured wave records. These included the Blackman-Tukey method, the direct Fourier transform method, which are two classical or non-parametric methods and the maximum entropy method, which is a parametric procedure. They found that different methods of spectral estimation did not have a significant effect on the variability of the spectral wave parameters whose magnitude depends on the overall spectrum. However, parameters that depend on only a few spectral estimations such as the peak period, show a large variation between the spectral estimation methods. The estimation of the power spectrum by means of the maximum entropy method showed excellent statistical behaviour of the spectral wave parameters.

1.4 Motions in Waves at High Froude Numbers and Onset of Passenger Sickness

Accelerations, combined with the perception of motion through eye vision, are primarily responsible for the physical sensation of movement. Furthermore, accelerations of specific magnitude and frequency can lead to motion sickness and physical debilitation to both passengers and crew (see Smith (1995)). The speeds achieved by modern high-speed craft has taken them to unusually high Froude numbers and thus have also been responsible for an increase in resonant motion amplitudes (see Holloway (1998)) and accelerations, which have exacerbated the problem of motion sickness. Reason and Brand (1975) gave a broad overview of motion sickness where they discuss the extent of the problem, the nature of the phenomenon and the physiological aspects such as the nature of the stimulus and the role of the vestibular system before discussing personal susceptibility and preventative measures through drugs or otherwise.

Shaw (1954) and Geller (1940) according to Korvin-Kroukovsky (1961) proved that there was a direct connection between acceleration and sea sickness which subsequently

lead to a range of predictive measures for motion sickness, although it is widely considered that other factors play a significant yet unquantifiable part. Subsequently it was found that the various acceleration levels across the deck influenced personnel sense of well being depending on their position within the hull (see Lawther and Griffin (1980)). Various passenger surveys have also yielded supportive evidence of the factors that influence passenger illness (see Lawther (1983) reports one such survey).

The International Organisation for Standardisation, ISO 2631/3 (1985) document provides a basis for determining the limitation of human exposure to vibration transmitted to the body in the frequency range of 0.1 Hz to 0.63 Hz (the Australian Standard, AS 2670.3 (1990) is a similar document). The recommendation applied particularly to discrete-frequency and narrow-banded vibration and provisionally to random or non-periodic vibrations in the vertical z-axis direction. The tests were conducted with unadjusted sitting or standing young men and provided a guide to acceleration levels known as "comfort curves" plotted to a scale of log base 10, with centre frequencies of 1/3 octave bands against the root mean square (RMS) acceleration levels (see appendix F.2). The nominal discomfort boundaries were set as a function of frequency and exposure times of 30 minutes, 2 hours and 8 hours. The acceleration level occurring at one of these boundaries is a function of the exposure time t and follows the relationship a^2t = constant. "Severe discomfort" defined by these publications was the broad spectrum of motion sickness symptoms that occur successively in order of increasing severity. Individual symptoms progress from pallor and dizziness through nausea to vomiting and complete disability. These symptoms can vary from subject to subject in both severity and duration and that it can change for a given subject depending on circumstances and habitation. If the boundaries were exceeded it was expected that a significant proportion of human habitants would experience severe discomfort and temporarily disability. Whilst these values could be raised or modified to adapt for the acclimatized traveller, they could be considered to be optimistic in their application due to the many other factors that influence the inducement of motion sickness. Unfortunately, the range of frequencies within the tests that caused the most severe motion sickness in the participants generally coincided with a component of the frequency of response associated with high Froude number vessels.

The vertical direction arguably has a great effect on motion sickness but other modes of motion such as surge, sway, roll and pitch can reduce the acceleration comfort boundaries by up to 25%. Other factors such as age and gender will contribute to reduce these levels further. No specific experiments were conducted for women, children or elderly people but indications were that the sickness levels would be 25% higher than those given by the standard. In addition, no experimental data was available from typical irregular wave induced motions at sea.

The standard suggests that these boundaries will reflect the sickness levels for 85% of a population, indicating that 15% will be sick before these levels are reached. In order for these boundaries to be increased to reflect the sickness levels for 90% of a population, the acceleration levels would need to be reduced by about 20%. The incidence of slamming experienced by a vessel will also contribute to passenger discomfort due to the violent vibrations initiated in the hull structure.

This approach for assessing motion sickness in vessels at sea has yet to be substantiated together with the adoption of 1/3 octave bands as a legitimate method of dividing up the range of acceleration response. It has been used in various vessel motion studies where the work of Hercus et al. (1991) and Adams (1996) are two examples.

The British Standards, BS 6841 (1987) define a motion sickness dose value (MSDV) to include acceleration, frequency and time exposure as variables (see also Lawther and

Griffin (1987) and Lawther and Griffin (1988) for a calculation and use of a motion dose).

Motion sickness incidence (MSI) or the percentage of persons to vomit as a result of experiencing accelerations of a given magnitude and frequency over a two hour period, was first proposed by O'Hanlon and McCauley (1974) after conducting a study on the effects of sinusoidal motion at various frequencies on human sickness (see mathematical description in appendix F.1). This was later refined with the follow up work of McCauley et al. (1976) to include exposure time of the human subject as an independent variable.

Colwell (1994) expressed the inadequacy in most approaches (that are well reviewed) to sea sickness or human proficiency at sea for the naval environment because firstly, they are not related to task performance, secondly, they do not cover the full spectrum of problem types and finally they are essentially exclusively based on short-term exposures to motion. He presented a new approach by describing a method that accounts for the reduction in motion sickness incidence due to the adaptation of personnel with long term exposure to motion, giving more realistic values for motion sickness in the naval environment.

More recently, Smith (1997) (see also Smith and Koss (1995)) presented a new measure of Kinetosis acceleration that took on the frequency weighted function defined by British Standards, BS 6841 (1987) and included a time based accumulation and recovery represented by a constant parameter, first order differential equation. Some work reported by Smith and Koss (1997) involved field studies of various hull types that included catamarans.

1.5 Development of Motion Control Systems

Development of motion control systems for high Froude number vessels began in the late 1980s as these craft began to enter service to improve the resonant heave responses (see Adams (1994)). Some developmental aspects of control theories, strategies and numerical computations were discussed for example by Haywood (1995), Haywood et al. (1995), Klaka (1997) and Haywood and Duncan (1997) (see also Haywood et al. (1994), Swanton et al. (1999)). Motion control systems were however already in existence for a range of low speed applications such as for luxury motor yachts, where the effects of cavitation were less of a problem (see Gaillarde (2002) and Redmayne(ed.) (2003) for a discussion on seakeeping of luxury yachts).

1.5.1 Active Control Devices

Motion control systems installed on high Froude number vessels have largely adopted the use of hydrofoils, interceptors or transom tabs as hydrodynamic devices among the range available (see Kubinec (2001)). The interceptor was introduced to high-speed craft when Ponomarev (1991) demonstrated through full-scale tests on a mono-hull planning their effectiveness as hydrodynamic force devices in controlling roll, pitch and trim. Further work was also conducted by Ponomarev et al. (1995) where they were fitted to the trailing edge of propeller blades to improve the propulsive performance. These devices were recognised as an alternative to the transom tab installation on high Froude number vessels from 1992 (see Duffy (1999)) where there were some obvious benefits compared with the transom tab (see Wilson(ed.) (2000)) such as reduced fabrication, operation and maintenance costs and reduced hydraulic operating power requirements. Some installations also utilize them for trimming on small high-speed

craft (see Pike (2003)). They can even be used as a high speed steering device (see Widmark (2001)). Ericson (2002) looked at a comparison of the lift and drag characteristics between the interceptor and transom tab through wind tunnel tests and numerical analysis. The force characteristics between the devices are different, thus making a selection between the devices for a particular application depend on factors such as vessel operating speed, machinery configuration and weight requirements.

Another device contemplated for high Froude number vessels include the lift dumping foil (see Shock and Thiagarajan (1998)). Other devices not so prominent on high-speed craft include the transversely actuated moving mass (see Anonymous (1999) for an example of a 100 tonne moving mass for an oceanographic research vessel), the use of actively controlled rudders (see Goodwin et al. (2000), Perez et al. (2000)) and active tanks (see Treakle (1998), Coyle (2000) and Knaggs(ed.) (2000)). These devices are more common on large mono-hulls with a comparatively low metacentric height.

The higher speeds of recently designed vessels makes cavitation an issue that must be considered and managed through material selection (see Ito et al. (1997) for cavitation erosion tests on high tensile stainless steels for a Techno-Superliner) and foil design. Super cavitating foils or possibly an unproven type of intercepted foil may be required in some cases to address these issues. Weight considerations in hull design have given rise to the need to produce lighter foils from materials such as high strength steels, aluminium, titanium or composites (Moan et al. (1991)).

1.6 Objective of Present Investigation

Model tests for the purpose of validation and experimentation are made possible by the scaling laws on which they are based and provide an environment that can be customized and controlled with greater certainty than with full scale measurements. Similarity between model and full scale in both the physical model and the wave environment has been achieved to a certain extent with the differences dealt with through the use of correlation coefficients (particularly in resistance tests). Clauss et al. (1999) discusses the uncertainties in wave modelling, which included the full scale measurement of the real wave field environment and their analysis through mathematical modelling. It also includes the mechanical restrictions in the wave generation process, their propagation and decay over the length of the tank, instrumentation accuracy, their measurement and linear spectral analysis. Whilst full scale measurements also share some of these problems, they do not need to deal with issues of scaling and wave reproduction. However, they do need to deal with the issues of measurement and instrumentation so as to obtain an accurate record that provides a complete understanding of the events measured and recorded for use during the analysis of the data.

Transfer functions or response amplitude operators (RAO) can be derived if sufficiently long time records are available to resolve cross spectra of signals accurately. When deriving a specific energy spectrum of ship response it is necessary for the measurements of the wave environment and ship response to be taken over a relatively short duration where the wave conditions can be considered to remain constant to obtain a useful result. However, under the assumption of linear ship response it is not essential for the sea conditions to remain identical when deriving transfer functions as all the ensemble averages of wave spectra and response spectra can be averaged together, provided the data can be organised into groups of constant wave direction, vessel speed and even wave height if linearity is an issue. With the vessel encountered wave direction changing significantly during a period of measurement from 0 to 360 degrees, resolving wave directions aft of the beam with ship mounted wave measurement devices

becomes difficult without complex equipment. Therefore, central to such observations is the measurement of the sea surface profile using either radar and ultrasonic sensors mounted on the vessel bow from which the wave encounter spectra can be derived.

This thesis seeks to develop some of the techniques and practices involved in performing full scale motion measurements with instrumentation mounted on an 81 and 86 metre aluminium twin-hull car/passenger ferries operating in an omni-directional wave environment. Assumptions and simplification of the measurement records were made to enable a comparison of the data through spectral analysis with a numerical time domain prediction method for waves encountered on the bow (head seas). The numerical computations predicted the motion responses at Froude numbers of 0.235 to 0.798 (12.5 to 45.5 knots) through the use of a time domain strip theory program (see Holloway (1998)) with the inclusion of motion control surfaces.

1.6.1 Limitations of the Results

The approach of this research was to involve both experimental and computational results to achieve a balance of outcomes. The scope of measurements achieved and the type of experiments undertaken were restricted by limitations that include:

- the experimental tests were carried out with the use of a full-scale craft where the wave environment could not be controlled or regulated. The measurement of the wave climate did not take into account its three dimensional nature and so some assumptions had to be made to account for this. No model scale experimental motion data from a towing tank was available to further validate the results, due to time and financial constraints. Ideally, some results from a towing tank would have provided more credence to the outcomes due to the ability of such experiments to isolate and limit the measured variables. This would have been a useful comparison however, the scope of the present work was necessarily limited to comparison of full-scale and computed responses.

- the recording of experimental data during the course of normal ship operations due to the high cost for dedicated ship time. The implication was that without measuring every influencing variable of the ship motions (for example, whether the motion control system was on or off, although in practice the motion control system was invariably active), some ambiguity remained in the results due to broad assumptions and averaging of the data. In addition, operational requirements overwhelmingly dictated the preferred course of the vessel relative to the predominant wave direction, so the probability of obtaining data for all wave directions reduced considerably.

- the motion control system algorithm implemented on the vessel was not known exactly for reasons of commercial security. As a result the control algorithm could not be exactly modelled in the numerical computation and certain assumptions had to be made about its method of operation. However, the general principle of the motion control system is to act as a damper and it was considered that this was sufficient to represent the motion controls in the numerical computation, and

- time and the availability of computational resources meant that only head seas could be modeled for comparison with the experimental data. The ability to model other wave directions may have yielded more information about the response of the vessel in omni-directional seas similar to the type of waves encountered in the experimental measurements.

1.6.2 Thesis Outline

The present chapter has introduced the wave-induced motions of high Froude number craft with some background discussion of the literature relevant to this research topic. Chapter 2 covers the methods employed in the experimental work and introduces a solution to resolving the measured dominant wave direction to allow data analysis to be conducted for known directions for the encountered sea. Chapter 3 presents the methods employed in the computational simulation. Chapter 4 presents the results of the full-scale measurements through transfer functions, spectra and response measurements. Chapter 5 presents the results of the numerical computation through transfer functions and response spectra for bow waves at two loading conditions for the hull configured both with and without motion control surfaces. Chapter 6 contains a discussion that brings the results of full-scale measurements and numerical computations together and finally Chapter 7 forms the conclusion and highlights some areas of possible future research.

Chapter 2

Experimental Methods For Full-Scale Wave Response Measurements

2.1 Overall Strategy

Experimental measurements were conducted on two twin-hull type car/passenger vessels illustrated in figures 2.1 and 2.2. Measurements commenced on an 81 meter vessel (Incat hull number 038) and concluded on a second 86 metre vessel (Incat hull number 042) (see Appendix A for further details on these vessels). The hull form features a chine below the waterline with cantilevered, low volume hulls in the bow above the waterline. The sectional beam at the waterline of each demi-hull is greater than any underwater section, unlike the underwater shape of the Small Water plane Area Twin Hull (SWATH) or the semi-SWATH (see Holloway and Davis (1997)). These generally have a waterline beam in the extreme aft end that is greater than any underwater section, but in the forward end the greatest section beam is well below the still waterline. The 81 and 86 metre hull forms of this study are thus conventional in general form.

A data acquisition system fitted to each vessel was left to operate largely unsupervised to accumulate data. The 81 metre vessel after its delivery to the United Kingdom, operated between Weymouth, Guernsey and Jersey in the English Channel, whilst the 86 metre vessel, which eventually replaced the 81 metre vessel, operated on the same route for a further 12 months before all measuring equipment was removed (see Hynds (1997) for some background information of the 86 metre vessel on this route).

The delivery voyage of the 81 metre vessel started in Hobart, Australia on 8^{th} March 1996 before proceeding to Perth Australia, Seychelles, Djibouti, Suez Canal and Malta before arriving in Portland, England on 3^{rd} April 1996, some 26 days later. Data was collected during the delivery voyage and during sea trials conducted out of Portland before the vessel went into service shortly after the 19^{th} April 1996. The last measurement of the vessel in service was taken on the 3^{rd} December 1996, some 228 days later.

The delivery voyage of the 86 metre vessel also started in Hobart Australia on 14^{th} December 1996 before proceeding to Sydney Australia, Perth Australia, Seychelles, Suez Canal and Malta before arriving in Portland, England on 15^{th} January 1997, some 32 days later. Data was collected during the delivery voyage prior to the vessel going into service about 1^{st} February 1997. The last measurement of the vessel in service was taken on the 7^{th} May 1998, some 460 days later.

Figure 2.1: 81 metre (Incat Hull 038) - first experimental measurements

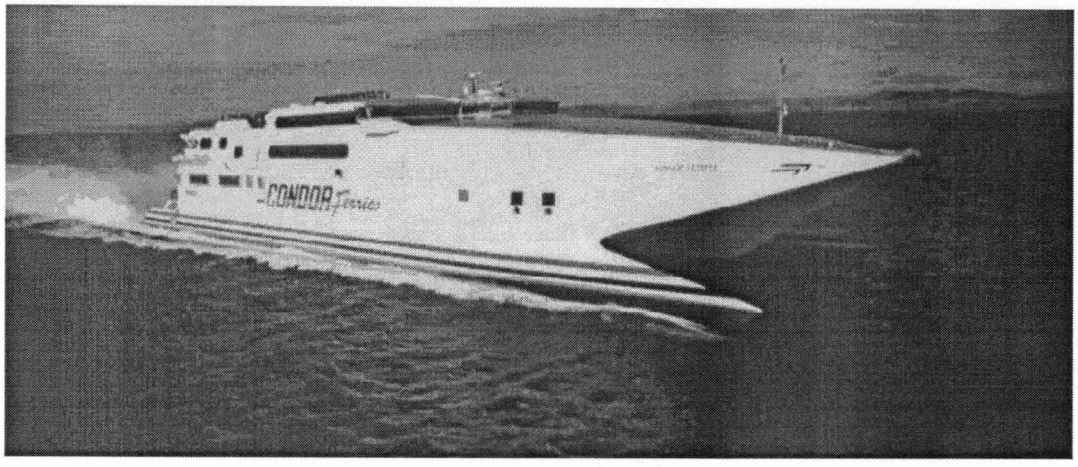

Figure 2.2: 86 metre (Incat Hull 042) - second experimental measurements

2.1.1 Hull Configuration

2.1.1.1 Hull Particulars

The hull displacement throughout the delivery could vary significantly because of the substantial fuel usage between fuel stops. For the 81 metre vessel, the fuel load was over 360 tonnes and over 380 tonnes for the 86 metre vessel, which represents approximately 30% of the total vessel displacement. Whilst it was not feasible to calculate the precise displacement of the vessel for each data record, the overall range of possible loading conditions was calculated. During the delivery voyage, the change in loaded displacement occurred due to fuel reduction, whilst during service operations, the variation in displacement was due to the daily variation in passenger and vehicle numbers combined with fuel usage.

Implicit in the calculation for the loading of the vessel was the corresponding range of radius of gyration in roll, pitch and yaw. These were estimated for each vessel at the departure and the 10% arrival[1] conditions for both the delivery voyage and service operating conditions. These estimations showed that there was only a small change

[1]10% arrival condition represents for a given loading departure condition the corresponding loading condition of the vessel toward the end of its journey where the fuel and other liquid expenditure or usage has diminished to the 10% capacity level. For some liquids this merely involves a transfer from one tank to another within the vessel but for items like fuel these weights are lost to the atmosphere after combustion in the engines.

in the roll gyration radius for both the delivery and service configurations whilst a larger variation occurred for the pitch and yaw gyration radii. This was not surprising with the fuel tanks concentrated near amidships and the loading areas extending well forward and aft. The range of loading conditions considered for each vessel are listed in Appendix A.

2.1.1.2 Motion Control Configuration

Throughout the period of data acquisition, each vessel was fitted with transom mounted trim tabs, which were an extension of the hull's underside shell plating. The tab was pivoted about a hinge line on the leading edge about one metre forward of the transom with a 2 metre chord and a 4 metre span located vertically above the hull baseline 1.4 and 1.296 metres for the 81 and the 86 metre vessel respectively. Up and down deflection of this surface by a hydraulic ram would increase or decrease the hydrodynamic lift force near the transom. After the delivery voyage to the United Kingdom and prior to operational service, both vessels were fitted with a horizontal foil on the forward keel of each demi-hull which was connected to the keel by a single vertical strut to form an inverted tee shape, a configuration commonly known as a T-foil. These were located 55.8 and 61.8 metres forward of the transom for the 81 and 86 metre vessels respectively and 0.2 metres above the hull baseline (or approximately 0.5 metres below the local keel). These T-foils could also create both upward and downward lift through two hydrodynamic processes. The first was by inducing an angle of attack through the vertical movement of the foil as the vessel heaved and pitched or by the controlled deflection of the trailing edge flap.

2.2 Measurement of Encountered Wave Surface

Measurement of the encountered wave surface profile used a bow mounted TSK type microwave radar wave meter. It measured the relative velocity of the free surface by timing the Doppler phase shift of the return signal relative to the output signal. The relative wave displacement was then be found by the integration of this signal with respect to time. The mounting of this device at the forward most bow position was suited to the twin-hull vessel where the target area on the water surface was well clear of any interference of the hull on the sea surface. In close proximity was an accelerometer suspended on a gimbal mechanism in a bath of viscous fluid. By twice integrating the accelerometer signal with respect to time, the relative displacement in time of the bow was calculated. Calculation of the wave profile under the microwave sensor subtracted the relative displacement between the water surface and the microwave sensor from the bow displacement (determined from the accelerometer). The position reference was determined through integration of each signal over a long-term average level.

The centre bow arrangement on both the 81 and 86 meter vessels provided a suitable mounting platform for the transducer providing a downward view of the water surface that was free from any obstruction by the hull. This unit proved to be more effective than ultrasonics transducers at the time as there was no manufacturer at the time that produced any units suitable for this type of measurement in both range and sampling frequency.

2.2.1 Wave Meter Sample Rate

It can be shown that for a given forward speed, the greatest wave encounter frequency ω_e will occur with the waves encountered directly on the bow. Predicted transfer functions

for these vessels in head, bow-quartering and beam seas show that a dimensionless encounter frequency (ω_e^*) of 8 (2.9 rad/s or 0.46 Hz, where assumed length is 76.412m) was sufficient to capture the diminishing upper frequencies tail of the heave and pitch transfer functions. To capture the high frequency wave energy of a 3 to 4 second average period wave spectrum with a vessel forward speed of 42.5 knots required a high frequency cut off of at least 15 rad/s (2.4 Hz). The established sampling frequency of 10 Hertz of the sea surface transducer was therefore greater than the required sample rate whilst also sufficient to prevent aliasing of the frequencies below the required 2.4 Hertz by remaining above the minimum sampling frequency of 4.8 Hertz. Similarly, the lowest frequency of vessel response can extend down to the DC level. The ability of the transducer to detect this will depend upon its signal to noise level. Ideally, the transducer should be able to detect frequencies down to 0.15 rad/s (0.024 Hz) to capture waves up to 20 second average period although there will be higher frequency components within this spectrum.

If the sampling frequency (f_s) is set at the Nyquist frequency of $2\omega_{e(\max)}$, it can be shown that the minimum measurable regular wave length ($\lambda_{\min}$) in deep water is given by

$$f_s = \frac{1}{\pi}\left[\sqrt{\frac{2\pi g}{\lambda_{\min}}} - \frac{2\pi}{\lambda_{\min}} U\cos\mu\right] \tag{2.1}$$

where U the forward speed (m/s) and μ is the wave heading. The sample frequency can be either positive where the hull encounters the waves on their front face or negative where the hull encounters the waves on their rear face. The solutions are shown in figure 2.3 with the minimum measurable wave length $\lambda_{\min}$ against $U\cos\mu$. For some values of $U\cos\mu$ there are two solutions of f_s, which are apparent in figure 2.3. This condition is similar to the relationship discussed by Lloyd (1989) between wave encounter, wavelength and the speed term $U\cos\mu$. It highlights the problem that waves detected and measured by a single point transducer encountered aft of the beam can introduce an ambiguity by the fact that there can be two possible solutions of wave length under certain conditions.

Both vessels were fitted with a TSK wave meter that sampled the relative sea surface distance at a frequency of 20 Hertz [2]. With the vessel top speed of approximately 42.5 knots, the minimum measurable wave length was less than 5 meters or 6.5% of the waterline length. This sample rate was higher than would normally be required for this type of experiment, but provides the opportunity for the sample rate of the raw data to be reduced through data decimation, which effectively reduced the sample frequency to 5 Hertz for spectral analysis.

In this analysis, a maximum encounter frequency in the transfer functions of say $\omega_e^* = 10$ corresponds to a deep water wave length of approximately 54.5 meters (71% of the hull waterline length) at a forward speed of 42.5 knots in head seas.

[2]Ideally the TSK unit should of had a low pass filter of 10 Hertz (or less) but it is unknown what type of filtering the TSK contained to prevent aliasing.

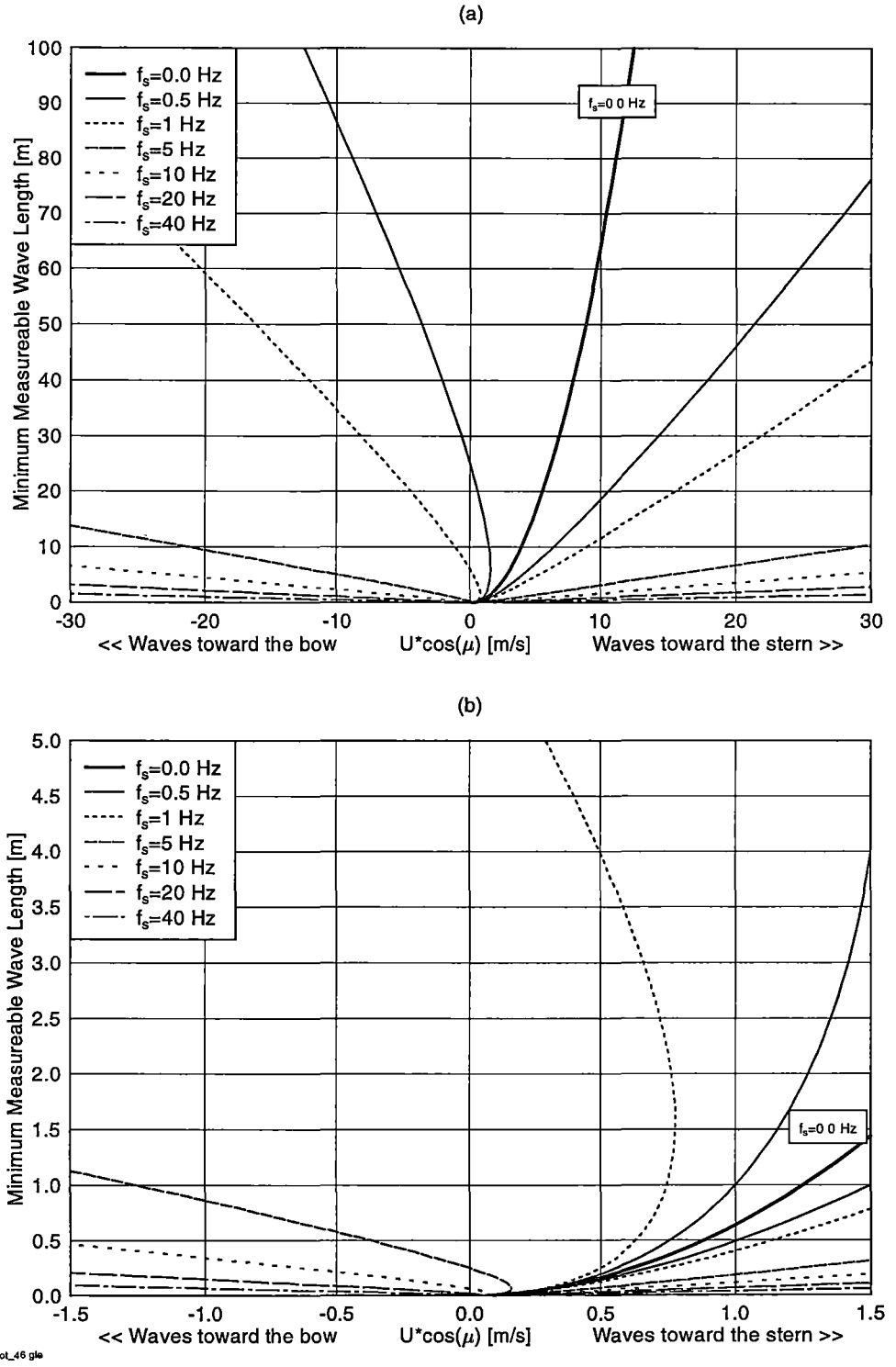

Figure 2.3: Minimum measurable wave length by a sea surface transducer given its sampling frequency, the vessel speed and the encountered wave direction for (a) long wave lengths and (b) short wave lengths.

2.3 Determination of Primary Wave Direction

A vessel instrumented with a sea surface sensing radar has the capacity to only measure the encountered wave surface profile in the vicinity underneath the bow where it was mounted. On a mono-hull vessel, this is difficult to achieve because of the wake disturbance near the bow created by the forward movement of the vessel. On a twin-hull vessel however, the sea surface beneath a bow-mounted sensor was generally free from the disturbing influence of the side hulls because of the spacing between them. The transducer only measures the distance between the sea surface and the sensor itself and when combined with a double integrated vertical acceleration measurement from the same location was able to produce a profile of the sea surface in time. This provides only an indication of the wave height with no indication of wave direction, surface orientation or wave celerity with respect to the direction of vessel forward speed. To acquire this information from the wave environment, a more complex wave-sensing device was required. Such devices based on radar sensing are in use on some ferries and may in the future become part of a compulsory ship monitoring system. Where the wave sensing device has limited capacity to gather sufficient information for the production of motion response spectra, the only practical approach was to use the hull motions as the means to determine wave direction. For a vessel in commercial service, this removes the reliance on crew to obtain visual wave data, which can be unreliable, particularly at night when there may be poor visibility. Visual wave data can however be useful to provide confirmation for the recorded or computed wave data.

Whilst twin-hull vessels have heave, roll and pitch motions that are prone to excitation at relatively short wave encounter periods, the heave transfer functions with respect to wave height or wave slope which are close to unity in longer wave encounter periods. On this basis, it was reasonable to assume that the wave direction could be determined through full-scale measurements of roll and pitch displacement magnitudes combined with the heave velocity at the vessel's centre of gravity.

The solution was implemented assuming small angle rotations with a right handed coordinate system with its origin located at the hull centre of gravity (CG) with x forward, y to port and z upwards such that the notation η_4 is for roll positive starboard side down, η_5 for pitch positive bow down and η_3 for heave positive up. A unit vector was constructed at the CG (see figure 2.4) and fixed in the z-direction of the hull body coordinates such that as the hull rolls (η_4) and pitches (η_5) the unit vector remains perpendicular to the deck on the z_B-axis. In the presence of waves as the hull rolls and pitches, components of this unit vector can be projected onto the non rotating x, y and z trihedron, which moves forward with the vessel thus creating components a, b, c and m giving an instantaneous direction of deck slope (denoted x_{6w}).

From this notation the following relationships are created

$$\tan^2(x_s) = \frac{m^2}{b^2} \tag{2.2}$$

$$m^2 = c^2 + a^2 \tag{2.3}$$

$$\tan(\eta_4) = \frac{c}{b} \tag{2.4}$$

$$\tan(\eta_5) = \frac{a}{b} \tag{2.5}$$

$$\tan(x_{6w}) = \frac{c}{a} \tag{2.6}$$

Substituting equation 2.4 and 2.5 into 2.3 for c and a, then substituting equation

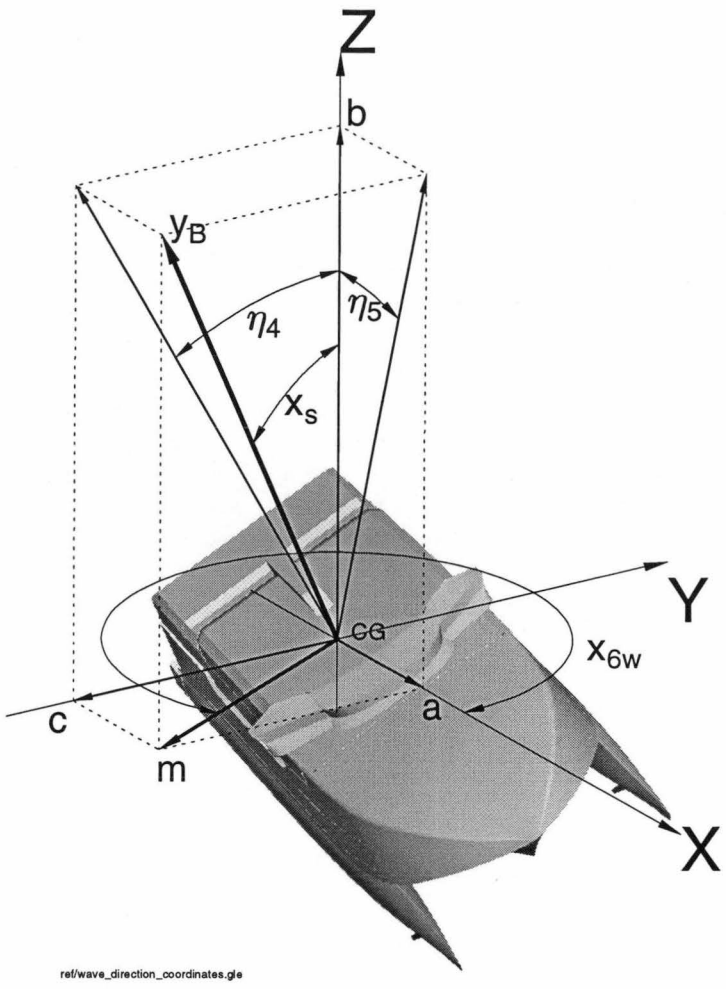

Figure 2.4: Nomenclature and geometry used for the determination of the primary wave dirction (μ) . z_B is perpendicular to the deck. Roll (η_4) and pitch (η_5) angles are exagurated for clarity.

2.3 into 2.2, it can be shown from equation 2.2 that the magnitude of the deck slope x_s at any instant in time can be determined with

$$\tan^2(x_s) = \tan^2(\eta_4) + \tan^2(\eta_5) \tag{2.7}$$

where x_s will always be positive. In addition, by substituting equations 2.4 and 2.5 into equation 2.6 for c and a the direction of the deck slope x_{6w} at an instant in time can be determined by

$$\tan(x_{6w}) = \frac{\tan(\eta_4)}{\tan(\eta_5)} : \eta_4, \eta_5 \neq \pm\frac{\pi}{2} \tag{2.8}$$

where x_{6w} will always be in the direction of downward deck slope. To ensure the correct orientation of x_{6w} from equation 2.8 within the 0° to 360° range rather than a ±90° range, table 2.1 shows the required corrections based on figure 2.5. A corrected x_{6w}

indicates a downward deck slope magnitude that has a direction in degrees to port from the bow such that a deck with a roll angle to port and a bow down pitch angle of equal magnitude would give $x_{6w} = 45°$.

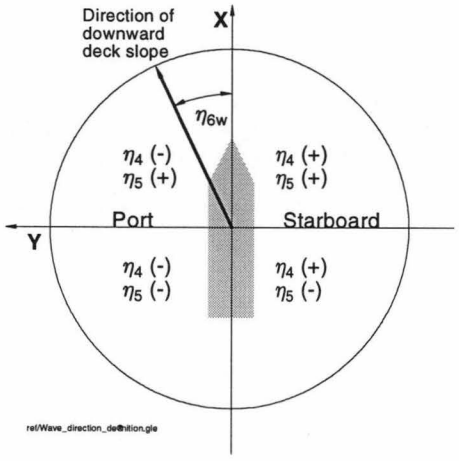

Figure 2.5: Sign of roll (η_4) and pitch (η_5) angles for various angles of downward deck slope (η_{6w}).

x_{6w} quadrant	Pitch sign	Roll sign	Correction to x_{6w} result
1	$\eta_5\,(+)$	$\eta_4\,(-)$	$x_{6w} + \frac{\pi}{2}$
2	$\eta_5\,(-)$	$\eta_4\,(-)$	$x_{6w} + \frac{\pi}{2}$
3	$\eta_5\,(-)$	$\eta_4\,(+)$	$x_{6w} - \frac{\pi}{2}$
4	$\eta_5\,(+)$	$\eta_4\,(+)$	$x_{6w} - \frac{\pi}{2}$

Table 2.1: Correction to the downward deck slope result of equation 2.8

From the relationships of 2.7 and 2.8 it was possible to determine both the magnitude (x_s) and direction (x_{6w}) of the instantaneous deck slope from both the roll displacement (η_4) and pitch displacement (η_5). Under the assumption the vessel was operating in the presence of a significant wave environment, two maximum values of deck slope (x_s) emerge that correspond with two values of deck slope direction (x_{6w}) that differ by approximately 180° (see plot (2a) in figures 2.6 to 2.8). One of these maximum values will correspond with the primary wave direction (denoted $x_{x_s(+)}$) and the other will correspond with the wave encounter direction relative to the vessel (denoted $x_{x_s(-)}$). However, it was not clear which of the two represents the primary wave direction and which the wave encounter direction. The distribution of deck slope magnitude (x_s) as a function of deck slope direction (x_{6w}) can be improved by a summation of all the instantaneously measured data within each increment of deck slope direction (x_{6w}) of say 5° (see plot (2b) in figures 2.6 to 2.8). This reduces the data whilst emphasising the directions of deck slope that contain a higher number of data points.

With a similar approach to that described for the deck slope (x_s), the instantaneous heave velocity ($\dot{\eta}_3$) as a function of deck slope direction (x_{6w}) can be determined. This yields two maximum values of heave velocity ($\dot{\eta}_3$) that will differ by approximately 180°, but in this case, one will be positive and the other negative. A positive maximum value indicates the vessel was on the front face of a wave heaving upwards and a negative maximum indicates the vessel was on the back face of a wave heaving downwards (see plot (1a) in figures 2.6 to 2.8). It was of course obvious that the deck slope

direction (x_{6w}) that corresponds with the former will correspond with the primary wave direction (denoted by $x_{\dot{\eta}_3(+)}$) and the later will correspond with the direction of wave encounter (denoted by $x_{\dot{\eta}_3(-)}$). As with the case of deck slope, the distribution of heave velocity ($\dot{\eta}_3$) as a function of deck slope direction (x_{6w}) can be improved through similar reasoning by a summation of all the instantaneously measured data within each increment of deck slope direction (x_{6w}) of say 5° (see plot (1b) in figures 2.6 to 2.8). It was clear however, that the sign convention of the heave velocity will in this case remove the ambiguity present when considering only the deck slope (x_s) as a function of deck slope direction (x_{6w}) by yielding the primary wave direction ($x_{\dot{\eta}_3(+)}$) and the wave encounter direction ($x_{\dot{\eta}_3(-)}$).

The two elements of instantaneous heave velocity ($\dot{\eta}_3$) and instantaneous deck slope (x_s) can be multiplied such that the product $x_s\dot{\eta}_3$ is made a function of the deck slope direction (x_{6w}). This yielded two maximum values that differed by approximately 180° (see plot (3) in figures 2.6 to 2.8). Firstly, a positive maximum occurred that is coincident with a value of deck slope direction (x_{6w}), which indicated the primary wave direction (denoted μ) such that a positive maximum of 180° indicates the waves are encountered on the bow of the vessel . Secondly, a negative maximum occurred that is coincident with a value of deck slope direction (x_{6w}), which indicated the wave encounter direction (μ_e).

In an irregular short crested wave environment, there is a degree of wave spreading, which implies that not all waves are travelling precisely in the same direction as the primary wave direction. This phenomenon combined with the possibility that the roll or pitch transfer function may independently vary to some extent from unity (although this is assumed to be small) for a given wave encounter frequency, means that there will be varying magnitudes in the product $x_s\dot{\eta}_3$. The distribution of the product $x_s\dot{\eta}_3$ as a function of deck slope direction (x_{6w}) will vary between the positive maximum corresponding to the primary wave direction (μ) and a negative maximum corresponding to the direction of wave encounter (μ_e), a difference of approximately 180°. It is clear that it would be convenient for the primary wave direction to be defined at exactly one direction for the duration of a data sampling period, so that the positive and negative maximums of $x_s\dot{\eta}_3$ should in theory be exactly 180° apart. Therefore, by taking the mean of these two values (μ and μ_e) which are already approximately in opposite directions and adding $\pm 90°$ as appropriate, both values will contribute to determining the most probable primary wave direction relative to the vessel. Based on this approach, it can be shown that the mean primary wave direction $\bar{\mu}$ can be determined by

$$\bar{\mu} = \frac{(\mu + \mu_e)}{2} + 90\frac{(\mu - \mu_e)}{|\mu - \mu_e|} \tag{2.9}$$

It is implied by the assumptions that in the presence of a significant wave environment the vessel must undergo roll, pitch and heave motions of sufficient magnitudes to use the hull as a directional wave buoy for estimating the primary wave direction ($\bar{\mu}$) from equation 2.9. To ensure a data set contains the characteristics that makes it suitable for determining the primary wave direction, some experience with the data set showed the following. Firstly, the absolute heave acceleration should be of sufficient magnitude. Second and thirdly, the deck slope directions of $x_{\dot{\eta}_3(+)}$ and $x_{\dot{\eta}_3(-)}$ should correspond closely with the wave direction (μ) and the wave encounter direction (μ_e) respectively. Fourthly, the wave direction (μ) and the wave encounter direction (μ_e)

should be approximately 180° apart. These four criteria are summarized as,

$$|\ddot{\eta}_3|_{\max} > 0.07g \quad (2.10)$$

$$|x_{\dot{\eta}_3(+)} - \mu| < 45° \quad (2.11)$$

$$|x_{\dot{\eta}_3(-)} - \mu_e| < 45° \quad (2.12)$$

$$|180 - |\mu - \mu_e|| < 45° \quad (2.13)$$

The important aspect of the selected bow acceleration criterion level was that the other lower criteria could have been satisfied whilst the vessel was under the influence of very small motions, causing it to roll and pitch only a modest amount. For the vessel to show vertical accelerations greater than the underlying noise level that might be recorded in nominally calm water, there was thus reasonable certainty that the vessel was at sea and responding to significant waves. The data recorded was thus not obtained in low wave heights or even in calm conditions. However, the acceleration level for data collection may well have been lower or higher than 0.07g at the vessel's centre of gravity. It can be seen that 0.07g measured at the vessel's centre of gravity is about four times smaller than the trigger level set for general data acquisition from the bow accelerometer. In some typical cases this was the approximate difference in acceleration levels between the bow and centre of gravity positions. Had the general trigger level of the bow accelerometer that initiated the data acquisition sequence been lower, then the criterion level of 0.07g at the vessel's centre of gravity would also have been effectively lower. The acceleration value therefore was not particularly critical provided it served its purpose of removing data records of low motion levels and therefore not of interest in the analysis.

Figures 2.6, 2.7 and 2.8 present three sets of sample results for head, bow quartering and beam sea primary wave directions respectively. The figures represent the derivation of $x_s\dot{\eta}_3$ as a function of deck slope direction (x_{6w}) from the raw data of deck slope and heave velocity. Each value in plots (1b), (2b) and (3) represents the summation of all values that lay within a narrow band, which in this case was a 5° increment. The raw data displayed in each of the figures represent a time record of 4096 samples taken at the sampling rate of 20 Hertz. For the case where a head sea was predicted (see plot (3) of figure 2.6) a distinct positive maximum peak value (μ) can be identified near the deck slope direction (x_{6w}) of 180°. In the case where a bow quartering sea was predicted (see plot (3) of figure 2.7) a distinct positive maximum peak value (μ) can be identified near the deck slope direction (x_{6w}) of 225°. In the case where a port beam sea was predicted (see plot (3) of figure 2.8) a distinct positive maximum peak value (μ) can be identified near the deck slope direction (x_{6w}) of 90°. In each instance there is a corresponding negative maximum approximately 180° out of phase confirming the wave encounter direction (μ_e) such that between the two, the mean primary wave direction ($\bar{\mu}$) can be determined according to equation 2.9. The peak of each of these examples can vary in sharpness depending on how well the primary wave direction has been distinguished from less pronounced waves from surrounding directions, or how long or short crested the sea surface is. A sharp peak would tend to define a well defined wave direction whilst a less defined peak produces only a moderately defined wave direction. Typically, the magnitude of the product $x_s\dot{\eta}_3$ is reduced to half its peak level within a directional bandwidth of ±45° and in the circumstance of a well defined outcome this directional bandwidth is reduced to less than ±10°.

An issue with this method is firstly, the possibility that the vessel's course will occasionally change because of operational requirements or because of inadequate directional stability and course tracking control, which can also have the secondary effect

of course correction through an automatic or manually operated helm. Other distinguishing nonlinear events were also noted in the following sea wave directions where the ship course could vary by up to 20° because of phase lags in the autopilot of the ship steering system. As the sea overtakes the vessel, the steering mechanisms attempt to correct the induced yawing moment but the over correction results in the vessel following a zigzag course, which is evident in the wake of the vessel. Under these circumstances, the pitch angles and velocities or accelerations are of similar magnitude to the roll induced motions as the vessel undergoes yaw oscillations across the wave front. Because of this phenomenon, this method of determining the wave direction can become unreliable in seas between the beam and following directions. However, the low level of accelerations in such seas resulted in inadequate data being collected for the purpose of transfer function and sea direction analysis. Secondly, the likelihood that the speed can fluctuate with a data record or across a data group means that the selection of suitable data records where these variations were maintained below an acceptable threshold is important. These variations are inevitable, so the data collected that is related to the sea state in some form will not remain constant as would be the case in ideal conditions. Finding and being exposed to conditions of sufficient duration so as to collect enough data for this type of analysis and spectral derivation is a real issue that to some extent was inadequately achieved during the time frame of this work. With this proposition much of the data records had to branded with the assumption of linearity, particularly with regard to wave amplitude, the sector size of wave directions so that wave spectra, ship response and finally the derived transfer functions could be created.

These results present a clear case that the primary wave direction in certain circumstances may be determined where the broad criterion of 2.10 to 2.13 are at least satisfied. However, without further confirmation from additional independent inputs that can provide wave direction in a fixed reference frame such as wind speed and direction transducers, three-dimensional wave sensing radar or simultaneous metrological data this method can in no wise guarantee that a sufficient description of the wave conditions has been achieved. This approach is presented as the means by which the primary wave direction was predicted for each sampled data set wherein each data set was assigned to the nearest $45° \pm 22.5°$ centre banded increment from 0° to 360°. However, only the primary wave directions coinciding with the centre bands of 90°, 135°, 180°, 225° and 270° were further developed to produce the motion responses and transfer functions in this work. In particular, these specific wave directions represent the wave encounter directions of head, bow-quartering and beam seas. Data obtained in aft-quartering to following sea wave directions, although present, did not emerge through this process, as these conditions created ambiguous results that were typified by low accelerations and less pronounce motions that made them difficult to determine with any certainty their primary wave direction. Removal of this data occurred after applying the criteria of 2.10 to 2.13. Further, the data collected was triggered by a signal based on the bow accelerations, which was greatest in bow to beam sea wave directions and of much less significance in the beam to following sea wave encounter directions for which very little data was collected. Other wave directions sampled and grouped outside of the specific wave directions of head (180°), bow-quartering (135° or 225°) and beam (90° or 270°) seas (see table 4.1 for the 81 metre and table 4.2 for the 86 metre vessels) were excluded from further analysis as presenting this data would not add meaningfully to the discussions raised in this analysis.

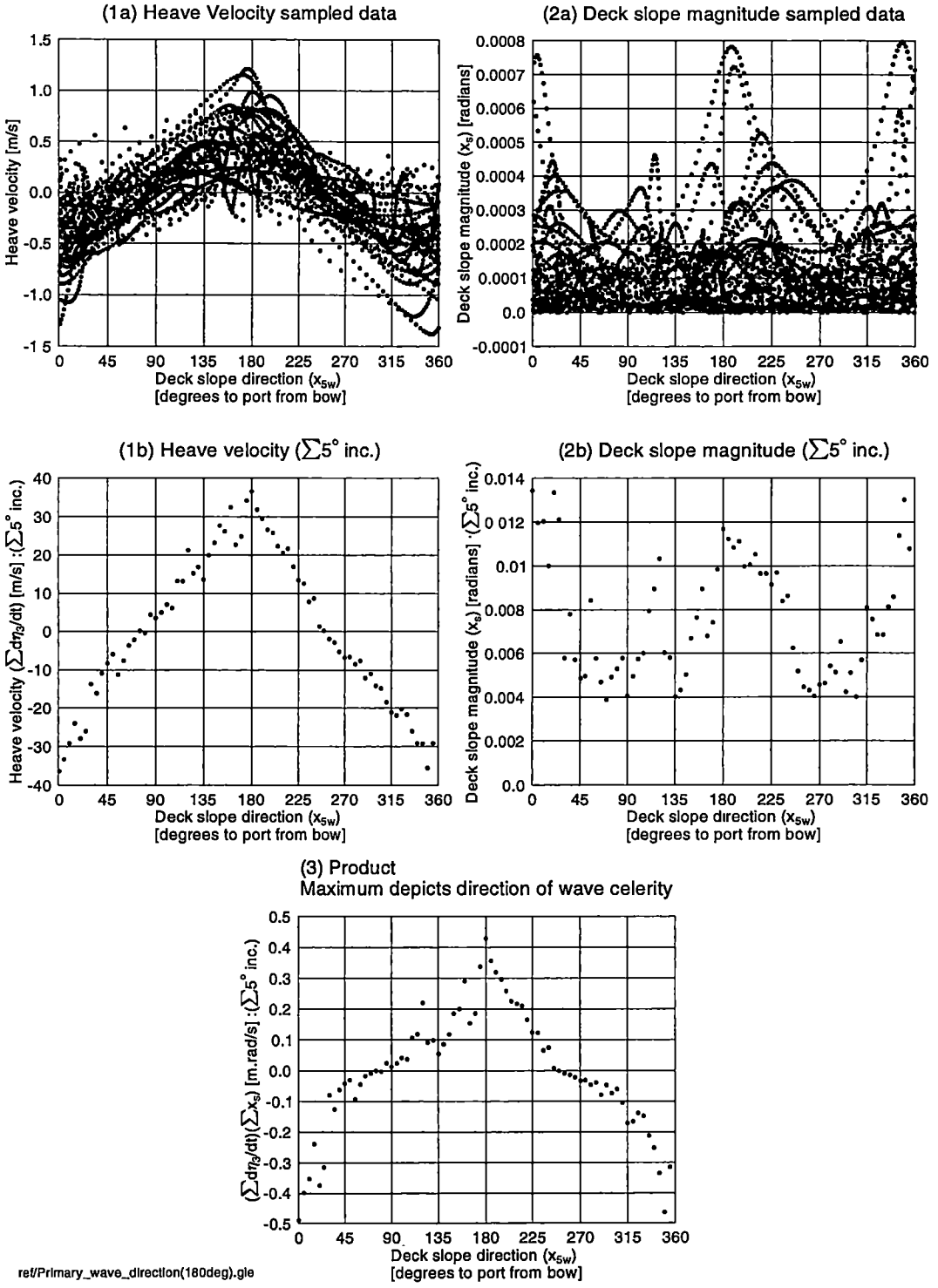

Figure 2.6: Primary wave direction predicted at 180° (Head sea wave direction). (Moderately well defined wave direction)

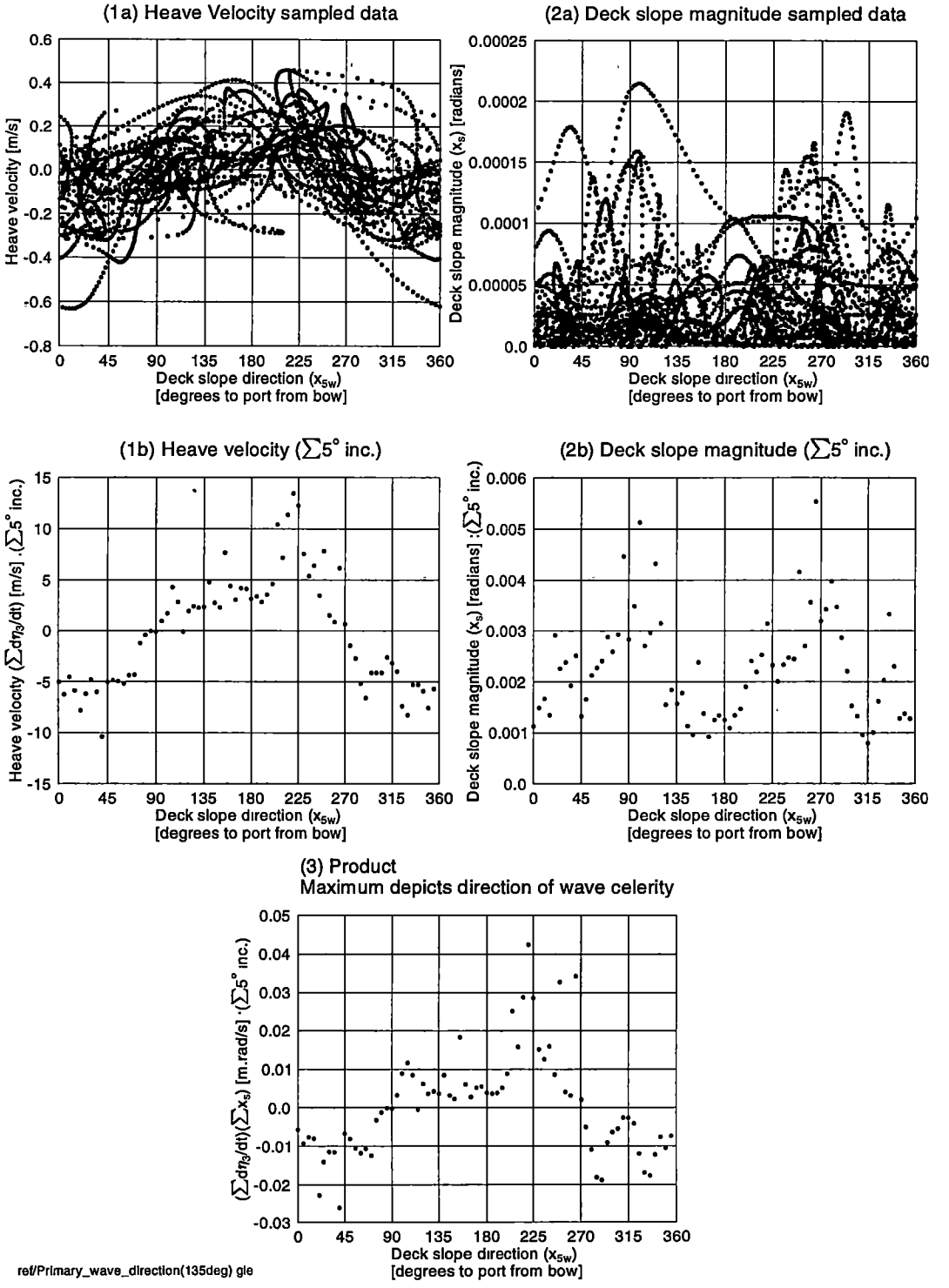

Figure 2.7: Primary wave direction predicted at 225° (Port bow-quartering wave direction) (Moderately well defined wave direction)

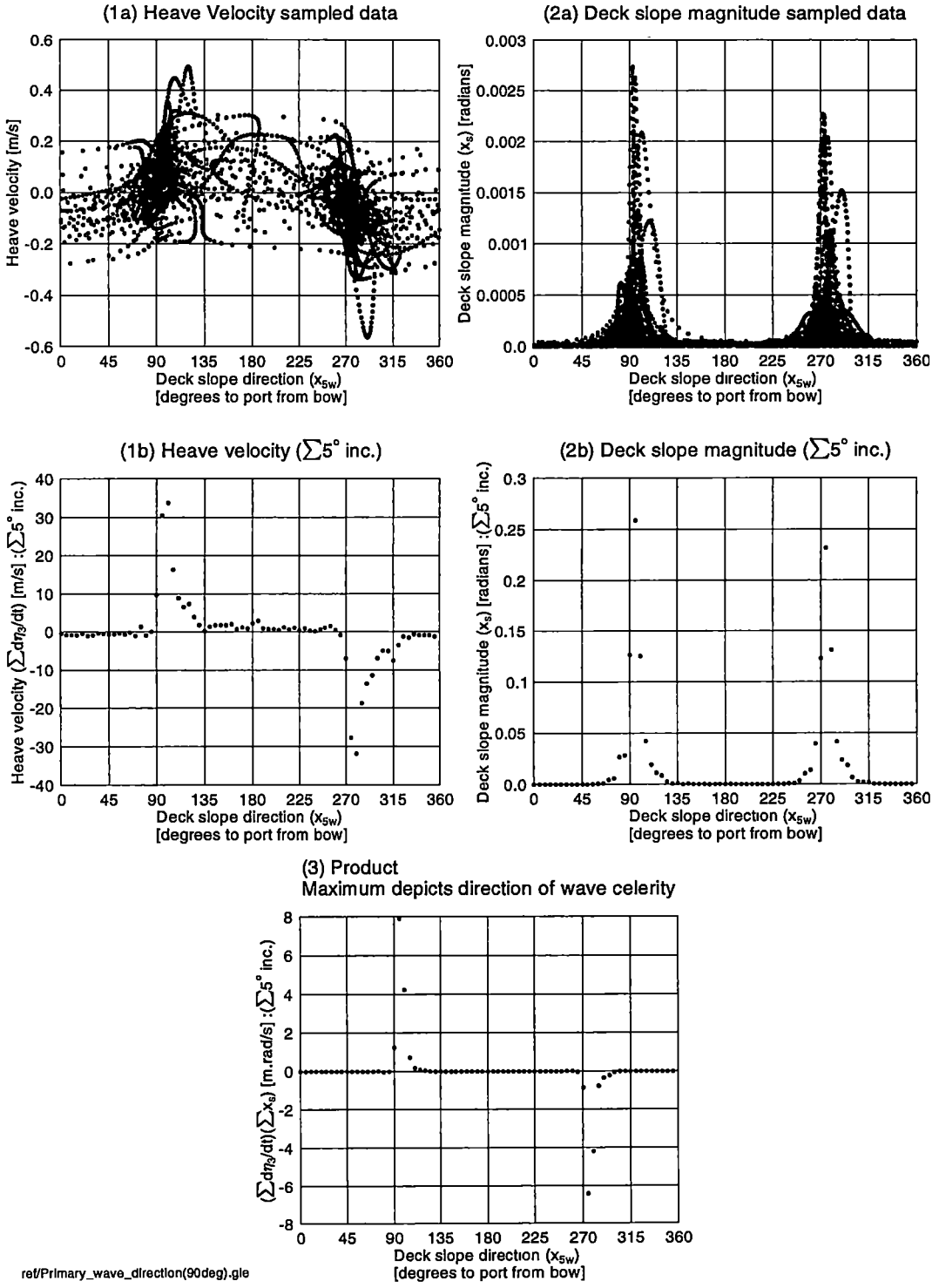

Figure 2.8: Primary wave direction predicted at 90° (Starboard beam wave direction) (Well defined wave direction)

2.4 Measurement of Vessel Motions

Experimental motion measurements on the 81 metre vessel proceeded with a vertical accelerometer and gyroscopic angular rate sensors located near the vessel's centre of gravity (CG). The angular rate was converted to a signal that was proportional to the roll and pitch motions prior to reaching the acquisition system, which were recorded with the data. A vertical accelerometer was also placed at the CG and at the bow.

The 86 metre vessel only used vertical accelerometers placed at the CG, bow, stern and port side adjacent to the CG. The roll and pitch angles were calculated by combining the signals of two or more vertical accelerometers with a known separation distance in the transverse and the longitudinal planes respectively. Calculation of hull motions or displacements in time was conducted through double integration of the vertical and the rotational acceleration signals.

2.5 Data Acquisition

The platform for shipboard data acquisition consisted of a portable notebook computer installed with instrumentation software and a hard disk drive for data storage. Connected through the computer's parallel port was an analogue to digital (A/D) card module which provided an interface between the computer and the motion transducers consisting of vertical accelerometers and/or electronic rate gyroscopes. Also connected, was a Global Positioning System (GPS) and bow mounted microwave radar from Tsurumi Seiki Co. Ltd. (TSK) (see TSK (2003)) for relative water surface distance measurement that operated in a similar fashion to the unit described by Yasuda et al. (1985).

The computer was a portable Toshiba T2130CS DX486 75MHz notebook (PC) that contained 8 MB of random access memory (RAM) and 350 MB of available hard disk storage space (500 MB total) running on a Microsoft Windows version 3.11 operating system. There was sufficient data storage with this arrangement for approximately six months of data before downloading of the hard disk was required. The analog to digital (A/D) conversion system was a 16 channel IOtech DBK112B daqbook device connected to the PC through the parallel port and contained a screw terminal card as an interface with the ship wiring connections.

Power interruptions would frequently occur as power was switched from ship to shore based supply. In the event of a power failure or interruption from the ship's 240-volt supply, the PC battery would keep the system going for a short period whilst also providing some protection from power surges. Should the PC shut down completely, a manual reboot was required to restore the power, after which the instrument-based software would automatically initialize itself. For the remaining equipment and transducers, no independent power backup was available, but these were generally able to function without supervision.

Data was sampled from the Global Positioning System (GPS) at less than 0.1 Hertz through a serial connection. The data consisted of the ship speed, global position coordinates, heading relative to north and universal mean time (UMT).

The smaller 81 metre vessel was fitted with an electronic rate gyroscope located in close proximity to the vessel's centre of gravity and a vertical accelerometer at the bow. The 86 metre vessel had only vertical accelerometers located on the port beam, the hull centreline near the vessel's centre of gravity, and at the bow and stern.

An electrical ground loop detected on the 81 meter vessel between the computer and the motion control system caused interference with other systems such as the

transom flaps. The only solution available was a temporary disconnection of the system during manoeuvring. This issue was solved on the subsequent 86 meter vessel by the installation of an optical-isolator between the ship motion control system and the data acquisition system, which prevented the reference voltages of the analogue to digital (A/D) card from interfering with the reference voltages of the ship motion control system.

The retention of raw data also provided the flexibility to analyse and interrogate data in various ways after completion of the measurements. Acquisition of data on the 81 and 86 metre vessels, was accomplished with the portable PC programmed with the National Instruments software product Labview, version 3.1, to acquire data automatically by continuously monitoring the acceleration of the bow due to the wave induced motions. Provided a recording sequence was not currently underway, and the bow accelerations exceeded a predefined threshold, a new recording sequence was initiated where data was held in memory from the motion sensing transducers, bow mounted wave measurement transducer and the Global Positioning System (GPS) before being stored to the hard disk drive. This was clearly a demanding task for the computer hardware system to perform efficiently and would often result in modest delays while the system wrote data to disk before a new acquisition sequence could commence.

2.5.1 Data Initialisation Trigger Level

The initialisation of a data recording sequence commenced when the constantly monitored signal of the bow accelerometer exceeded a predefined threshold. The bow accelerometer was chosen because its location generally had the largest motion levels in most wave conditions and so provided a greater range over which to select a suitable trigger level. The trigger level on the 81 metre vessel was set to an acceleration level of between 0.05g and 0.5g. Similarly, the trigger level on the 86 metre vessel was set to an acceleration level of between 0.05g and 0.5g where the acceleration level was defined over and above the acceleration due to gravity and typically ended up at least about 0.3g for many of the data records. In retrospect it may have been better to maintain a low level and thus acquired a greater amount of data for motion analysis. However, data storage was relatively expensive at the time of the measurements and it was not known how much potential there was to acquire data of sufficient quality. Taking a conservative approach it was decided to limit the data records to those that contained reasonable levels of motion. This ensured the data storage would not run out of space before a data download could be achieved and that significant measurement opportunities were not missed.

The trigger level was based on machine units that could be converted to acceleration provided the transducer calibration was known together with the voltage range. The bow accelerometer had a range of $\pm 2g$ about its mean level of 1g and the 12 bit data acquisition board had the voltage range of ± 5V (see appendix B). This gave a machine unit trigger level (TL) setting of $TL = \frac{4095}{5}V = \frac{4095}{2}g$, where V is the equivalent voltage level and g is the equivalent non-dimensional acceleration. By example, a trigger level of 0.05g or 0.3g over the acceleration due to gravity required a setting of 2150 and 2662 respectively.

2.5.2 81 metre Vessel Data Records

Data records of the 81 metre vessel were sampled at 10 Hertz over a 102.4 or 204.8 second period. This data was stored in compact uncalibrated binary format on the data acquisition computer. After retrieval of this data from the ship, it was calibrated

and converted to ASCII text format ready for analysis. To maintain an ordered file sequence, each raw data file was designated by the month in which it was sampled followed by a monthly sequence number. For example, the 87^{th} file recorded in April was named 'apr_87.bin'. The raw data acquired from the transducers included

1. bow vertical accelerometer;
2. vertical accelerometer at the hull centre of gravity;
3. roll displacement derived from the rate gyroscope;
4. pitch displacement derived from the angular rate gyroscope;
5. port tab hydraulic ram;
6. starboard tab hydraulic ram;
7. vertical displacement of the bow measured by the accelerometer associated with the microwave wave radar;
8. sea surface relative distance measured by the microwave wave radar;
9. significant wave height as calculated by the microwave wave radar processor, and
10. average wave period as calculated by the microwave wave radar processor.

Measurements of the port and starboard transom tabs in items 5 and 6 above, used a linear transducer made from a resistance multi-turn potentiometer mounted on the hydraulic ram of each transom tab. Calibrated resistance potentiometers provided a voltage of the ram displacement in time that could be logged by the data acquisition system. After a short period into the delivery voyage, these measurements ceased when the equipment broke beyond repair.

The statistical information associated with each data file was simultaneously stored by creating a single line entry into a statistical summary file. This information describing the circumstances in which the file was created was considered just as important as the measured data itself. Therefore, each file had a name that matched the month in which it was first created, followed by a sequence number for the given month and the year in which it was created. For the example previously used, the statistical information would be stored in a file called "apr1_96.sum", where this file was the first statistical summary file created in April of 1996. These files were limited to a nominal figure of 250 entries before creating a new file, so it was possible to have more than one statistical summary file in a month. The summary file for each analogue input channel consisted of the

1. minimum value;
2. maximum value;
3. RMS value;
4. standard deviation, and
5. average value.

A general header was also included containing a list of the channel numbers, the channel gains, the trigger source, the trigger level, the number of scans per data file, the sample rate and the polarity of each channel.

Data received from the GPS serial string was summarized at the end of each acquisition and saved to file after which the original data was discarded. This summary file consisted of

1. final GPS time stamp;
2. GPS average speed for the duration of the data record;
3. PC's last time stamp;
4. PC's last date stamp, and
5. raw data file's monthly incremental run number.

2.5.3 86 metre Vessel Data Records

The configuration of the data acquisition on the 86 metre vessel recorded eight consecutive data files after the initiation of an acquisition sequence through the automatic trigger. Each of these eight data files contained four sets of 1024 samples taken at 20 Hertz, thus giving 4096 samples per file. This configuration complied with limitations in the IOtech daqbook drivers supplied with the A/D module for the Labview acquisition software where after each 1024 data samples the software had to be reset before sampling could continue. The separation time created by the reset was system dependant so could not be guaranteed to be consistent with the general timing of the sample intervals.

Data received from the GPS serial string was stored separately for future retrieval and a summary of the GPS data acquired with each 4096 sample file was also recorded at the end of each acquisition. The summary file consisted of

1. data binary file name;
2. GPS data file name;
3. computer day and date;
4. computer time;
5. GPS local time;
6. GPS Universal Mean Time;
7. average GPS speed over ground for the period of the data file recording;
8. minimum GPS speed over ground for the period of the data file recording;
9. maximum GPS speed over ground for the period of the data file recording;
10. variation in GPS speed over ground for the period of the data file recording;
11. average true north heading for the period of the data file recording;
12. variation in true north heading for the period of the data file recording;
13. average magnetic north heading for the period of the data file recording;

14. variation in magnetic north heading for the period of the data file recording;
15. latitude and longitude position, and
16. number of samples acquired by the raw data file.

This information was stored in ASCII text format because of its relatively small storage requirement and included a file header containing the channel numbers used, the gains for each channel, the trigger source, the trigger level, the number of scans per data file, the sample rate, and polarity of each channel. Data acquired from transducers included

1. bow vertical accelerometer;
2. vertical accelerometer near the hull centre of gravity;
3. aft vertical accelerometer;
4. port side vertical accelerometer;
5. vertical displacement of the bow as measured by the accelerometer associated with the microwave wave radar;
6. relative distance from the microwave wave radar to the sea surface;
7. sea surface profile as calculated by the microwave wave radar processor, and
8. significant wave height as calculated by the microwave wave radar processor.

In a similar approach to that used for the 81 metre vessel, the recorded data was stored in uncalibrated binary format. During post analysis the data was calibrated and converted to ASCII text format for further analysis. Each data file was named according to the month in which it was sampled, followed by a sequenced sample number within a group of 8 consecutively sampled data files. For example, the 5^{th} data file recorded in the 17^{th} group in December was named "Dec175.bin". Likewise, the corresponding GPS serial data was named "Dec175.gps".

2.6 Data Analysis Methods

2.6.1 Data Manipulation

When full-scale measurements are conducted at sea under a variety of operating conditions and wave climates, the measurements will include any number of conceivable wave heights, directions and periods within the sampled data records. They will also include variations of hull motion control configuration, loading condition and operational speed. Full-scale measurements therefore do not have the freedom to isolate and manipulate the measured variables to the extent available with model tests conducted in a controlled environment. The variation within and across the data records of these experiments were therefore managed collectively by grouping the data into categories where multiple records within each category were averaged together. Variation of record wave heights, wave periods or vessel loading conditions were not considered and a range of these variables were therefore included in each group of data. Vessel speeds were divided into 5 knot increments from 2.5 to 42.5 knots ($\pm$2.5 knots), although only speeds from 12.5 knots were analysed as data below this speed generally represented

data recorded manually in sheltered calm water near the vessel's port facilities. By assuming that the vessel response to waves was symmetrical about the hull longitudinal centre-line, the wave directions recorded from 0° to 360° were grouped in sectors from 0° to 180° in 45° increments. With the limitation that only waves forward of the beam could be more effectively resolved in the wave measurements, only results for bow ($180° \pm 22.5°$), bow quartering ($135° \pm 22.5°$) and beam ($90° \pm 22.5°$) seas were considered in the spectral analysis. The sector angles were kept at 45° to encompass most of the limited quantities of data available whilst also acknowledging the difficulty of showing that the method of determining the wave direction could be resolved with sufficient accuracy to sector sizes less than 45°.

Each vessel had two distinct hull configurations of motion control equipment on each demi-hull consisting of only a transom tab for the delivery voyage and then a transom tab and forward mounted T-foil during subsequent operational service. Whilst no distinction was made in the analysis between the control surfaces being in active or fixed mode, the vast majority of measurements were conducted with the controls in active mode, and inactive controls were selected only on very rare occasions. Therefore, grouping the results created 144 possible record groups of 9 speeds (2.5 to 42.5kn), 8 wave directions (0° to 360° in 45° increments) and 2 hull configurations (trim tabs only or trim tabs and T-foils). However, not every record group contained usable data such as the two lowest speeds and following sea wave directions for reasons explained. Thus truncating the speeds and selecting the bow, bow quartering and beam wave directions left 42 record groups of 7 speeds (12.5 to 42.5kn), 3 wave directions (180°, 135° and 90°) and 2 hull configurations (trim tabs only or trim tabs and T-foils) that could be used for spectral analysis and presentation. A summary of the data within each record group is discussed later in more detail and shown in table 4.1 for the 81 metre vessel and table 4.2 for the 86 metre vessel.

2.6.2 Data Analysis

Post analysis of the data proceeded with the use the National Instruments software package Labview that contained modules suitable for digital signal processing with regard to filtering, integration and spectral analysis. It was apparent from the outset that with the large quantity of data, a certain amount of automation had to be built into the analysis, firstly to determine into which data group (see preceding section 2.6.1 for a description of the basis for these groups) each individual data record should be placed and finally to perform spectral analysis on the data within each group.

2.6.2.1 Integration and Filtering

Of the issues involved with spectral analysis of full-scale measurement data, the conversion of time wise vertical acceleration data acquired from accelerometers to displacement in time through integration is of particular interest. Over the time frame of any particular data record, the average mean position in heave, pitch or roll will be constantly changing due to non-linear variables such as vessel speed, wind forces on the hull, wave encounter direction, statistical variations in the wave profile, drift in the electronic transducers and changes in the hull displacement. Unless an accurate average of the time-wise signal is known prior to integration, the integrated signal will contain an element of drift that must be removed through high pass filtering at each stage of the integration process. In many applications where a time varying shift in the average condition does not occur, drift in the integrated signal is greatly reduced, making integration of long record durations possible, with less high pass filtering. In the

present investigation, the data records were sectioned over relatively short durations, then integrated and averaged together over all the records contained within each data group.

When acceleration data was digitally converted during the analysis, a 0.16 Hertz high pass filter was applied at each stage of the integration to remove the low frequency drift associated with the integration of time records whilst a 0.6 Hertz low pass filter was applied to remove high frequency noise. The filter applied was a linear-phase finite impulse response (FIR) filter with equiripple characteristics using a Parks-McClellan algorithm. When measured wave data was employed in the spectral analysis no digital filtering was imposed on the data records obtained from the TSK wave meter.

The effect of the low and high pass filtering on the energy represented by the measured acceleration response spectra was small (see section 4.4). This is because the filter was only applied during the integration process as the measured acceleration data was converted to velocity and displacement to create the motion transfer functions. In this case the results were truncated as this filtering removed any reliability in the outcome for frequencies below 0.16 Hertz. The transfer functions derived from measured data are further described in section 4.5. Clearly no significant amounts of energy was removed from the signal obtained from the wave data as no further digital filtering was applied.

2.6.2.2 Power Spectrum Derivation

To enable the use of efficient fast Fourier transform (FFT) techniques, the data sample records were made up of a factor of 2^n samples such that a typical data file of 4096 data samples was split into segments of 1024 samples with a 50% overlap (see Welch (1967) in which a similar approach was used). Furthermore the data segments were increased through data decimation to reduce the effective sample rate to 5 Hertz, thus maintaining a sample rate which was more than twice the Nyquist frequency ($f_s/2$) or the highest of all the applied low pass filters being 2 Hertz. To achieve a sample rate of 5 Hertz on both the 81 and 86 metre vessel, the data was decimated by a factor of 2 and 4 respectively. This also had the effect of increasing the number of data sets that could be averaged together after obtaining a spectrum for each. This segmented record length also provided sufficient spectral resolution (δf) calculated as

$$\delta f = \frac{f_s}{n} : [Hertz] \tag{2.14}$$

where n is the number of samples, f_s is the sample frequency to give an approximate spectral resolution (δf) of 0.01 Hertz and 0.02 Hertz for the 81 and 86 metre vessels respectively. Each data segment had a Hamming spectral window applied before performing an FFT on the data to obtain both a set of response spectra and wave spectra. As many sets of spectra that were available from a particular record group (defined by vessel speed, wave direction and hull control surface configuration) were combined to obtain an averaged power spectral density function with the units of $V_{rms}^2/\left(\frac{rad}{s}\right)$ (where V represents the input data unit). This computation was performed on the wave data to obtain wave spectra and on the heave, roll and pitch data to obtain the corresponding response spectra. To check data integrity the coherence function was calculated for each data segment between the sampled wave data and response data where a value greater than 0.4 for a given encounter frequency was considered sufficient for spectral results to be presented.

In the event of encounter frequency spectra being required as wave frequency spectra, the transformation of the abscissa was made with the deep water wave relationship of

$$\omega_e = \omega - \frac{\omega^2 U}{g} \cos \mu \tag{2.15}$$

and the transformation of the ordinate $S_\zeta(\omega_e)$ to $S_\zeta(\omega)$, whilst preserving the variance with the relationship

$$S_\zeta(\omega) = S_\zeta(\omega_e) \left| 1 - \frac{2\omega U}{g} \cos \mu \right| \tag{2.16}$$

$$= S_\zeta(\omega_e) \frac{d\omega_e}{d\omega} \tag{2.17}$$

Chapter 3

Prediction of Vessel Response

3.1 Review of Alternative Methods Available

A broad introduction to analytical ship motion methods has been given in section 1.2.2. Strip theory suitable for numerical computations developed from the theory of Korvin-Kroukovsky and Jacobs (1957). Their theory has been recognized as a significant contribution to seakeeping because it introduced many of the concepts now used in more recent methods. Further development and improvements to this method were made by Salvesen et al. (1970) which is now a more recent standard theory which has provided the means to extract both motions and loads through the integration of hull hydrodynamic pressures.

Despite the considerable progress made with numerical solutions to the three-dimensional unsteady fluid domain problem, these techniques involve greater complexity and computational time, making their practical application to engineering problems currently unsuitable using affordable desk top computers. Some of these methods for example included those developed by Nakos and Sclavounos (1991); Beck et al. (1993), Beck (1994), Beck et al. (1994); Zhu and Katory (1995) and Zhu and Katory (1998). Strip theories by comparison are of lesser complexity and will solve a numerical computation in a relatively short time frame, making the results (which are often satisfactory for conventional hulls) an acceptable compromise whilst incurring only a modest loss of accuracy. Indeed, three dimensional methods are sensitive to conditions aft of and near to the transom. This leads to difficulty in predicting pitch by such methods at high Froude number (see Davis and Holloway (2003a)). The application of strip theories make them especially suitable for the analysis of slender hull forms that generally have the required geometrical characteristics required by the constraining assumptions. Hulls with non-slender geometrical characteristics in the strict sense require a three-dimensional theory to represent the fluid domain, although some strip theories have been adapted to overcome some of these shortfalls. Holloway (1998) identified that validity of some of the notable theories can be characterized by hull slenderness, wavelength and speed. These categories are reproduced in table 3.1, where the low Froude number theories are notably frequency domain formulations and the "non-slender hull" formulations are not strip theory.

The conventional strip theories, developed from the work of Korvin-Kroukovsky and Jacobs (1957) to the more recent standard theory of Salvesen et al. (1970), were primarily designed to provide reasonable predictions for the low speed ships at relatively high wave frequencies or short wavelengths. Although critical forward speed effects were neglected in the formulation, Faltinsen (1993) states that "Generally speaking, strip theories are still the most successful theories for wave-induced motions of conventional

	slender hull		non-slender hull
	short λ (high frequency)	any λ (any frequency)	any λ (any frequency)
low F_n (Frequ. domain)	Salvesen et al. (1970)	Newman (1978) (unified)	Newman (1991) (3D)
any F_n (time domain)	Yeung and Kim (1981)	Yeung and Kim (1984) (comprehensive)	Linear 3D
high (i.e. any) F_n with steady interaction	Faltinsen and Zhao (1991)		Nakos and Sclavounos (1991)

Table 3.1: Relationship between various strip or strip-like theories and some 3D theories (Reproduced from table 4.1 of Holloway (1998))

ships at forward speed". This was generally true because the "conventional ships" on which strip theory calculations were based for many years were relatively slow vessels with low length based Froude numbers. Thus the emergence of problems associated with high Froude numbers were not apparent until the advent of large high-speed displacement hull forms.

Two-dimensional transverse strips of the hull in traditional theory have been formulated to have independence from each other with no interaction. This had not been so important at low Froude numbers where gradual changes in hull geometry essentially produce transverse wave radiation at low forward speed and interaction between the strips is less critical for obtaining reasonable motions results.

The unified theory of Newman (1978) attempted to address some of the three-dimensional effects ignored by traditional strip theory by modifying the two-dimensional strips to impose some interaction between them to match a three dimensional solution.

Yeung and Kim (1981) proposed a forward speed strip theory with a pseudo-time variable that was designed to address the forward speed terms and provide a solution to the high speed restrictions imposed by conventional strip theory. This formed the basis of an advancement to a more comprehensive theory later given by Yeung and Kim (1984) that contained no restrictions on forward speed and frequency of oscillation.

Faltinsen and Zhao (1991) developed a strip theory method that took account of forward speed effects. While acknowledging the deficiencies of conventional strip theory they sought to improve these areas and keep the method relatively simple without adopting a complete three-dimensional theory. The effect of the local steady flow was included in the body boundary conditions, free surface conditions and the pressure calculations. Their solution starts at the bow where it assigns a zero value to the velocity potential and its x-derivative before stepping the solution of the unsteady free surface and velocity potential in the downstream direction. The free-surface condition differs from the ordinary strip theory formulation in that the terms proportional to the forward velocity squared are retained, which are neglected in the ordinary strip theory.

The three-dimensional theory of Newman (1991) was not so much intended to be a practical procedure as to obtain a solution to the ship motion problem and obtain results that could remove the uncertainty inherent in experimental comparisons. This may be where three-dimensional theories that can prove their worth through accurate validations, given the available computing power. As computer speed increases this will become less of an issue.

The work of Nakos and Sclavounos (1991) represents a new phase of computational

ship hydrodynamics that seeks to solve the time-harmonic three-dimensional ship motion problem by a Rankine Panel method. A new free surface condition is derived which is shown to be valid uniformly for all Froude numbers and frequencies and provides a solution that gives improvement over strip theory. Once again, the intention is that a good solution to the unsteady ship motion problem could provide an alternative to experimental results for numerical comparison. The adoption of some strip theories to partially account for the forward speed effects has implied that they can no longer be strictly designated as two-dimensional in which case they are often labelled $2\frac{1}{2}$-dimensional theories.

3.2 Basis of High Speed Strip Theory Method

The high speed strip theory implemented in this analysis was developed by Holloway (1998) as a time domain alternative to conventional frequency domain strip theories, with particular differences in the fundamental treatment of the free surface boundary condition. It departs from the moving reference frame formulation used in traditional strip theories and replaces it with a stationary reference frame that is fixed in the absolute reference frame of the water. This eliminates the need for the $\partial/\partial x$ terms in the free surface boundary condition. In doing this it solves the potential problem for each strip of water in a stationary reference frame, thus removing any speed dependent terms in the free surface boundary condition. Prior to the hull passing by, each strip of water remains undisturbed until the bow progresses into the strip of water, which commences to generate waves. As each section of the hull passes through the strip of water, the waves initiated by the first strip at the bow continue to propagate away from the hull whilst the hydrodynamic effects of each subsequent hull section contribute to the wave pattern of each strip of water until the hull has completely passed the fixed water strip. This is unlike traditional strip theory in so far as that at no time does a strip of water have waves that extend to infinity. Also each hull section is fully influenced by the waves generated by the hull forward of its position. Traditional strip theory and this method will only produce similar results at zero forward speed.

As with traditional strip theory, the hull boundary condition for each strip is exactly satisfied. However, in this case the linearised free surface boundary condition is necessary in each two-dimensional solution owing to the form of the Green function used.

The rationale behind the time domain strip theory is that it has the potential for non-linear wave and vessel behaviour to be introduced to the numerical problem. It also allows for forward speed effects and obviates the need to consider them in the free surface boundary condition. The non-linear problem that is accounted for in the method is the changing hull submergence as it oscillates in waves. By using a free surface Green function panel method, the need for source distributions on the free surface is eliminated without any need for special treatment in the problem where the hull intersects the free surface. However, many of the strip theory assumptions must still apply.

The objective for implementing a strip theory is to approximate the motions of a hull form in a three-dimensional fluid without the complexity and computational demand necessarily required by a full three-dimensional computational method. If this can be achieved without a significant loss in the solution accuracy then a strip theory approach may well be applied to many modern hull shapes with reasonable success. The assumptions inherent in traditional strip theory were expressed by Salvesen et al. (1970) and Newman (1977). Most of these apply to the time domain method adopted

for this analysis and when strictly applied would include the assumptions of small wave amplitude, small ship motions and hull slenderness.

$$\frac{(B,T)}{L} \ll 1 \tag{3.1}$$

That is, the hull beam and draft should be small compared with the hull length and that the hull cross section and fluid domain properties thus vary slowly longitudinally. This assumption is consistent with most high speed hull forms used at high Froude number, which are the focus of investigation in this analysis. However, the restriction that traditional strip theory should only be applied to high frequencies and low speeds ($F_n < 0.4$) no longer apply.

Being a time domain computation with no special treatment required at the hull boundary intersection with the free surface, it is possible for the hull shape above and below the still water free surface level to be considered in the computation. Non-linearities due to the variation of immersed hull section shape are considered. Added mass and damping terms are not introduced specifically as they are in traditional strip theory. Increasing the computed wave height on a non-wall sided hull form will thus alter the hull response per unit wave height. This can be important when comparing numerical solutions with experimental results obtained in sea waves that are large compared with the vessel draft and beam.

3.2.1 Synopsis of the Green Function Method

The Green function formulation used in this analysis, derived by Holloway (1998) and presented here for reference, lends itself to the application of ship motions as a practical solution to the body boundary and fluid surface boundary conditions to determine the hydrodynamic forces on a slender hull form using a form of strip theory. The rigid body hull motions can be determined from the hydrodynamic forces and moments on the hull such that the problem is only concerned with the disturbance flow field about the moving hull form instantaneously submerged below the free surface.

To put this in perspective, the linearised full three-dimensional disturbance potential due to the moving ship in waves is defined in the fluid domain by the equation

$$\frac{\partial^2\phi}{\partial x^2} + \frac{\partial^2\phi}{\partial y^2} + \frac{\partial^2\phi}{\partial z^2} = 0 \tag{3.2}$$

and on the equilibrium free surface ($z = 0$) by the equation

$$\frac{\partial^2\phi}{\partial t^2} + g\frac{\partial\phi}{\partial z} = 0, \tag{3.3}$$

on the hull surface by the equation

$$\nabla\phi \cdot \mathbf{n} = (\mathbf{v} - \nabla\phi_I) \cdot \mathbf{n} \tag{3.4}$$

where ϕ_I is the incident wave potential. The far field is represented by

$$\nabla\phi \longrightarrow 0 \tag{3.5}$$

where z is in the vertical and x in the forward direction of the ship.

All strip theories by their definition use a two dimensional form of the fluid field equation that is expressed as

$$\frac{\partial^2\phi}{\partial y^2} + \frac{\partial^2\phi}{\partial z^2} = 0, \tag{3.6}$$

which is justified on the basis that slender ships generate fluid motions (at least near the hull) that are essentially in planes perpendicular to the centreline. Three dimensional effects in the far-field is unlikely to introduce significant errors in the hull forces and motions because of the distant proximity of these areas to the immediate hull disturbance flow field about the moving hull.

Traditional strip theory further approximates the solution by adopting a moving reference frame, in which the free surface boundary condition is expressed in its full form as

$$\left(\frac{\partial}{\partial t} - U\frac{\partial}{\partial x}\right)^2 \phi + g\frac{\partial\phi}{\partial z} = 0, \tag{3.7}$$

where the $U\frac{\partial}{\partial x}$ terms must be neglected in a strip theory. For ships moving with increasingly high forward speed or in particular, high length based Froude numbers, this approximation becomes difficult to justify on the basis that the forward speed effects are an important contribution to a reasonable numerical outcome.

However, by using a fixed reference frame approach as proposed, presented and solved by Holloway (1998) (see also, Holloway and Davis (2001b), Holloway and Davis (2001a), Holloway and Davis (2002a), Davis and Holloway (2003a)), where stationary strips of water are created numerically through which the ship penetrates as it moves forward, the original free surface boundary condition can be retained thus avoiding any need for approximation of equation 3.7. The outcome of this procedure is that the solution is necessarily transient, even for regular motions.

This has necessitated a solution to the transient two dimensional motion problem for spatially fixed sections of the water orientated in a perpendicular plane to the direction of forward motion. The method adopted uses a boundary element method based on a Green function given by Wehausen and Laitone (1960) as

$$\begin{aligned} f(z,t) &= \frac{Q(t)}{2\pi}\ln(z-c(t)) - \frac{Q(t)}{2\pi}\ln(z-\bar{c}(t)) \\ &\quad -\frac{g}{\pi}\int_0^t Q(\tau)\int_0^\infty \frac{1}{\sqrt{gk}} e^{-\imath k(z-\bar{c}(\tau))}\sin\left[\sqrt{gk}\,(t-\tau)\right] dk\, d\tau \end{aligned} \tag{3.8}$$

where Q is the source strength, k is the wavenumber, c is the source location and $\bar{c}$ its complex conjugate. This function satisfies the conditions above, hence it is only necessary to locate the sources on the hull surface without the need to also include the free surface of the surrounding fluid. This provides a simplification of the computation and thus avoids problems often associated with the boundaries of the free surface at a distance from the hull and its disturbance flow field.

The complex velocity $W = u - iv$ is obtained by integrating $\frac{\partial f}{\partial z}$ over all sources positioned on the hull surface. Application of the hull boundary condition then leads to a set of equations for the source strength terms at each time step in terms of the hull motion and the previous time history integrals.

The contribution of a source of unsteady strength Q distributed over boundary element j with endpoints c_1 and c_2 to the velocity at a collocation point i at z is given by

$$W_{i,j} = \frac{Q}{2\pi}\left(e^{-i\beta}\ln\left(\frac{z-c_1}{z-c_2}\right) - e^{i\beta}\ln\left(\frac{z-\bar{c}_1}{z-\bar{c}_2}\right)\right) - i\sqrt{\frac{g}{\pi}}\int_0^t e^{i\beta(\tau)}Q(\tau)\left[\frac{e^{w^2}\operatorname{erf} w}{\sqrt{i(z-\bar{c})}}\right]_{w_1}^{w_2} d\tau \tag{3.9}$$

where the slope of the source element is $\beta = arg(c_2 - c_1)$. If the sources are distributed over a finite number of elements, the hull boundary condition then leads to the equations for the source strengths in matrix form as

$$[A]\{Q\} = \{R\}. \tag{3.10}$$

Here the unknown source strengths at the current time step ($\{Q\}$) are separated from the historical source strengths appearing in the convolution integral of $W_{i,j}$ by putting

$$A_{i,j} = -\operatorname{Im}\left\{\frac{e^{i\alpha}}{2\pi}\left[e^{-i\beta}\ln\left(\frac{z-c_1}{z-c_2}\right) - e^{i\beta}\ln\left(\frac{z-\bar{c}_1}{z-\bar{c}_2}\right)\right]\right\} \tag{3.11}$$

and

$$R_i = (\mathbf{v} - \nabla\phi_I)\cdot\mathbf{n} - \operatorname{Im}\left\{e^{i\alpha}\left[i\sqrt{\frac{g}{\pi}}\sum_{j=1}^{n}\sum_{k=0}^{n_t-1} C\Delta t e^{i\beta(\tau)}Q_j(\tau)\left[\frac{e^{w^2}\operatorname{erf} w}{\sqrt{i(z-\bar{c})}}\right]_{w_1}^{w_2}\right]\right\} \tag{3.12}$$

where $\tau = k\Delta t$, $n_t = \frac{t}{\Delta t}$, α = slope of the hull surface at point i, C is a trapezoidal integration coefficient ($= \frac{1}{2}$ for $k = 0$ or 1 otherwise), $w = \frac{i(t-\tau)}{2}\sqrt{\frac{-ig}{z-\bar{c}}}$, $w_k = w(c_k(\tau))$, $(\mathbf{v} - \nabla\phi_I)$ is the local hull element velocity in a stationary reference frame relative to the wave particle motion in the absence of the hull (i.e. $\mathbf{v}$ is the local hull velocity, $\nabla\phi_I$ is the local wave particle velocity) and the source strength history is approximated by discrete values at time intervals Δt where the radiated and diffracted waves are treated together. The source strengths may then be determined as $[A]^{-1}\{R\}$, where there is an equal number of source elements and collocation points.

The hull forces are obtained from pressures calculated over the hull surface, which can be determined from $p = -\rho\frac{\partial\phi}{\partial t}$. Integrating $\frac{\partial f}{\partial t}$ over each element and summing for all source elements the contribution at point i from a single element j can be shown to be

$$\frac{\partial\phi_{i,j}}{\partial t} = \operatorname{Re}\left\{\frac{e^{-i\beta}}{2\pi}\left[(A_k + (z-c_k)B)\ln\left(e^{-i\gamma}(z-c_k)\right)\right]_{k=1}^{2} - \frac{e^{-i\beta}}{2\pi}\left[\left(\bar{A}_k + (z-c_k)\bar{B}\right)\ln(z-\bar{c}_k)\right]_{k=1}^{2} + \frac{2ig}{\sqrt{\pi}}\int_0^t e^{i\beta(\tau)}Q(\tau)\int_{w_1}^{w_2}\left(e^{w^2}\operatorname{erf} w + \frac{1}{w\sqrt{\pi}}\right)dw\,d\tau\right\} \tag{3.13}$$

where $A_k = Q\frac{dc_k(t)}{dt}$, $B = -\frac{dQ}{dt} + iQ\frac{d\beta}{dt}$. The result is independent of γ provided that the path of integration of the logarithm terms crosses the positive real axis, and this can be guaranteed by adopting $\gamma = \arg\left(z - \frac{1}{2}(c_1(t) + c_2(t))\right)$ if $z \neq \frac{1}{2}(c_1(t) + c_2(t))$, otherwise $\gamma = \left(\arg(c_2 - c_1) + \frac{\pi}{2}\right)$.

This computational method was also validated by Holloway and Davis (2002a) with reference to analytic solutions for the wave-maker problem and the transient response of a floating cylinder, as well as against numerous steady or periodic motion problems.

With the instantaneous wetted hull sections being panelled up to the free surface as the time marching solution proceeds it is possible for large amplitude motions to be considered, even to the extent of non-wall sided hull forms. This nonlinearity, coupled with the effects of the motion control surfaces has the potential to bridge the gap between the linear motion solution and the full scale measured solution of hull response, which will be addressed in the proceeding chapters. However, this nonlinear benefit obtained with the Green function formulation does not extend to the free surface where the boundary condition is linearised. Other non-linear effects associated with the free surface cannot be directly considered with this procedure. These effects are not considered to have a significant contribution in the motions of high Froude number vessels.

Methods for solving the potentially unstable numerical integration of the equations have been presented by Holloway and Davis (2001b) and Holloway and Davis (2002b) (see also Davis and Holloway (2003a)) where the reader is left to refer to these for further detail.

With each stationary strip of water transferring the unsteady disturbance history down stream, so too do the steady flow disturbance due to the hull forward motion get included in the solution. With the hull free to trim and sink in the solution it is possible to determine these properties in solutions where no incident waves are included. In the results presented by this analysis these results are revealed at the zero frequency of the motion transfer functions ($\omega_e^* = 0$) presented generally in chapter 5.

3.2.1.1 Frictional effects

Frictional effects not considered by the Green function formulation in reality will have some contribution to the motion solution. Some frictional effects are thought to have a greater effect at model scale than full scale (see Davis and Holloway (2003a) and Davis et al. (2003) for further discussion). Therefore, a small viscous correction of the form $D = \frac{1}{2}C_s\rho U v B$ (where D is the force per unit length, C_s is a drag coefficient, B is the local beam, U the forward speed of the ship and v is the local vertical velocity relative to the local water surface) was added to the sectional transverse potential forces to realistically account for dissipative effects that find their origin through a variety of mechanisms. These include skin friction, flow separation, vortex shedding, bow wave breaking and the lift associated with separated flow at the transom. The tendency for potential based motion predictions published in the open literature to almost always show an over prediction of peaks may possibly be contributed to the frictional effects but these effects are likely to be modest with a value for the drag coefficient being generally less than 0.15. In this analysis a value of 0.1 was generally applied to all motion solutions because it was not considered necessary to spend time iterating the magnitude of the transfer function peaks in demonstrating the outcomes in comparison with the experimental results.

The high speed strip theory described has previously been extensively validated for hull motions against model tests on conventional mono-hulls, catamarans and SWATHs at Froude numbers ranging up to 1.14 with good agreement (see Davis and Holloway (2003a), Holloway and Davis (2001a), Holloway and Davis (2002b) and Holloway (1998)). The motion solutions have generally shown a substantial improvement to classical strip theory, particularly at the high Froude numbers.

3.3 The High Speed Strip Theory Program BESTSEA

Details of the computational modelling of ship motions and hydrodynamic loads are presented in this section. This includes a method for modelling the ride control system which has been incorporated into the time-domain ship motions program BESTSEA for regular head sea waves. Issues of hull definition and other input parameters required by the ship motions program are presented. Transfer functions of the heave and pitch motions with various configurations of motion control devices are combined with a Bretschneider wave spectrum of 2.5 metre significant wave height and 7 second average period to determine the vessel accelerations.

3.3.1 Code Overview

The computational modelling of hull motions and hydrodynamic loads was undertaken with a modified version of BESTSEA, a program written in Fortran 90 (Holloway (1998)). When compiled in the appropriate format, the program will run either on an IBM compatible personal computer running Windows NT or on a UNIX workstation. Its method of operation was to compute a numerical time-domain solution for a vessel progressing in long-crested regular head sea waves. It computes the unsteady hydrodynamic hull forces and the resulting ship motions which can be further post-processed to determine the motion transfer functions, phases, structural bending moments and shear forces.

BESTSEA considers a single hull that moves forward in head seas at a constant speed U in the positive x direction where the system coordinates are stationary and fixed relative to the equilibrium position of the water. Each strip of water lays undisturbed forward of the bow prior to the hull advancing onto the strip. When the bow reaches a strip of undisturbed water the strip observes the heave and pitch motion of the vessel while solving for the hydrodynamic forces on the hull by the Green Function method. The solution for each water strip commences as the pointed bow enters it and is terminated as the stern leaves it, after which the strip is discarded. The method requires that the vessel hull is slender (has a high length to beam ratio) so that the two dimensional deformation of each water strip can be considered a realistic representation of the free surface and water motion process. No forward motion terms have been neglected which makes the solution valid for high Froude Numbers as the free surface boundary condition is satisfied in a spatially fixed reference frame. For low length to beam ratios hulls and low Froude numbers where the deformation of the free surface becomes strongly three-dimensional the code is less applicable. This approach however, suits the slender hulls measured and analysed in this work, which typically had a length to beam ratio of 17.7 and Froude numbers of 0.2 to 0.8 (12.5 to 42.5 knots).

Modification to the program BESTSEA permitted the modelling of the hydrodynamic forces exerted on the vessel through one or more ride control surfaces, which in this work comprised a transom tab and forward mounted T-foil as only one hull of the twin hull vessel was considered for the head sea case. Other investigations with a twin hull solution have shown that interference between the two hulls is not significant for the Froude numbers and hull spacing of the analysed hull forms. The lift generated by these devices could be controlled in time as the solution proceeded by careful selection of the control feedback gain parameters that demand a change in the angle of attack of the tab or flap as the vessel heaves and pitches through regular waves in the time stepped solution. The output of the program produced time records of the computed heave and pitch motions and hydrodynamic loads for each section of the hull.

The number of sections required to define the hull shape has a direct relationship

to the number of time steps required by the program to complete a solution. In addition, the number of sections must be sufficient to maintain adequate resolution in the descretization of time and length to allow an accurate completion of a solution. The BESTSEA method of calculation advanced the hull shape forward one hull section length Δx ($\Delta x = \frac{L}{n_s}$, where L is the length of hull geometry and n_s is the number of regularly spaced hull geometry sections) with each time step where the fluid domain computation would retain the information from the previous time step. Thus a single time step Δt is defined as

$$\Delta t = \frac{\Delta x}{U} = \frac{L}{n_s U} \tag{3.14}$$

where U is the vessel speed in metres per second.

To ensure a smooth transition of forces between each time step, a minimum number of eight time steps was nominated over a single regular wave length. The defined hull therefore must satisfy the relationship $\frac{T_e}{\Delta t} \geq 8$, where T_e is the wave encounter period. By substitution of Δt in equation 3.14 it can be shown that the number of sections must meet the broad requirement of

$$n_s \geq \frac{8L\omega_e^*}{U2\pi}\sqrt{\frac{g}{L}} \tag{3.15}$$

where ω_e^* is the dimensionless wave encounter frequency $\left(\omega_e^* = \omega_e\sqrt{\frac{L}{g}}\right)$.

A typical hull geometry will contain between twenty to fifty sections and as a general rule the number of sections required will increase as the ship speed decreases. At higher Froude numbers, proportionately fewer sections have proved satisfactory.

The total number of time steps required to complete a computation is dependant on the numerical solution reaching a steady periodic response at the given frequency. This is a function of the wavelength, vessel speed and the number of sections defining the hull. Experience with previous solutions has shown that when measuring the hull trim in calm water whilst at speed the computation requires at least four hull lengths for the transient disturbances to disappear. In waves, the computation requires the hull to pass through an additional three wavelengths to achieve a reasonable steady state solution. It can thus be shown that the approximate minimum number of time steps required in a computation is

$$ts = N_1\frac{2\pi U n_s}{\omega_e L} + N_2 n_s \tag{3.16}$$

where $T_e/\Delta t$ is the number of time steps per wavelength, and n_s is the number of sections defining a hull surface. N_1 and N_2 are factors selected by the user, which experience has shown to be best selected as a value of 3 and 4 respectively. This clearly shows that as the wave encounter frequency decreases, the speed decreases, or as the number of hull sections is increased, the number of time steps will increase. Experience with a run time solution at a low vessel speed with dimensionless frequencies (ω_e^*) down to 1, required a solution of up to 422 time steps. Running the program on a Pentium-4 with a single 2.4GHz central processor requires between 2.5 to 6 hours to compute 45 frequencies at one forward speed to derive one set of associated transfer functions.

3.4 Modelling of Motion Control Surfaces

Motion measurements on the full-scale vessels were for the majority of time conducted whilst the vessel was operating under the influence of an active motion control system. The system initially consisted of active transom mounted trim tabs throughout the delivery voyage and later included the T-foils mounted towards the bow when the vessel went into regular service. The manner in which the ride control system could alter the characteristics of the motion transfer functions was not well known and so the modelling of these devices was an essential area of investigation.

The force exerted on a ship by a submerged lifting surface is a function of the lifting surface aspect ratio, plan area, section form, depth below the free surface and its angle of attack to the free stream flow. The trim tab force is derived by changing the momentum of the fluid and thus increasing the pressure on the underside of the hull whereas the hydrofoil generates a lift force by producing a circulation or a pressure differential between its upper and lower surfaces. The force generated by the transom tab could be controlled through a change in its angle or for the T-foil a change in the flap angle. In BESTSEA the feedback signal, which controlled the control surface deflections was made proportional to a linear combination of acceleration, velocity and displacement in both heave and pitch. Set at a constant angle, the forces remained constant except where the vertical hull motions relative to the water induced a change in the free stream incidence angle of the foil thus increasing the lift force.

It was assumed that the tab, not operating as a lifting foil outside the hull effect, was not affected by the motion of the hull relative to the water but produced a force that was directly proportional to the tab deflection only.

3.4.1 T-foil Force Model

The T-foil was mounted forward on the hull as close to the bow of the demi-hull as the geometric constraints permitted and consisted of a vertical strut connected to the keel that extended downwards to support a horizontal foil at its mid span that had the profile approximately of a NACA 0009 or 0012 section. The foil was comprised of two segments consisting of a fixed forward section and a trailing edge flap. The fixed forward section had a backward swept leading edge, which was forced to move and rotate with the hull motions through a rigid connection of the vertical strut. The trailing edge flap was rectangular in plan form and had a chord of 40% of the total mean chord length and force was generated when the free stream incidence angle was greater than zero ($|\alpha| > 0$) to the main foil section or by deflection of the trailing edge flap ($|\delta| > 0$) that could be actuated by the hydraulics of the motion control system.

An angular defection of a trailing edge flap (δ_i) thus generates lift even whilst the main foil remained at zero incidence angle ($\alpha_i = 0$). Plotting this effect on a lift curve would change the y-intercept of the lift slope curve an amount proportional to the flap defection while the lift slope $\left(\frac{dC_l}{d\alpha}\right)$ remained constant (Hoerner and Borst (1975)). The total lift coefficient could therefore be expressed as a function of free stream incident angle (α_i) and trailing flap deflection (δ_i)

$$C_l(\alpha_i, \delta_i) = \frac{dC_l}{d\alpha_i}\alpha_i + C_{l_0}(\alpha_i) + \frac{dC_l}{d\delta_i}\delta_i \tag{3.17}$$

Since there is symmetry in the sectional geometry of the T-foil no zero offset is required and thus $C_{l_0}(\alpha_i) = 0$. The lift force is therefore expressed as

$$F_i(\alpha_i, \delta_i) = \left(\frac{dC_l}{d\alpha_i}\alpha_i + \frac{dC_l}{d\delta_i}\delta_i\right)\frac{1}{2}\rho U^2 A_i \tag{3.18}$$

where A_i is the plan area of the foil (m^2), ρ is the water density (kg/m^3) and U the vessel forward speed (m/s).

The flap deflection (δ_i) relative to the chord line of the forward fixed section was controlled by feedback from the control system motion sensors. The lift force was determined by the free stream incidence angle (α_i) which was a function of the initial angle in the foil relative to the hull base line, the instantaneous pitch displacement, the instantaneous pitch or heave velocities, and the water velocity due to the presence of waves (see figure 3.1). The free stream incidence angle (α_i) is therefore

$$\begin{aligned} \alpha_i &= \alpha_0 - \eta_5 + \alpha_{x\dot{\eta}_5} - \alpha_{\dot{\eta}_3} + \alpha_w \\ &= \alpha_0 - \eta_5 + \frac{x_{\frac{1}{4}c}\dot{\eta}_5}{U} - \frac{\dot{\eta}_3}{U} + \alpha_w \end{aligned} \tag{3.19}$$

where α_0 is the angle of incidence of the fixed part of T-foil relative to the hull baseline, η_5 is the pitch displacement, $\dot{\eta}_5$ is the pitch velocity, $\alpha_{\dot{\eta}_3}$ is the angle of the free stream flow due to the heave velocity and the vessel forward speed, $\alpha_{x\dot{\eta}_5}$ is the angle of the free stream flow due to the pitch velocity and the vessel forward speed, α_w is the flow incidence angle due to the presence of waves (ignoring the presence of hull), $x_{\frac{1}{4}c}$ is the distance of the control surface quarter chord point from the LCG (+ve forward) and U is the vessel forward velocity.

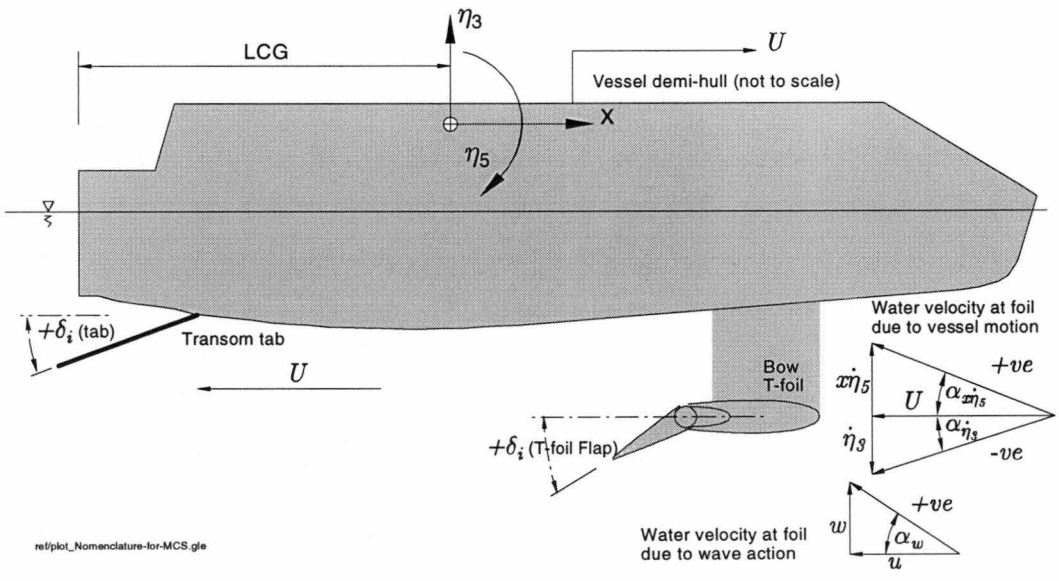

Figure 3.1: Diagram showing the variables applied in the lifting surface computation where the δ_i represents the deflection of the active component for the i^{th} independent control surface (the hull and foil geometry exaggerated for clarity)

3.4.1.1 Incidence Change Due to Wave Particle Velocity

According to linear wave theory (Lewis (1988a), Lloyd (1989), Tucker (1991)) regular wave water particles in deep water [1] move with a circular motion in the vertical plane parallel to the wave direction. On the free surface the orbit path has a radii of $\bar{\zeta}$ which decreases with depth in proportion to e^{kz}, where z is the water depth from the mean water level (taken as negative). The plane of this orbit coincides with the vertical plane of motion of the vessel as it moves forward in a long crested head sea and has the effect of altering the free stream velocity over the lifting surface and changing the incident angle of the foil. For a vessel travelling at 30 knots in three metre high waves, this effect can alter the incident angle of the foil by up to 4° provided the foil is mounted clear of the hull effect. Geometrically, the vertical (w) and the horizontal (u) particle velocity due to a regular long crested wave in time (t) and space in the x and z directions are given by

$$u = \bar{\zeta} e^{-kz_{cs}} \omega \cos(\omega_e t + k x_{\frac{1}{4}c}) \tag{3.20}$$

$$w = -\bar{\zeta} e^{-kz_{cs}} \omega \sin(\omega_e t + k x_{\frac{1}{4}c}) \tag{3.21}$$

where $\bar{\zeta}$ is the wave amplitude, k is the wave number, z_{cs} is the vertical distance of the control surface to the mean water level, ω is the wave frequency and $x_{\frac{1}{4}c}$ is the longitudinal distance between the hull centre of gravity and the centre of foil force application, which in this case is assumed to be at the quarter chord position.

In deep water the horizontal and vertical velocity components are considered equal $\left(u = w = -\bar{\zeta} e^{-kz_{cs}} \omega\right)$. The maximum orbital velocity occurs at the free surface with amplitude $u_{\max} = -\bar{\zeta}\omega$ (where $e^{-kz_{cs}} \doteq 1$) and reduces with depth such that it can be shown that the velocity amplitude of the water particles reduces to 1% ($u = 0.01 u_{\max}$) of the surface velocity at a depth (z) of $z = \frac{1}{k} \ln\left(\frac{0.01 u_{\max}}{-\bar{\zeta}\omega}\right) = \frac{1}{k} \ln\left(\frac{0.01(-\bar{\zeta}\omega)}{-\bar{\zeta}\omega}\right) = -0.733\lambda$. In comparison the T-foil is submerged approximately 2 metres below the still water level which is within the influence of wave action.

The change of incidence angle (α_w) on a lifting surface due to the orbital velocity of the water particles is expressed as

$$\alpha_w = \frac{w}{u + U}$$

where the velocity of fluid over the foil is $u + U$.

3.4.1.2 Control Surface Depth Effects

The shallow draft of the vessels modelled in this analysis implies that adequate submergence depth of a T-foil in waves may not be possible. The extension of the foil below the keel by a strut increases the submergence, however a reduction or even a loss of lift will occur as the foil approaches or breaks through the free surface. A reduction in pressure over the foil surface will initiate cavitation and eventually ventilation if an air source is created. Fossen (1994) modelled the reduction in foil lift due to the free surface proximity, but neglecting any effect due to the nearby hull as

[1] Deep water in this sense means for practical purposes that the depth is greater than $\frac{\lambda}{2}$.

$$\begin{array}{rl} \frac{h}{c} \geq 0 & : C_l(h) = 0 \\ 0 > \frac{h}{c} > -1 & : C_l(h) = \frac{C_{l_\infty}}{2}\left(1 - \frac{h}{c}\right) \\ \frac{h}{c} \leq -1 & : C_l(h) = C_{l_\infty} \end{array} \tag{3.22}$$

where h is the depth of the quarter chord point of the hydrofoil below the free surface (h is positive upwards from the mean surface level), c is the chord length, $C_l(h)$ is the piece wise lift coefficient and C_{l_∞} is the deeply submerged lift coefficient.

Cavitation also has a real and detrimental effect on the lift generated by a T-foil (see Tornblad (1987) for effects on propellers and Lewis (1988b) for general information) under certain operating conditions. As water passes around the foil surface, cavitation occurs when an increase in the fluid velocity causes a sufficient reduction in the local fluid pressure for vapour bubbles to form. This is often assumed to occur when the fluid pressure has fallen to the local water vapour pressure (p_v), which is dependant on temperature. However, this is considered optimistic and cavitation may occur at higher pressures, particularly in sea water (see Lewis (1988b, p173)). Once formed, the cavitation vapour bubble will collapse when it moves into a region of sufficiently high pressure. For a foil at a particular operating condition, the point of cavitation onset can be described by the cavitation number

$$\sigma = \frac{p_0 - p_v}{q} \tag{3.23}$$

where p_0 is the total static pressure equal to the sum of the atmospheric (p_a) and hydrostatic ($\rho g h$) pressures ($p_a + \rho g h$) and q is the dynamic or stagnation pressure $\left(1/2.\rho V_0^2\right)$ and is dependant on the fluid density (ρ) and free stream velocity (V_0). If a foil is subjected to sufficient bubbles of cavitation over its surface then a loss of lift can occur. In this situation the assumption made is that the lift force is truncated to the value obtained at the flap deflection prior to the onset of cavitation.

If one was to assume that vapour pressure was sustained on the low pressure side of the foil such that cavitation was occurring and that static pressure was sustained on the high pressure side of the foil, then the total lift on the foil would be equivalent to $(p_0 - p_v) A$, where A is the foil area. Foil lift is also expressed as $1/2.\rho V_0^2 A C_l$. It would be reasonable to assume that cavitation onset had been exceeded in this described condition, therefore an approximation for the onset of cavitation is when the lift coefficient is greater than or equal to the cavitation number (i.e. $C_l \geqslant \sigma$). Therefore, to avoid cavitation on the foil the lift coefficient should be kept at some point less than the cavitation number. This approach is only approximate and a more rigorous approach would be required in critical applications. Further consideration was outside the scope of the present analysis but would normally be considered in the design of a new T-foil application. The exact section profile used on the full-scale vessels is unknown for use in the present analysis as this is proprietary manufacturing technology and so estimates of foil lift potential were used.

3.4.2 T-foil Force

Due to the influence of the surface boundary layer, particularly near the trailing edge, experimental results for the lift coefficient slope $\left(\frac{dC_L}{d\alpha_i}\right)$ tend to be lower than the equivalent theoretical predictions. For example, a symmetrical two dimensional foil has a theoretical lift coefficient slope of $\left(\frac{dC_L}{d\alpha_i}\right)_{2D} = 2\pi \text{ rad}^{-1}$ $\left(0.11 \text{ deg}^{-1}\right)$, which is

unachievable for practical applications with foils of finite span according to Glauert (1959). He showed that the theoretical lift slope for an elliptical airfoil is

$$\frac{dC_l}{d\alpha} = \frac{\pi A}{1 + \frac{\pi}{a_0} A} \tag{3.24}$$

and a rectangular foil is

$$\frac{dC_l}{d\alpha} = \frac{A}{0.33 + 1.04 \frac{A}{a_0}}, \tag{3.25}$$

where A is the airfoil aspect ratio and a_0 is equivalent to $\left(\frac{dC_L}{d\alpha_i}\right)_{2D}$. It is assumed that in a practical application the lift coefficient slope can only achieve 75% of the theoretical value such that $a_0 = 0.75\,(2\pi) = 4.7124$.

The T-foil used in the computations had a span of 2.395 metres and a plan area of 3 square metres (aspect ratio (AR) of 1.91). Therefore, with an aspect ratio of 1.91 a practical lift coefficient slope based on equations 3.24 and 3.25 give 2.6395 and 2.541 respectively. Thus taking an average one obtains

$$\frac{dC_l}{d\alpha} = 2.591 \text{ rad}^{-1} \left(0.045 \text{ deg}^{-1}\right), \tag{3.26}$$

which should be a suitable approximation to adopt for a T-foil of aspect ratio 1.91 in this analysis.

Hoerner and Borst (1975) provide some experimental data showing the flap effectiveness ratio for a foil with a 40% flap and aspect ratio of 1.92 to be

$$\frac{d\alpha}{d\delta} = 0.744 \tag{3.27}$$

giving a flap lift coefficient slope of

$$\begin{aligned} \frac{dC_l}{d\delta} &= \frac{dC_l}{d\alpha}\frac{d\alpha}{d\delta} \\ &= (2.578)\,(0.744) \\ &= 1.92 \text{ rad}^{-1} \left(0.0335 \text{ deg}^{-1}\right) \end{aligned} \tag{3.28}$$

The lift force given by equation 3.18 may be expressed as the sum of the lift generated by the fixed foil and the additional lift generated by the flap deflection

$$F_l\left(\alpha_i, \delta_i\right) = F_{\alpha_i} + F_{\delta_i} \tag{3.29}$$

where $F_{\alpha_i} = \left(\frac{dC_l}{d\alpha_i}\right) \alpha_i \frac{1}{2}\rho U^2 A_i$ and $F_{\delta_i} = \left(\frac{dC_l}{d\delta_i}\right) \delta_i \frac{1}{2}\rho U^2 A_i$.

By separating the variables from the constants in equation 3.18 the total lift force generated by a T-foil is

$$F_i\left(\alpha_i, \delta_i\right) = \left[\left(\frac{F_{\alpha_i}}{\alpha_i U^2}\right)\alpha_i + \left(\frac{F_{\delta_i}}{\delta_i U^2}\right)\delta_i\right](U+u)^2 \tag{3.30}$$

where $\left(\frac{F_{\alpha_i}}{\alpha_i U^2}\right) = 3964$ kg/(m.rad) (69.2 kg/(m. deg)) and $\left(\frac{F_{\delta_i}}{\delta_i U^2}\right) = 2952$ kg/(m.rad) (51.5 kg/(m. deg)).

The T-foil lift force was applied at the positions of 55.79m and 61.19m forward of the transom for the 81 and 86 metre vessels respectively. The vertical position was 0.2m above the hull baseline for both vessels.

Sometimes a poorly designed or loaded hull form will be unable to achieve its optimum running trim[2] at forward speed through the deflection of the trim tab alone. In this case the T-foil may be used to assist the transom tab by imposing a mean deflection to the T-foil flap. In such conditions, the maximum unsteady force capacity of the T-foil is reduced because the maximum flap deflection about its new mean operating position has been effectively truncated by an amount equivalent to the imposed offset. Such limitations were not included in the motion computations carried out here.

3.4.3 Transom Tab Force Model

The transom mounted trim tabs have two purposes in the effective operation of the vessel. These are firstly, to provide a lifting force at the aft end which will alter the running trim of the vessel thus improve the hull efficiency and secondly, to provide an active motion control force. The device consists of a rigid flat or near flat plate hinged at its leading edge and connected to the hull at or just forward of the transom lower edge. The bottom surface is flush with the hull underside at its leading edge and its angle of incidence is controlled with a hydraulic ram attached to the transom that actuates a hinge mechanism interconnected between the transom and the upper side of the flap towards the trailing edge. An increasing upward hydrodynamic lift force is exerted on the hull when the tab deflection is increased in a downward direction. For a tab that is of equal width to the underside of the hull, the lift force F_i according to Brown (1971) and later restated by Savitsky and Brown (1976) is

$$F_i = \frac{dC_l}{d\delta_i}\left(\frac{1}{2}\rho U^2 A_i\right)\delta_i : [N] \tag{3.31}$$

where the sea water density ρ is approximately 1025 kg/m^3, U is the ship forward speed [m/s], A_i is the tab area $[m^2]$ and δ_i is the flap deflection (+ve downwards [deg]).

It was assumed that the vessel trim, pitch velocity, heave velocity and the water movement due to wave action had little effect on the relative velocity of the free stream flow over the tab surface. This implies that the angular displacement δ_i of the tab was the only means of generating lift and a change in vessel trim had no effect on generating additional hydrodynamic forces.

3.4.4 Transom Tab Force

Equation 3.31 gives the transom flap lift coefficient per flap deflection to be 2.64 rad^{-1} $(0.046\ \text{deg}^{-1})$. When the flap deflection is zero the flap is parallel to the hull underside. The projected plan area of this flap on the 81 and 86 metre vessels was 8.0 square metres (4.0 meter span (s), 2.0 meter chord). Rearranging equation 3.31 to separate the variables and constants gives

$$\begin{aligned} \frac{F_i}{\delta_i U^2} &= \left(\frac{dC_l}{d\delta_i}\right)\frac{1}{2}\rho A_i \\ &= 10824\ kg/(m.rad) \text{ or } (188.9\ kg/(m.\text{deg})) \end{aligned} \tag{3.32}$$

According to Brown (1971) the lift force application point is 0.6 (span) metres forward of the tab trailing edge (giving 2.4 metres). For both vessels this position is 1.0 metre

[2] In order to obtain the greatest hull efficiency which is determined by acheiving the maximum speed.

forward of the transom. The vertical position is 1.4 and 1.296 metres above the hull base line for the 81 and the 86 metre vessels respectively.

In most instances in the use of a transom tab, part of the force produced by the device is used to reduce the stern trim of the vessel at speed to improve the hull efficiency through the water. In this work the tab was placed at a 6 degree offset with an operating range of ± 6 degrees for active motion control. Sometimes a poorly designed or loaded hull form will have an existing optimum running trim[3] at forward speed without the assistance of a transom tab offset. In such conditions, the tab is unable to operate about a mean position, which ideally would be in the middle[4] of its effective range[5] without creating an excessive bow down trim that is detrimental to the hull efficiency at forward speed. In this case the tab must operate at a zero mean deflection position thus removing any force that otherwise might have been produced through an upward deflection and therefore truncating any force capability in that direction. Such limitations were not included in the motion computations carried out in the present work.

3.4.5 Application of Control Surface Force in Numerical Model

In the case where the position of a motion control device may not coincide with the position of a numerical hull section, the hydrodynamic force generated by the lifting device must be distributed to the adjacent hull sections. This was implemented simply by allocating a proportion of the lift force to each section according to their relative longitudinal distance from the force application position of the device.

3.4.6 Force Capacity of Motion Control Surfaces

For a given forward vessel speed, the maximum limited force capability of each control device is a function of the frequency of motion and forward speed. Other effects creating a loss of lift include cavitation and ventilation, which are a function of the submergence depth. The net wave forces on the hull however increase with wave height and with decreasing wave encounter frequency. Therefore the influence of the motion control system on reducing the vessel motions can only be considered effective for a finite range of wave heights and frequencies. Thus, with the introduction of a motion control system to a numerical model there will be a unique solution of vessel response for each wave height, wave heading, wave frequency and vessel speed thus limiting the application of a linear solution to a single case should the motion control gains be set so as to maximise the control surface deflections for the particular conditions of the solution..

In a static sense the relative effect of a motion control device will depend on the hull's waterplane area and the hydrostatic restoring force. Reducing the water plane area of the hull will increase the relative force capacity of the motion control devices for controlling heave and pitch whilst reducing the metacentric height will improve the relative roll force capacity of the same devices. The static roll and pitch angles possible from the maximum deflection of the control surfaces fitted to the 81 and 86 metre vessels were determined through a simple static analysis by taking moments about the hull centreline for roll and the longitudinal centre of floatation for pitch. The results of this static analysis for the 81 and 86 metre vessels at their respective in service full

[3]Determined through the fact that adjustment of the trim has the tendency to reduce the maximum speed for a given engine power output.

[4]This is set at 6° for this analysis.

[5]This is set at 12° for this analysis.

load departure condition (see appendix A for details) are shown in figure 3.2. With this calculation having been obtained independently of BESTSEA, these results are referred to as a static analysis as they do not take into account the running trim of the vessel due to forward speed effects such as the radiated waves. Thus this calculation produced different results to those obtained from the steady state computation of BESTSEA shown in figures 3.3 to 3.5 and discussed hereafter. They do however provide a useful comparison of the contribution of each device to the control of vessel motions without the need to run a time domain solution. They show that the force developed by the control surfaces only ever achieve about 14% of the total vessel displacement so their influence in reducing the vessel motions will be limited. They also show that the static roll angle is only slightly greater than the static pitch angle for the 81 metre vessel. The differences are a little greater for the 86 metre vessel where the static roll angles are clearly greater in every case. Clearly apparent from these results is the diminished effect of the devices as the speed of the vessel is reduced and the fact that the transom tab can create a static roll or pitch angle that is approximately twice that of the forward mounted T-foil. However, one cannot conclude from this that contribution of the tab in reducing the vessel motions is also twice that of the T-foil as the dynamics involved in reducing the motions based on some motion criteria may well not be so apparent.

The unsteady excitation capacity of the motion control devices was computed with BESTSEA to determine the heave and pitch response with forward speed to the sinusoidal excitation of the transom tabs and T-foil flaps in a free surface with no incident waves. These results are shown in figure 3.3 for the 86 metre vessel with transom tabs only, in figure 3.4 for a hull with an oscillating T-foil flap only and in figure 3.5 for a hull with a fixed T-foil and an oscillating transom flap. In addition, the steady state condition is displayed for the control surface at $\omega_e^* = 0$. In figure 3.3 with only a transom tab, the zero frequency was computed with the tab at the full deflection of 12 degrees. In figure 3.4 with only a T-foil, the zero frequency was computed with the flap at the full deflection of 8 degrees. Finally, in figure 3.5 with an oscillating tab and a fixed T-foil, the zero frequency was computed with the tab at the full deflection of 12 degrees and the T-foil fixed at 0 degrees.

It can be seen that the pitch displacement at zero frequency ($\omega_e^* = 0$) for the steady state tab deflection of figure 3.3 and steady state T-foil flap deflection of figure 3.4 differ in some respects to the static pitch calculation of figure 3.2(b) where the tab produced the greatest difference. As stated, these differences are attributed to the fact that the BESTSEA computation also accounts for forward speed effects that influence the vessel trim.

A notable feature of the unsteady excitation plots is that the T-foil produced a heave and pitch response that reached a peak and on either side of this peak, the magnitude reduced gradually to both the low and high frequencies. The tab by comparison had similar characteristics in the pitch excitation but generated a trough at a frequency just below the maximum heave excitation magnitude. The differences between the tab and T-foil plots appear to be strongly influenced by their respective longitudinal position on the hull. These characteristics will most certainly influence their use and effectiveness in a control strategy.

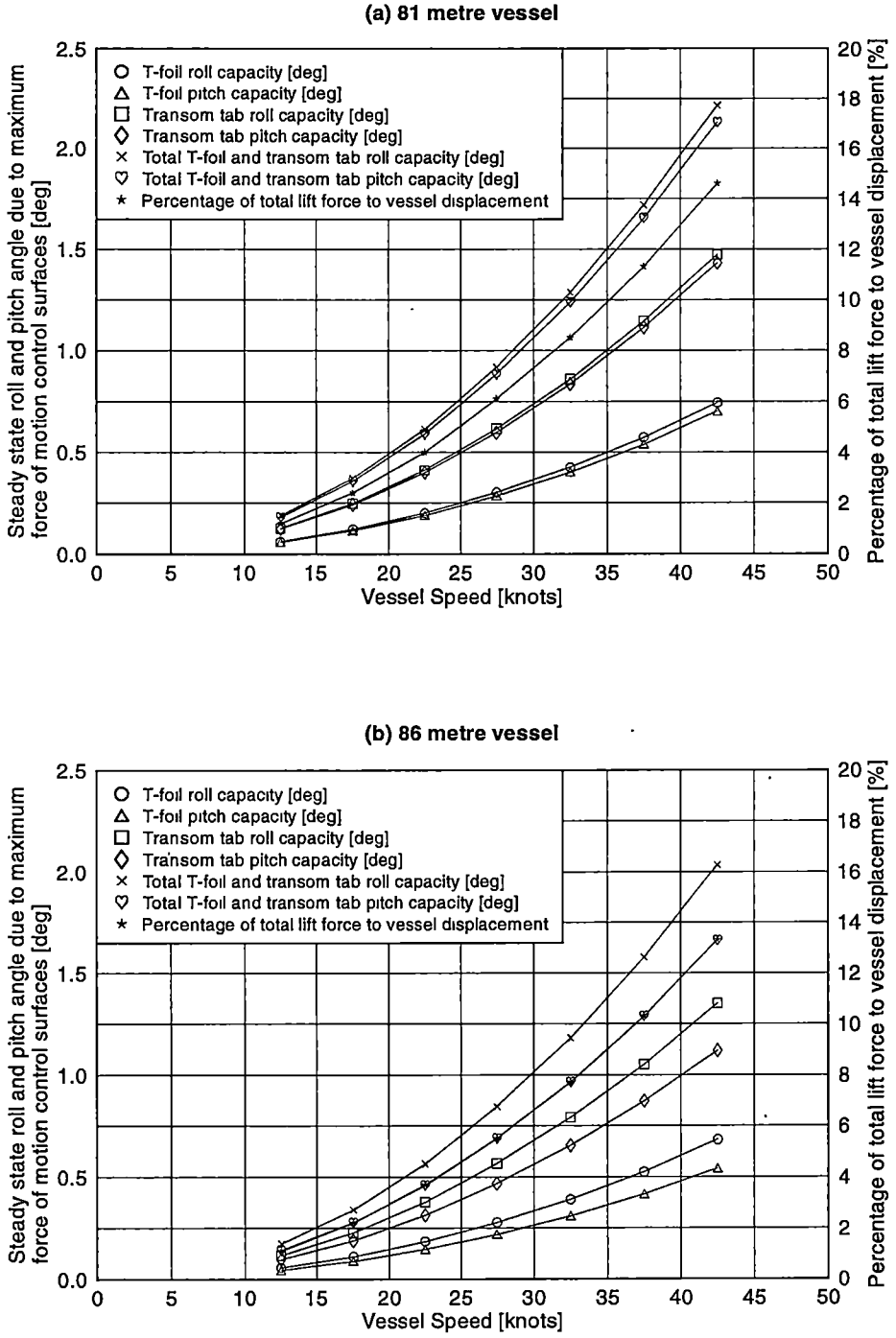

ref/MCD_force_capability(038 and 042) gle

Figure 3.2: Steady state roll and pitch angle due to the maximum deflection force of the motion control surfaces for the (a) 81 metre and (b) 86 metre vessel on free surface with no incident waves at a range of forward speeds (Full load in service departure conditions of 1138t and 1251t respectively). Calculation based only on hull parameters independant of BESTSEA output.

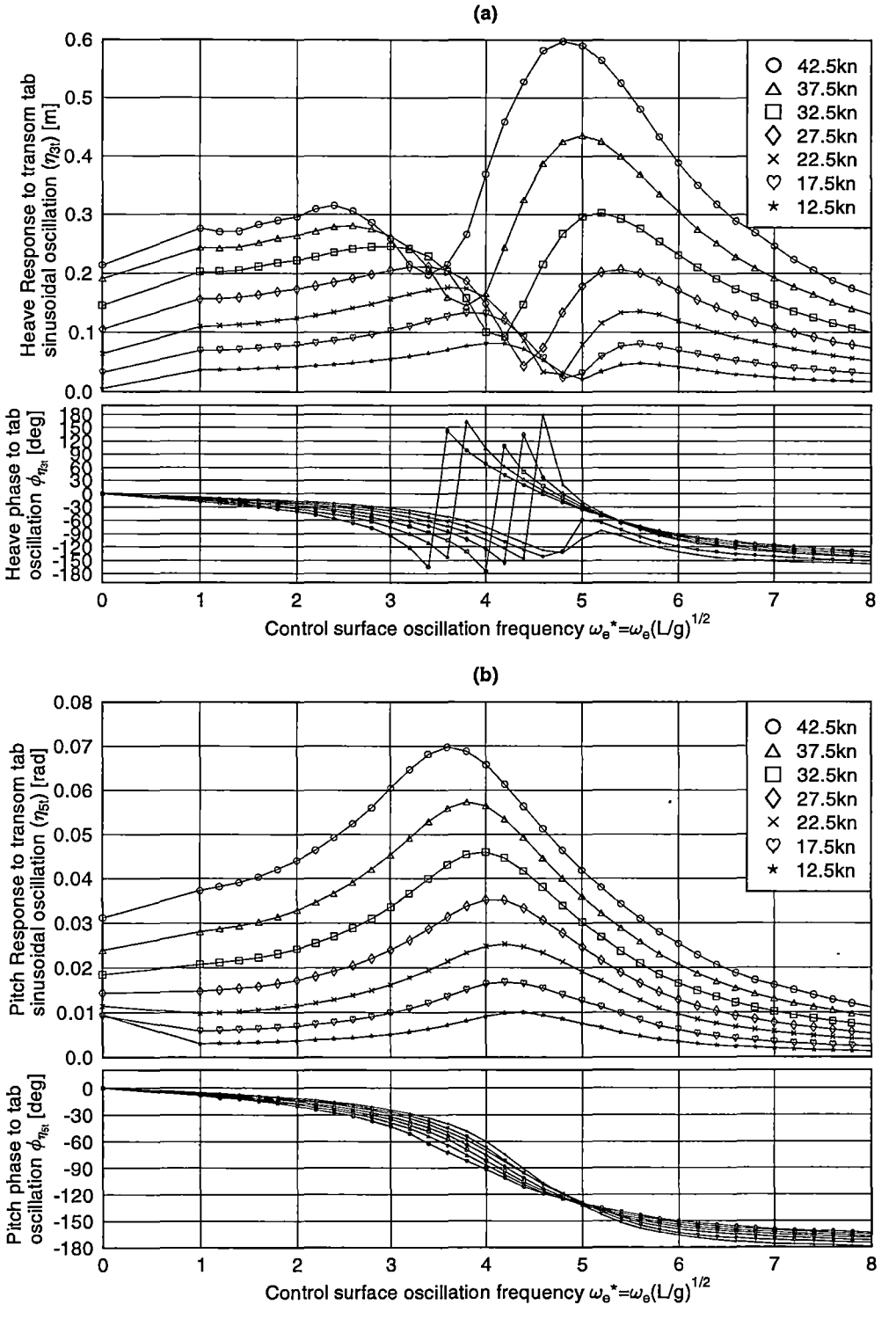

Figure 3.3: 86 metre vessel response at forward speed in (a) heave and (b) pitch to sinusoidal transom tab excitation (no T-foil) on free surface with no incident waves . When $\omega_e^* = 0$, surface is at full deflection ($\delta = 12°$, where mean position is $\delta = 6°$).

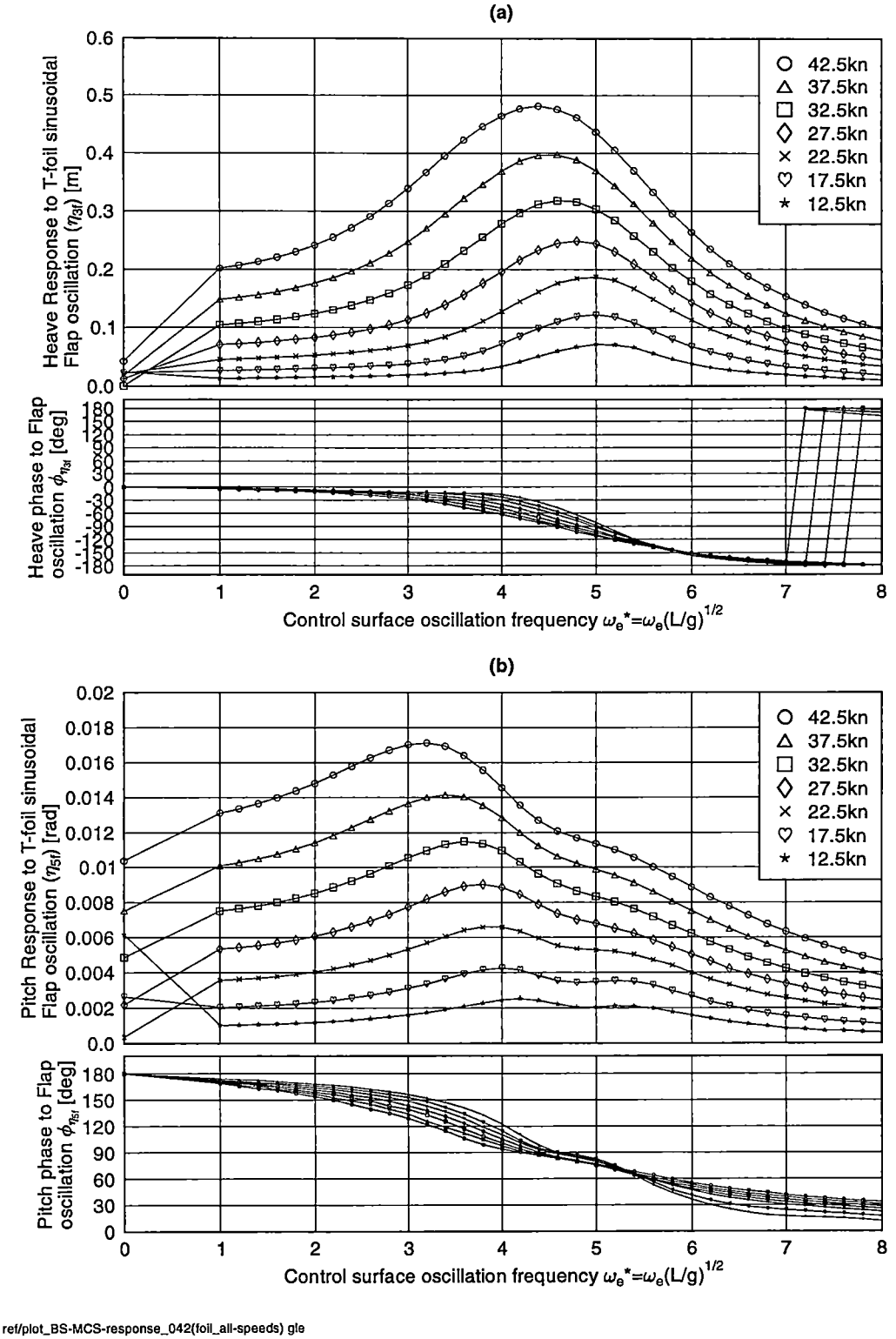

ref/plot_BS-MCS-response_042(foil_all-speeds) gle

Figure 3.4: 86 metre vessel response at forward speed in (a) heave and (b) pitch to sinusoidal T-foil flap excitation (no transom tab) on free surface with no incident waves. When $\omega_e^* = 0$, surface is at full deflection ($\bar{\delta} = 8°$, where mean position is $\delta = 0°$).

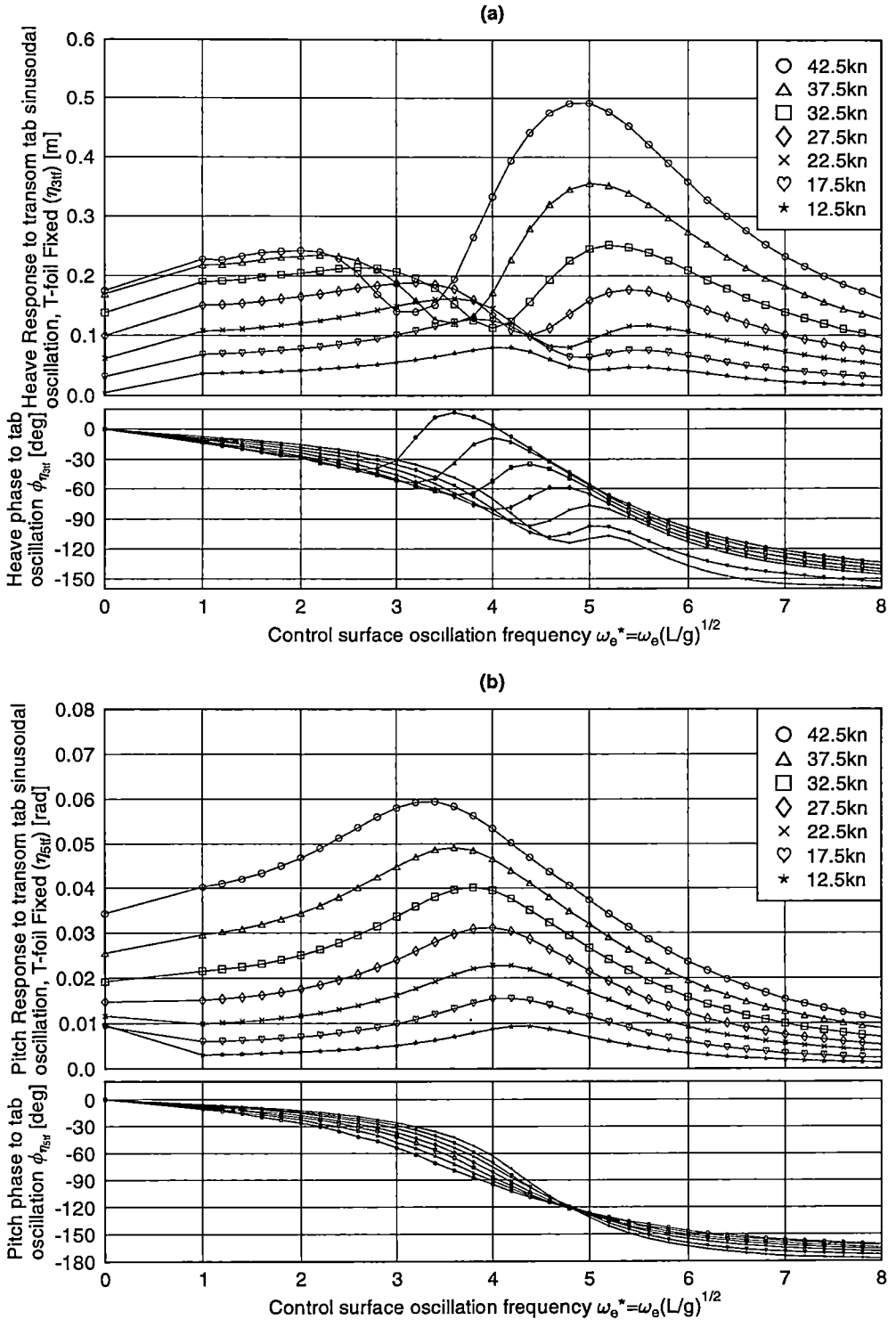

Figure 3.5: 86 metre vessel response at forward speed in (a) heave and (b) pitch to sinusoidal transom tab excitation with a fixed T-foil on free surface with no incident waves. When $\omega_e^* = 0$, surface is at full deflection ($\delta = 12°$, where mean position is $\delta = 6°$).

3.4.7 Motion Control Method

Each motion control device in the BESTSEA numerical computation had its unsteady deflection controlled though a feedback control algorithm based on the computed heave and pitch motions. These motions each comprised displacement, velocity and acceleration that were selected and weighted to achieve the desired flap deflection magnitude. Using these variables with appropriate gain settings, the deflection ($\delta_i(t)$) in time of the transom tab or T-foil flap was expressed as

$$\delta_i(t) = \sum_{j=1}^{6} K_{\ddot{\eta}_j i}\ddot{\eta}_j + K_{\dot{\eta}_j i}\dot{\eta}_j + K_{\eta_j i}\eta_j \tag{3.33}$$

where $K_{\ddot{\eta}_{j_i}}$, $K_{\dot{\eta}_{j_i}}$ and $K_{\eta_{j_i}}$ represent the gain values assigned to the acceleration $(\ddot{\eta}_j)$, velocity $(\dot{\eta}_j)$ and displacement (η_j) of the j^{th} degree of freedom of the i^{th} control surface respectively.

Selection of the appropriate gain settings is an iterative process where ship installed systems usually rely on an adaptive control algorithm. Real time control systems generally operate on the principle of adaptive gain control to achieve the best motion reduction based on a motion criterion objective function. With a modern control system and sufficient force capability it would be possible to minimise any one motion criterion from of a range of possible criteria. This task becomes more complex in an irregular sea where the control system must respond to and manage a range of frequency responses and degrees of freedom of motion created by the wave environment. This study does not have the scope to investigate this area thoroughly, particularly since only head seas were modelled, but it is reasonable to assume that given the relatively small force capability of the motion control devices it should be possible to obtain a practical idea of the level of motion reduction obtained by the use of these devices. In particular, the use of transom tabs and forward mounted T-foils were modelled in a range of combinations.

3.4.7.1 Motion Criterion

To determine the mode of operation for the motion control surfaces that would reduce the vessel motions to the largest extent, a motion criterion was defined as the average vertical acceleration over the longitudinal extent of the hull between the aft and forward perpendiculars. This averaging was determined over five equally spaced positions between the aft and forward perpendiculars in addition to the longitudinal centre of gravity position. When the average vertical acceleration had reached a minimum whilst varying the gains for the control surface actuator then it was clear that an optimum setting had been achieved.

3.4.7.2 Gain Finding Routine

To determine appropriate gain settings for each control surface whilst keeping iterations to a manageable level, a procedure has been devised that was well suited to the frequency domain in which the results were presented. Owing to the number of variables required for each control surface, a reduced number of forward speeds from the original seven are presented for this part of the analysis.

The selection of an appropriate control philosophy presents a number of options. Displacement feed back may be well suited for active motion control if the oscillations of the hull due to the waves always occurred about the calm water zero speed hydrostatic

condition. However, the hull sinkage and trim that occurs with forward speed would create a proportional offset demand in the control algorithm causing the motion control surfaces to exert a force to correct this condition of natural trim. This type of control most certainly has application where static heel or trim angles require correction or on hydrofoils, where ride height is important. Velocity or acceleration feedback for a displacement vessel would therefore be a more appropriate mechanism for control. Whilst acceleration creates the most crew and passenger discomfort it is uncertain that this signal alone would be appropriate for control. Davis and Holloway (2003a) were able to show through comparison of transfer function magnitudes that operating the controls in proportion to the local acceleration of the control surface they were unable to achieve any significant improvement in the magnitude and frequency of the maximum transfer function points. It will be shown in the results of this analysis that reducing the peaks of the motion transfer functions in heave and pitch may not alone guarantee the greatest motion reduction for a given sea spectrum that may have its peak located at different frequency. Therefore, the basis for motion reduction should be on the motion response. This ensures the effect of the sea spectrum at its modal frequency is considered in combination with the vessel transfer functions. In fact this is the practical basis on which ship adaptive control algorithms operate. As the wave conditions vary so too will the controller to achieve the best outcome based on its control philosophy. Davis and Holloway (2003a) were also able to show that operating the controls in proportion to the local velocity of the control surface they were able to achieve a greater reduction in the magnitude of the maximum transfer function points. Therefore, the basis of control for this analysis assumed a procedure based on velocity feedback whilst also making some comparisons (see chapter 5) based on the method of Davis and Holloway (2003a) comprising local velocity and acceleration feedback.

For a hull encountering long crested head sea waves at a particular frequency (ω_e), the deflection of a motion control device in time can be defined as a function of the heave and pitch velocity

$$\begin{aligned}
\delta_i(t) &= K_{\dot{\eta}_3 i}\frac{d\eta_3}{dt} + K_{\dot{\eta}_5 i}\frac{d\eta_5}{dt} \\
&= K_{\dot{\eta}_3 i}(\bar{\eta}_3\omega_e)\cos(\omega_e t + \varepsilon_{3v}) + K_{\dot{\eta}_5 i}(\bar{\eta}_5\omega_e)\cos(\omega_e t + \varepsilon_{5v}) \\
&= \cos(\omega_e t)\left[K_{\dot{\eta}_3 i}(\bar{\eta}_3\omega_e)\cos(\varepsilon_{3v}) + K_{\dot{\eta}_5 i}(\bar{\eta}_5\omega_e)\cos(\varepsilon_{5v})\right] \\
&\quad -\sin(\omega_e t)\left[K_{\dot{\eta}_3 i}(\bar{\eta}_3\omega_e)\sin(\varepsilon_{3v}) + K_{\dot{\eta}_5 i}(\bar{\eta}_5\omega_e)\sin(\varepsilon_{5v})\right]
\end{aligned} \tag{3.34}$$

where $K_{\dot{\eta}_3 i}$ and $K_{\dot{\eta}_5 i}$ are the respective heave and pitch velocity gains for the i^{th} control surface. $\bar{\eta}_3$ and $\bar{\eta}_5$ are the respective heave and pitch displacement amplitudes of the hull calculated at the wave amplitude of the numerical computation. $\bar{\eta}_3\omega_e$ and $\bar{\eta}_5\omega_e$ are the heave and pitch velocity amplitudes. ε_{3v} and ε_{5v} are the respective heave and pitch velocity phases that correspond with the heave and pitch velocity amplitudes such that $\varepsilon_{3v} = \varepsilon_3 + \frac{\pi}{2}$ and $\varepsilon_{5v} = \varepsilon_5 + \frac{\pi}{2}$ where ε_3 and ε_5 are the heave and pitch displacement phases.

Introducing two new variables, X_i and Y_i and setting them equal to two respective components of equation 3.34 and then converting the phases of velocity to phases of displacement, one obtains

$$\begin{aligned}
X_i &= \left[K_{\dot{\eta}_3 i}(\bar{\eta}_3\omega_e)\cos(\varepsilon_{3v}) + K_{\dot{\eta}_5 i}(\bar{\eta}_5\omega_e)\cos(\varepsilon_{5v})\right] \\
&= -K_{\dot{\eta}_3 i}(\bar{\eta}_3\omega_e)\sin(\varepsilon_3) - K_{\dot{\eta}_5 i}(\bar{\eta}_5\omega_e)\sin(\varepsilon_5)
\end{aligned} \tag{3.35}$$

$$\begin{aligned}
Y_i &= \left[K_{\dot{\eta}_3 i}(\bar{\eta}_3\omega_e)\sin(\varepsilon_{3v}) + K_{\dot{\eta}_5 i}(\bar{\eta}_5\omega_e)\sin(\varepsilon_{5v})\right] \\
&= K_{\dot{\eta}_3 i}(\bar{\eta}_3\omega_e)\cos(\varepsilon_3) + K_{\dot{\eta}_5 i}(\bar{\eta}_5\omega_e)\cos(\varepsilon_5)
\end{aligned} \tag{3.36}$$

such that equation 3.34 now becomes

$$\begin{aligned}\delta_i(t) &= X_i\cos(\omega_e t) - Y_i\sin(\omega_e t) \\ &= \sqrt{X_i^2+Y_i^2}\left[\cos(\omega_e t)\frac{X_i}{\sqrt{X_i^2+Y_i^2}} - \sin(\omega_e t)\frac{Y_i}{\sqrt{X_i^2+Y_i^2}}\right] \end{aligned} \quad (3.37)$$

The oscillation of the i^{th} control surface in regular waves will be of the form

$$\begin{aligned}\delta_i(t) &= \bar{\delta}_i\cos(\omega_e t+\phi_i) \\ &= \bar{\delta}_i\left[\cos(\omega_e t)\cos(\phi_i) - \sin(\omega_e t)\sin(\phi_i)\right] \end{aligned} \quad (3.38)$$

where $\bar{\delta}_i$ is the amplitude of oscillation or maximum deflection permitted by the mechanical arrangement of the control surface and ϕ_i is the oscillation phase angle of the control surface.

It can be seen that equations 3.37 and 3.38 are of similar form where $\bar{\delta}_i = \sqrt{X_i^2+Y_i^2}$, $\cos(\phi_i) = \frac{X_i}{\sqrt{X_i^2+Y_i^2}}$ and $\sin(\phi_i) = \frac{Y_i}{\sqrt{X_i^2+Y_i^2}}$. Therefore, by simple geometry

$$X_i = \bar{\delta}_i\cos(\phi_i) \quad (3.39)$$

$$Y_i = \bar{\delta}_i\sin(\phi_i) \quad (3.40)$$

and so $\phi_i = \arctan\left(\frac{Y_i}{X_i}\right)$ leads to the control surface phase (ϕ_i).

Also, one can conclude that the deflection of the control surface can be expressed as

$$\delta_i(t) = \sqrt{X_i^2+Y_i^2}\cos(\omega_e t+\phi_i) \quad (3.41)$$

where X_i and Y_i can be described as the abscissa and ordinate values in the phase plane that depicts the control surface's oscillation.

Equating equations 3.35 with 3.39 and 3.36 with 3.40, X_i and Y_i can be expressed as two simultaneous equations

$$\begin{aligned}\bar{\delta}_i\cos(\phi_i) &= -K_{\dot{\eta}_3 i}(\bar{\eta}_3\omega_e)\sin(\varepsilon_3) - K_{\dot{\eta}_5 i}(\bar{\eta}_5\omega_e)\sin(\varepsilon_5) \\ \bar{\delta}_i\sin(\phi_i) &= K_{\dot{\eta}_3 i}(\bar{\eta}_3\omega_e)\cos(\varepsilon_3) + K_{\dot{\eta}_5 i}(\bar{\eta}_5\omega_e)\cos(\varepsilon_5) \end{aligned} \quad (3.42)$$

Except for the control surface deflection amplitude $\bar{\delta}_i$, all variables in these equations are unknown and can only be determined through iteration. However, by considering each motion control surface independently the iterations can be greatly reduced. Using a previously computed hull motion solution that represents as near as possible the active motion control surface configuration under consideration, the variables $(\bar{\eta}_3\omega_e)$, $(\bar{\eta}_5\omega_e)$, ε_3 and ε_5 for a particular wave amplitude (ζ_0) and encounter frequency (ω_e) can be estimated. For example, a computation involving an active transom tab only can have the variables $(\bar{\eta}_3\omega_e)$, $(\bar{\eta}_5\omega_e)$, ε_3 and ε_5 estimated by initially adopting the results from a previously determined motion solution that has no control surfaces (bare hull). Similarly, a computation involving an active T-foil only can have the variables $(\bar{\eta}_3\omega_e)$, $(\bar{\eta}_5\omega_e)$, ε_3 and ε_5 estimated by initially adopting the results from a previously determined fixed T-foil solution. Any subsequent iterations conducted after this first iteration to obtain a better result can thereafter make use of a similar configuration. A full list of these relationships that can be applied in the first iteration are shown in table 3.2.

Solving the equations of 3.42, a value for $K_{\dot{\eta}_3 i}$ can be determined with

Active MCS configuration	Suggested 1st iteration estimation solution ("seed file")
Transom tab	Without control surfaces (bare hull)
Transom tab (fixed T-foil)	Fixed transom tab, fixed T-foil
T-foil	Fixed transom tab, fixed T-foil
Transom tab and T-foil	Fixed transom tab, fixed T-foil

Table 3.2: Previous motion solution used to estimate the variables of active motion control configuration

$$K_{\dot{\eta}_3 i} = \frac{\left(\frac{\bar{\delta}\cos(\phi_i)}{(\bar{\eta}_5\omega_e)\sin(\varepsilon_5)} + \frac{\bar{\delta}\sin(\phi_i)}{(\bar{\eta}_5\omega_e)\cos(\varepsilon_5)}\right)}{\left(\frac{(\bar{\eta}_3\omega_e)\cos(\varepsilon_3)}{(\bar{\eta}_5\omega_e)\cos(\varepsilon_5)} - \frac{(\bar{\eta}_3\omega_e)\sin(\varepsilon_3)}{(\bar{\eta}_5\omega_e)\sin(\varepsilon_5)}\right)} \tag{3.43}$$

and by substitution of $K_{\dot{\eta}_3 i}$ a value of $K_{\dot{\eta}_5 i}$ from

$$K_{\dot{\eta}_5 i} = \frac{\bar{\delta}\sin(\phi_i) - K_{\dot{\eta}_3 i}(\bar{\eta}_3\omega_e)\cos(\varepsilon_3)}{(\bar{\eta}_5\omega_e)\cos(\varepsilon_5)} \tag{3.44}$$

With the variables $(\bar{\eta}_3\omega_e)$, $(\bar{\eta}_5\omega_e)$, ε_3, ε_5 estimated and $\bar{\delta}_i$ known, multiple values of the heave and pitch gains $K_{\dot{\eta}_3 i}$ and $K_{\dot{\eta}_5 i}$ can be determined by substituting a range of motion control surface oscillation phase angles (ϕ_i) from 0 to 360 degrees in 45 degree increments for ϕ_i. Within this range, all the resulting values of the defined motion response criterion when plotted against the calculated phase angle ϕ_i, created a wave form of one cycle.

An example of the typical results of this procedure are shown in figures 3.8 and 3.9. In figure 3.8, the value on which an improvement is sought is shown as a horizontal line and represents the maximum average acceleration spectral response value. This value has been extracted from the response spectrum ("seed file") used for the initial estimation of the hull response with a motion control surface (see table 3.2). For example, the value in figure 3.8(a) which is the hull response to various tab oscillations of various phases corresponds with the peak of the acceleration response without control surfaces shown in figure 5.22(a). The polynomial curve has been fitted to the various acceleration response values of different phases (ϕ_i). Only one phase angle along this curve represents a maximum motion response where the transom tab or the T-foil was amplifying the hull motions and one phase represents a minimum where the same control surface was reducing the hull motions. It was found that 45 degree increments of the phase angle ϕ_i provided sufficient data points in the range of 0 to 360 degrees to position a curve of best fit between the data points from which the phase angle ϕ_i coinciding with the point of minimum motion could be extracted.

Whilst obtaining the correct phase angle ϕ_i is a relatively precise procedure, this value is only required for the purpose of directly calculating the unique gains values $K_{\dot{\eta}_3 i}$ and $K_{\dot{\eta}_5 i}$. By now reapplying these newly found gain values to a solution that not only consists of the single nominated frequency but to the full range of wave encounter frequencies using the corresponding "seed" file (to estimate the values of $(\bar{\eta}_3\omega_e)$, $(\bar{\eta}_5\omega_e)$, ε_3, ε_5), a solution with an active control surface may be obtained. Such results are presented in chapter 5 together all other computational results.

Once a computation using the optimised gain values $(K_{\dot{\eta}_3 i}$ and $K_{\dot{\eta}_5 i})$ for the active surface is completed, the resulting motions and phases would clearly differ to those initially assumed from the "seed" file. This implies that the resulting oscillation phase

angle of the i^{th} control surface (ϕ_i) may also change by a small amount from the value initially used to calculate the most appropriate gain values ($K_{\dot{\eta}_3 i}$ and $K_{\dot{\eta}_5 i}$). This will most likely be the case, especially since only one iteration has been conducted. However, after a new active motion control solution is obtained, a new value of ϕ_i can be calculated using the newly calculated values of ($\bar{\eta}_3\omega_e$), ($\bar{\eta}_5\omega_e$) , ε_3, ε_5 combined with the existing gain values of $K_{\dot{\eta}_3 i}$ and $K_{\dot{\eta}_5 i}$ using equations 3.35, 3.36 and either equation 3.39 or 3.40. Should there be a dramatic variation, further iterations to obtain a more correct motion response may be required.

Typical control installations on some ships operate with adaptive gain settings that are sensitive to the encountered wave period and significant wave height to maintain the optimum control system setting throughout their operation. In contrast, this analysis had the advantage of being based on the known vessel response to the selected wave environment and vessel forward speed and so the gain finding routine to target a specific wave environment could be implemented. The gain finding routine targeted a Bretschneider wave spectrum with an average wave spectral period of 7 seconds, as this produced one of the largest excitation responses in the vessel of any wave period[6] (see figure 5.25 in chapter 5). This wave period was the only one considered in all the computations that involved an active motion control system due to the necessary practical limitations placed on the scope of this analysis.

The gain finding routine focussed on reducing the motion response of the hull at the unique encounter frequency where the maximum hull response occurred. For example, at the forward speeds of 12.5 and 42.5 knots, the unique encounter frequency corresponded to a dimensionless frequency (ω_e^*) of 4 and 5 respectively for the Service-Full Departure loading condition (see also Average Acceleration Spectral Density response results in figure 5.20(a) for the 12.5 knot case and figure 5.23(a) for the 42.5 knot case)). Once the gain finding routine had been completed and a suitable phase angle (ϕ_i) identified at this unique encounter frequency, the heave and pitch gain values ($K_{\dot{\eta}_3 i}$ and $K_{\dot{\eta}_5 i}$) were held constant whilst solving the hull response for the remaining encounter frequencies. Thus, a complete solution with the selected heave and pitch gain values ($K_{\dot{\eta}_3 i}$ and $K_{\dot{\eta}_5 i}$) was conducted over the full range of wave encounter frequencies for each motion control device configuration. From the results, the complete heave and pitch motion transfer functions and phases were obtained for the active control system modelled.

This approach implied that whilst substituting a range of motion control surface oscillation phase angles (ϕ_i) and solving for the heave and pitch gain values ($K_{\eta_3 i}$ and $K_{\dot{\eta}_5 i}$), only a computation at one frequency was required to successfully complete the gain finding task[7]. This approach required 7 minutes per frequency at 42.5 knots, 9 minutes at 32.5 knots and 20 minutes per frequency at 12.5 knots, for one significant wave height and a single active control surface configuration. Overall this calculation required eight computations per speed and control surface so that on a computer running a 2.4 GHz CPU, the total computation could be executed in a time of 40 minutes

[6]The wave period selected is not critical, but should be indicative of the wave environment of interest. By selecting the wave period that caused the greatest response in the vessel, it was expected that greater motion reductions could be achieved in the selected example.

[7]Given the benefit of greater computing power or computation time, a better approach may be to minimize the average RMS acceleration rather than just the response for a single frequency. This would ensure the area under the response spectrum was minimized rather than just reducing the response peak at one frequency, although it is possible that a similar outcome would be achieved, but it is beyond the scope of this analysis to verify this. This implies that rather than conducting the gain finding routine at one frequency, all frequencies are solved for each substitution of the surface oscillation phase angle ϕ_i, thus increasing the computation time considerably. Since the wave energy spectra are quite narrow, the full spectral analysis was not considered essential at this stage.

for the higher speeds and up to 2 hours for the lower speeds.

This procedure was successfully completed for the 86 metre hull for each of its single active control surface configurations which included an active transom tab only, an active T-foil only and an active transom tab combined with a fixed (fixed flap) T-foil. Results obtained through only one iteration of this process at most speeds were encouraging where they provided a well defined solution of the required phase (ϕ_i), from which the gain values ($K_{\dot{\eta}_{3^i}}$ and $K_{\dot{\eta}_{5^i}}$) were calculated. A list of these values used for 0.5 metre regular wave height computations are shown in table 3.3 for two loading conditions of the computed 86 metre vessel. Shown is the estimated phase calculated with the use of the seed file and the corresponding heave ($K_{\dot{\eta}_{3^i}}$) and pitch ($K_{\dot{\eta}_{5^i}}$) gain values. The actual phase achieved with these gain values and the new motion solution after the first iteration are also shown together with a column showing the difference between the estimated phase and the actual phase achieved. Further iterations using the new data may produce better convergence of the solution, but in general this was not conducted because the result after only one iteration had reasonable convergence, so a significant improvement in the transfer functions or response spectra was not expected. To show this, a second iteration was conducted with an active transom tab configuration and the results are shown in table 3.4. The change in the phase angle was approximately 25° but a significant difference was not seen in the heave and pitch transfer functions shown in figure 3.6. In addition, the phase values used for 2.5 metre regular wave height computations are shown in table 3.5.

The general transfer functions obtained with active controls calculated by this method are shown in figures 5.8 to 5.13 of chapter 5 where they are also discussed.

This approach essentially resembled a simplified ship system that could be adapted either manually or automatically to provide the maximum motion attenuation in a given wave environment of a given wave height and period. Should the wave environment change, so too would the gains of the controller be required to change to maintain its optimum settings, as both the wave height and period would affect the gains of a well tuned control system. The wave height will also affect the proportion of force that can be delivered by a motion control device, which will influence the shape of the corresponding transfer functions. Thus, a transfer function generated by this process for a hull fitted with any form of motion control surface whether fixed or active, must also reference both the wave spectrum and the corresponding regular wave amplitude to which it applies. In particular for the controlled surface this implies that the wave amplitude at which full deflection of the control surfaces is attained should be stated for the result to be meaningful. This may also be true for a hull without control surfaces solution when there is a variation in hull cross section moving through the free surface in time that essentially removes the linearity assumption over the broad range of wave heights as could be the case with BESTSEA if the solution is applied to large wave heights. If the linearity assumption implied with the use of transfer functions begins to break down then a comparison with experimental data of various wave height becomes difficult whilst remaining with a frequency domain approach.

The remaining task was to apply control gains to the hull with two motion control surfaces combined, namely the configuration of a transom tab and a forward mounted T-foil. A similar procedure was adopted to determine the optimum phase for each surface in which all combinations of control surface phases were calculated. This amounted to 64 combinations that were computed where each control surface had a range of set phase angles (ϕ_i) of 0 to 360 degrees in increments of 45 degrees. The output of these solutions used to determine the optimum phase are shown in figure 3.9 where the plots shown are effectively a two-dimensional representation of a three-dimensional solution space in

"Service-Full departure" load condition						
Applied MCS	Speed [kn]	Initial phase estimate (φ_i) [deg]	Heave velocity gain ($K_{\eta 3i}$)	Pitch velocity gain ($K_{\eta 5i}$)	Actual phase achieved (φ_i) [deg]	Difference between actual and estimated phase [deg]
Active tabs						
tab	12.5	121.1	-0.2177	-1.0681	120.3	-0.8
tab	22.5	147.6	-16.9040	-287.2440	136.5	-11.1
tab	32.5	111.8	-0.0452	-2.6962	115.5	3.7
tab	42.5	112.9	-0.0401	-2.8694	118.7	5.8
Active T-foil						
T-foil	12.5	-67.3	0.5271	0.8460	-65.9	1.4
T-foil	22.5	-67.3	-0.1419	1.1044	-67.8	-0.5
T-foil	32.5	-91.8	-0.0470	2.2947	-90.7	1.2
T-foil	42.5	-98.7	-0.0455	2.9756	-97.3	1.4
Active tab, fixed T-foil						
tab	12.5	124.3	-0.2635	-1.0450	123.4	-0.9
tab	22.5	116.8	0.0118	-1.7120	117.8	1.0
tab	32.5	120.9	-0.0569	-3.0455	125.1	4.1
tab	42.5	125.0	-0.0522	-3.1817	130.5	5.5
Active tab and T-foil						
tab	32.5	124.6	-0.0666	-3.1384	128.7	4.1
T-foil	32.5	-100.4	-0.0783	1.6807	-99.8	0.6

"Delivery-10% arrival" loading condition						
Applied MCS	Speed [kn]	Initial phase estimate (φ_i) [deg]	Heave velocity gain ($K_{\eta 3i}$)	Pitch velocity gain ($K_{\eta 5i}$)	Actual phase achieved (φ_i) [deg]	Difference between actual and estimated phase [deg]
Active tabs						
tab	12.5	-174.5	0.0124	-2.3323	175.9	350.4
tab	22.5	157.4	0.0650	-1.9915	148.7	-8.7
tab	32.5	116.9	-0.0590	-2.8757	123.3	6.4
tab	42.5	113.6	0.0729	-0.8379	81.4	-32.2
Active T-foil						
T-foil	12.5	13.4	-2.5954	17.8788	8.4	-5.0
T-foil	22.5	-61.6	1.5687	4.3376	-48.7	12.9
T-foil	32.5	-81.6	-0.2093	0.9119	-84.1	-2.5
T-foil	42.5	-89.1	-0.0884	2.2320	-90.4	-1.3
Active tab, fixed T-foil						
tab	12.5	179.5	0.5409	-5.1745	-179.6	-359.1
tab	22.5	200.6	2.6568	2.3260	175.8	-24.8
tab	32.5	124.6	-0.0352	-2.6428	128.5	3.9
tab	42.5	123.5	-0.0356	-3.0629	129.8	6.3

Table 3.3: Motion control surface phase (ϕ_i) estimated prior to first iteration and actual phase (ϕ_i) achieved after the first iteration with the corresponding heave ($K_{\dot{\eta}_3 i}$) and pitch ($K_{\dot{\eta}_5 i}$) gain values calculated for the two loading conditions considered (86m vessel, Regular wave height of computation was 0.5m)

"Service-Full departure" load condition						
Applied MCS	Speed [kn]	Initial phase estimate (φ_i) [deg]	Heave velocity gain ($K_{\eta 3i}$)	Pitch velocity gain ($K_{\eta 5i}$)	Actual phase achieved (φ_i) [deg]	Difference between actual and estimated phase [deg]
Active tabs						
tab	32.5	116.1	-0.0660	-3.8607	91.2	-24.9

Table 3.4: Motion control surface phase (ϕ_i) estimated prior to second iteration and actual phase (ϕ_i) achieved after the second iteration with the corresponding heave ($K_{\dot{\eta}_3 i}$) and pitch ($K_{\dot{\eta}_5 i}$) gain values calculated for the two loading conditions considered (86m vessel, Regular wave height of computation was 0.5m)

"Service-Full departure" load condition						
Applied MCS	Speed [kn]	Initial phase estimate (φ_i) [deg]	Heave velocity gain ($K_{\eta 3i}$)	Pitch velocity gain ($K_{\eta 5i}$)	Actual phase achieved (φ_i) [deg]	Difference between actual and estimated phase [deg]
Active tabs						
tab	32.5	116.8	-0.0106	-0.8078	117.7	0.9
Active T-foil						
T-foil	32.5	-135.8	-0.0237	0.2636	-135.7	0.0
Active tab, fixed T-foil						
tab	32.5	129.7	-0.0143	-0.7823	131.1	1.4
Active tab & T-foil						
tab	32.5	129.7	-0.0143	-0.7823	126.4	-3.3
T-foil	32.5	-135.8	-0.0237	0.2636	-135.7	0.1

Table 3.5: Motion control surface phase (ϕ_i) estimated prior to first iteration and actual phase (ϕ_i) achieved after the first iteration with the corresponding heave ($K_{\dot{\eta}_3 i}$) and pitch ($K_{\dot{\eta}_5 i}$) gain values calculated for the one loading condition considered (86m vessel, Regular wave height of computation was 2.5m)

which the task was to determine the minimum. Results from this exercise shown in table 3.3 demonstrate that the calculated phases of this configuration did not significantly vary from those obtained when the control surfaces were considered independently. For example, referring to the "actual phase achieved" column of table 3.3 for the active tab configuration shows the calculated value to be 125.1°, compared with the solution with two control surfaces of 128.7°. Similarly, the T-foil result gave -90.7° for the single surface and -99.8° when combined with the tab. The difference these phases produce in the heave and pitch transfer functions are shown in figure 3.7. Therefore, the phase and gain values obtained for each control surface independently were also adopted as the gains for the multiple control surface configurations. Furthermore, conducting iterations with two independent controls would enormously increase the computational effort, only to achieve an outcome that would not necessarily improve the results and aim of this exercise, which was to approximate the best solution of minimum average vertical acceleration.

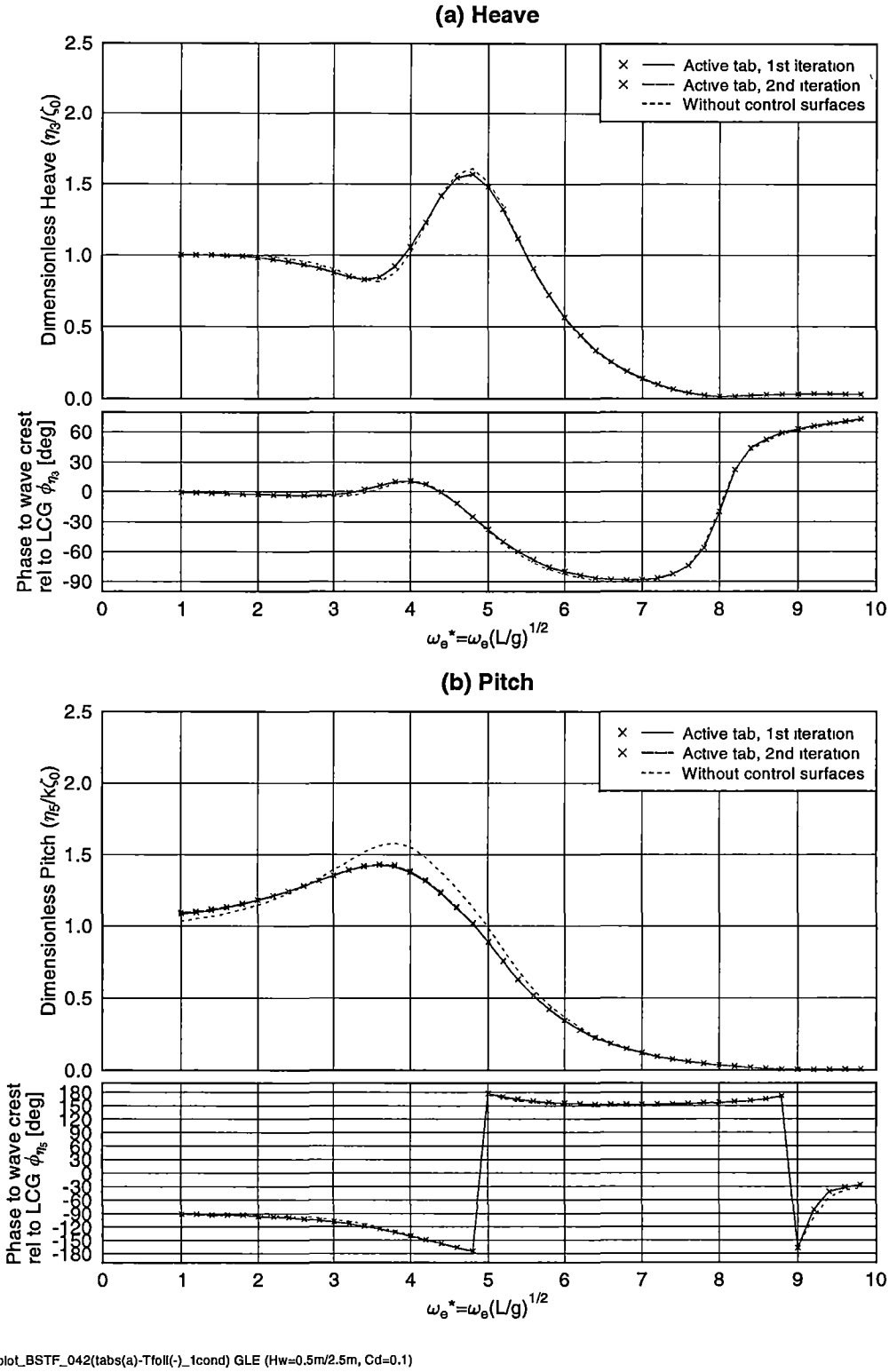

Figure 3.6: Variation in heave and pitch transfer functions between 1 and 2 iterations of the gain finding routine (86m vessel, 32.5kn, active tab only, Loading condition: Service-Full departure)

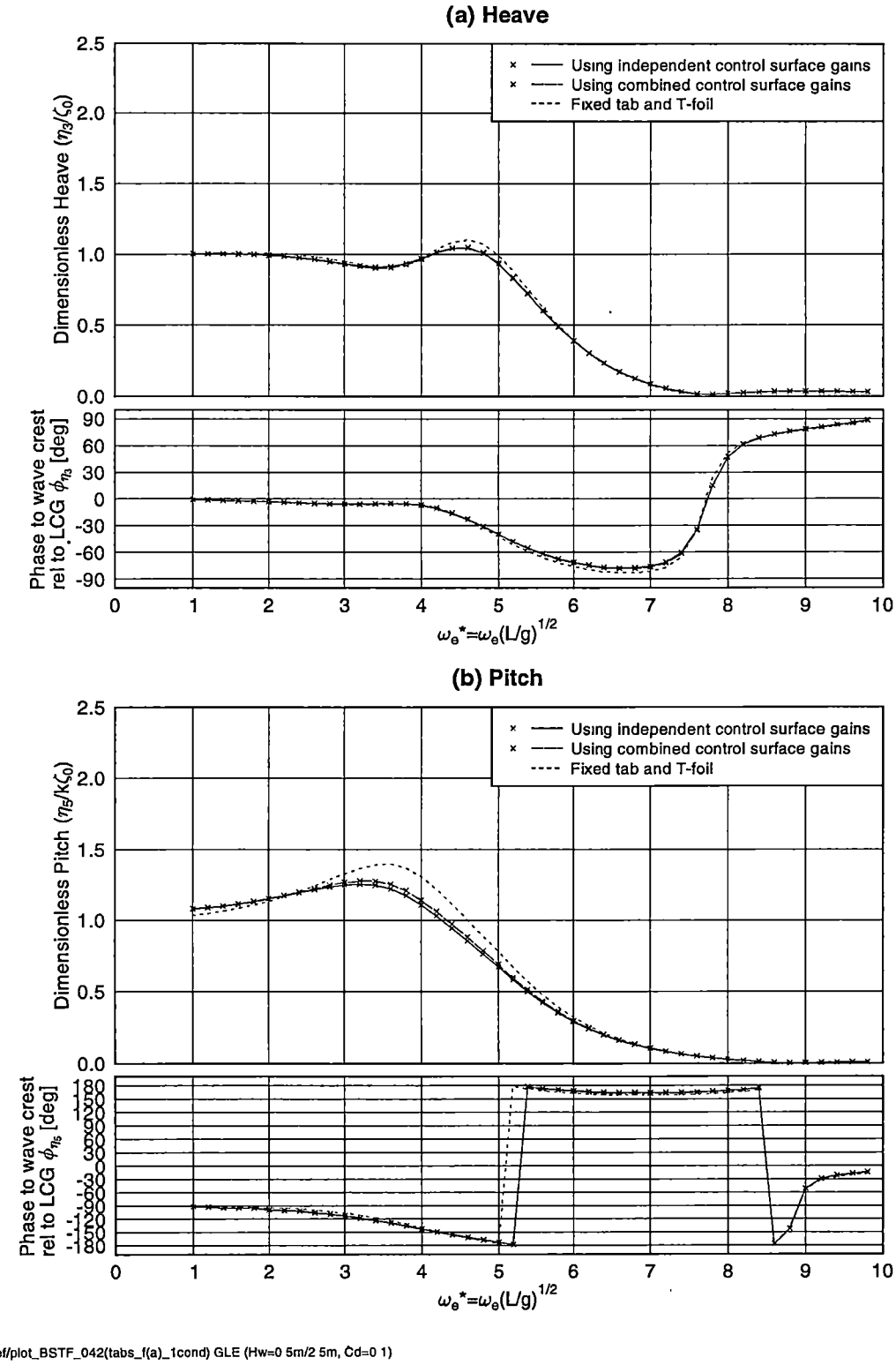

Figure 3.7: Variation in heave and pitch transfer functions (86m vessel, 32.5kn) for active tab and T-foil configuration when gains are determined for individual surfaces or combined. (Result after one iteration; Loading condition: Service-Full departure).

3.4.7.3 Local Velocity or Local Acceleration Based Feedback Control?

Local Velocity Based Feedback A motion control system approach proposed for high speed passenger vessels has been based on the force of the control surface (in the case of a transom tab or T-foil) opposing or acting 180° out of phase with the vertical velocity as calculated at the position of the motion control surface (see Haywood (1995)). To apply this particular method and determine how it compares with the procedure implemented in this analysis, the vertical velocity $\left(\dot{\xi}_i(t)\right)$ at the position of the control surface in terms of heave (η_3) and pitch (η_5) for waves encountered on the bow, can be expressed following a similar procedure to that given previously to give

$$\begin{aligned}
\dot{\xi}_i(t) &= \frac{d\eta_3}{dt} - x\frac{d\eta_5}{dt} \\
&= (\bar{\eta}_3\omega_e)\cos(\omega_e t + \varepsilon_{3v}) - x(\bar{\eta}_5\omega_e)\cos(\omega_e t + \varepsilon_{5v}) \\
&= \cos(\omega_e t)\left[(\bar{\eta}_3\omega_e)\cos(\varepsilon_{3v}) - x(\bar{\eta}_5\omega_e)\cos(\varepsilon_{5v})\right] \\
&\quad - \sin(\omega_e t)\left[(\bar{\eta}_3\omega_e)\sin(\varepsilon_{3v}) - x(\bar{\eta}_5\omega_e)\sin(\varepsilon_{5v})\right]
\end{aligned} \tag{3.45}$$

where $\bar{\eta}_3$ and $\bar{\eta}_5$ are the respective heave and pitch displacement amplitudes of the hull calculated at the wave amplitude of the numerical computation. $\bar{\eta}_3\omega_e$ and $\bar{\eta}_5\omega_e$ are the heave and pitch velocity amplitudes. ε_{3v} and ε_{5v} are the respective heave and pitch velocity phases such that $\varepsilon_{3v} = \varepsilon_3 + \frac{\pi}{2}$ and $\varepsilon_{5v} = \varepsilon_5 + \frac{\pi}{2}$ where ε_3 and ε_5 are the heave and pitch displacement phases. x is the distance between the LCG and the centre of lift of the control surface (+ve forward). There is no need for an overall gain to be included as the object of this analysis is to obtain the phase of the control surface oscillation as a result of this method.

Introducing two new variables, X_{v_i} and Y_{v_i} and setting them equal to two respective components of equation 3.45 and then converting the phases of velocity to phases of displacement, one obtains

$$\begin{aligned}
X_{v_i} &= \left[(\bar{\eta}_3\omega_e)\cos(\varepsilon_{3v}) - x(\bar{\eta}_5\omega_e)\cos(\varepsilon_{5v})\right] \\
&= -(\bar{\eta}_3\omega_e)\sin(\varepsilon_3) + x(\bar{\eta}_5\omega_e)\sin(\varepsilon_5) \qquad (3.46) \\
Y_{v_i} &= \left[(\bar{\eta}_3\omega_e)\sin(\varepsilon_{3v}) - x(\bar{\eta}_5\omega_e)\sin(\varepsilon_{5v})\right] \\
&= (\bar{\eta}_3\omega_e)\cos(\varepsilon_3) - x(\bar{\eta}_5\omega_e)\cos(\varepsilon_5) \qquad (3.47)
\end{aligned}$$

such that equation 3.45 now becomes

$$\begin{aligned}
\dot{\xi}_i(t) &= X_{v_i}\cos(\omega_e t) - Y_{v_i}\sin(\omega_e t) \\
&= \sqrt{X_{v_i}^2 + Y_{v_i}^2}\left[\cos(\omega_e t)\frac{X_{v_i}}{\sqrt{X_{v_i}^2 + Y_{v_i}^2}} - \sin(\omega_e t)\frac{Y_{v_i}}{\sqrt{X_{v_i}^2 + Y_{v_i}^2}}\right]
\end{aligned} \tag{3.48}$$

The oscillation of the i^{th} control surface in regular waves will be of the form

$$\begin{aligned}
\dot{\xi}_i(t) &= \bar{\delta}_i\cos(\omega_e t + \phi_{v_i}) \\
&= \bar{\delta}_i\left[\cos(\omega_e t)\cos(\phi_{v_i}) - \sin(\omega_e t)\sin(\phi_{v_i})\right]
\end{aligned} \tag{3.49}$$

where $\bar{\delta}_i$ is the amplitude of oscillation or maximum deflection permitted by the mechanical arrangement of the control surface and ϕ_{v_i} is the phase of the hull vertical velocity at the location of the control surface.

It can be seen that equations 3.48 and 3.49 are of similar form where $\bar{\delta}_i = \sqrt{X_{v_i}^2 + Y_{v_i}^2}$, $\cos(\phi_{v_i}) = \frac{X_{v_i}}{\sqrt{X_{v_i}^2+Y_{v_i}^2}}$ and $\sin(\phi_{v_i}) = \frac{Y_{v_i}}{\sqrt{X_{v_i}^2+Y_{v_i}^2}}$. Therefore, by simple geometry

$$X_{v_i} = \bar{\delta}_i \cos(\phi_{v_i}) \tag{3.50}$$

$$Y_{v_i} = \bar{\delta}_i \sin(\phi_{v_i}) \tag{3.51}$$

Also, one can conclude that the deflection of the control surface can be expressed as

$$\dot{\xi}_i(t) = \sqrt{X_{v_i}^2 + Y_{v_i}^2} \cos(\omega_e t + \phi_{v_i}) \tag{3.52}$$

where X_{v_i} and Y_{v_i} can be described as the abscissa and ordinate values in the phase plane that depicts the vertical hull velocity at the location of the control surface.

The oscillation phase the control surface must adopt to oppose the local vertical hull velocity $\left(\dot{\xi}_i(t)\right)$ is therefore

$$\phi_{vi} = \arctan\left(\frac{Y_{v_i}}{X_{v_i}}\right) + \pi \tag{3.53}$$

where π is added to ensure the control surface force opposes the vertical velocity. (see discussion below in section 3.4.7.3)

Local Acceleration Based Feedback Whilst opposing the hull local vertical velocity with a control surface may provide effective damping at particular encounter frequencies and hull forward speeds, the question of whether acceleration instead of velocity could be an effective control philosophy for reducing hull motions remains. In this instance, the control would then effectively be increasing the system effective mass. In a similar approach to that presented above for local velocity based feedback, the oscillation phase angle solution of the control surface operated to oppose the local hull acceleration can be calculated through the expression

$$\begin{aligned} \ddot{\xi}_i(t) &= \frac{d^2\eta_3}{dt^2} - x\frac{d^2\eta_5}{dt^2} \\ &= \cos(\omega_e t)\left[\left(\bar{\eta}_3\omega_e^2\right)\cos(\varepsilon_{3a}) - x\left(\bar{\eta}_5\omega_e^2\right)\cos(\varepsilon_{5a})\right] \\ &\quad -\sin(\omega_e t)\left[\left(\bar{\eta}_3\omega_e^2\right)\sin(\varepsilon_{3a}) - x\left(\bar{\eta}_5\omega_e^2\right)\sin(\varepsilon_{5a})\right] \end{aligned} \tag{3.54}$$

where $\bar{\eta}_3$ and $\bar{\eta}_5$ are the respective heave and pitch displacement amplitudes of the hull calculated at the wave amplitude of the numerical computation. $\bar{\eta}_3\omega_e^2$ and $\bar{\eta}_5\omega_e^2$ are the heave and pitch acceleration amplitudes. ε_{3a} and ε_{5a} are the respective heave and pitch acceleration phases such that $\varepsilon_{3a} = \varepsilon_3 + \pi$ and $\varepsilon_{5a} = \varepsilon_5 + \pi$ where ε_3 and ε_5 are the heave and pitch displacement phases. x is the distance between the LCG and the centre of lift of the control surface (+ve forward). Once again, there is no need for an overall gain to be included as the object of this analysis to obtain the phase of the control surface oscillation as a result of this method.

Introducing two new variables, X_{a_i} and Y_{a_i} and setting them equal to two respective components of equation 3.54 and then converting the phases of acceleration to phases of displacement, one obtains

$$\begin{aligned} X_{a_i} &= \left[\left(\bar{\eta}_3\omega_e^2\right)\cos(\varepsilon_{3a}) - x\left(\bar{\eta}_5\omega_e^2\right)\cos(\varepsilon_{5a})\right] \\ &= -\left(\bar{\eta}_3\omega_e^2\right)\cos(\varepsilon_3) + x\left(\bar{\eta}_5\omega_e^2\right)\cos(\varepsilon_5) \end{aligned} \tag{3.55}$$

$$\begin{aligned} Y_{a_i} &= \left[\left(\bar{\eta}_3\omega_e^2\right)\sin(\varepsilon_{3a}) - x\left(\bar{\eta}_5\omega_e^2\right)\sin(\varepsilon_{5a})\right] \\ &= -\left(\bar{\eta}_3\omega_e^2\right)\sin(\varepsilon_3) + x\left(\bar{\eta}_5\omega_e^2\right)\sin(\varepsilon_5) \end{aligned} \tag{3.56}$$

such that equation 3.54 now becomes

$$\begin{aligned}\ddot{\xi}_i(t) &= X_{a_i}\cos(\omega_e t) - Y_{a_i}\sin(\omega_e t) \\ &= \sqrt{X_{a_i}^2 + Y_{a_i}^2}\left[\cos(\omega_e t)\frac{X_{a_i}}{\sqrt{X_{a_i}^2 + Y_{a_i}^2}} - \sin(\omega_e t)\frac{Y_{a_i}}{\sqrt{X_{a_i}^2 + Y_{a_i}^2}}\right] \end{aligned} \quad (3.57)$$

The oscillation of the i^{th} control surface in regular waves will be of the form

$$\begin{aligned}\ddot{\xi}_i(t) &= \bar{\delta}_i\cos\left(\omega_e t + \phi_{a_i}\right) \\ &= \bar{\delta}_i\left[\cos(\omega_e t)\cos\left(\phi_{a_i}\right) - \sin(\omega_e t)\sin\left(\phi_{a_i}\right)\right] \end{aligned} \quad (3.58)$$

where $\bar{\delta}_i$ is the amplitude of oscillation or maximum deflection permitted by the mechanical arrangement of the control surface and ϕ_{a_i} is the phase of the hull vertical acceleration at the location of the control surface.

It can be seen that equations 3.57 and 3.58 are of similar form where $\bar{\delta}_i = \sqrt{X_{a_i}^2 + Y_{a_i}^2}$, $\cos\left(\phi_{a_i}\right) = \frac{X_{a_i}}{\sqrt{X_{a_i}^2+Y_{a_i}^2}}$ and $\sin\left(\phi_{a_i}\right) = \frac{Y_{a_i}}{\sqrt{X_{a_i}^2+Y_{a_i}^2}}$. Therefore, by simple geometry

$$X_{a_i} = \bar{\delta}_i\cos\left(\phi_{a_i}\right) \quad (3.59)$$

$$Y_{a_i} = \bar{\delta}_i\sin\left(\phi_{a_i}\right) \quad (3.60)$$

Also, one can conclude that the deflection of the control surface can be expressed as

$$\ddot{\xi}_i(t) = \sqrt{X_{a_i}^2 + Y_{a_i}^2}\cos\left(\omega_e t + \phi_{a_i}\right) \quad (3.61)$$

where X_{a_i} and Y_{a_i} can be described as the abscissa and ordinate values in the phase plane that depicts the vertical hull velocity at the location of the control surface.

The oscillation phase the control surface must adopt to oppose the local vertical hull acceleration $\left(\ddot{\xi}_i(t)\right)$ is therefore

$$\phi_{a_i} = \arctan\left(\frac{Y_{a_i}}{X_{a_i}}\right) + \pi \quad (3.62)$$

where π is added to ensure the control surface force opposes the vertical acceleration. The phase solution from this approach compared with the phase solution based on the gain finding method already described are presented in figure 3.10 for the transom tab and the T-foil configurations at two loading conditions.

Local Velocity or Local Acceleration Feedback Discussion The phase solution from this approach compared with the phase solution based on the gain finding routine are presented by way of example in figures 3.8 and 3.9 where it is clear that the local velocity feedback method is correct only for the T-foil control surface (see figure 3.8(b)) in the sense that it has a similar phase angle to that determined by the gain finding routine already described. Using the local velocity approach with the transom tab produced a phase angle in this figure that was typically in error by some offset. However, these plots show one instance only and an overall comparison can be made with the results of figure 3.10, which shows the calculated phase angles for three control surface configurations, two loading conditions and four speeds based on the previously described gain finding routine, the local velocity feedback method just described and the local acceleration feedback method described below in section 3.4.7.3. It is apparent from these results that the velocity feedback method is suitable for the T-foil at all speeds

whilst the local acceleration feedback method was not. In the case of the transom tab, the local velocity feedback method almost becomes beneficial at the lowest speed of 12.5 knots whilst the local acceleration feedback seems beneficial at only one speed somewhere between 12.5 and 17.5 knots for either loading condition.

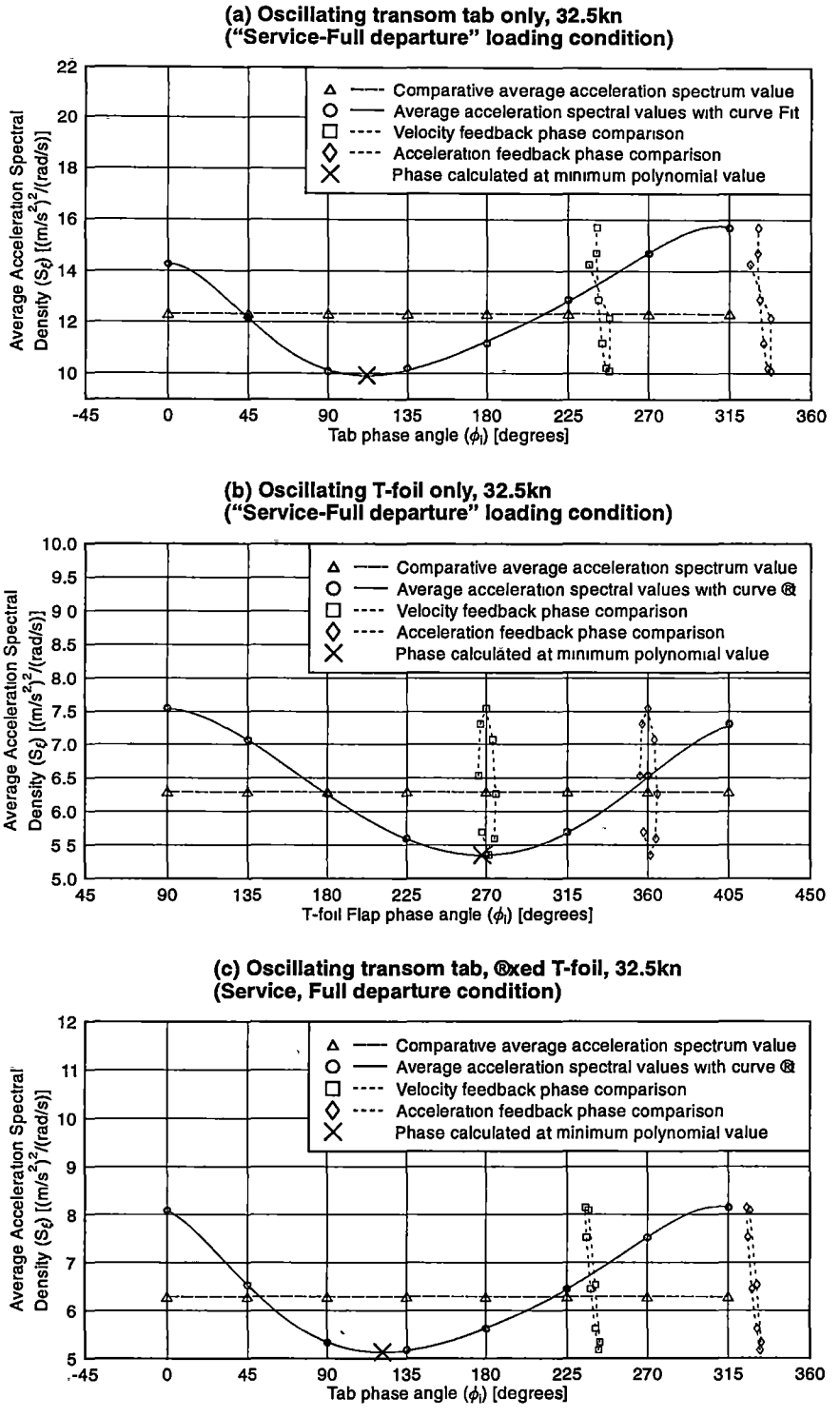

Figure 3.8: 86 metre vessel examples of gain optimisation for (a) transom tab only, (b) T-foil only and (c) transom tab with fixed T-foil. The horizonal line (Δ symbols) is the uncontrolled average vertical acceleration spectral response on which a reduction is sought. Thus, the minimum value on the curve is the ideal phase. Also shown are the corresponding phases calculated by local velocity and local acceleration feedback control methods for comparison.

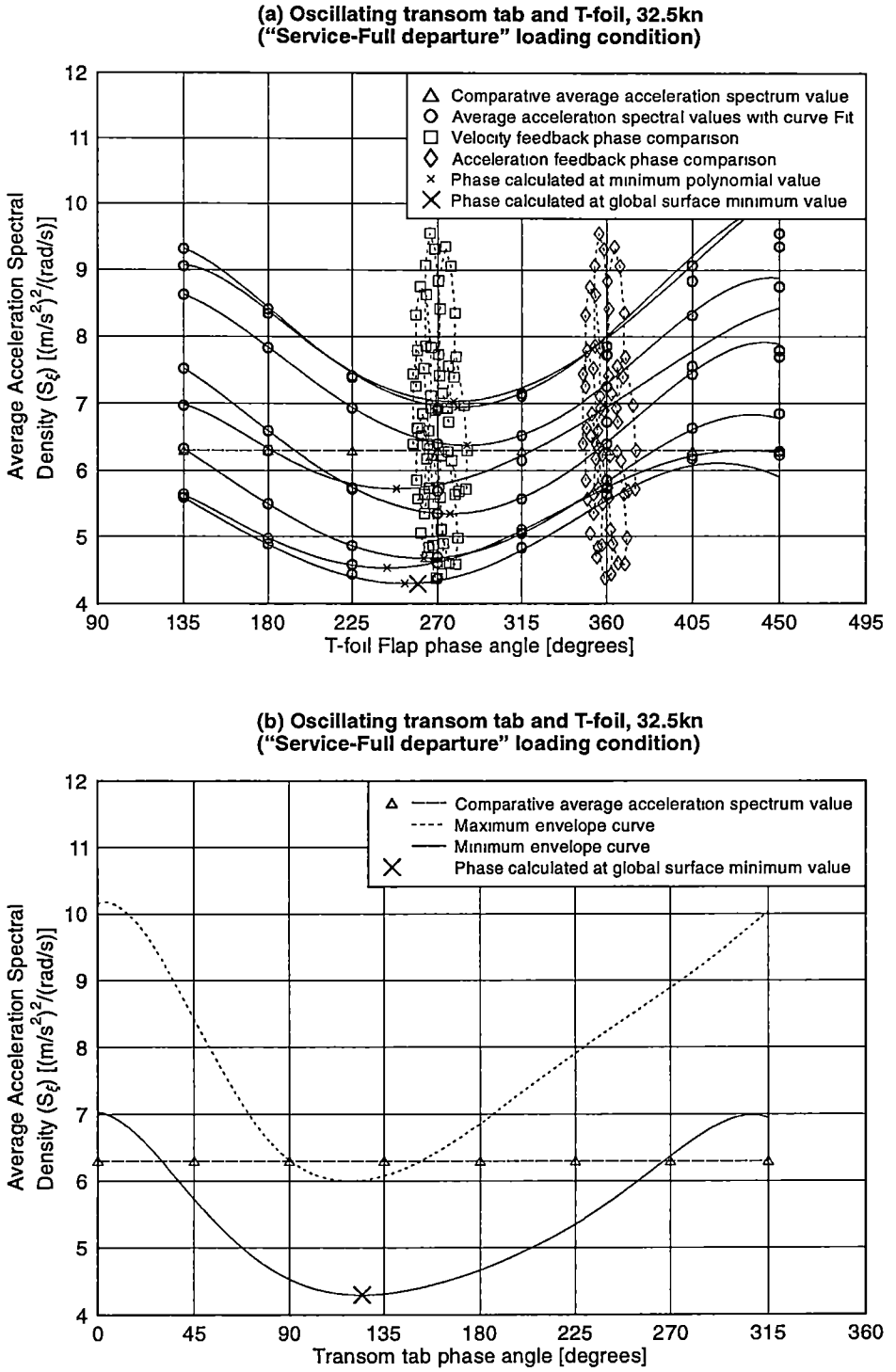

Figure 3.9: 86 metre vessel example of gain optimisation for two simultaneously oscillating control surfaces. (a) representation of solution space showing change in response against T-foil phase (each curve represents a constant tab phase (0° to 360°, 45° increments) whilst (b) represents the two-dimensional envelope of solution space of plot "a" against various tab phases. The minimum response of the three dimensional solution space has been shown in both plot (a) and (b). The horizonal line (Δ symbols) is the uncontrolled average vertical acceleration spectral response on which a reduction is sought.

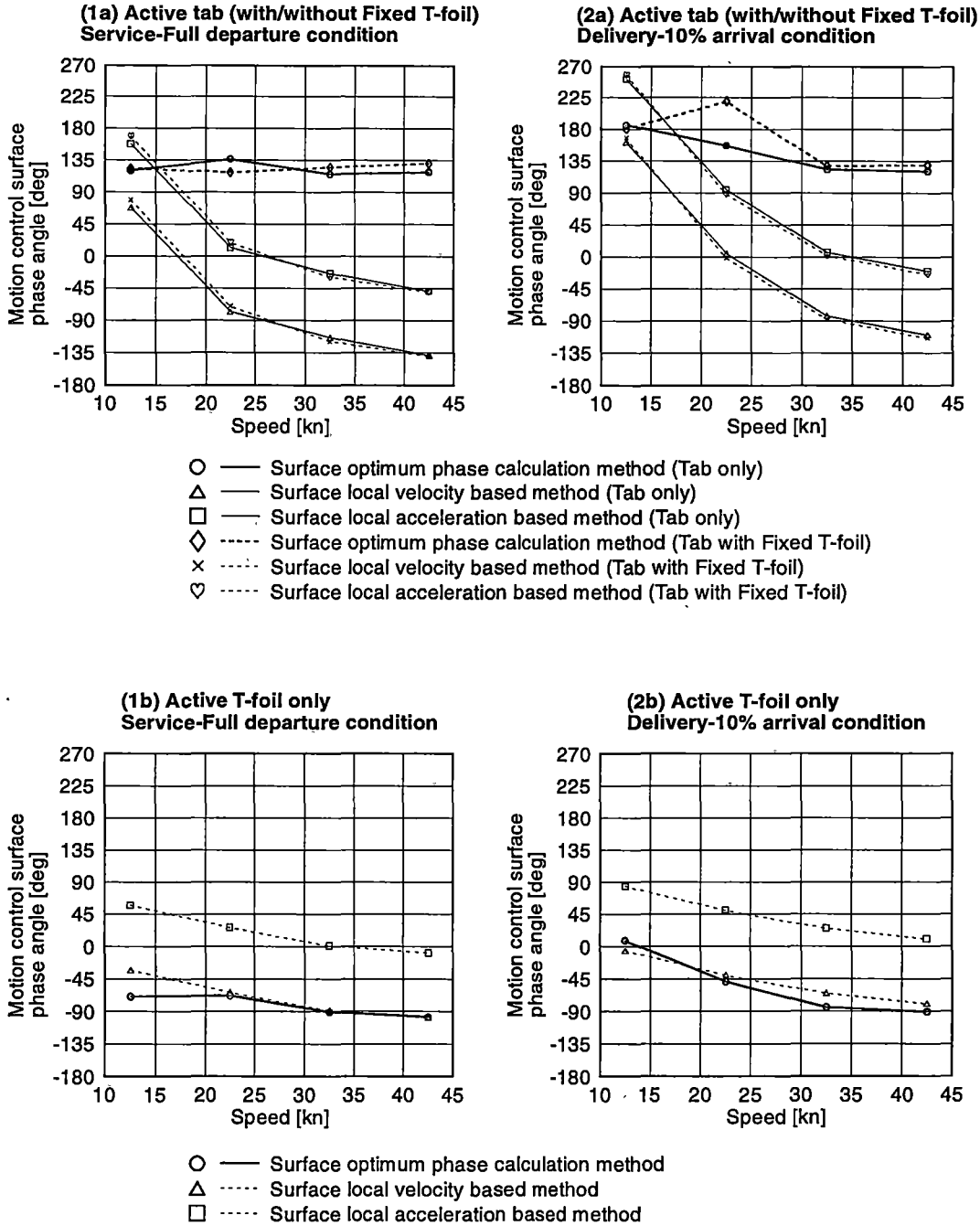

Figure 3.10: 86 metre vessel optimum oscilation phase angle (Hence gains) for the (a) transom tab (with/without a fixed T-foil), (b) T-foil, for the (1) Service full departure loading condition and (2) Delivery, 10% arrival loading condition. All results were obtained after a single iteration.

3.4.8 Deflection Velocity and Acceleration Restriction

In ship applications where the control surfaces are deflected by means of a hydraulic system, practical limitations must be imposed on the deflection rates as a result of the finite hydraulic power capability. These practical limits for commercial reasons were not known for the vessels analysed. Therefore, the deflection of the control surfaces in the computation had velocity and acceleration limits imposed that prevented them from exceeding the rates defined by a sinusoidal path based on the maximum deflection and the wave encounter frequency. Thus, the amplitude of angular velocity could not exceed $\dot{\delta}_i = \bar{\delta}_i \omega_e$ and the amplitude of angular acceleration could not exceed $\ddot{\delta}_i = \bar{\delta}_i \omega_e^2$ (where $\bar{\delta}_i$ is the maximum deflection of the i^{th} control surface)[8]. This implies that the surface deflection could not go from full positive deflection to full negative deflection within the course of one time step. The velocity limit was imposed in the current $\left(i^{th}\right)$ time step by ensuring the deflection (δ_i) was less than $\pm\left(\Delta t\right)\dot{\delta}_i + \delta_{(i-1)}$ and similarly the acceleration limit was imposing in the current $\left(i^{th}\right)$ time step by ensuring the deflection (δ_i) was less than $\pm 2\left(\Delta t\right)\ddot{\delta}_i + 2\delta_{(i-2)} - \delta_{(i-1)}$, where Δt is the size of the time step in seconds (see equation 3.14).

3.4.9 Application of Motion Control with Transfer Functions

One particular aspect of the BESTSEA time domain computation is that the computed wave height from which the motion transfer functions are derived can be selected by the user. With the addition of motion control surfaces to the hull in a numerical computation, a new approach is required that allows the results to be presented in the frequency domain. The linear assumption that is generally made with frequency domain computations implies that the hull response increases proportionally with wave height. In contrast, the force generated by a motion control appendage essentially remains constant for a given speed irrespective of wave height. Furthermore, its influence on the motion response of the hull is a function of the exciting wave forces acting on the hull, which in broad terms relates to both the wave height and period. So clearly the additional modelling of a control surface will remove to some extent the linear proportional hull response to wave height that may have existed for the hull configuration without control surfaces. However, if linearity in the solution of a hull with motion control appendages can be implied, if only for a reduced range of wave heights, then it may be still feasible to present a transfer function for the vessel based on a limited range of wave heights. Thus, in the case of a hull modelled with motion control appendages, the wave height and to a lesser extent the wave spectrum, will become unique for each transfer function solution.

The transfer function derived from the computations of this work were generally calculated at the regular wave height of 0.5 metres, but the regular wave height at which most results were required for this analysis was 2.5 metres this being a typical wave height for the data acquired through measurements. The regular wave height of 2.5 metres was used to have some equivalence with the Bretschneider wave spectrum used for deriving motion responses at 2.5 metres significant wave height and 7 seconds average period. It could be argued that whilst maintaining the significant wave height

[8]In the numerical computation the maximum deflection of the transom flap was 6° (0.105 radians) about a mean offset of 6°. At the dimensionless wave encounter frequency of 5, this implied a velocity limit of 10.7 deg/s and an acceleration limit of 19.3 deg/s^2. Similarly for the T-foil flap, which had a maximum deflection of 8° (0.140 radians) about a mean offset of 0°. At the dimensionless wave encounter frequency of 5, this implied a velocity limit of 14.3 deg/s and an acceleration limit of 25.7 deg/s^2.

of the wave spectrum at 2.5 metres, a regular wave height smaller than 2.5 metres should be computed, particularly if the results were sensitive to this parameter. In the case of the Bretschneider spectrum where the significant wave height is equivalent to 4 standard deviations, the average spectral wave height of 2.5 standard deviations may be more appropriate. However, this question can only be answered by investigation of the non-linear characteristics over the range of wave heights within the wave spectrum or by looking at the variation in hull response when various computed regular wave heights are applied. Should there be a significant variation in the hull response for various wave heights within the wave spectrum, then it is likely that the force generated by a control surface would be under estimated for the lower range of wave heights and over estimated at the higher wave heights. This implies that the hull motions would be over predicted at lower wave heights and under predicted at higher wave heights.

The use of regular wave heights other than 2.5 metres based on some rationale may in fact be justified for calculating the motion response with a Bretschneider wave spectrum of 2.5 metres significant wave height and 7 seconds average period, but this was not considered necessary. The reason for this will not be given here but will be investigated further in chapter 5 (with particular reference to the results of tables 5.1, 5.3, 5.4 and figure 5.33).

To model the appropriate force of the control surface with respect to the wave force on the hull, the forces generated by the transom tab and the T-foil were scaled by limiting the deflection of the flaps by a factor equivalent to the ratio of the computed regular wave height (in this case was 0.5 metres) divided by the simulated regular wave height (in this case was 2.5 metres) (see also Sections 3.4.2, 3.4.3). This was equivalent to saying that the deflection angles of the motion control surfaces were scaled so that full deflection from the control gains was only achieved in a 2.5 metre regular wave height. Scaling the inflow angle relative to the main foil section was not necessary in this case as the free stream incident angle to the foil was already scaled by the proportionally smaller computed regular waves.

3.5 Development of Operating Interface Programs

The BESTSEA solver was created as a command line executable requiring input data files to initialize variables in its computational procedure. The two types of input files consisted of a hull geometry file and a general hull particulars data file. These files contained the variables required to run a number of individual time-wise solutions for a single speed at discrete frequencies such that a completed multiple solution computation would provide sufficient information to complete one transfer function. The input file included the essential hull particulars such as hull displacement, pitch radius of gyration, hull length, longitudinal centre of gravity, nominal draft and wave height. When modelling the hydrodynamic lifting devices of a motion control system, the input files would also contain the variables for these devices.

The *hull geometry file* specified the hull shape, defined by evenly distributed sections from the bow to the stern by listing the vertical and transverse coordinates from the keel to the deck edge. The first section of the defined geometry commenced one section aft of the bow stem and continued through to the transom. A right hand coordinate system relative to the nominal hull centre of gravity defined the x-axis toward the bow, the y-axis to port and the z-axis vertically upwards. Although the computation considers changes in the user defined hull geometry up to the free surface boundary, the program will assume a vertical hull side if the height of the hull definition is lower than the local free surface.

To facilitate the creation of the input files, a Windows based LABVIEW program (BESTINPUT) was created to partly automate the input of data to file that was required to compute the transfer functions for multiple speeds. The LABVIEW program presented the user with all the required inputs. After the manual entry of these inputs, the information could be saved and retrieved for later use (see appendix D for a view of the screen interface).

The output created by BESTSEA consisted of the time-wise motion results of heave and pitch and where appropriate, the deflection in time of each control surface. Hydrodynamic force and moment distributions were also supplied and could be used to determine the wave induced global loads. To process this data and create the results required by this analysis, a dedicated post-processing program (BESTVIEW) was created with the National Instruments software package LABVIEW.

3.5.1 Motion Analysis

Kvalsvold et al. (1995) showed that the differences in the longitudinal distribution of vertical motion between conventional hulls and SWATH hulls can vary significantly. Therefore, the computational motion analysis of the 86 metre vessel has particularly considered the longitudinal distribution of vertical motion for the headsea case. Yoo et al. (1997) suggested that the most severe motions occurred in bow quartering seas and that for particular wave frequencies and forward speeds, beam seas may create accelerations exceeding those produced by head-seas. This suggests that it is difficult to make generalizations about the response of any particular hull form without understanding the entire solution space made up of all wave frequencies, wave heights and directions. However, Davis and Holloway (2003a) showed that the higher sea states of 3 metres, head seas produced some of the worst case motions of all headings whilst in smaller wave heights the more severe conditions were in the bow quartering (120°) wave direction. Wave heights considered here were at 2.5 metres (top of sea state 4) so head seas are invariably going to produce the most severe acceleration magnitudes of all wave directions.

Over a sufficient number of time steps, the BESTSEA computation will achieve a regular sinusoidal motion and the vessel adopts a natural trim position. This condition was clearly visible in the displacement time trace of the output data. A regular response condition was defined when the maximum difference between three successive amplitudes of the time wise dimensionless transfer function was less than 0.05.

Within the time stepping routine of BESTSEA the phase was defined relative to the hull longitudinal centre of gravity where for the heave phase in time was relative to the wave displacement and the pitch phase in time was relative to the wave slope. A positive phase is in advance of the wave and a negative phase lags the wave. For low encounter frequencies, the heave phase therefore approached zero and the pitch phase approached -90 degrees.

The wave profile was defined by the expression $\eta = A\cos(\omega_e t + kx)$ where in the first time step, the value of $t = 0$. This cosine wave profile was reproduced in the post processing routine where the phase had to be advanced one time step for it to correspond the BESTSEA computation. From equation 3.14, one time step $\Delta t = \frac{L}{n_s U_0}$, or $\frac{\Delta t}{T_e} = \Delta t.f_e$ cycles $(360.\Delta t.f_e$ degrees). For the wave profile of the postprocessor to be synchronized with the BESTSEA output data, the first time step data output had to correspond to the wave profile which had been advanced by $2\pi.\Delta t.f_e$ radians such that $\eta = A\cos(\omega_e t + kx + 2\pi.\Delta t.f_e)$. This occurs because the first output from BESTSEA is the computed result at the end of the first time step.

With the wave profile known, the heave and pitch phase were determined using a

cross phase power spectrum within BESTVIEW and extracting the calculated phase at the corresponding encounter frequency. From this, the phase information was extracted from the spectrum at the predetermined wave encounter frequency of the BESTSEA computation.

3.5.2 Motion Derivation about the LCG

A vessel in a long crested wave environment defined by a fixed frame wave spectrum $S_\zeta(\omega)$ will encounter the waves at a different frequency due to the forward speed of the vessel and the wave heading relative to the waves, thus transforming the wave spectrum to $S_\zeta(\omega_e)$. The magnitude of motion displacement or acceleration at a given location on a rigid vessel can be derived from the displacement transfer functions that describe the vessel's six degrees of freedom, namely surge, sway, heave, roll, pitch and yaw (η_i where $i = 1$ to 6 respectively). Defining the displacement transfer functions at the vessel centre of gravity (CG) as $H_i(\omega_e)$ (where $i = 1$ to 6), the displacement transfer function at some other position about the vessel CG will be $H_i(x, y, z, \omega_e)$.

The response at some position (x, y, z) on the vessel has the response spectrum $S_j(\omega_e)$ determined by the expression

$$S_j(x, y, z, \omega_e) = |H_i(\omega_e)|^2 S_\zeta(\omega_e) \tag{3.63}$$

The k^{th} moment of the response spectrum is defined by

$$m_k = \int_0^\infty |\omega_e|^k |H_i(\omega_e)|^2 S_\zeta(\omega_e)\, d\omega_e : k = 1, 2, 3, 4, ...,: [metres^2/\sec ond^k]$$

The statistical properties of the vessel response can be calculated from the response spectrum moments. In particular the variance σ^2 of the response is the zeroth moment of the response spectrum (m_0) and the standard deviation is the square root of the zeroth moment such that $\sigma = \sqrt{m_0}$. The significant response value is four times the standard deviation$\left(4\sigma = 4\sqrt{m_0}\right)$ (see Lloyd (1989)).

In all the instances where the acceleration response is required instead of the displacement response, the displacement transfer function $H_i(\omega_e)$ can be interchanged with the acceleration transfer function $\ddot{H}_i(\omega_e)$ which is derived by multiplying by the factor ω_e^2 (Lloyd (1989)) such that $\ddot{H}_i(\omega_e) = H_i(\omega_e)\omega_e^2$.

In determining the local response at some position (x, y, z) about the CG, the vertical displacement transfer function for that position was first calculated as a function of the heave ($\bar{\eta}_3$), roll ($\bar{\eta}_4$) and pitch ($\bar{\eta}_5$) magnitudes and their respective phases.

$$\eta_3(x, y, z) = \left\{ \begin{array}{l} [\bar{\eta}_5 r_x \cos(\phi_5) - \bar{\eta}_4 r_y \cos(\phi_4) + \bar{\eta}_3 \cos(\phi_3)]^2 \\ +[\bar{\eta}_5 r_x \sin(\phi_5) - \bar{\eta}_4 r_y \sin(\phi_4) + \bar{\eta}_3 \sin(\phi_3)]^2 \end{array} \right\}^{\frac{1}{2}} \tag{3.64}$$

where r_x and r_y are the distances from the centre of gravity in the x and y directions respectively.

According to Michel (1999) (see also Lloyd (1989) and Tucker (1991)) the period of response can be determined from the spectral moments. The zero crossing period is defined as $T_2 = T_z = 2\pi\sqrt{\frac{m_0}{m_2}}$, the peak or mean crest period as $T_p = T_c = 2\pi\sqrt{\frac{m_2}{m_4}}$, and the average period as $T_1 = \bar{T} = 2\pi\frac{m_0}{m_1}$.

3.5.3 Position of Minimum Motion in Regular Head Sea Waves

In regular head sea waves, the harmonic heave (η_3) and pitch (η_5) displacements in time will produce a unique longitudinal position of minimum vertical displacement that can be determined through simple analysis (Holloway and Davis (1998)). It can be shown that the vertical displacement (ξ_3) in time at any longitudinal position (x) within the vessel length is

$$\xi_3(x,t) = \eta_3(t) - x\eta_5(t) \tag{3.65}$$

where x is the distance to the centre of gravity. The ship motion in heave is given by

$$\begin{aligned} \eta_3(t) &= \bar{\eta}_3 \sin(\omega_e t + \varepsilon_3) \\ &= \bar{\eta}_3 \sin(\omega_e t' + \varepsilon_3 - \varepsilon_5) \end{aligned} \tag{3.66}$$

and pitch by

$$\begin{aligned} \eta_5(t) &= \bar{\eta}_5 \sin(\omega_e t + \varepsilon_5) \\ &= \bar{\eta}_5 \sin(\omega_e t') \end{aligned} \tag{3.67}$$

where $t' = t + \frac{\varepsilon_5}{\omega_e}$. Thus using equation 3.65, 3.66 and 3.67, the vertical motion $\xi_3(x,t)$ at a position x from the centre of gravity is given by

$$\begin{aligned} \xi_3(x,t) &= \bar{\eta}_3 \sin(\omega_e t' + \varepsilon_3 - \varepsilon_5) - x\bar{\eta}_5 \sin(\omega_e t') \\ &= \bar{\eta}_3 \sin(\omega_e t') \cos(\varepsilon_3 - \varepsilon_5) + \bar{\eta}_3 \cos(\omega_e t') \sin(\varepsilon_3 - \varepsilon_5) \\ &\quad -x\bar{\eta}_5 \sin(\omega_e t') \\ &= (\bar{\eta}_3 \cos(\varepsilon_3 - \varepsilon_5) - x\bar{\eta}_5) \sin(\omega_e t') + (\bar{\eta}_3 \sin(\varepsilon_3 - \varepsilon_5)) \cos(\omega_e t') \\ &= X_m \sin(\omega_e t')) + Y_m \cos(\omega_e t') \end{aligned} \tag{3.68}$$

where X_m and Y_m are defined as

$$X_m = (\bar{\eta}_3 \cos(\varepsilon_3 - \varepsilon_5) - x\bar{\eta}_5) \tag{3.69}$$

$$Y_m = (\bar{\eta}_3 \sin(\varepsilon_3 - \varepsilon_5)) \tag{3.70}$$

such that equation 3.68 now becomes

$$\begin{aligned} \xi_3(x,t) &= X_m \sin(\omega_e t')) + Y_m \cos(\omega_e t') \\ &= \sqrt{X_m^2 + Y_m^2} \left[\sin(\omega_e t') \frac{X_m}{\sqrt{X_m^2 + Y_m^2}} + \cos(\omega_e t') \frac{Y_m}{\sqrt{X_m^2 + Y_m^2}} \right] \\ &= \sqrt{X_m^2 + Y_m^2} \left[\sin(\omega_e t') \cos(\beta) + \cos(\omega_e t') \sin(\beta) \right] \\ &= \sqrt{X_m^2 + Y_m^2} \sin(\omega_e t' + \beta) \end{aligned} \tag{3.71}$$

where $\cos(\beta) = \frac{X_m}{\sqrt{X_m^2+Y_m^2}}$ and $\sin(\beta) = \frac{Y_m}{\sqrt{X_m^2+Y_m^2}}$. The magnitude of $\xi_3(x,t)$ squared is clearly now

$$\begin{aligned} |\xi_3(x,t)|^2 &= X_m^2 + Y_m^2 \\ &= (\bar{\eta}_3 \cos(\varepsilon_3 - \varepsilon_5) - x\bar{\eta}_5)^2 + (\bar{\eta}_3 \sin(\varepsilon_3 - \varepsilon_5))^2 \\ &= \bar{\eta}_3^2 - 2\bar{\eta}_3\bar{\eta}_5 x \cos(\varepsilon_3 - \varepsilon_5) + x^2\bar{\eta}_5^2 \end{aligned} \tag{3.72}$$

The distance (x) to the location of minimum motion from the LCG can be found by putting

$$\begin{aligned} \frac{d\left(|\xi_3(x,t)|^2\right)}{dx} &= 0 \\ &= 2x\bar{\eta}_5^2 - 2\bar{\eta}_3\bar{\eta}_5\cos\left(\varepsilon_3 - \varepsilon_5\right) \\ x &= \frac{\bar{\eta}_3}{\bar{\eta}_5}\cos\left(\varepsilon_3 - \varepsilon_5\right) \end{aligned} \tag{3.73}$$

Figure 3.11 shows the position of minimum motion for the 81 and 86 metre vessels at 32.5 knots for a range of loading conditions without motion control surfaces. It also shows the position of minimum motion for the in "service - full departure" loading condition at a range of speeds. All instances show the result relative to amidships and the centre of gravity. These results show that the position of minimum motion generally lies aft of amidships and moves further aft relatively close to the transom at the frequency of maximum heave response. Both vessels show similar behaviour and the result is only moderately influenced by the loading condition and vessel forwards speed. At some frequencies the theoretical position of minimum motion actually extends aft beyond the hull transom, in which case the position of minimum motion within the hull would lie at the transom.

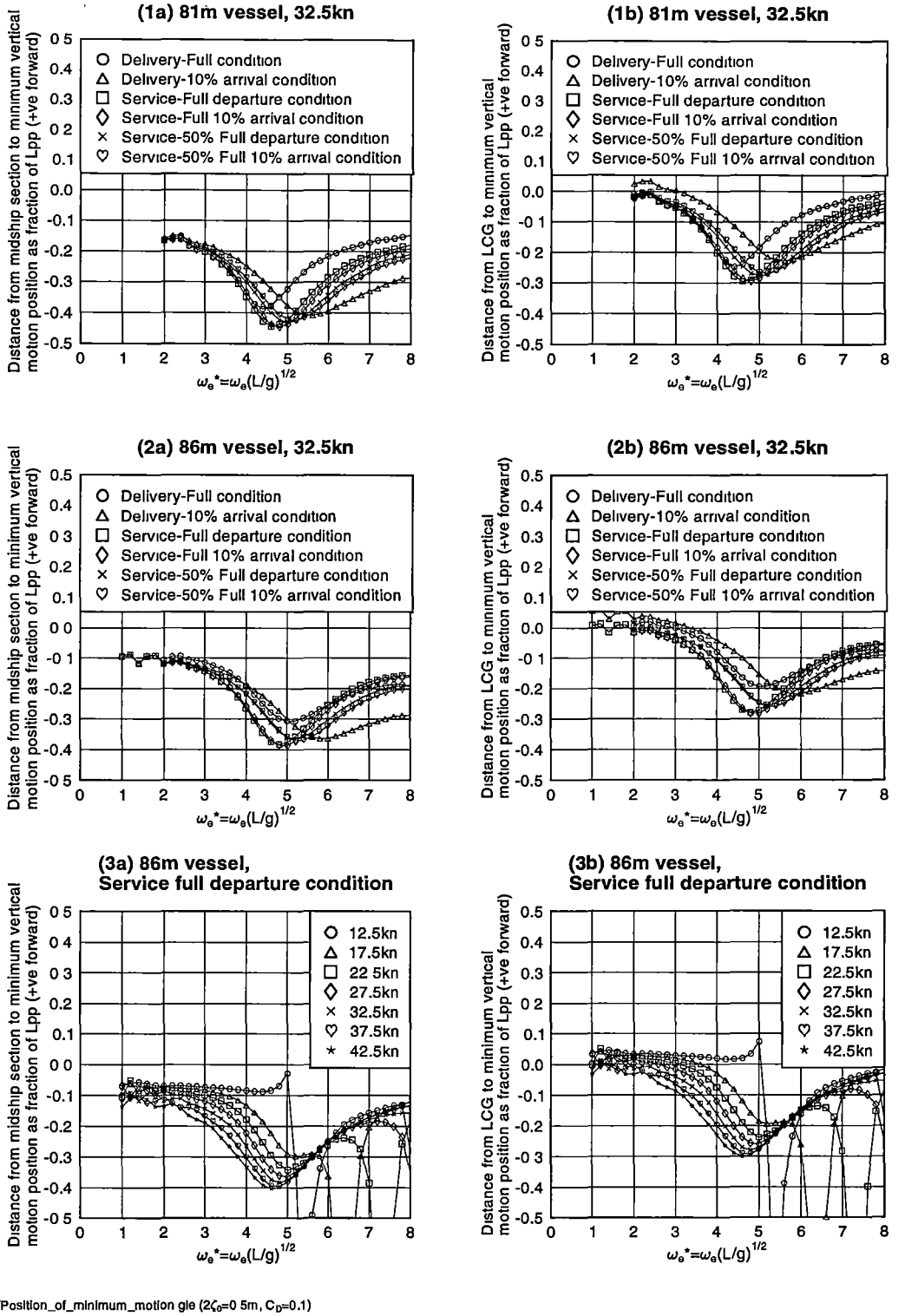

Figure 3.11: Variation in position of minimum vertical motion with encounter frequency (bare-hull, no motion control surfaces) for (1) 81 metre and (2) 86 metre vessel at 32.5 knots for a range of loading condtions and (3) 86 metre at one loading condition for a range of speeds. (See appendix A for hull particulars)

Chapter 4

Full-Scale Experimental Results

4.1 Introduction

Data records collected during full-scale motion measurements with both the 81 and 86 metre vessels are presented in this chapter comprising wave spectra, acceleration spectra and motion transfer functions. The arrangement of data and its presentation format is primarily based on the vessel type, control surface configuration, vessel speed and observed primary wave direction using the method presented in chapter 2.

4.2 Overview of Data Records

From the data records obtained during full-scale measurements on the 81 and 86 metre vessels during their delivery voyages and operational service, there was a proportion of the total data records for which the primary wave direction could be determined. This allowed further analysis of the data to be conducted where it was categorised according to speed and observed primary wave direction sectors. The remaining records for which the primary wave direction could not be determined through the procedure described in section 2.3 were discarded from further analysis and are not reflected in the results of this chapter. This generally also excluded all wave directions encountered aft of the beam where low encounter frequencies and low vertical acceleration responses were imposed on the vessel. In comparison, wave directions encountered forward of the beam had a progressively higher encounter frequency and higher vertical acceleration response as the sea direction moved toward the bow. These measurements also had generally better defined steady periodic motions that allowed more certainty in predicting the encountered wave direction.

The duration of data records allocated to each data group according to forward speed (12.5 to 42.5kn in 5kn increments $\pm$2.5kn) and wave direction (90°, 135° and 180°) for the 81 metre vessel are shown in table 4.1. The duration of data records created during the delivery voyage where only transom tabs were fitted are shown in this same table as well as the duration details of data created during operational service when the vessel had T-foils in addition to transom tabs. The data in table 4.1 represent over 30 hours or 87% of the total data collected during the delivery voyage and 41 minutes or 50% of the total data collected during service operations on the English Channel that was retained for subsequent analysis. Throughout this period, the instrumentation was saving data to disk at an average of 81 minutes per day during the delivery voyage and only 0.4 minutes per day during passenger service operations. Obviously the time spent on the delivery voyage for the 81 metre vessel was more efficient in generating useful data than the time spent during passenger service

operations since severe conditions occurred on the delivery voyage whilst more mild conditions occurred during the introduction to service of the 81 metre vessel. In any event the calender period during which service data was collected on the 81 metre vessel was 228 days before the instrumentation was moved to the 86 metre vessel so it is expected that there may have been times when data was not recorded due to instrumentation or software problems that were not corrected in a timely manner.

The delivery voyage data is grouped into directional sectors that include, head sea waves containing 63.6% of the data, bow quartering waves with 22.9% and beam seas with the remaining 13.5% of the data. In operational service only 12.5% of the data was in head seas with 37.5% in bow quartering seas and 50.0% in beam seas. This was not unexpected as the route of this vessel between Weymouth on the south coast of England and the Channel Islands gave it exposure to the swells from the Atlantic that the vessel would have generally encountered on the beam to the bow quarter on the outward bound journey and the beam to stern quarter on the return journey. These circumstances would have left a very small proportion of the time where head sea encounters could have occurred unless from wind generated waves from some other direction or the vessel took a different course than would normally be part of its route.

The delivery voyage data was limited to speeds less than 30 knots due to engine problems that persisted for the duration of the voyage, so it cannot be implied that the speed of measurement was necessarily influenced by the wave conditions. Once the vessel had entered operational service the measured speeds increased to over 35 knots which is reflected in these tables.

As previously discussed in chapter 2, in cases where a data acquisition sequence commenced automatically, the bow accelerometer trigger level was set between 0.05 to 0.5g but typically at about 0.3g for the 81 metre vessel. This decision affected the total amount of data collected by eliminating the number of records in smaller wave heights. The wave data will show in this chapter that most measurements were taken in significant wave heights of 0.8 metres ($\geq$ 0.2m RMS) or more. This aspect of the data acquisition will also be reflected in the acceleration results presented later in this chapter.

The total durations of data records allocated to a data group according to forward speed (12.5 to 42.5 $\pm$2.5kn) and wave directions from the beam to the bow for the 86 metre vessel are shown in table 4.2. This table shows the duration of data records created during the delivery voyage where only transom tabs were fitted as well as for data records created during operational service when the vessel had T-foils fitted in addition to the transom tabs. The data in these tables represent over 46 hours or 44% of the data collected during the delivery voyage and over 88 hours or 54% of the data collected during service operations on the English Channel that was retained for subsequent analysis. Throughout this period, the instrumentation was saving data to disk an average of 198 minutes per day during the delivery voyage and 21 minutes per day during passenger service operations. Just like the experience with the 81 metre vessel, the time spent on the delivery voyage for the 86 metre vessel was more efficient in generating useful data for analysis owing to more severe conditions on the delivery voyage. Overall the records for the 86 metre vessel exceeded those of the 81 metre vessel on the delivery voyage by 3 times, during service operations by 120 times and overall by more than 7 times. This is largely because the instrumentation was left in place for up to 460 calendar days of service operations where it remained on-line for most of this period.

The delivery voyage data of table 4.2 is grouped into directional sectors that include, head sea waves containing 7% of the data, bow quartering waves with 63% of the data

and beam seas with the remaining 30% of the data. In operational service only 2.4% of the data was in head seas with 52% in bow quartering seas and 45.6% in beam seas. This was not unexpected as this vessel operated the same route as its predecessor (the 81 metre vessel) between Weymouth on the south coast of England and the Channel Islands giving it the same exposure to the swells from the Atlantic where beam to the bow quarter waves would be typical on the outward bound journey and the beam to stern quarter on the return journey. These circumstances gave rise to the small volume of head sea data obtained from the vessel once in service.

The 86 metre vessel also had a greater amount of data collected during the delivery and operational service than the 81 metre vessel. Furthermore, once in service the variety of speeds measured were much greater and of longer duration. The greatest amount of recorded time was at 37.5 knots constituting 43% of the data, this being the design speed of the vessel.

Data collected on the two vessels that was not grouped and shown in tables 4.1 and 4.2 and thus not utilised for subsequent analysis was made up of data that was recorded either manually whilst the vessel was tied up in harbour, in waves encountered aft of the beam, in small waves that induced only small heave accelerations or in waves with a broad directional spreading that made determining the primary wave direction difficult or not possible.

The total length of data, which is needed to form the basis of spectral analysis or variance analysis is difficult to specify. In general, variance analysis is less demanding than energy spectral analysis, which in turn is less demanding than cross spectral analysis. Further, the question of the required length of data records is considerably complicated by the variability of sea conditions, in particular the sea direction, wave height and period associated with each speed and direction subset. For example, if there is relatively little spectral energy in the frequency band of significant motion response then clearly a much longer total record is needed to resolve an energy or cross spectrum. It is often suggested that 30 minutes forms a minimum record length, although this is only an approximate estimate made by experienced observers. On this basis, almost all of the subsets of data for each speed and direction shown in tables 4.1 and 4.2 would appear to be adequate. Perhaps the greatest barrier to a formal analysis of the statistical reliability of the results obtained is the variability of sea direction over each subset of data for a particular speed and direction. It must be realised that the data in each subset is not generated from concurrent records, but may have been contributed over intervals of days, weeks or months and so the extent to which the sea direction is defined or somewhat confused is itself not a constant factor over a particular subset of data. In these circumstances the outcomes of the analysis (e.g. irregularity of spectra) were perhaps the only sensible indicators of probable statistical reliability. It was considered beyond the scope of the present project to attempt an analysis of statistical reliability of variance and spectral outcomes. Whilst this aspect should not be overlooked in considering the needs of future research projects, it seems that particular provision in the data acquisition process would need to be made to take account of variability of nominal condition parameters such as vessel speed, sea direction, wave height and wave period, and the extent to which the sea direction is well defined as opposed to being confused.

81 metre vessel delivery voyage (Active tabs only)

Days equipment installed	26
Total data record duration [s]	126,669
Average recording time per day [min]	81.2
Percentage of data used	87.2%

0° is following waves

Seconds of data

Middle of speed range ±2.5kn	90° ±22.5°	135° ±22.5°	180° ±22.5°	Total [s]	Total [hrs]	Total [%]
12.5	204.8	409.6	1843.2	2457.6	0.68	2.2%
17.5	6348.8	10649.6	24780.8	41779.2	11.61	37.8%
22.5	7577.6	13516.8	39424	60518.4	16.81	54.8%
27.5	819.2	716.8	4198.4	5734.4	1.59	5.2%
32.5	-	-	-	0.0	0.00	0.0%
37.5	-	-	-	0.0	0.00	0.0%
42.5	-	-	-	0.0	0.00	0.0%
Total [s]	14950.4	25292.8	70246.4	**110,490**		
Total [hrs]	4.15	7.03	19.51		**30.7**	
Total [%]	13.5%	22.9%	63.6%			**100%**

81 metre vessel in operational service (Active tabs and T-foils)

Days equipment installed	228
Total data record duration [s]	4,915
Average recording time per day [min]	0.4
Percentage of data used	50.0%

0° is following waves

Seconds of data

Middle of speed range ±2.5kn	90° ±22.5°	135° ±22.5°	180° ±22.5°	Total [s]	Total [hrs]	Total [%]
12.5	-	-	-	0.0	0.00	0.0%
17.5	-	-	-	0.0	0.00	0.0%
22.5	-	-	-	0.0	0.00	0.0%
27.5	-	-	-	0.0	0.00	0.0%
32.5	-	-	-	0.0	0.00	0.0%
37.5	1126.4	614.4	102.4	1843.2	0.51	75.0%
42.5	102.4	307.2	204.8	614.4	0.17	25.0%
Total [s]	1228.8	921.6	307.2	**2,458**		
Total [hrs]	0.34	0.26	0.09		**0.7**	
Total [%]	50.0%	37.5%	12.5%			**100%**

C:\1Nigel\038DATA\cor_1filebasis\tf1count(tabs and tabs_f)-038(45deg inc).xls

Table 4.1: Measurement record durations (81m vessel) at various speeds and observed wave heading sectors

86 metre vessel delivery voyage (Active tabs only)

Days equipment installed	32
Total data record duration [s]	379,904
Average recording time per day [min]	197.9
Percentage of data used	44.0%

0° is following waves

Seconds of data

Middle of speed range ±2.5kn	90° ±22.5°	135° ±22.5°	180° ±22.5°	Total [s]	Total [hrs]	Total [%]
12.5	8601.6	4096	614.4	13312.0	3.70	8.0%
17.5	18432	25600	3072	47104.0	13.08	28.2%
22.5	4710.4	1433.6	204.8	6348.8	1.76	3.8%
27.5	10240	43008	3276.8	56524.8	15.70	33.8%
32.5	7987.2	30515.2	4505.6	43008.0	11.95	25.7%
37.5	409.6	614.4	-	1024.0	0.28	0.6%
42.5	-	-	-	0.0	0.00	0.0%
Total [s]	50380.8	105267.2	11673.6	**167,322**		
Total [hrs]	13.99	29.24	3.24		**46.5**	
Total [%]	30.1%	62.9%	7.0%			**100%**

86 metre vessel in operational service (Active tabs and T-foils)

Days equipment installed	460
Total data record duration [s]	591,053
Average recording time per day [min]	21.4
Percentage of data used	53.8%

0° is following waves

Seconds of data

Middle of speed range ±2.5kn	90° ±22.5°	135° ±22.5°	180° ±22.5°	Total [s]	Total [hrs]	Total [%]
12.5	204.8	2048	1638.4	3891.2	1.08	1.2%
17.5	5324.8	6963.2	2048	14336.0	3.98	4.5%
22.5	3481.6	7372.8	-	10854.4	3.02	3.4%
27.5	21504	34816	-	56320.0	15.64	17.7%
32.5	40345.6	45465.6	2457.6	88268.8	24.52	27.8%
37.5	69632	64921.6	1433.6	135987.2	37.77	42.8%
42.5	4300.8	3891.2	-	8192.0	2.28	2.6%
Total [s]	144793.6	165478.4	7577.6	**317,850**		
Total [hrs]	40.22	45.97	2.10		**88.3**	
Total [%]	45.6%	52.1%	2.4%			**100%**

C:\1Nigel\042DATA\cor_1filebasis\tf1count(tabs and tabs_f)-042(45deg inc).xls

Table 4.2: Measurement record durations (86m vessel) at various speeds and observed wave heading sectors

4.3 Encountered Sea Conditions

4.3.1 Wave Height and Period

4.3.1.1 Combined Data of Both Vessels

The measured average wave period against RMS wave height for the 81 and the 86 metre vessels are shown in figure 4.1 for each data record retained for subsequent analysis and included as part of the duration data displayed in tables 4.1 and 4.2. The average values for each data record displayed in figure 4.1 are shown in table 4.3.

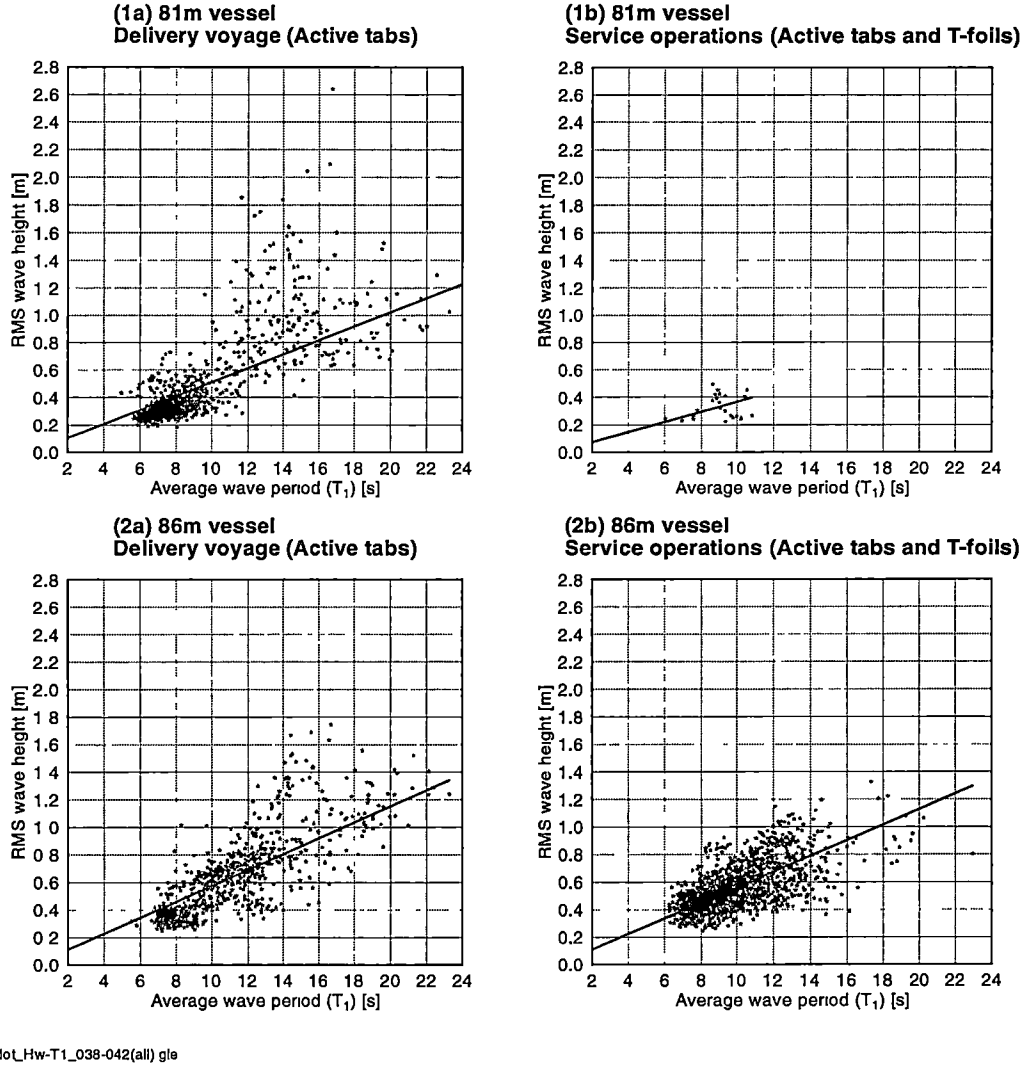

Figure 4.1: Measured RMS wave height verse wave period of each data record of the (1) 81 and (2) 86 metre vessels, (a) active tabs only (delivery voyage), (b) active tabs and T-foils (operational service). Shows lines drawn between average values and origin.

It is clear from figure 4.1 that the waves encountered during the delivery voyages of both vessels were generally higher than those encountered whilst the vessel was in passenger service across the English Channel. The maximum RMS wave height encountered by the 81 metre vessel was over 2.6 metres (approximately 8.8m significant wave height). Further detailed inspection of the data revealed that these waves were encountered on the port beam to the port bow quarter where the largest wave measured

Hull, configuration	Average RMS wave height [m]	corresponding significant wave height ($Hs=4(m_0)^{0.5}$) [m]	Average, average wave period (T_1) [s]	Period / Wave height [s/m]
81m, delivery voyage	0.464	1.856	9.1	19.6
81m, in service operations	0.327	1.309	8.9	27.2
86m, delivery voyage	0.629	2.516	11.0	17.4
86m, in service operations	0.562	2.247	10.0	17.7

ref/042data\cor_1filebasis\038-042(wave summary)-from rms files xls

Table 4.3: Overall measured averages of wave height, average wave period, and their ratio

during this period was over 10.6 metres whilst the vessel was proceeding north at 19.5 knots in the Atlantic Ocean near the Bay of Biscay. Similarly, the maximum RMS wave height encountered by the 86 metre vessel during delivery was approximately 1.74 metres or 5.3 metres significant wave height on the port beam where the largest wave measured during this period was approximately 7.1 metres whilst the vessel was proceeding at 14 knots heading west one day out of Fremantle in the Indian Ocean. However, once in service a restriction of 3 to 4 metres significant wave height would have applied, resulting in the amount of data above 0.75 to 1 metre (RMS) to be greatly reduced. This is reflected in the data of the 86 metre vessel.

Table 4.3 shows that the wave periods presented for the 81 metre vessel delivery voyage averaged 9.1 seconds (average wave period) where most were between 6 to 10 seconds with some as high as 23 seconds. The small amount of data obtained in service for this vessel means that no real conclusion can be made about the periods but those that were measured were typical of the Atlantic swells the vessel would encounter during passenger service operations across the English Channel. These records contained an average period of 8.9 seconds.

The 86 metre vessel experienced slightly longer wave periods during its delivery of 11 seconds (average wave period) where most were between 6.5 and 14 seconds with some periods up to 23 seconds. During service operations in the English Channel the vessel experienced the majority of periods of between 6 and 14 seconds as indicated in figure 4.1 and an average period of 10 seconds.

The wave heights against period in figure 4.1 indicate that as the wave period increases there is a general increase in the wave height. This increase is reflected in the slope of a line taken through the average data values (shown in table 4.3) and the origin, the inverse slope of which is given in table 4.3. Firstly, it should be noted that there is a considerable scatter of data on the wave height to wave period diagrams. This would be due to variation in the origin of wave generation and combination of waves due to local wind and swell. However, as table 4.3 shows, there is a tendency for the service conditions to have a rather large wave period to wave height ratio, reflecting most likely the influence of ocean originated swell on the service route conditions.

4.3.1.2 Data of 81 metre Vessel

The wave statistics presented previously in figure 4.1 for all vessels are presented in figure 4.2 specifically for the 81 metre vessel where the data has been further divided into categories of speed and wave direction. The delivery voyage statistics are shown in the speed range of 12.5 to 27.5 knots whilst the statistics collected during operational

service are shown for 37.5 and 42.5 knots.

It is clear that of the data collected for this vessel, a reasonable amount was obtained at 17.5 and 22.5 knots whilst only a modest amount was collected at the other speeds on both the delivery and service operations. At 17.5 knots the majority of the data was obtained between the wave period of 6 to 10 seconds and wave heights of 0.2 to 0.8 metres (RMS). A similar observation can be made about the majority of 22.5 knot data, which is also between 6 to 10 seconds but has a smaller range of wave heights being 0.2 to 0.6 metres (RMS). For these two speeds there did not appear to be a particular wave heading that featured more prominently as the wave height increased. At 22.5 knots, as the wave period increased the minimum wave height also increased and the wave heights measured tended to expand in range.

Table 4.4 shows a summary of the average wave heights (RMS) and periods for each wave heading for the data contained in figure 4.2 where the zero crossing period (T_z), peak period (T_p) and average wave period (T_1) are defined in section 3.5.2. With the small quantity of data contained in some of these groups it is not possible to draw valid conclusions about their distribution. The results obtained for the 81m vessel were significantly limited by the low speeds maintained during the delivery voyage and by the low efficiency of data collection whilst in service.

Table 4.5 shows the ratio of measured average wave period to RMS wave height based on the individual data records displayed in figure 4.2. The ratio of wave period to wave height is an indication of the wave length relative to wave height, where lower values tend to represent waves that are increasing in steepness or wave slope. It can be seen in this table for the 81 metre vessel that the ratio of wave period to wave height has a strong tendency to increase with speed in head and bow quartering wave directions. In beam sea directions this tendency is not so apparent where the period to wave height ratio tended to decrease in the mid speed range of 22.5 to 27.5 knots before increasing again at 37.5 and 42.5 knots.

4.3.1.3 Data of 86 metre Vessel

The wave statistics presented previously in figure 4.1 for all vessels is presented in figures 4.3 to 4.5 for the 86 metre vessel where the data has been further divided into categories of speed and wave direction. The delivery voyage statistics (tabs only configuration) are shown on the left side ("a" plots) whilst the operational service statistics (tabs and T-foils configuration) are shown on the right side ("b" plots).

Modest quantities of data was obtained at most speeds and configurations except at 37.5 knots (figure 4.4(6a)) where only a few data points exist. Whilst the amounts of data varied between speeds and between delivery and service operations, the range of wave periods did not vary significantly although the range did include all the most probable periods anyway. Wave periods ranged from 6 to 20 seconds for the operational service data ("b" data) and 6 to 24 seconds for the delivery voyage data ("a" data).

In service the wave height rarely exceeded 1.0 metres (RMS), which is approximately the regulatory limiting significant wave height of 3 to 4 metres for service operations. The range of speeds in these diagrams had a similar range of wave heights and periods indicating that whilst operating on this route in the English Channel there is not a clear relationship between the vessel speed and the wave height or period.

Table 4.4 shows a summary of the average wave heights and periods for each wave heading for the data contained in figures 4.3 to 4.5 (see section 3.5.2 for definitions). From this data, of which there is a substantially greater volume than obtained from the 81 metre vessel, one cannot draw an absolutely clear conclusion that the vessel speed decreased as the wave height increased or that a change in the wave period might have

been responsible for a change in the vessel speed. However, there is some evidence of a trend for the speed to reduce as the wave height increases. For example, the 86 metre vessel in service data with waves encountered on the bow quarter shows an average wave height of 0.83 metres RMS at 12.5 knots decreasing to 0.49 metres RMS at 37.5 knots. Whilst this trend is not totally regular, similar effects can be seen for some of the other directions, both in service and on delivery.

Table 4.5 shows the ratio of measured average wave period to RMS wave height and is based on individual data records also displayed in figures 4.3 to 4.5. As previously mentioned, the ratio of wave period to wave height is an indication of the wave length relative to wave height where lower values tend to reflect waves that are increasing in steepness or wave slope. It can be seen in this table for the 86 metre vessel that the ratio of wave period to wave height has a strong tendency to increase with speed in head and bow quartering wave directions in a similar manner seen in the results for the 81 metre vessel. The beam sea directions had a similar tendency observed for the 81 metre vessel of the period to wave height ratio tending to decrease in the mid speed range of 22.5 to 27.5 knots before increasing again at 37.5 and 42.5 knots.

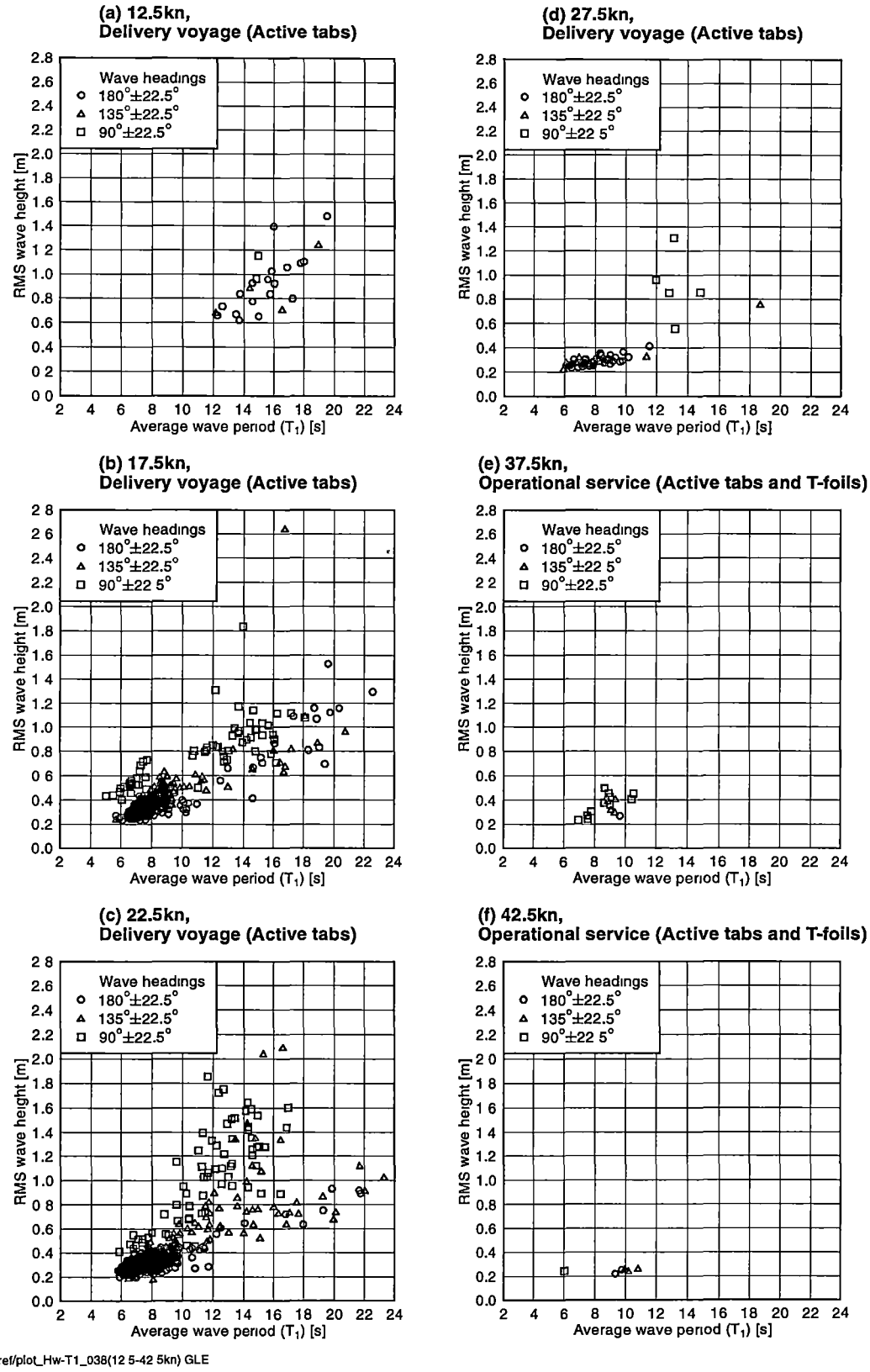

Figure 4.2: 81 metre vessel measured RMS wave height verses average wave period (T_1) (12.5 to 42.5kn). Various observed wave heading sectors. Configurations: active tabs (delivery voyage), active tabs and T-foils (operational service). (See table 4.4 for the average values of this data and table 4.5 for the period to wave height ratios based on speed and wave direction)

	Head sea				Bow-quarter sea				Beam sea			
Speed (±2.5) [kn]	RMS wave height $(m_0)^{0.5}$ [m]	T_z [s]	T_p [s]	T_1 [s]	RMS wave height $(m_0)^{0.5}$ [m]	T_z [s]	T_p [s]	T_1 [s]	RMS wave height $(m_0)^{0.5}$ [m]	T_z [s]	T_p [s]	T_1 [s]
81 metre, delivery voyage (tabs only)												
12.5	0.92	13.5	5.5	16.0	0.88	13.4	5.4	16.1	1.06	12.9	5.2	14.9
17.5	0.37	8.4	4.8	10.2	0.50	9.3	5.0	10.9	0.79	9.6	4.1	11.7
22.5	0.32	7.2	4.7	8.2	0.54	9.8	5.2	11.6	1.04	10.3	4.9	11.9
27.5	0.29	7.0	4.6	8.2	0.35	8.3	4.5	10.8	0.91	7.5	3.6	9.2
32.5	-	-	-	-	-	-	-	-	-	-	-	-
37.5	-	-	-	-	-	-	-	-	-	-	-	-
42.5	-	-	-	-	-	-	-	-	-	-	-	-
81 metre, service operations (tabs and T-foils)												
12.5	-	-	-	-	-	-	-	-	-	-	-	-
17.5	-	-	-	-	-	-	-	-	-	-	-	-
22.5	-	-	-	-	-	-	-	-	-	-	-	-
27.5	-	-	-	-	-	-	-	-	-	-	-	-
32.5	-	-	-	-	-	-	-	-	-	-	-	-
37.5	0.27	8.7	5.7	9.7	0.35	7.9	4.6	8.9	0.36	7.5	3.7	8.9
42.5	0.23	8.8	6.2	9.6	0.26	9.0	4.8	10.3	0.24	5.4	3.6	6.0
86 metre, delivery voyage (tabs only)												
12.5	0.64	8.7	3.7	11.0	0.65	7.8	3.9	9.6	1.30	11.8	4.5	14.1
17.5	0.58	8.7	4.3	10.8	0.52	7.9	3.8	9.6	0.91	13.1	4.6	16.4
22.5	0.52	8.3	4.5	10.3	0.69	10.5	5.3	12.5	0.96	12.7	4.2	15.9
27.5	0.65	9.6	5.5	10.8	0.58	9.6	5.3	11.0	0.76	9.8	4.0	11.8
32.5	0.42	10.4	5.7	12.0	0.39	7.8	4.7	9.0	0.53	9.9	5.4	11.6
37.5	-	-	-	-	0.62	12.6	4.6	16.3	0.49	12.0	5.3	14.6
42.5	-	-	-	-	-	-	-	-	-	-	-	-
86 metre, service operations (tabs and T-foils)												
12.5	0.85	8.1	5.0	8.9	0.83	7.9	4.7	8.8	0.55	12.2	3.6	16.6
17.5	0.49	9.6	4.2	11.5	0.75	8.9	4.2	10.7	0.68	7.2	3.6	8.9
22.5	-	-	-	-	0.55	8.5	3.9	10.2	0.62	9.2	4.4	10.9
27.5	-	-	-	-	0.49	7.5	3.8	9.0	0.57	8.2	3.9	10.0
32.5	0.44	9.0	4.8	10.5	0.49	8.0	4.4	9.3	0.64	8.6	4.2	10.5
37.5	0.47	11.1	5.5	12.8	0.54	9.4	5.1	11.0	0.58	9.0	4.5	10.8
42.5	-	-	-	-	0.56	10.9	5.9	12.5	0.61	12.0	5.5	14.3

C:\1Nigel\042DATA\cor_1filebasis\038-042(averages table)-from rms files xls Wave height-period

Table 4.4: Measured wave heights (RMS) and wave periods grouped according to speed and observed wave direction sectors (81 and 86m vessels)

	Head sea			**Bow-quarter sea**			**Beam sea**		
Speed (±2.5) [kn]	Ratio (T_z / $(m_0)^{0.5}$) [s/m]	Ratio (T_p / $(m_0)^{0.5}$) [s/m]	Ratio (T_1 / $(m_0)^{0.5}$) [s/m]	Ratio (T_z / $(m_0)^{0.5}$) [s/m]	Ratio (T_p / $(m_0)^{0.5}$) [s/m]	Ratio (T_1 / $(m_0)^{0.5}$) [s/m]	Ratio (T_z / $(m_0)^{0.5}$) [s/m]	Ratio (T_p / $(m_0)^{0.5}$) [s/m]	Ratio (T_1 / $(m_0)^{0.5}$) [s/m]
81 metre, delivery voyage (tabs only)									
12.5	14.7	6.0	17.4	15.2	6.1	18.3	12.2	5.0	14.1
17.5	22.7	12.9	27.5	18.7	10.1	22.0	12.2	5.2	14.9
22.5	22.1	14.5	25.4	18.3	9.7	21.7	9.9	4.7	11.5
27.5	24.4	15.9	28.3	23.9	13.0	30.9	8.3	4.0	10.2
32.5	-	-	-	-	-	-	-	-	-
37.5	-	-	-	-	-	-	-	-	-
42.5	-	-	-	-	-	-	-	-	-
81 metre, service operations (tabs and T-foils)									
12.5	-	-	-	-	-	-	-	-	-
17.5	-	-	-	-	-	-	-	-	-
22.5	-	-	-	-	-	-	-	-	-
27.5	-	-	-	-	-	-	-	-	-
32.5	-	-	-	-	-	-	-	-	-
37.5	32.9	21.3	36.4	22.4	13.1	25.3	20.6	10.3	24.4
42.5	37.5	26.4	40.9	35.1	18.6	40.3	22.3	15.1	24.9
86 metre, delivery voyage (tabs only)									
12.5	13.6	5.8	17.2	12.0	5.9	14.6	9.0	3.4	10.9
17.5	15.1	7.5	18.8	15.3	7.4	18.6	14.4	5.0	17.9
22.5	15.8	8.6	19.6	15.2	7.7	18.1	13.3	4.3	16.6
27.5	14.8	8.5	16.7	16.5	9.0	18.9	12.8	5.3	15.5
32.5	24.8	13.6	28.6	19.9	11.8	22.8	18.7	10.3	22.0
37.5	-	-	-	20.3	7.4	26.3	24.7	10.8	30.0
42.5	-	-	-	-	-	-	-	-	-
86 metre, service operations (tabs and T-foils)									
12.5	9.5	5.9	10.5	9.5	5.7	10.6	22.0	6.6	29.9
17.5	19.5	8.6	23.3	12.0	5.7	14.3	10.6	5.3	13.1
22.5	-	-	-	15.3	7.0	18.4	14.8	7.1	17.6
27.5	-	-	-	15.5	7.9	18.6	14.3	6.9	17.4
32.5	20.4	11.0	23.9	16.1	8.9	18.8	13.6	6.5	16.5
37.5	23.6	11.8	27.3	17.5	9.4	20.6	15.5	7.7	18.6
42.5	-	-	-	19.4	10.5	22.2	19.6	8.9	23.3

C:\1Nigel\042DATA\cor_1filebasis\038-042(averages table)-from rms files.xls

Table 4.5: Ratio of wave period to measured wave heights (RMS) grouped according to speed and observed wave direction sectors (81 and 86m vessels)

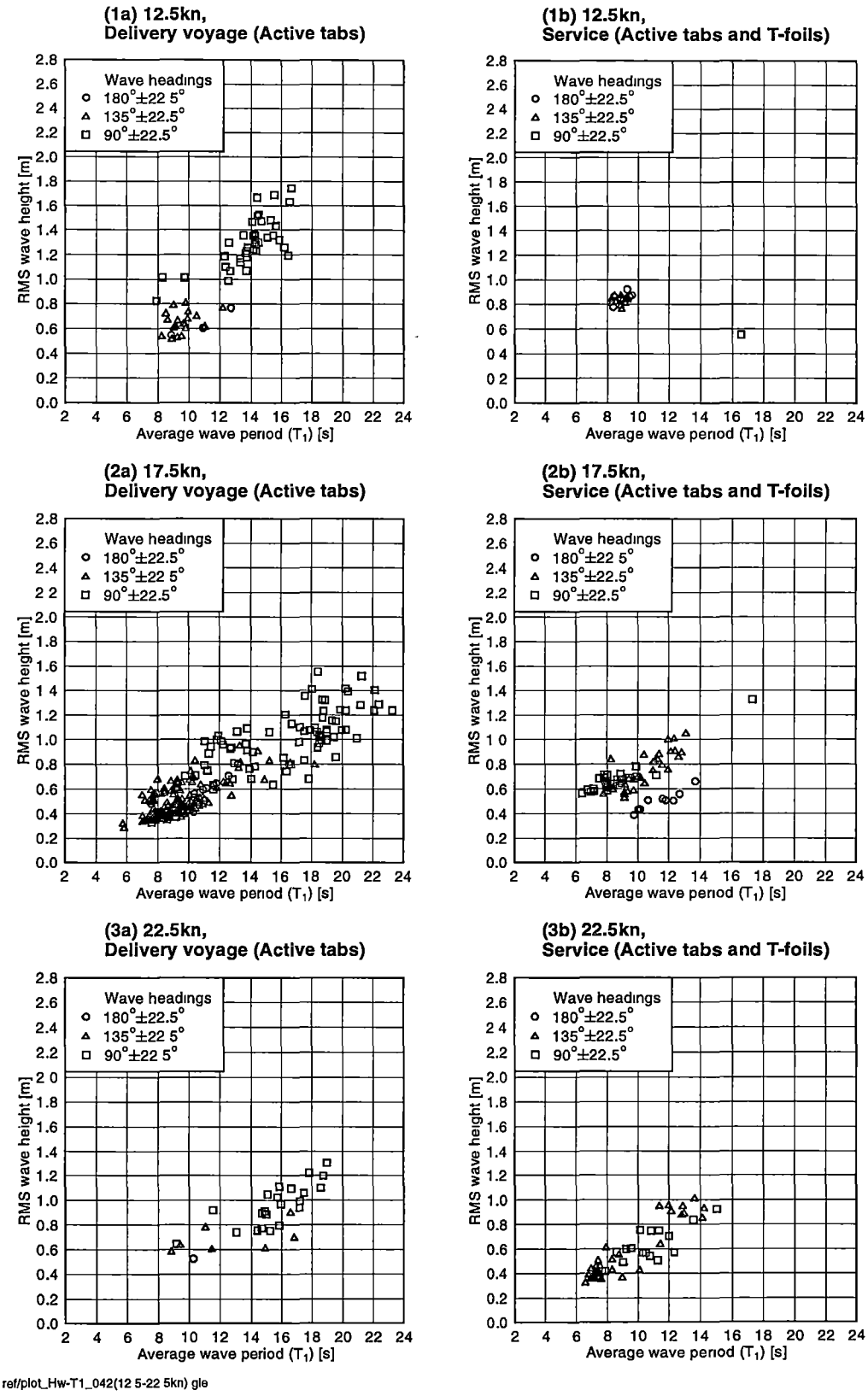

Figure 4.3: 86 metre vessel measured RMS wave height verses average wave period (T_1) (12.5 to 22.5kn). Various observed wave heading sectors. Configurations: active tabs (delivery voyage), active tabs and T-foils (operational service). (See table 4.4 for the average values of this data and table 4.5 for the period to wave height ratios based on speed and wave direction)

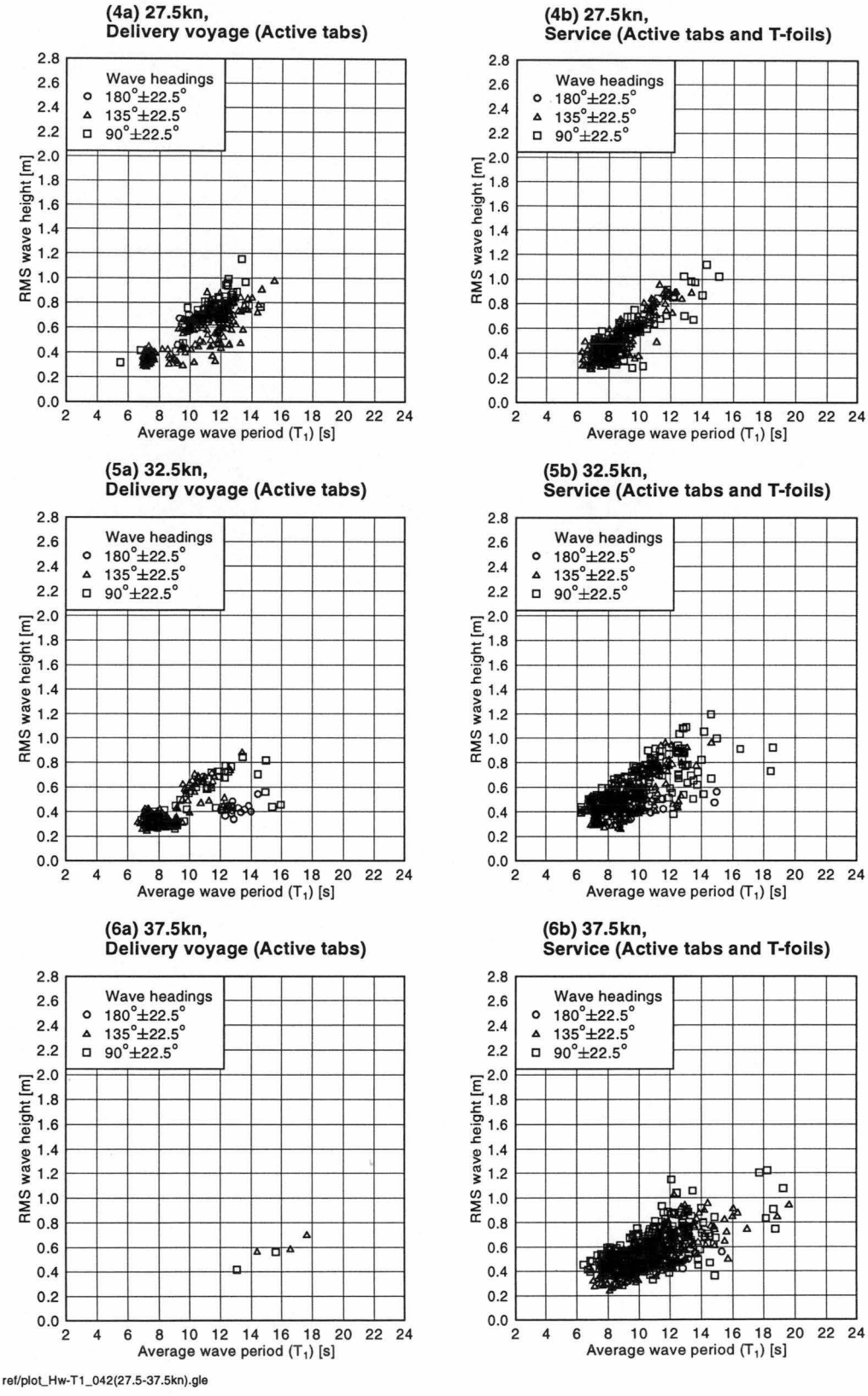

Figure 4.4: 86 metre vessel measured RMS wave height verses average wave period (T_1) (27.5 to 37.5kn). Various observed wave heading sectors. Configurations: active tabs (delivery voyage), active tabs and T-foils (operational service). (See table 4.4 for the average values of this data and table 4.5 for the period to wave height ratios based on speed and wave direction)

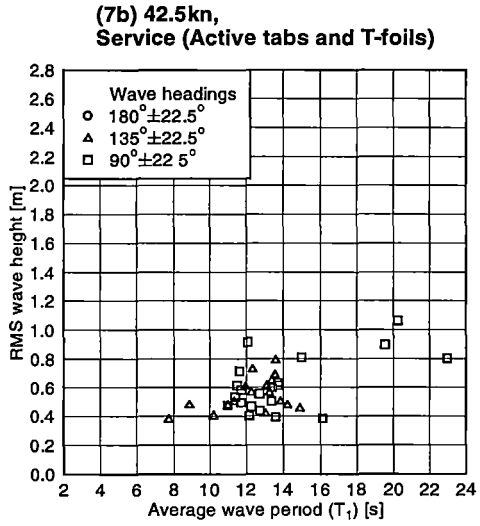

Figure 4.5: 86 metre vessel measured RMS wave height verses average wave period (T_1) (42.5kn). Various observed wave heading sectors. Configuration: active tabs and T-foils (operational service). (See table 4.4 for the average values of this data and table 4.5 for the period to wave height ratios based on speed and wave direction)

4.3.2 Derived Wave Spectra

4.3.2.1 Spectra for 81 metre Vessel

The process of collecting the data records taken from measurements during the delivery voyage and service operations has previously been discussed. In particular the process of grouping this data according to vessel speed and observed wave direction for subsequent data processing has also been applied in the derivation of spectra. All files contained within each group were averaged in the frequency domain to obtain the wave spectra at each speed and for each wave heading sector. The result of this process is shown for the 81 metre vessel in figure 4.6 for measurements with active tabs only and in figure 4.7 for measurements with active tabs and T-foils. The average wave energy spectra in figure 4.6 shows that in head and bow quartering seas, the most severe wave spectrum is at a forward speed of 12.5 knots whilst in beam seas the spectra for a range of speeds from 12.5 to 27.5 knots have similar magnitudes. The average wave spectra for service operations in figure 4.7 is generally smaller than the delivery voyage spectra, thus supporting the fact that the waves were on average smaller. This also can be seen in the statistics shown previously in figure 4.1. Further generalisations about this data are not warranted because the amount of data used to derive these spectra was small.

With the wave energy spectra shown in these figures derived by taking the average of all wave spectra within each data group it was also possible to derive the corresponding bandwidth parameter for each averaged spectrum, which has two formulations. One given by Lloyd (1989) $\left(\text{i.e. } \varepsilon = \sqrt{1 - \frac{m_2^2}{m_0 m_4}}\right)$, which can be used to determine the significant wave height $\left(\text{i.e. } H_{1/3} = 4\sqrt{1 - \frac{\varepsilon^2}{2}}\sqrt{m_0}\right)$ (see also appendix E) and relates to the ratio between the average period of the peaks and the average zero-crossing period. The other proposed by Tucker (1991) $\left(\text{i.e. } \nu = \sqrt{\frac{m_0 m_2}{m_1^2} - 1}\right)$ is regarded by the same author as a more appropriate form because it removes the dependence on the fourth spectral moment (m_4) and is the normalised radius of gyration of the spectrum about its mean frequency value. Tucker's bandwidth parameter is also used in the formulation of spectral skewness $\left(= \left(m_0^2 m_3 / m_1^3 - 3\nu^2 - 1\right) / \nu^2\right)$. However, both bandwidth formulations will approach zero for narrow bandwidths and both will approach unity for broad spectral bandwidths, but they will both give different results where there is a significant spectral tail in the high frequency region.

The bandwidth parameters shown in table 4.6 are relatively high compared with the well documented Pierson–Moskowitz (P-M) wave spectrum, which has a value of $\nu = 0.426$, the Modified Pierson–Moskowitz or Bretschneider wave spectrum, which has a value of $\nu = 0.425$ and the JONSWAP spectrum, which has a value of $\nu = 0.39$ (with $\gamma = 3.3$, $\sigma_A = 0.7$, $\sigma_B = 0.9$) (see Tucker (1991) p 97). Compared with the bandwidth parameter from Lloyd (1989), the Modified Pierson–Moskowitz or Bretschneider wave spectrum has a value of $\varepsilon = 1$ and in the strict sense makes it broadbanded. However, in most cases the high frequency tail would be truncated at the frequencies of significant vessel response, thus removing the high frequency components that only contribute to increase the bandwidth but not to alter the vessel motions, in which case the bandwidth parameter ε would be much less than unity and may even approach the narrow band case of $\varepsilon = 0$. This indicates the possibility of the measured wave spectra being the result of a combination of long wavelength swells and more local shorter length wind generated waves. Visual observations in some regions where data was acquired did indicate the presence of swells from one direction and wind waves from a different direction, but these values show the combination of the two types of waves of unknown

specific directions was quite general amongst the data.

The skewness parameter of table 4.6 range from 0.80 to 4.58 compared with the value of the typical P-M wave spectrum of 5.60, which includes the high frequency tail. The parameter however is sensitive to the high frequency tail and if the spectrum is truncated to a value that is three times the mean spectral frequency, this value is reduced to 1.91. It is evident from the rather low values of the skewness in table 4.6 that the measured wave spectra probably are limited by truncation of the high frequency tail, but this should not be of importance in determination of the vessel response functions. Also, evaluation of the skewness is very sensitive to the spectra being bi-modal due to contributions form wind waves and swell. Thus the large range of skewness evident in the data is to be expected.

It is evident that the spectra shown in figures 4.6 and 4.7 are generally rather irregular. This comes about because they represent the averaged wave energy spectra obtained on different occasions for which the sea conditions may be individually quite different. Thus the spectra are mainly of interest in the context of indicating the conditions under which the vessel response was determined and it is not to be expected that the wave energy spectra obtained will indicate any more than the conditions to which the vessel was on average exposed during data collection.

4.3.2.2 Spectra for 86 metre Vessel

In a similar manner to that presented for the 81 metre vessel, the wave spectra derived from measurements made on the 86 metre vessel at various speeds and observed wave headings during the delivery voyage and service operations are shown in figures 4.8 and 4.9 respectively.

The wave energy spectra in head seas (figure 4.8) show that for a number of operational speeds two dominant wave frequencies were present in the overall set of data at approximately 0.3 and 0.9 radians per second. The precise reason for this is not clear but it seems that this is simply due to the variation of sea conditions, which at times may have been in proximity to a coastline and at times in relatively open ocean. Much of this head sea data was collected during the early stages of the delivery voyage between Sydney and Perth. Overall there is a trend for the spectral density in the 0.2 to 0.6 rad/s range to reduce as speed increased from 12.5 to 32.5 knots, but the trend was not entirely regular at intermediate speeds. In the 0.7 to 1.0 rad/s range there was little wave energy encountered at the highest speed (32.5kn) but a significant level of energy was measured when operating at lower speeds up to 27.5 knots. For the quartering seas encountered there is again evidence of seas with most energy in either the 0.2 to 0.6 rad/s range or the 0.7 to 1.0 rad/s range. The maximum spectral density occurred at the lowest wave frequency (0.2 rad/s) when the vessel was operating at the highest speed (37.5kn). However, at lower speeds there was no clear trend in the energy spectra with speed in the lower frequency range, but once again in the higher frequency range there was a tendency for greater wave energy to be associated with the lower operating speeds. In beam seas (figure 4.8(b)) there was no evidence of encounter seas with energy in the higher frequency range and there was a clear trend for the spectral density to be lower as the speed increased. It is difficult to draw firm conclusions from these results regarding the sea conditions encountered during the delivery voyage, but it is evident that relatively short seas and relatively long seas were both encountered in head and bow quartering conditions, whilst only longer seas were encountered in beam sea conditions. There is some evidence of lower speeds being associated with higher wave spectral energy, but this is not entirely a clear relationship.

The average wave spectra in figure 4.8 shows there is no particular distinction

Speed (±2.5) [kn]	Head sea			Bow quartering sea			Beam sea		
	Bandwidth parameter (Lloyd, 1989)	Bandwidth parameter (Tucker, 1991)	Skewness (Tucker, 1991)	Bandwidth parameter (Lloyd, 1989)	Bandwidth parameter (Tucker, 1991)	Skewness (Tucker, 1991)	Bandwidth parameter (Lloyd, 1989)	Bandwidth parameter (Tucker, 1991)	Skewness (Tucker, 1991)
81 metre, delivery voyage (tabs only)									
12.5	0.91	0.64	3.86	0.92	0.67	3.72	0.91	0.58	4.58
17.5	0.82	0.69	1.23	0.84	0.62	1.84	0.90	0.70	3.00
22.5	0.75	0.57	0.80	0.85	0.64	2.01	0.88	0.59	3.11
27.5	0.76	0.59	0.80	0.84	0.82	1.15	0.88	0.70	2.40
32.5	-	-	-	-	-	-	-	-	-
37.5	-	-	-	-	-	-	-	-	-
42.5	-	-	-	-	-	-	-	-	-
81 metre, service operations (tabs and T-foils)									
12.5	-	-	-	-	-	-	-	-	-
17.5	-	-	-	-	-	-	-	-	-
22.5	-	-	-	-	-	-	-	-	-
27.5	-	-	-	-	-	-	-	-	-
32.5	-	-	-	-	-	-	-	-	-
37.5	0.76	0.47	1.78	0.81	0.52	2.21	0.87	0.64	2.41
42.5	0.71	0.43	1.31	0.85	0.57	2.49	0.74	0.49	1.13
86 metre, delivery voyage (tabs only)									
12.5	0.91	0.78	2.60	0.87	0.70	2.03	0.93	0.67	4.07
17.5	0.87	0.74	1.77	0.87	0.70	2.02	0.94	0.75	3.92
22.5	0.84	0.73	1.35	0.86	0.64	2.13	0.94	0.76	4.33
27.5	0.82	0.52	2.26	0.84	0.56	2.26	0.91	0.69	3.21
32.5	0.84	0.58	2.12	0.80	0.56	1.65	0.84	0.61	1.91
37.5	-	-	-	0.93	0.82	3.38	0.90	0.69	2.99
42.5	-	-	-	-	-	-	-	-	-
86 metre, service operations (tabs and T-foils)									
12.5	0.79	0.47	2.14	0.80	0.48	2.28	0.95	0.92	4.18
17.5	0.90	0.65	3.09	0.88	0.65	2.51	0.86	0.73	1.81
22.5	-	-	-	0.89	0.67	2.62	0.88	0.65	2.49
27.5	-	-	-	0.86	0.65	2.14	0.88	0.69	2.28
32.5	0.84	0.61	2.10	0.83	0.61	1.86	0.88	0.69	2.28
37.5	0.87	0.59	2.83	0.84	0.62	2.03	0.87	0.67	2.23
42.5	-	-	-	0.84	0.55	2.65	0.89	0.65	2.99

C:\1Nigel\042DATA\cor_1filebasis\038-042(averages table)-from rms files.xls

Table 4.6: Measured bandwidth parameters from averaged experimental wave spectra based on Lloyd 1989 ($= \sqrt{1 - \frac{m_2^2}{m_0 m_4}}$) and Tucker 1991 ($= \sqrt{\frac{m_0 m_2}{m_1^2} - 1}$). Also skewness ($= (m_0^2 m_3/m_1^3 - 3v^2 - 1)/v^2$) grouped according to measured speed and observed wave direction sectors (81 and 86m vessels). Note: Bretschneider wave spectrum bandwidth Parameter (Lloyd) = 0 to 1; (Tucker) = 0.426; Skewness (Tucker) = 5.6

between the speeds within the head and bow quartering wave headings but the beam sea (figure 4.8(c)) shows that as the wave spectrum increased the vessel speed decreased. Furthermore, the lower speeds in beam seas were larger than any of the spectra from the other wave direction sectors.

The average wave spectral densities measured during service operations and shown in figure 4.9(a) for head sea conditions show that the encountered waves were much less variable then during the delivery voyage, the energy spectra showing a single broader maximum without the presence of a second frequency of maximum wave energy. Also the maximum spectral density occurred at the lowest vessel speed (12.5kn) with progressive reduction as speed increased to 32.5kn but with a moderate increase in spectral density at 37.5kn (although still much lower than at 12.5kn).

For quartering seas shown in figure 4.9(b), the spectra are quite broad and irregular. The largest volume of data was collected in quartering seas when in operational service and it seems that this has produced the widest range of encountered sea states. The maximum spectral energy density occurred at 12.5kn, and reduced as the speed increased to 32.5kn, but higher speeds to 42.5kn (for which the data volume was small) the spectral energy density increased again.

In beam seas shown in figure 4.9(c), the wave energy density encountered indicated dominance of lower frequency long period and longer length waves with a concentration of wave spectral energy density around 0.3 rad/s at all speeds. The maximum wave spectral density was highest at the lowest speed and reduced as speed increased to 32.5kn, but once again larger spectral energy density values were measured at the highest speed.

In general it can be seen that the sea conditions encountered in service operation were somewhat less varied than during the delivery cruise for head and bow quartering seas. Beam sea encounter showed a dominance of longer lower frequency seas, in both delivery and service operations.

Once again, the skewness values for this vessel (table 4.6) ranged from 0.80 to 4.58 in comparison with the P-M wave spectrum that was discussed previously that could range from 1.91 to 5.60 depending on the truncation point of the high frequency tail. So it appears that this outcome in the measurements may be partly due to truncation of the measured spectra at high frequency (possibly due to the low pass filter applied to the signals during data analysis, which was set at 2 Hertz).

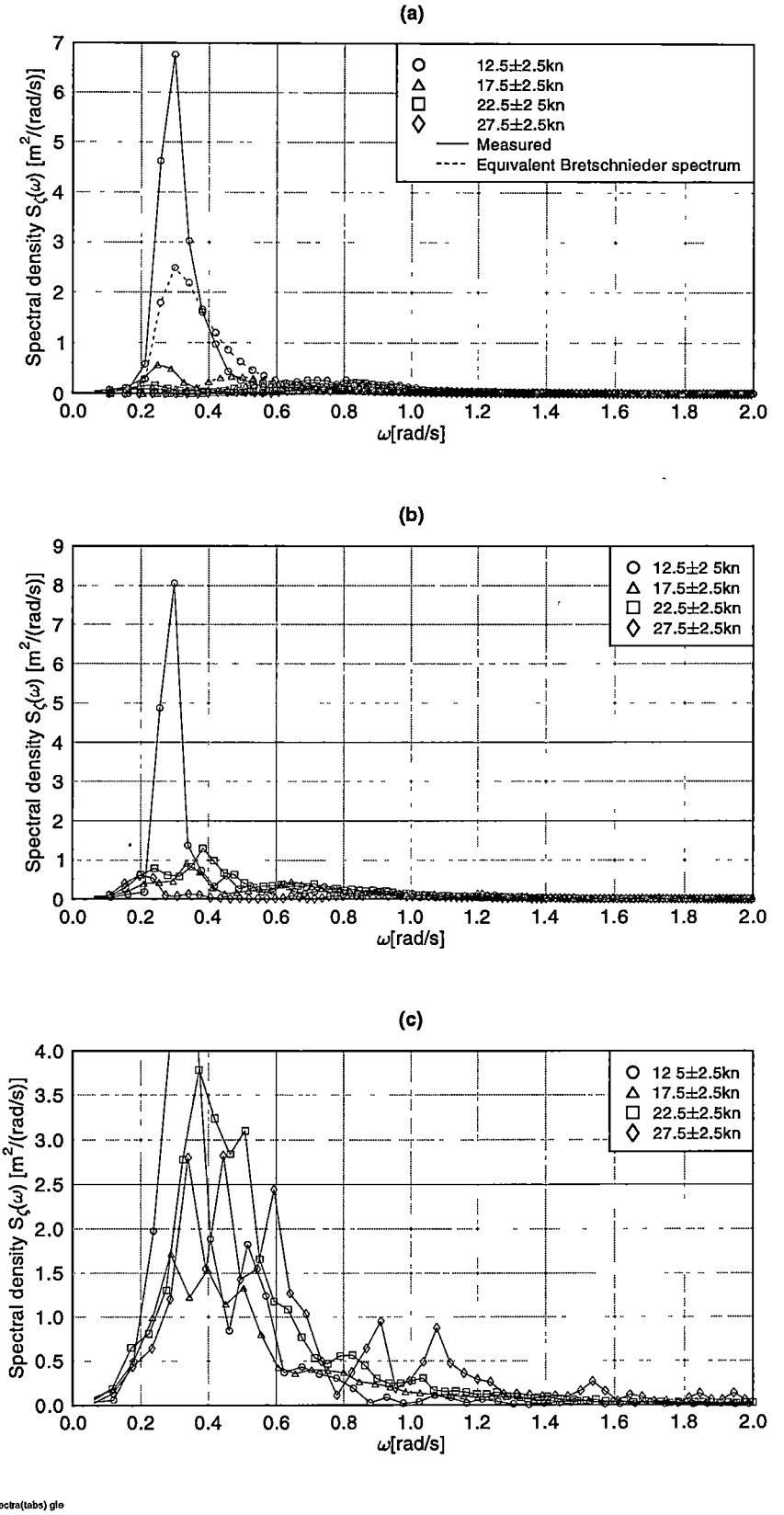

rel/plot_038_Wave-spectra(tabs) gle

Figure 4.6: Measured wave spectra (81m vessel, active tabs only). Observed wave heading sectors: (a) Bow (180° ±22.5°), (b) Bow-quarter (135° ±22.5°) and (c) Beam (90° ±22.5°).

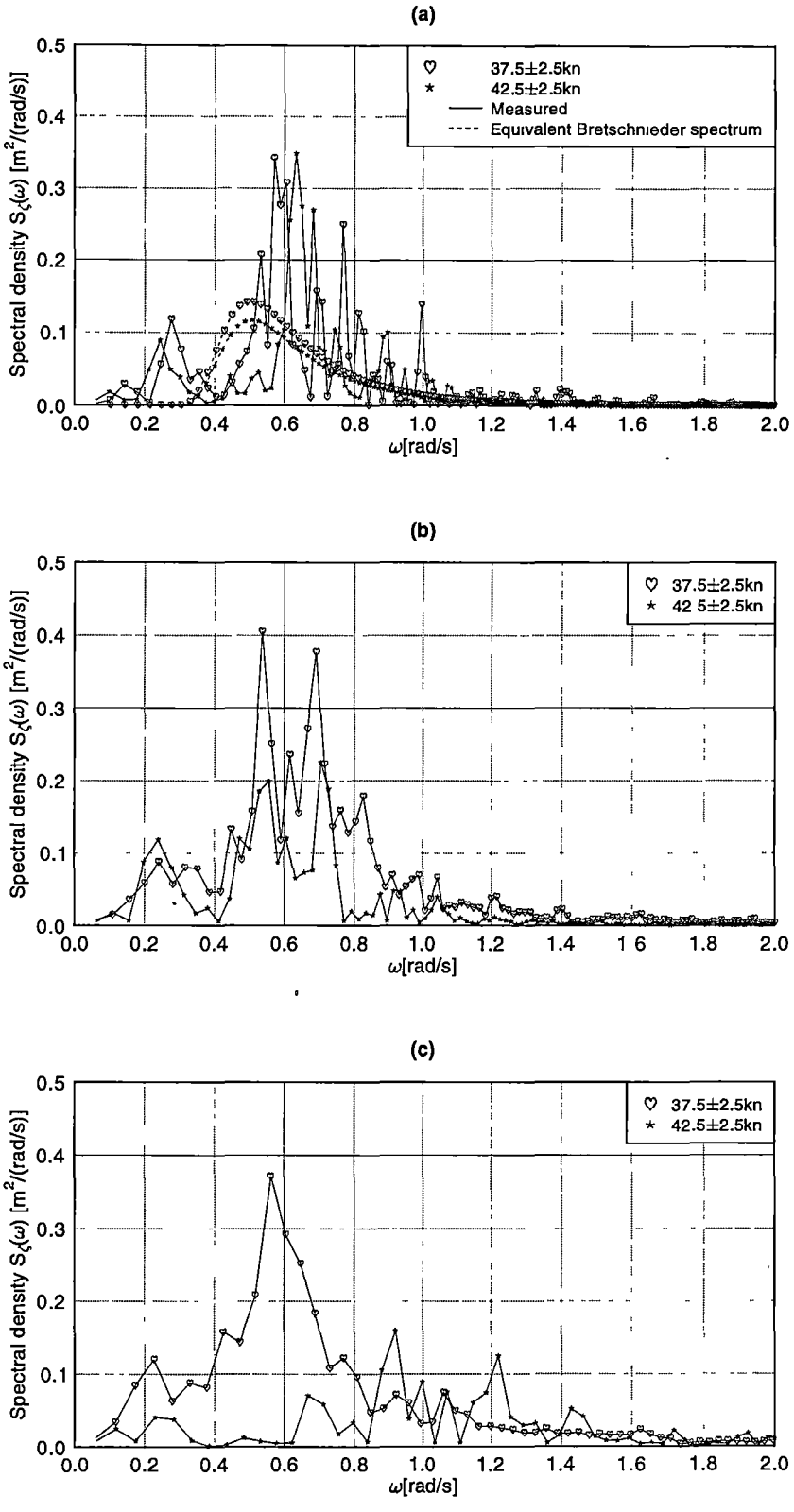

Figure 4.7: Measured wave spectra (81m vessel, active tabs and T-foils). Observed wave heading sectors: (a) Bow (180° ±22.5°), (b) Bow-quarter (135° ±22.5°) and (c) Beam (90° ±22.5°).

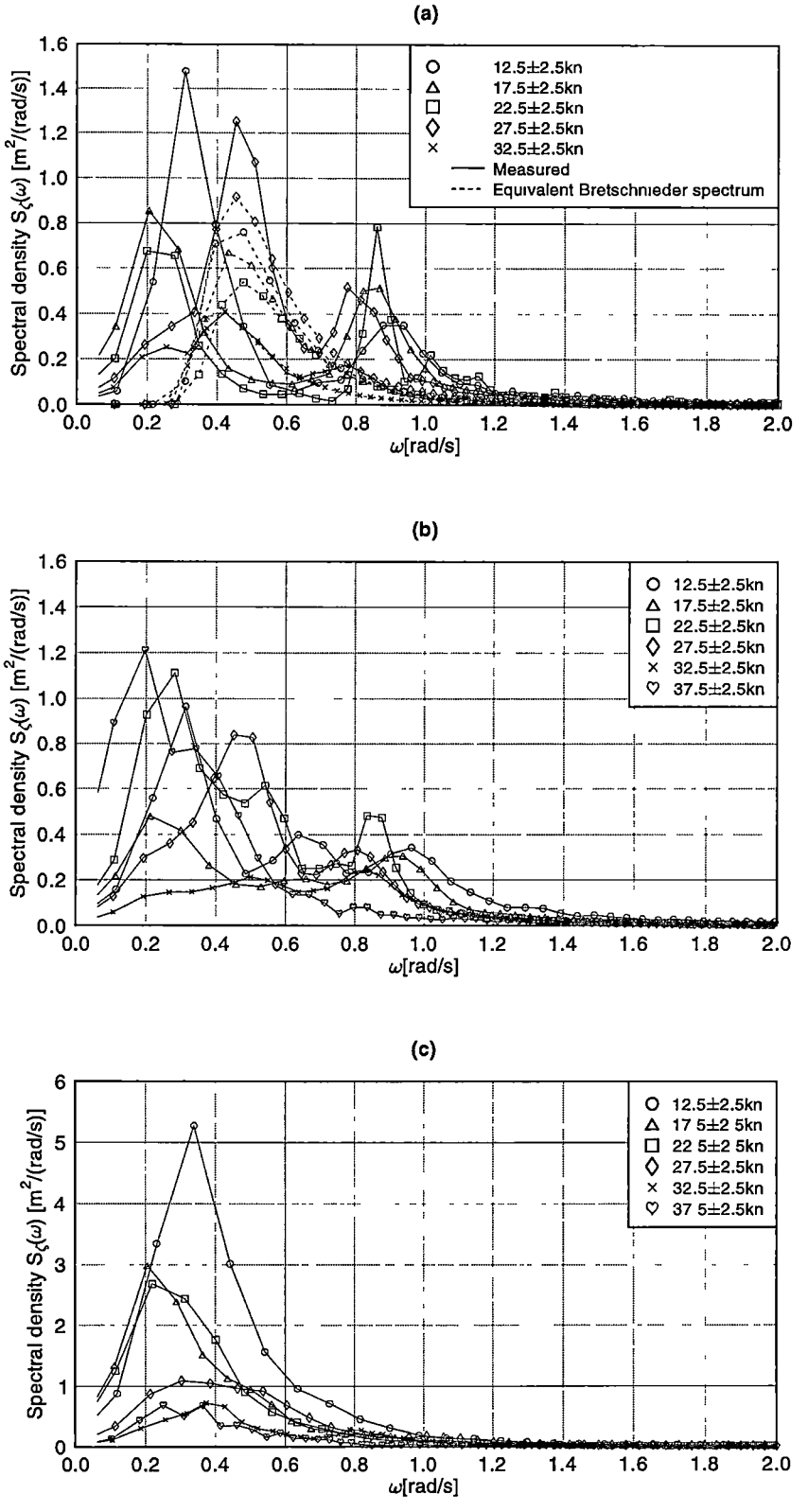

rel/plot_042_Wave-spectra(tabs).gle

Figure 4.8: Measured wave spectra (86m vessel, active tabs only). Observed wave heading sectors: (a) Bow (180° ±22.5°), (b) Bow-quarter (135° ±22.5°) and (c) Beam (90° ±22.5°).

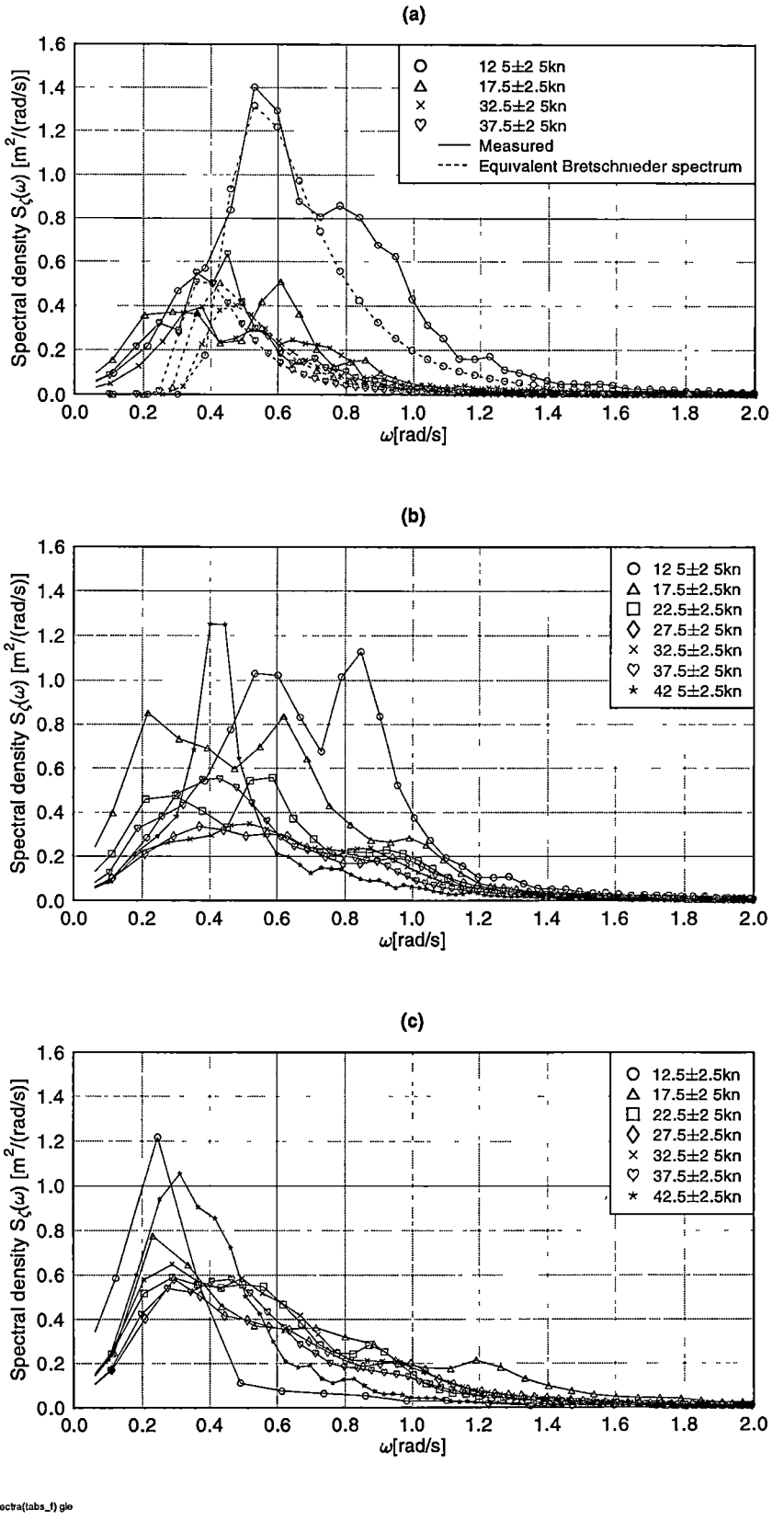

Figure 4.9: Measured wave spectra (86m vessel, active tabs and T-foils). Observed wave heading sectors: (a) bow (180° ±22.5°), (b) bow-quarter (135° ±22.5°) and (c) beam (90° ±22.5°).

4.4 Vertical Accelerations

4.4.1 Variation of Relative Acceleration with Longitudinal Position on Vessel

The average vertical accelerations recorded during experimental measurements on both the 81 and 86 metre vessels are shown as longitudinal distributions in figures 4.10 to 4.12. It is clear from these diagrams that the vertical acceleration toward the bow is often more than twice the vertical acceleration at the LCG and the aft end, particularly when the vessel had only transom tabs installed. When the T-foils were installed the difference is less pronounced particularly as the speed increases. In head seas the LCG acceleration is typically about 0.1g/m whilst the bow acceleration was as high as 0.3g/m. It is significant to observe that the LCG acceleration of the 86 metre vessel with active tabs and T-foils in head seas only fell below 0.1g/m at the speed of 12.5 knots. At the remaining speeds the acceleration was approximately equal to or greater than 0.1g/m.

The 81 metre vessel generally had higher accelerations than the 86 metre vessel but the distribution of acceleration showed similar characteristics.

The acceleration relative to wave height (g/m RMS) is the parameter shown in figures 4.10 to 4.12 and it is based on the assumption that the vessel motion response to the encountered wave height is linear in nature. As has been explained previously, the data acquired in these series of full-scale trials was not sufficient to form the basis of a full spectral investigation of the effect of wave height and by implication the nonlinear nature of the vessel response (although in section 4.4.2 which follows, consideration is given to the effect of wave height and period on the relative acceleration RMS values). However, factors other than wave height will have a bearing on the acceleration relative to wave height. In particular the average wave period in relation to the frequency of maximum response of the vessel will have a direct effect on the acceleration relative to wave height. In particular for conditions where the encountered wave period corresponds closely to the frequency of maximum response it is to be expected that larger accelerations relative to wave height will be observed. Thus, whilst acceleration relative to wave height is a parameter of direct interest to operators and designers, it must be borne in mind that such values will necessarily reflect the sea conditions encountered, in particular the wave period. Thus whilst the result of figures 4.10 to 4.12 indicate that rather large accelerations relative to wave height is observed for both vessels, particularly at the bow, when on the delivery voyage, it may be that this is due to the difference of wave conditions encountered on delivery and in service as well as to the installation of the T-foils for service operations. Nevertheless, the results do seem to indicate that the T-foils have contributed to reduced bow motions for speeds between 17.5 and 32.5 knots.

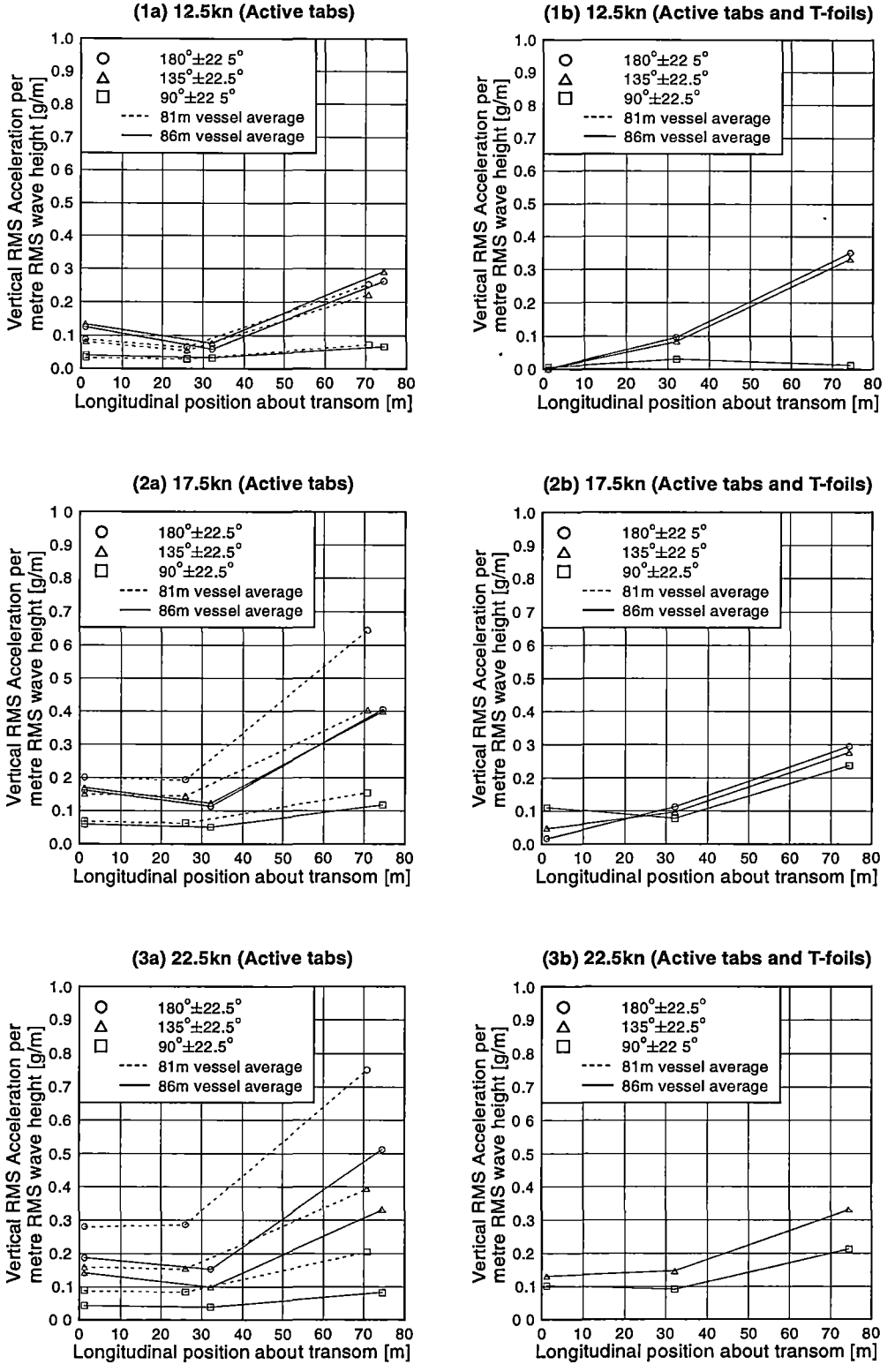

Figure 4.10: Measured acceleration verses hull position (81m and 86m vessels, 12.5 to 22.5kn). Various observed wave heading sectors. Configurations: (a) active tabs (Delivery voyage) and (b) active tabs and T-foils (Operational service).

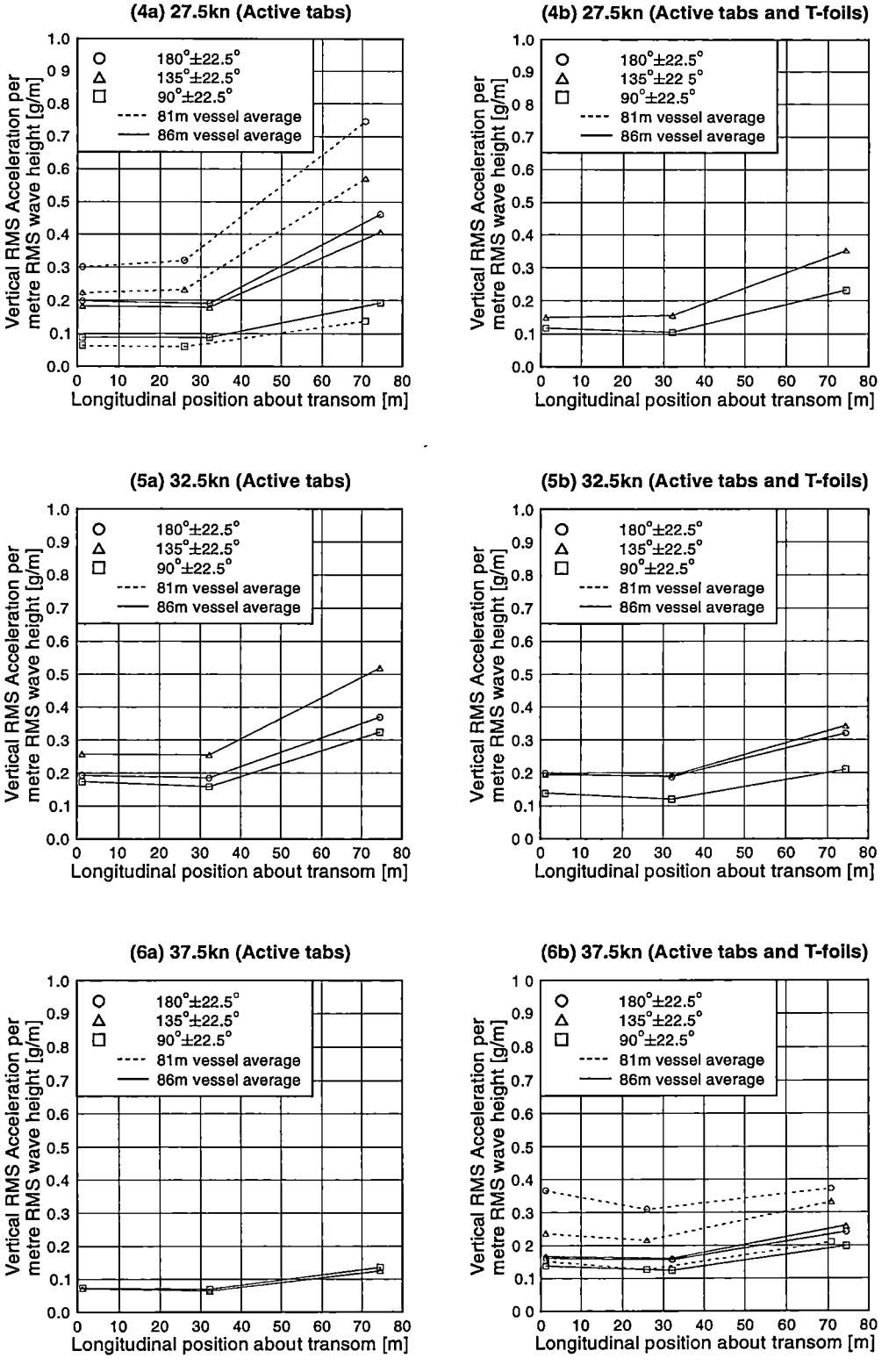

Figure 4.11: Measured acceleration verses hull position (81m and 86m vessels, 27.5 to 37.5kn). Various observed wave heading sectors. Configurations: (a) active tabs (Delivery voyage) and (b) active tabs and T-foils (Operational service).

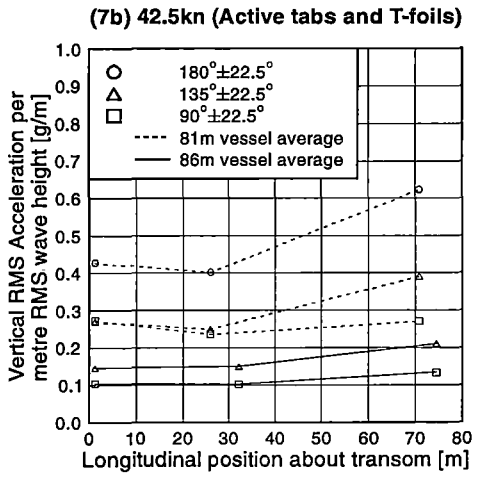

ref/plot_rmsDist_(42 5kn) gle

Figure 4.12: Measured acceleration verses hull position (81m and 86m vessels, 42.5kn). Various observed wave heading sectors. Configurations: (b) active tabs and T-foils (Operational service).

4.4.2 Variation of Relative Acceleration with Wave Height

4.4.2.1 Data for 81 metre Vessel

The ratio of vertical acceleration to wave height (RMS) against the wave height (RMS) for the 81 metre vessel is shown in figure 4.13. Once again the most detailed data in these diagrams was obtained at the 17.5 and 22.5 knot ranges. It is apparent that as the wave height increases the ratio of acceleration with wave height decreases except at the wave height of approximately 0.3 metres where there is a large range of acceleration values in the data record at the one wave height. One cause for this may be the variation in vessel displacement and another cause may be a greater range of variability of period and direction in the encountered waves at the lower wave heights.

Table 4.7 shows the average wave heights and acceleration values for the various speeds and corresponds with figure 4.13. It can be seen that in head seas the average acceleration at the LCG tends to increase in both magnitude and in proportion with the unit wave height whilst the wave height actually decreases. These same observations apply to the bow quartering wave direction but not so clearly to the beam sea wave direction, which shows a reduction at the highest speed (27.5kn).

4.4.2.2 Data for 86 metre Vessel

The ratio of vertical acceleration to wave height (RMS) against the wave height (RMS) for the 86 metre vessel is shown in figures 4.14 to 4.16. Many of these diagrams clearly show in some cases a large reduction in the ratio of acceleration per metre wave height as the wave height increases. This characteristic may in part be due to effects of a nonlinear nature but could also be related to variations in ship displacement, vessel speed, changing wave periods, wave directions and wave directional spreading. These variables have not been accounted for in the presentation of these results and would certainly contribute to the broad range of values displayed in these results.

Table 4.7 shows the average wave heights and acceleration values for the various speeds and corresponds with the previous figures 4.14 to 4.16. It can be seen that during the delivery voyage in head seas the speed tended to increase from 12.5 to 32.5 knots as the RMS wave height decreased from 0.47 to 0.32 metres. Also, the acceleration relative to wave height shows an increasing trend as the speed increases, except that at the highest speed in each case where the data was sparse as evident in figures 4.15 and 4.16. In considering the variations in acceleration relative to wave height with wave height for both vessels shown in figures 4.13 to 4.16 it should be borne in mind that the wave period varies with wave height as discussed in section 4.3. It thus seems most likely that the reduction in acceleration relative to wave height with increasing wave height as evident in figures 4.13 to 4.16 is in fact due to variance of wave period rather than of the wave height itself. This will be considered further in section 4.4.3 which follows.

	Head sea			Bow quartering sea			Beam sea		
Speed (±2.5) [kn]	RMS wave height $(m_0)^{0.5}$ [m]	RMS LCG accel [g]	Ratio [g/m]	RMS wave height $(m_0)^{0.5}$ [m]	RMS LCG accel [g]	Ratio [g/m]	RMS wave height $(m_0)^{0.5}$ [m]	RMS LCG accel [g]	Ratio [g/m]
81 metre, delivery voyage (tabs only)									
12.5	0.92	0.061	0.066	0.88	0.049	0.056	1.06	0.032	0.030
17.5	0.37	0.071	0.193	0.50	0.071	0.144	0.79	0.050	0.063
22.5	0.32	0.093	0.286	0.54	0.083	0.155	1.04	0.088	0.085
27.5	0.29	0.093	0.321	0.35	0.081	0.232	0.91	0.055	0.061
32.5	-	-	-	-	-	-	-	-	-
37.5	-	-	-	-	-	-	-	-	-
42.5	-	-	-	-	-	-	-	-	-
81 metre, service operations (tabs and T-foils)									
12.5	-	-	-	-	-	-	-	-	-
17.5	-	-	-	-	-	-	-	-	-
22.5	-	-	-	-	-	-	-	-	-
27.5	-	-	-	-	-	-	-	-	-
32.5	-	-	-	-	-	-	-	-	-
37.5	0.27	0.082	0.310	0.35	0.076	0.216	0.36	0.046	0.127
42.5	0.23	0.094	0.402	0.26	0.064	0.249	0.24	0.057	0.236
86 metre, delivery voyage (tabs only)									
12.5	0.64	0.038	0.059	0.65	0.050	0.077	1.30	0.043	0.033
17.5	0.58	0.065	0.113	0.52	0.063	0.123	0.91	0.046	0.050
22.5	0.52	0.080	0.153	0.69	0.068	0.098	0.96	0.038	0.039
27.5	0.65	0.123	0.191	0.58	0.104	0.179	0.76	0.067	0.088
32.5	0.42	0.077	0.185	0.39	0.100	0.254	0.53	0.083	0.158
37.5	-	-	-	0.62	0.039	0.063	0.49	0.033	0.068
42.5	-	-	-	-	-	-	-	-	-
86 metre, service operations (tabs and T-foils)									
12.5	0.85	0.082	0.096	0.83	0.070	0.084	0.55	0.017	0.031
17.5	0.49	0.055	0.112	0.75	0.072	0.096	0.68	0.053	0.077
22.5	-	-	-	0.55	0.081	0.146	0.62	0.057	0.091
27.5	-	-	-	0.49	0.076	0.156	0.57	0.060	0.104
32.5	0.44	0.082	0.187	0.49	0.095	0.192	0.64	0.076	0.120
37.5	0.47	0.074	0.157	0.54	0.086	0.160	0.58	0.072	0.124
42.5	-	-	-	0.56	0.084	0.149	0.61	0.063	0.102

C:\1Nigel\042DATA\cor_1filebasis\038-042(averages table)-from rms files.xls

Table 4.7: Measured wave heights (RMS) and vertical accelerations (RMS) grouped according to speed and predicted wave direction (81 and 86m vessels)

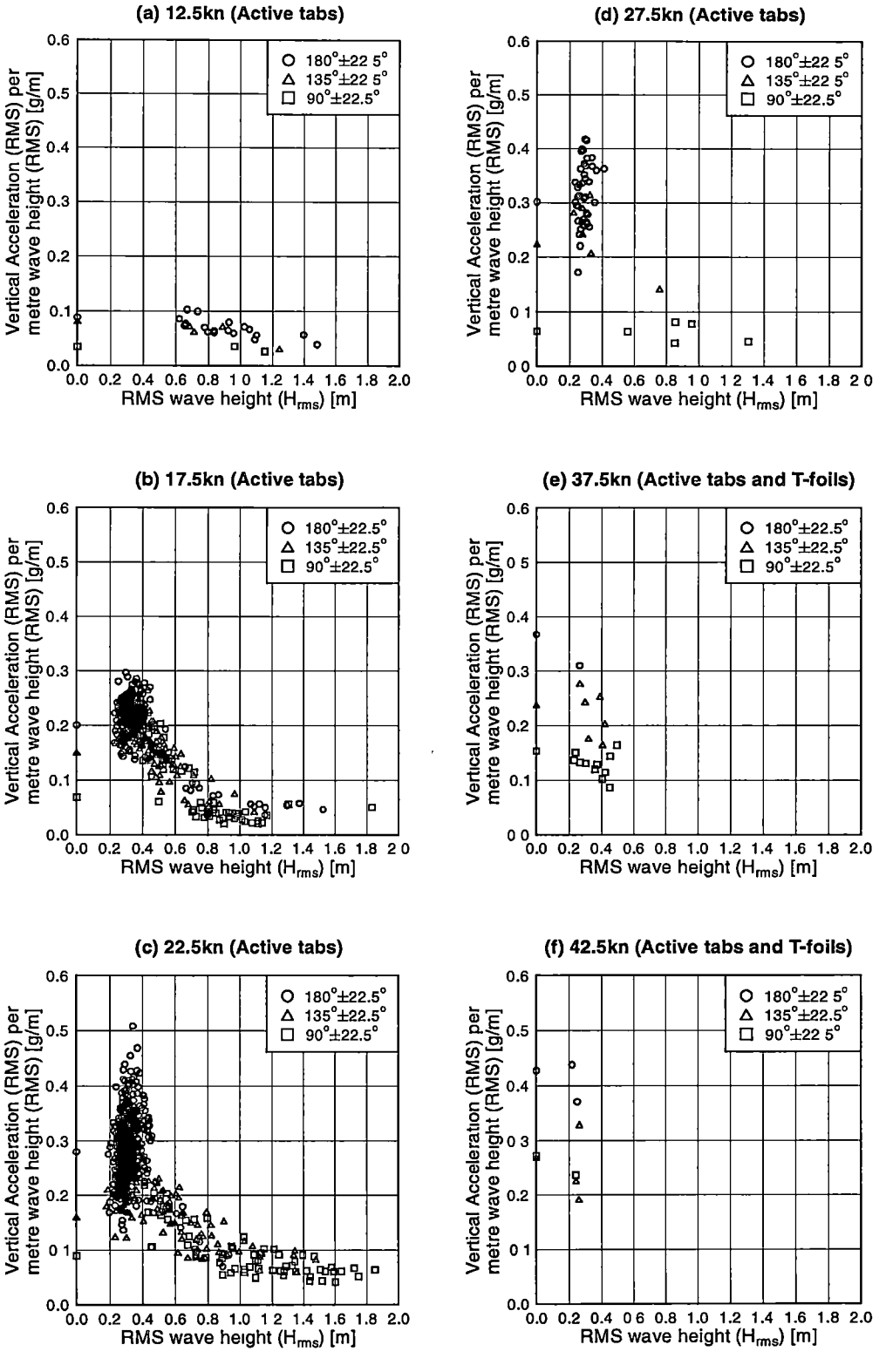

ref/plot_rmsAccel-Hs_038(12 5-42 5kn) gle

Figure 4.13: Measured LCG acceleration verses wave height (81m vessel, 12.5 to 42.5kn). Various predicted wave heading sectors. Configurations: active tabs (Delivery voyage) and active tabs and T-foils (Operational service).

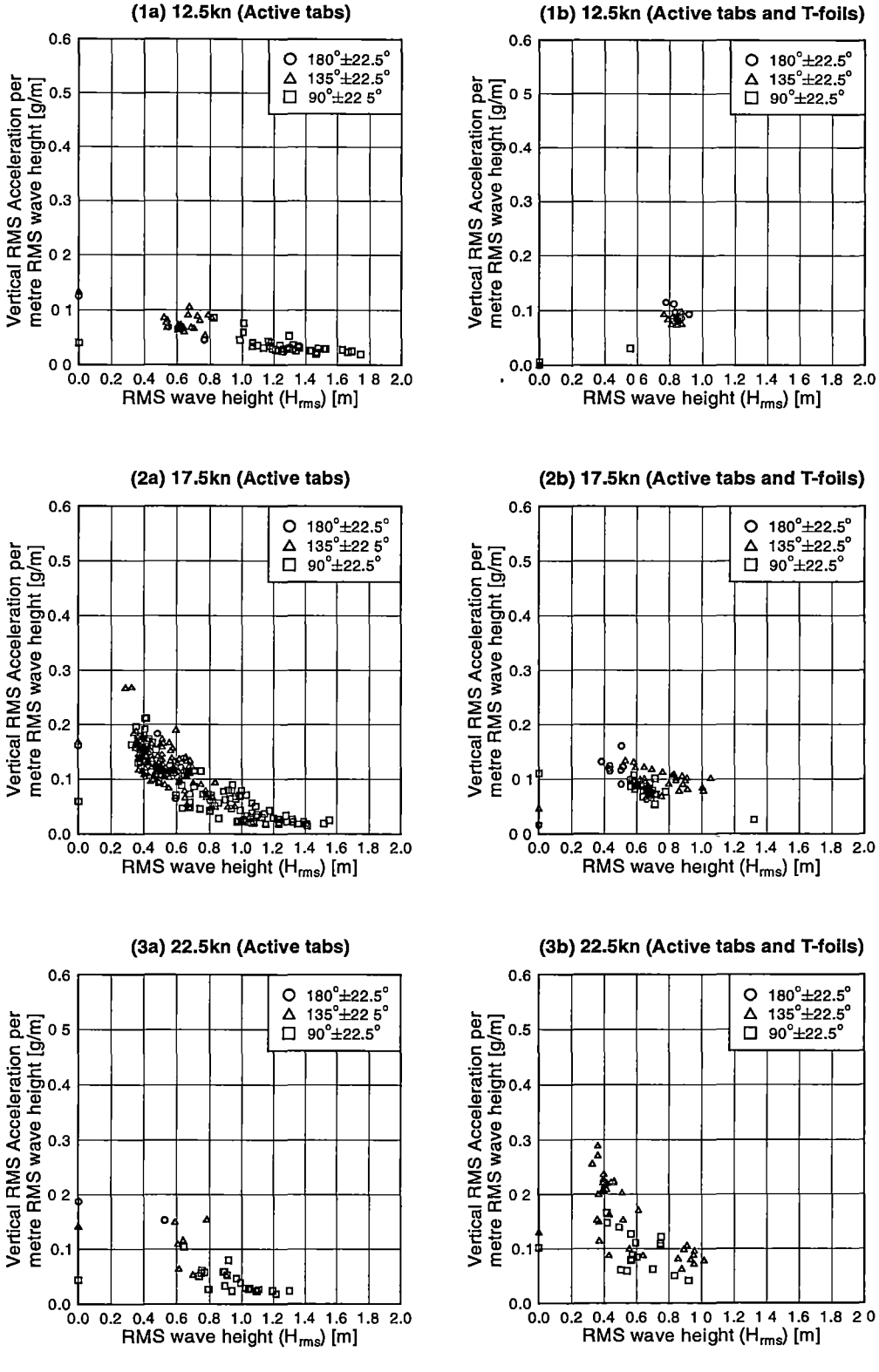

Figure 4.14: Measured LCG acceleration verses wave height (86m vessel, 12.5 to 22.5kn). Various predicted wave heading sectors. Configurations: active tabs (Delivery voyage) and active tabs and T-foils (Operational service).

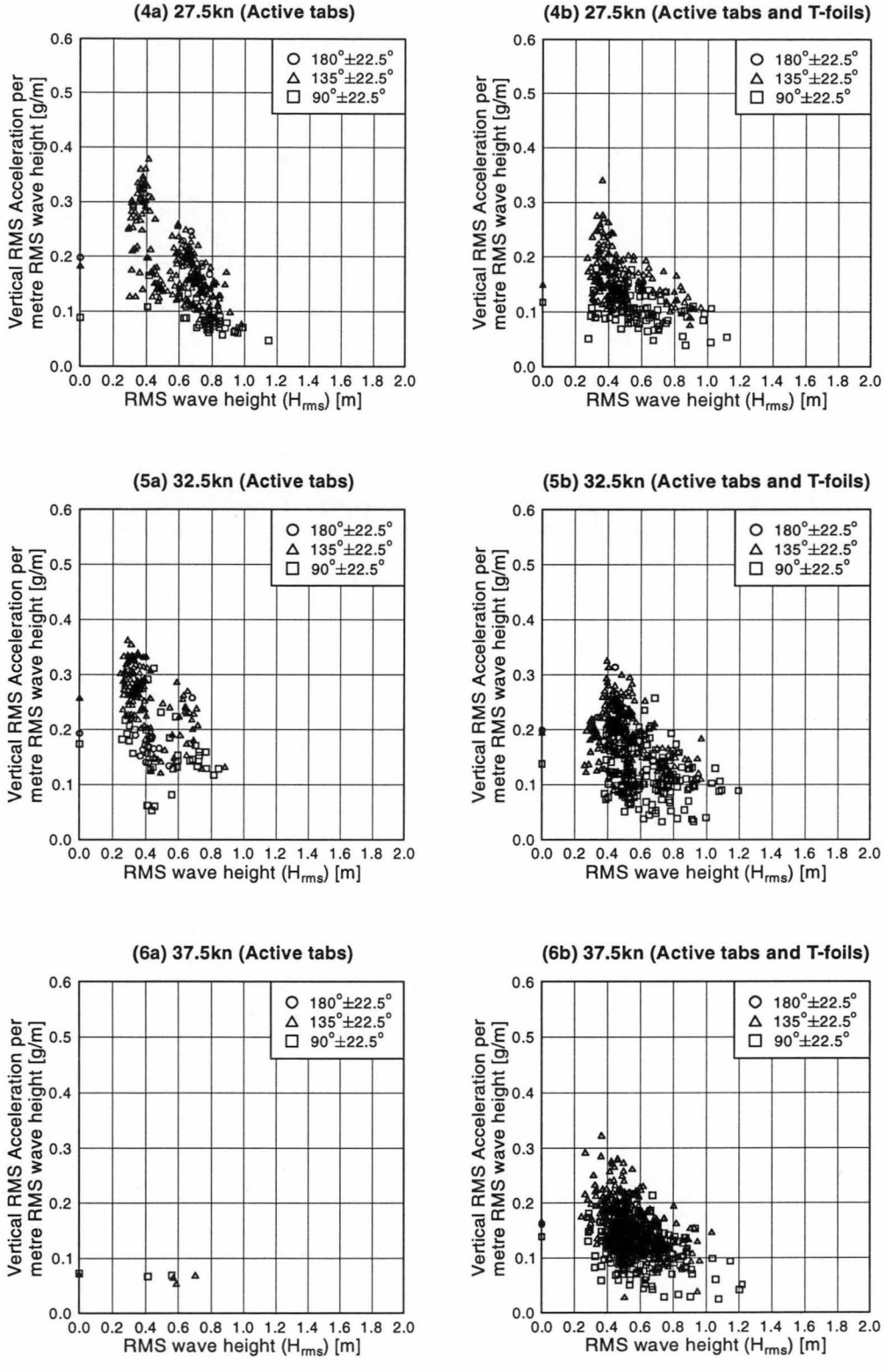

Figure 4.15: Measured LCG acceleration verses wave height (86m vessel, 27.5 to 37.5kn). Various predicted wave heading sectors. Configurations: active tabs (Delivery voyage) and active tabs and T-foils (Operational service).

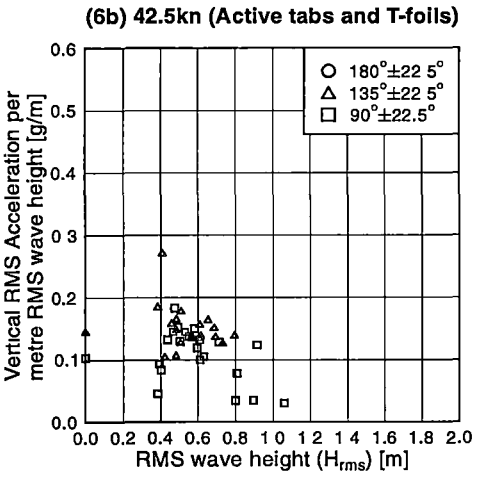

ref/plot_rmsAccel-Hs_042(42.5kn).gle

Figure 4.16: Measured LCG acceleration verses wave height (86m vessel, 42.5kn). Various predicted wave heading sectors. Configuration: active tabs and T-foils (Operational service).

4.4.3 Variation of Relative Acceleration with Wave Period

4.4.3.1 Data for 81 metre Vessel

The ratio of vertical acceleration to wave height (RMS) against the average wave period for the 81 metre vessel is shown in figure 4.17. It can be seen that as the wave period increases, the vertical acceleration relative to wave height tends to decrease generally for all speeds and control surface configurations. This outcome is expected where the accelerations should indeed increase up to a wave period where heave resonance occurs, which for the 81 metre vessel appears to be at the wave period of 7 to 9 seconds depending on the speed. Unfortunately there is insufficient data at the higher speeds to confirm this observation.

Table 4.8 summarises the averages of the results in figure 4.17 and it can be seen that in service operations and on delivery there is a trend for longer period seas to be taken at lower speed.

4.4.3.2 Data for 86 metre Vessel

The ratio of vertical acceleration to wave height (RMS) against the average wave period for the 86 metre vessel is shown in figures 4.18 to 4.20. As with the 81 metre vessel, as the wave period increases the vertical acceleration relative to wave height tends to decrease generally for all speeds and control surface configurations. The wave period where maximum accelerations occurred was approximately 8 seconds for all speeds whilst there was a reduction in acceleration as the wave periods increased up to 20 seconds. The implication of this is that the accelerations were reduced primarily by the vessel encountering a longer wave period for a given speed. As with previous results there still remains a broad range of accelerations for a given wave period but this may be attributed to the change in vessel displacement, variation in vessel speed, wave height variations and directional wave spreading. All these variations may have enough influence to have caused the variations of acceleration relative to wave height, which are evident, but nevertheless the period of maximum relative motions remains clearly identifiable at around the period of 8 seconds. There was not much data appearing below this period so it was not possible to detect a peak as the wave periods decreased to 3 or 4 seconds.

Table 4.8 summarises the averages of the periods and accelerations for the various speeds and wave headings from figures 4.18 to 4.20. It shows no clear trends for variation of wave period with the speeds analysed for this vessel. This is no doubt merely a consequence of the particular conditions encountered and the operational response of the crew to these conditions. In this respect there appears to be a difference with the operation of the 81m vessel, for which data was mainly collected during delivery when quite severe conditions were encountered. Under these conditions of large long period waves it seems that the crew of the 81m vessel during its delivery elected to reduce speed although there were known engine problems during this period that were also known to contribute to a reduced speed independently of wave conditions.

The general outcome of the results shown in figures 4.17 to 4.20 is that the variation of acceleration relative to wave height is primarily caused by variation of average wave period. As the wave period increases, in conjunction with increases of wave height, so that period becomes much longer than the period of maximum acceleration response of the vessel. Thus there is less wave energy in the range of dominant vessel response and so the acceleration relative to wave height is reduced. This general conclusion will be reemphasised by the spectra of vessel accelerations discussed in section 4.4.4, which follows.

	Head sea			Bow quartering sea			Beam sea		
Speed (±2.5) [kn]	T_1 [s]	RMS LCG accel [g]	Ratio [g/m]	T_1 [s]	RMS LCG accel [g]	Ratio [g/m]	T_1 [s]	RMS LCG accel [g]	Ratio [g/m]
81 metre, delivery voyage (tabs only)									
12.5	16.0	0.061	0.066	16.1	0.049	0.056	14.9	0.032	0.030
17.5	10.2	0.071	0.193	10.9	0.071	0.144	11.7	0.050	0.063
22.5	8.2	0.093	0.286	11.6	0.083	0.155	11.9	0.088	0.085
27.5	8.2	0.093	0.321	10.8	0.081	0.232	9.2	0.055	0.061
32.5	-	-	-	-	-	-	-	-	-
37.5	-	-	-	-	-	-	-	-	-
42.5	-	-	-	-	-	-	-	-	-
81 metre, service operations (tabs and T-foils)									
12.5	-	-	-	-	-	-	-	-	-
17.5	-	-	-	-	-	-	-	-	-
22.5	-	-	-	-	-	-	-	-	-
27.5	-	-	-	-	-	-	-	-	-
32.5	-	-	-	-	-	-	-	-	-
37.5	9.7	0.082	0.310	8.9	0.076	0.216	8.9	0.046	0.127
42.5	9.6	0.094	0.402	10.3	0.064	0.249	6.0	0.057	0.236
86 metre, delivery voyage (tabs only)									
12.5	11.0	0.038	0.059	9.6	0.050	0.077	14.1	0.043	0.033
17.5	10.8	0.065	0.113	9.6	0.063	0.123	16.4	0.046	0.050
22.5	10.3	0.080	0.153	12.5	0.068	0.098	15.9	0.038	0.039
27.5	10.8	0.123	0.191	11.0	0.104	0.179	11.8	0.067	0.088
32.5	12.0	0.077	0.185	9.0	0.100	0.254	11.6	0.083	0.158
37.5	-	-	-	16.3	0.039	0.063	14.6	0.033	0.068
42.5	-	-	-	-	-	-	-	-	-
86 metre, service operations (tabs and T-foils)									
12.5	8.9	0.082	0.096	8.8	0.070	0.084	16.6	0.017	0.031
17.5	11.5	0.055	0.112	10.7	0.072	0.096	8.9	0.053	0.077
22.5	-	-	-	10.2	0.081	0.146	10.9	0.057	0.091
27.5	-	-	-	9.0	0.076	0.156	10.0	0.060	0.104
32.5	10.5	0.082	0.187	9.3	0.095	0.192	10.5	0.076	0.120
37.5	12.8	0.074	0.157	11.0	0.086	0.160	10.8	0.072	0.124
42.5	-	-	-	12.5	0.084	0.149	14.3	0.063	0.102

C:\INigel\042DATA\cor_1filebasis\038-042(averages table)-from rms files xls

Table 4.8: Measured wave periods and vertical accelerations (RMS) grouped according to speed and predicted wave direction (81 and 86m vessels)

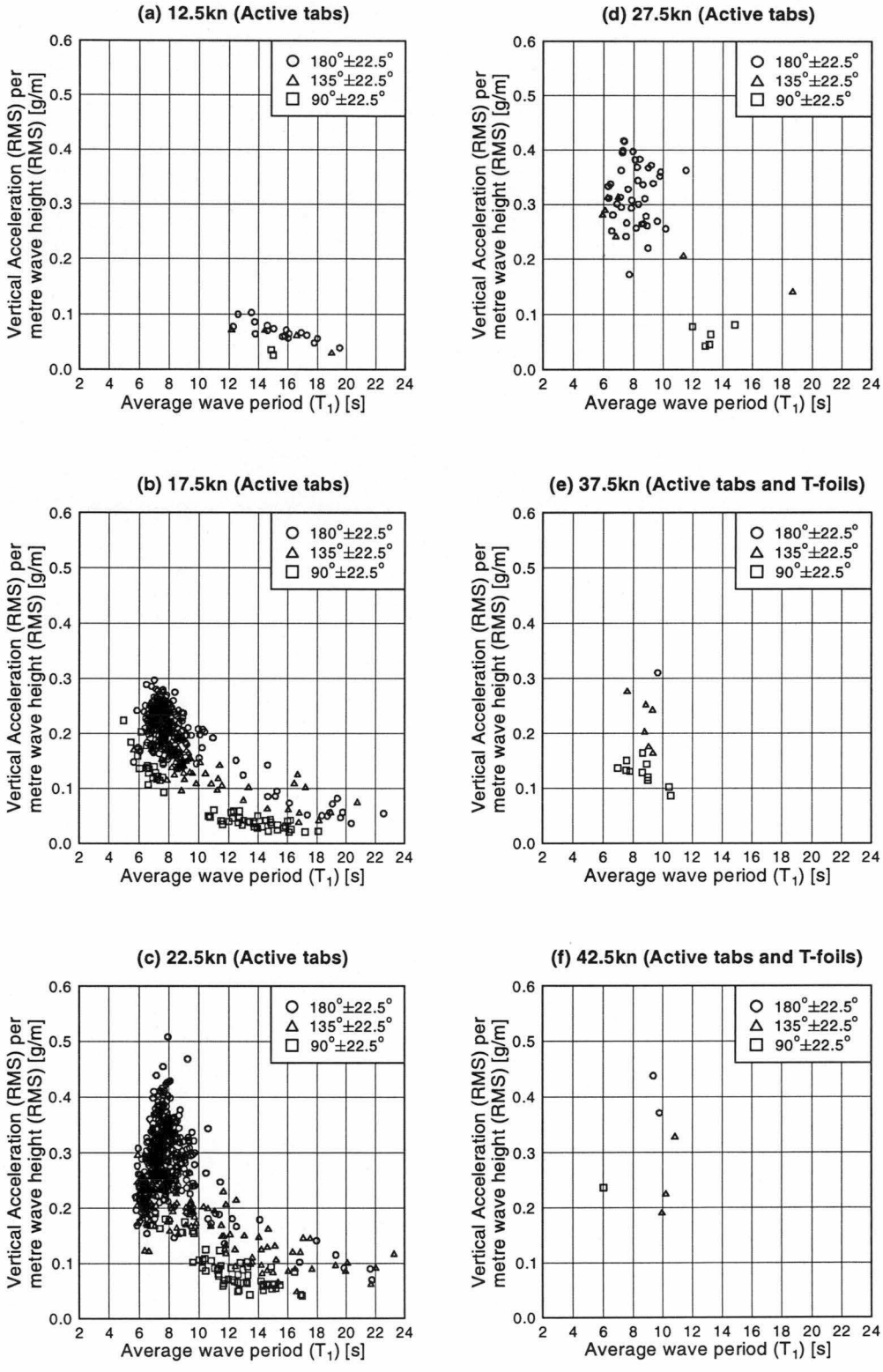

Figure 4.17: Measured LCG acceleration verses average wave period (T_1) (81m vessel, 12.5 to 42.5kn). Various predicted wave heading sectors.Configurations: (a) active tabs (Delivery voyage) and (b) active tabs and T-foils (Operational service).

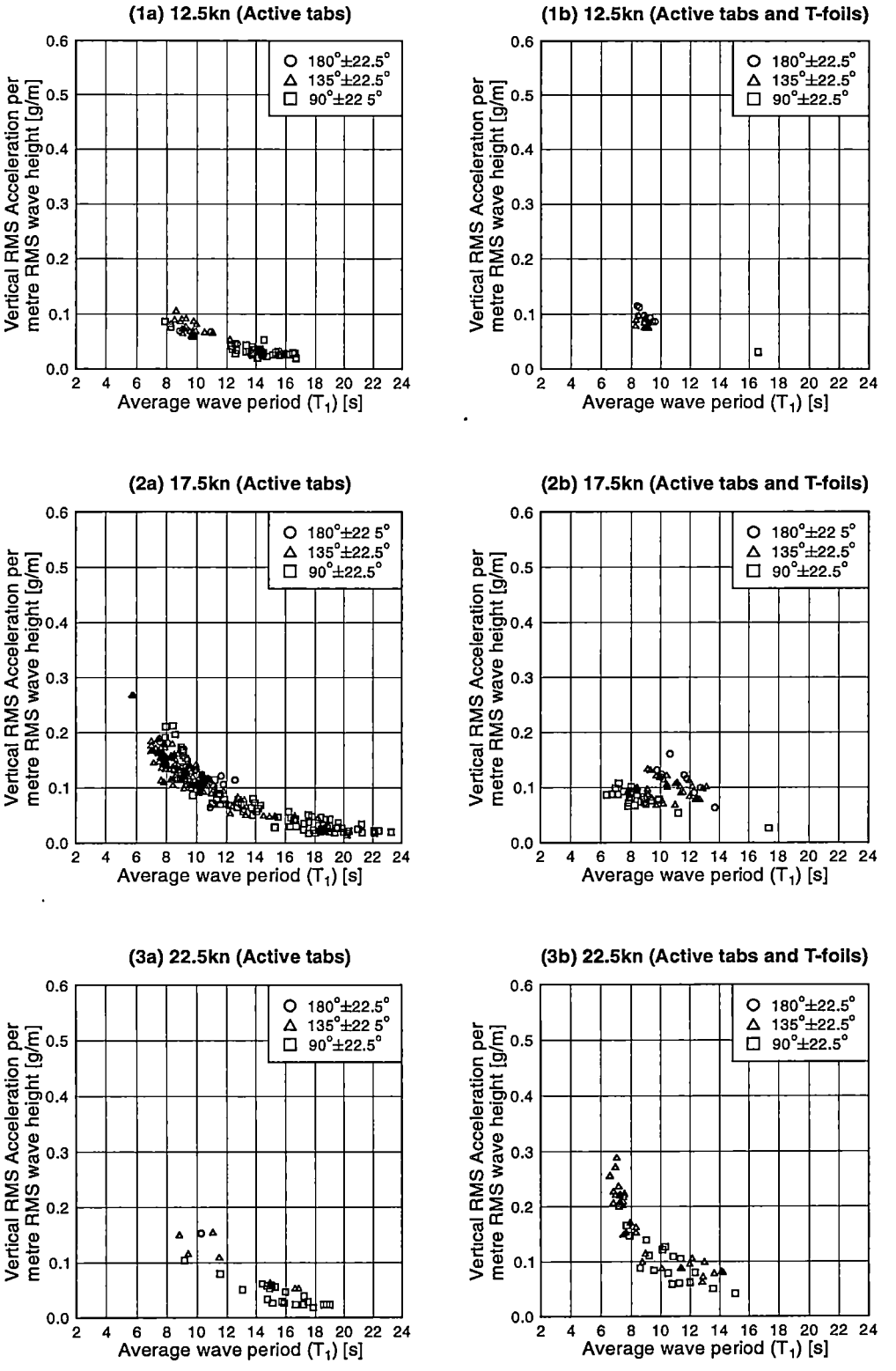

Figure 4.18: Measured LCG acceleration verses average wave period (T_1) (86m vessel, 12.5 to 22.5kn). Various observed wave heading sectors. Configurations: (a) active tabs (Delivery voyage) and (b) active tabs and T-foils (Operational service).

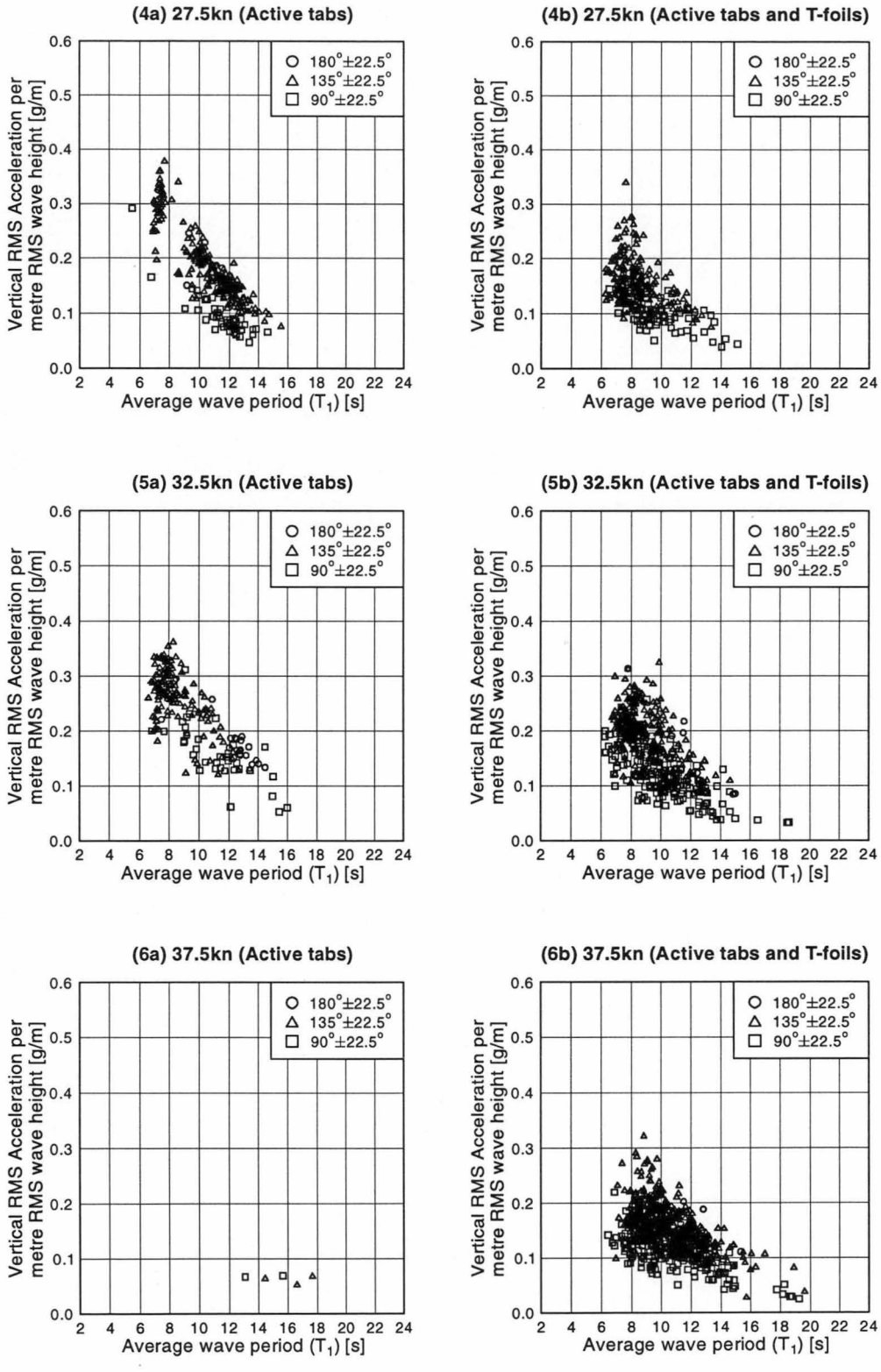

Figure 4.19: Measured LCG acceleration verses average wave period (T_1) (86m vessel, 27.5 to 37.5kn). Various observed wave heading sectors. Configurations: (a) active tabs (Delivery voyage) and (b) active tabs and T-foils (Operational service).

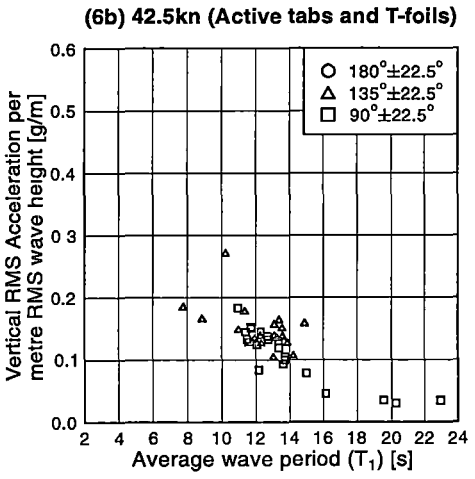

ref/plot_rmsAccel-T1_042(42 5kn) gle

Figure 4.20: Measured LCG acceleration verses average wave period (T_1) (86m vessel, 42.5kn). Various observed wave heading sectors. Configuration: (b) active tabs and T-foils (Operational service).

4.4.4 Measured Acceleration Spectra

4.4.4.1 Spectra for 81 metre Vessel

The derived LCG acceleration response spectra derived from the measurements on the 81 metre vessel during the delivery voyage are shown in figure 4.21 where the control surface configuration consisted of transom tabs only. Shown are the wave headings and variations of speed. It can be seen that the dimensionless frequency of maximum acceleration response is between 4 and 5. It is evident from these results that the double peak found in the wave energy spectra for the delivery voyage of this vessel in particular are not reflected in the measured acceleration spectra. This outcome demonstrates quite clearly, the controlling and over-riding influence of the inherent vessel acceleration response in determining the consequent on board accelerations. The vessel effectively filters the encountered wave energy and limits response energy to the range of frequency of vessel responsiveness. Also, it can be seen that the controlling influence of the vessel response is evident (figure 4.21) in that the acceleration spectral density is greatest at the highest vessel speeds. The reason for this will become apparent when the vessel transfer functions are discussed in section 4.5, which follows.

The LCG acceleration response spectra derived from service operations data where the vessel had tabs and T-foils is shown in figure 4.22. It can be seen that the maximum response was again mostly about the dimensionless frequency of 4. Some speeds were slightly lower and some were slightly higher. It can also be seen that for the 81 metre vessel, the accelerations were only significant between the dimensionless frequencies of 2 to 5. Outside this region the accelerations were negligible for all speeds and headings. However, it must be borne in mind that relatively little data was collected for this vessel during its service operations.

4.4.4.2 Spectra for 86 metre Vessel

The LCG acceleration response spectra derived from the measurements on the 86 metre vessel during the delivery voyage are shown in figure 4.23 where the control surface configuration consisted of transom tabs only. These results appear more regular than for the 81 metre vessel as a result of the increased quantity of data available. A reduction in speed generally leads to a reduced spectral density, except at the highest speeds. As with the 81 metre vessel, it can be seen that the dimensionless frequency of maximum acceleration response is between 4 and 5.

In the case of the LCG acceleration response spectra derived from the service operations data on the English Channel shown in figure 4.24 where the vessel had tabs and T-foils, the maximum response was between the dimensionless frequencies of 3 and 4. Except for some instances in beam seas, the accelerations were only significant between the dimensionless frequencies of 2 to 6. Outside this region the accelerations were for the most part negligible for most speeds and headings.

The general implication of the measured acceleration spectra is that the on board accelerations are strongly controlled by the vessel response. Furthermore, it can be seen that as with the variation of acceleration relative to wave period discussed in section 4.4.3, the vessel essentially acts as a filter to the encountered wave energy. This means that it is the vessel response which controls the dominant frequency of on board accelerations with direct consequences for passenger comfort and motion sickness incidence values.

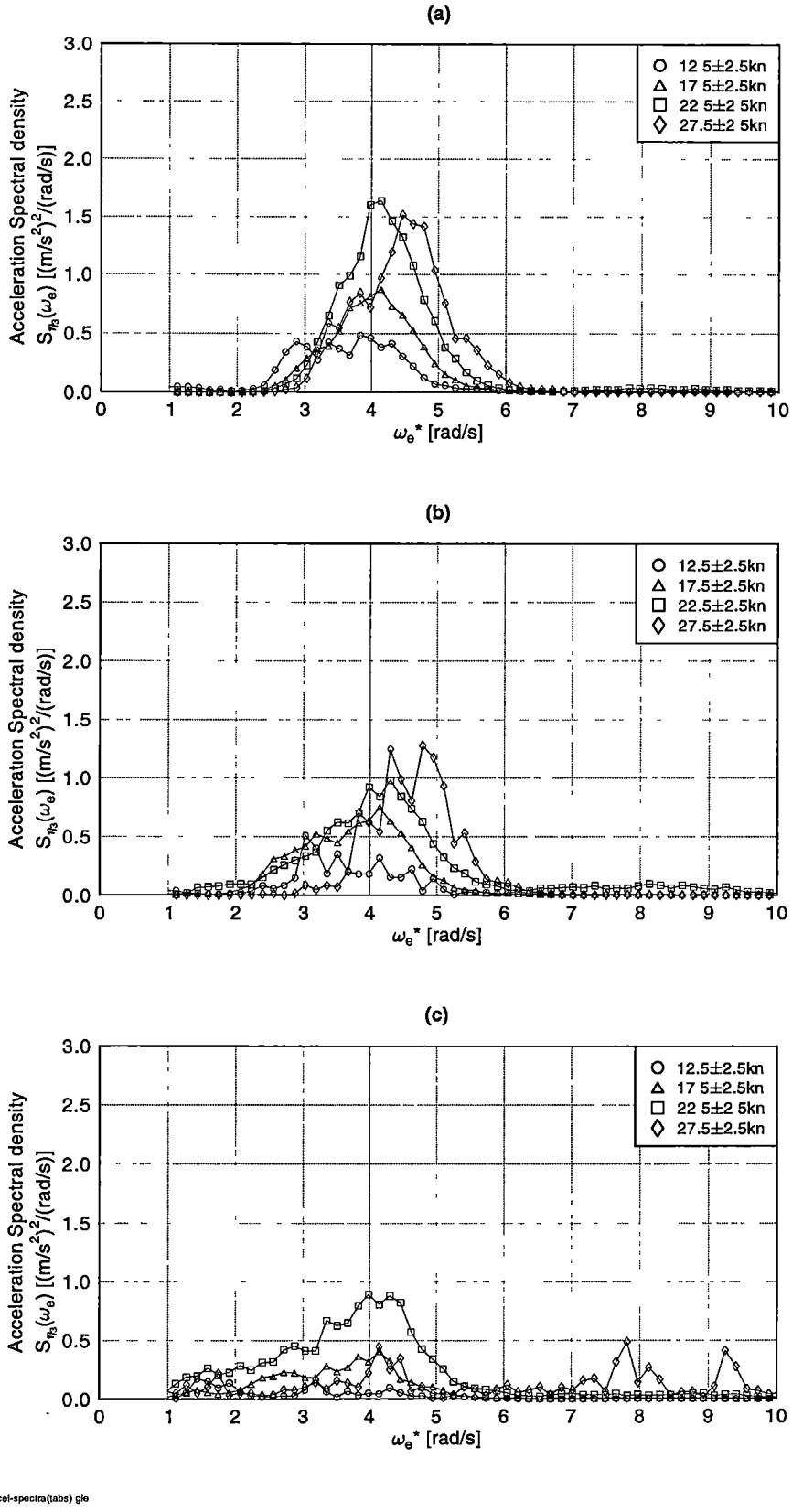

ret/plot_038_Accel-spectra(tabs) gle

Figure 4.21: Measured LCG acceleration response spectra (81m vessel, active tabs only). Observed wave heading sectors: (a) bow (180° ±22.5°), (b) bow-quarter (135° ±22.5°) and (c) beam (90° ±22.5°).

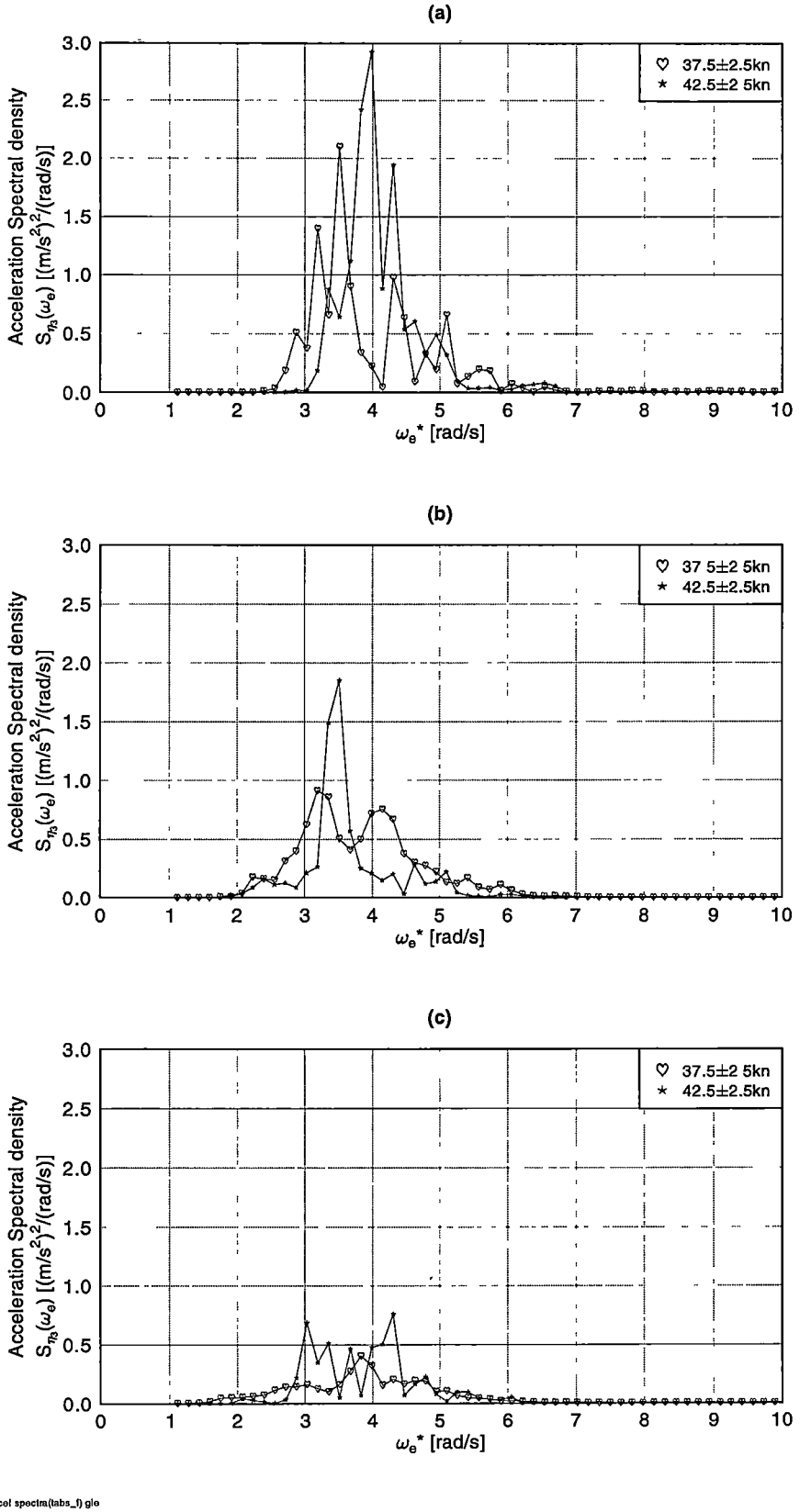

Figure 4.22: Measured LCG acceleration response spectra (81m vessel, active tabs and T-foils). Observed wave heading sectors: (a) bow (180° ±22.5°), (b) bow-quarter (135° ±22.5°) and (c) beam (90° ±22.5°).

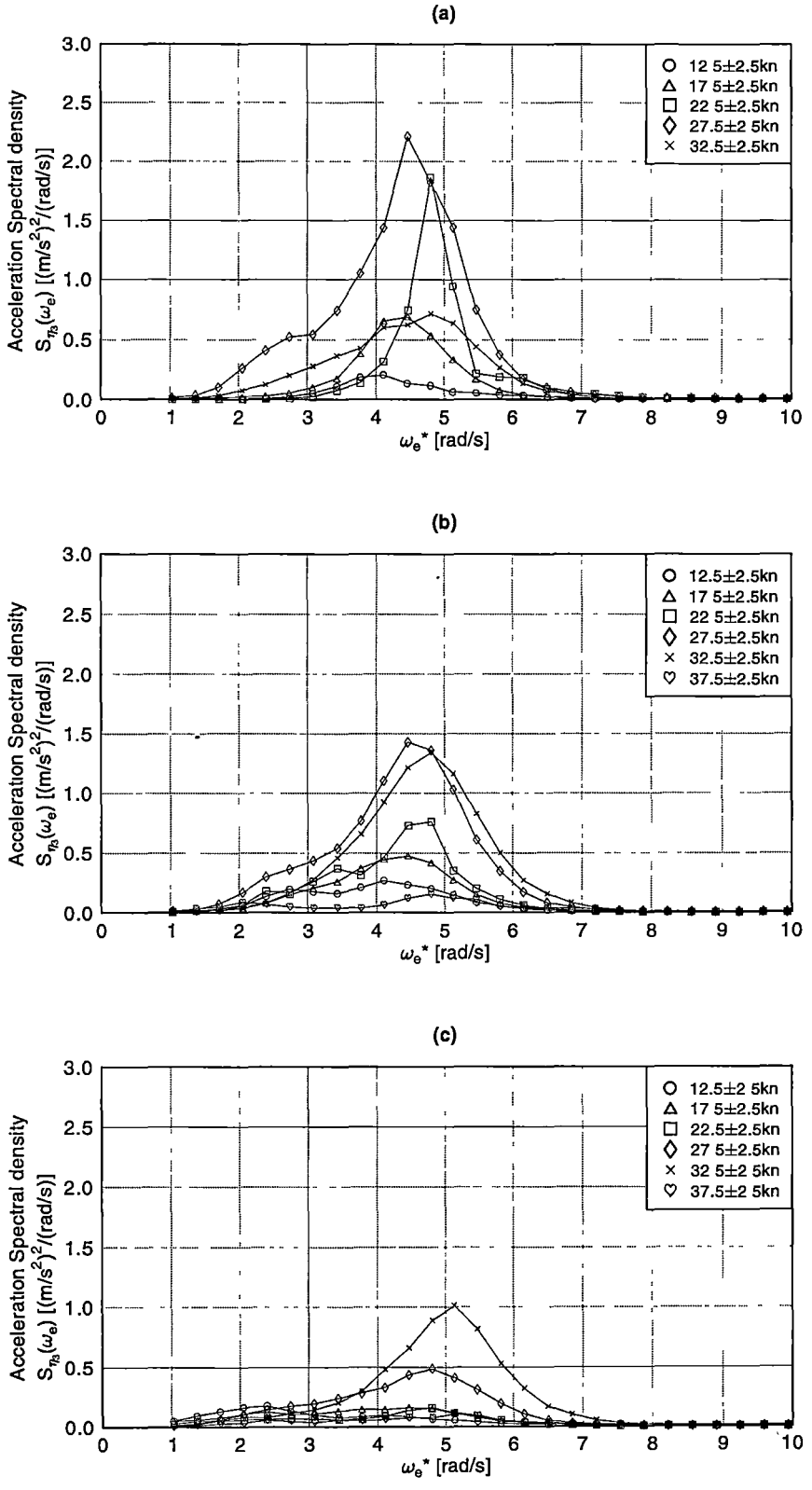

ret/plot_042_Accel spectra(tabs) gle

Figure 4.23: Measured LCG acceleration response spectra (86m vessel, active tabs only). Observed wave heading sectors: (a) bow (180° ±22.5°), (b) bow-quarter (135° ±22.5°) and (c) beam (90° ±22.5°).

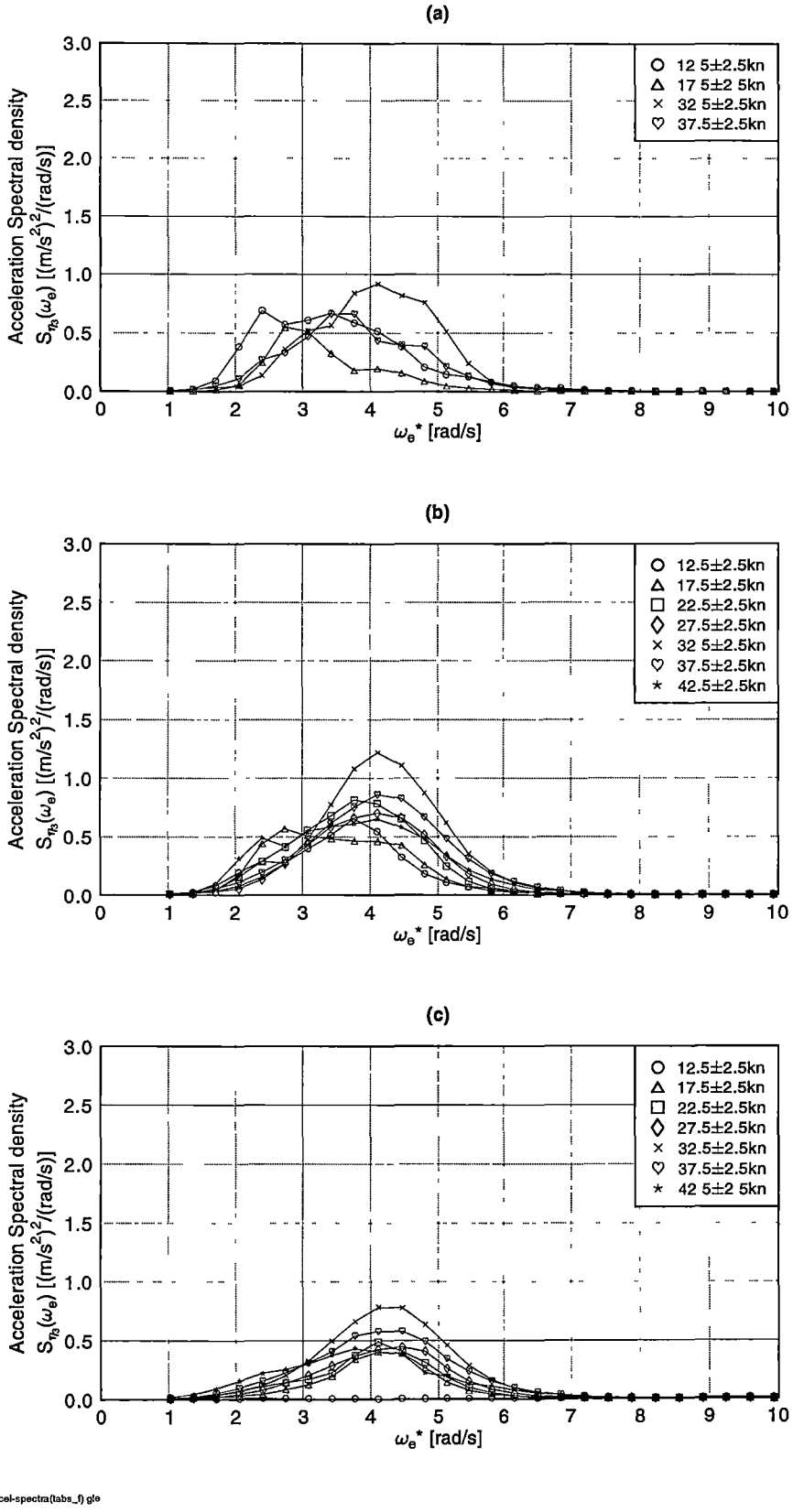

rel/plot_042_Accel-spectra(tabs_f).gle

Figure 4.24: Measured LCG acceleration response spectra (86m vessel, active tabs and T-foils). Observed wave heading sectors: (a) bow (180° ±22.5°), (b) bow-quarter (135° ±22.5°) and (c) beam (90° ±22.5°).

4.5 Measured Transfer Functions

The derived transfer functions in heave, roll and pitch are presented in this section and were created by grouping data records within categories defined by speed, observed wave direction sector and vessel configuration. The transfer functions are a result of the assemble averages of the measured wave spectra and measured response spectra and are therefore subject to the assumptions made in their derivation. The implication of evaluation of the vessel transfer functions is that a linear motion response to encountered wave height is assumed to exist. As has been indicated previously, the volume of data available and the limited range of wave heights established by the data collection trigger levels created conditions where it was not possible to investigate the wave amplitude nonlinearity of the transfer functions. As will be seen, the task of evaluating transfer functions for particular wave headings and speeds was about the limit of what could realistically be achieved.

4.5.1 Measurements with Tabs Only on Delivery Voyages (81m and 86m vessels)

The transfer functions derived for the 81 and 86 metre vessels with transom tabs only are presented in figures 4.25 to 4.27 for heave, roll and pitch respectively. Each of these figures show a variety of speeds where there was data available to make a derivation in each of the wave headings analysed (head, bow quartering and beam sea directions).

The heave results in figure 4.25 show a reduction in maximum heave in beam seas compared with the head and bow quartering wave direction sectors whilst clearly showing a reduction in heave in all directions as the vessel speed is reduced, although this result could not be strictly applied to each speed. In some case there was inconsistent behaviour in the transfer functions at some speeds which were not consistent with the other data leading one to conclude that the data may be of lesser quality. For example the 37.5 knots heave transfer function in bow quartering seas (figure 4.25(b)) is unusually low compared with the other speeds. Inspection of the record duration in table 4.2 shows this record has approximately 10 minutes of data, which may be less than ideal.

The frequency of maximum heave response with tabs only was just under the dimensionless frequency of 4 in head and bow quartering waves whilst it was just above 4 for the beam sea wave direction. The resonant peaks were typically about 2 for the higher speed of 42.5 knots, reducing to a value less than unity at lower speeds showing no sign of resonance. The heave did not appear to be significant at dimensionless frequencies greater than 8, but the diagrams displayed the results up to 10 for consistency with the predicted results.

The frequencies below 2.8 were not displayed because a 0.16 Hertz high pass filter was applied to the acceleration response data to remove the low frequency drift as it was double integrated to obtain the corresponding displacement (see section 2.6.2.1). Therefore it was not possible to resolve the transfer functions at frequencies lower than the 0.16 Hertz filter high pass cut off, which was equivalent to the dimensionless frequencies of 2.6 and 2.8 for the 81 and 86 metre vessels respectively.

Most of the data from the 81 metre vessel is of lesser quality owing to the shorter record lengths but some results showed similar trends to the 86 metre vessel where higher magnitudes at the resonant frequencies can be seen at the higher speeds and a reduction with speed. In head seas the magnitude was closer to 2.5 although the frequency of resonant response is about the same as the 86 metre vessel.

The roll transfer functions of the 81 and 86 metre vessels are shown in figure 4.26 for the configuration with transom tabs. The transfer functions of the 86 metre vessel are

much more variable than the heave transfer functions whilst the 81 metre roll transfer functions showed little resonance. In head seas of long crested waves one would not expect to see large responses shown in figure 4.26(a), which in some cases exceed unity by more than a factor of two. A likely reason for this is that there was a significant amount of wave spreading or waves from other directions than the bow that induced roll motions in the vessel. In these results, the mid speed range of 22.5 and 27.5 knots had the highest response compared with both the low speeds and the highest speed of 42.5 knots, which was below 1.75. One aspect of these results is that the frequency of maximum response reduced with speed, so that dimensionless frequencies were near 4 at the higher speeds reducing to 3 at the lower speeds.

Similar changes in the frequency of maximum roll response can also be seen in the bow quarter wave direction for the 86 metre vessel, which were also between 3 and 4. This wave direction shows a more uniform spread of results, but once again the 22.5 and 27.5 knot speeds show the highest roll response was about 2 compared with both the lower and higher speeds, which are all below 1.75.

In beam seas, the maximum roll peak of 3 occurred at 32.5 knots, which is relatively high whilst the peaks at other speeds were below 2. The dimensionless frequency of maximum response remained between 3 and 4 for all speeds.

Generally in roll the frequency of response did not change significantly between the wave headings and the peaks were reasonably well behaved but a few peaks were quite high.

The pitch transfer functions of the 81 and 86 metre vessels are shown in figure 4.27 for the configuration with transom tabs. The pitch in head seas of the 86 metre vessel shows an unusually high peak at 22.5 knots with the remaining speeds below 2. The maximum frequencies of response for all speeds and both vessels were between 3 and 4, which is similar to the vessels maximum response frequency in both heave and roll. The maximum frequency of response for the 81 metre vessel was slightly less than the 86 metre vessel. It appears from figures 4.25 to 4.27 that the 86 metre vessel, head sea, 22.5 knot data is significantly in error. This is probably because of the low quantity of data available being less than 4 minutes in total.

In bow quartering seas, the magnitude of the peaks remained lower than all head sea cases at a value of 1.5 at 27.5 knots whilst the 22.5 and 32.5 knot speeds were slightly lower. The 12.5 and 37.5 knot speeds had peaks below unity

The pitch in beam seas was generally small for both vessels but because the response was greater than zero there was still sufficient waves to pitch the vessels and to create a peak close to unity at 32.5 knots. All other speeds remained below unity.

4.5.2 Measurements with Tabs and T-foils for Operational Service (81m and 86m vessels)

The transfer functions derived for the 81 and 86 metre vessels with transom tabs and T-foils are presented in figures 4.28 to 4.30 for heave, roll and pitch respectively. Each of these figures show a range of speeds where there was sufficient data available to make a derivation in each of the wave headings analysed (head, bow quartering and beam sea directions).

The heave results of figure 4.28 for the 86 metre vessel at 32.5 knots show a similar response to that shown previously for the transom tabs only configuration. The speeds of 12.5 and 17.5 show a reduction in magnitude as the speed reduces. There was a general reduction in the response magnitude of the peaks, which occurred at a frequency between 3 and 4, starting at 2 and reducing to unity as the speed reduced.

Most of the data from the 81 metre vessel characterises similar trends in the shape of the transfer functions to those of the 86 metre but contain large variations in their magnitudes and are of lesser quality. This is simply because of the limited volume of in service data for this vessel.

The roll transfer functions of the 81 and 86 metre vessels are shown in figure 4.29 for the configuration with transom tabs and T-foils. In head seas the maximum roll response remained below unity for all the measured speeds up to 37.5 knots. No significant change in the frequency of maximum response occurred. Once again it is evident that variability of the actual sea direction has caused the vessel to roll significantly in sea that were nominally classified as head seas.

In the bow quarter wave direction the 86 metre vessel showed a maximum roll response at 32.5 knots which reduced almost equally as the speed increased to 37.5 knots and as the speed reduced to 27.5 knots to a value of 1.7. The frequency of maximum response remained at about 3.7. At the lower speeds 12.5 and 17.5 knots the response dropped to near unity. The highest speed of 42.5 knots showed strong reduction in roll to about 1.25, but relatively modest amounts of data was obtained at this speed.

In beam seas, the maximum roll peak of 2 occurred at 22.5 knots, which was almost exactly matched at 27.5 knots. The magnitude continued to decrease at 32.5 knots, 37.5 knots and up to 42.5 knots where the peak was only about 1.35. The dimensionless frequency of maximum response remained between 3.5 and 3.8 for all speeds. Recent motion computations reported by Davis et al. (2003) using a twin hull omnidirectional time domain code (BEAMSEA, similar to the head sea code BESTSEA used for monohulls in the present analysis) have shown that the maximum predicted roll transfer function does reduce with speed in beam seas over the range for 1.8 to 1.0 at 37.5 knots and 17.5 knots. The results of figure 4.29(c) are thus consistent with these more recent predictions.

Generally in roll the frequency of maximum response did not change significantly between the wave headings and the peaks were reasonably well formed and showed that the maximum roll response generally occurred in the mid speed ranges.

Compared with the configuration with transom tabs only, the addition of the T-foils reduced the roll response component of the vessel noticeably in the head, bow quartering and beam sea wave directions. Further reductions appear possible as resonant peaks greater than unity remained and further motion damping is feasible.

The pitch transfer functions of the 81 and 86 metre vessels are shown in figure 4.30 for the configuration with transom tabs and T-foils. The pitch in head seas (figure 4.30(a)) of the 86 metre vessel shows a peak of 1.4 at the dimensionless frequency of 3.4. In this case most speeds had a similar peak magnitude which did not appreciably change from the high to the lower speeds. Compared with the vessel with only transom tabs, there was a reduction in the magnitude but not a significant change in the frequency of maximum response.

In bow quartering seas, the pitch magnitude of the 86 metre vessel was close to unity for most speeds, which also represents an improvement on the previous configuration with transom tabs only, where the peaks of maximum response had values of 1.5.

The pitch in beam seas was generally small for both vessels but the response shows values greater than zero indicating there was still sufficient wave energy to pitch the vessels and to create a peak at values less than unity for all speeds. This is probably because of variability of sea direction within the sea direction classified here as beam seas, not always being exactly on the beam.

The heave, roll and pitch transfer functions were not significant at dimensionless fre-

quencies greater than 8, but the diagrams displayed the results up to 10 for consistency with the predicted results.

As with the previous results of section 4.5.1, the frequencies below 2.8 were not displayed because a 0.16 Hertz high pass filter was applied to the acceleration response data to remove the low frequency drift as it was double integrated to obtain the corresponding displacement (see section 2.6.2.1). Therefore it was not possible to resolve the transfer functions at frequencies lower than the 0.16 Hertz filter high pass cut off, which was equivalent to the dimensionless frequencies of 2.6 and 2.8 for the 81 and 86 metre vessels respectively.

4.6 Summary

This chapter has presented the measured results for the 81 and 86 metre vessels considered in the present analysis. Key findings from these results include:

Data records

1. Only the primary wave direction between head and beam seas were investigated because of the very small motions for primary wave directions from the aft sectors. Furthermore, the level of wave directional spreading could not be determined. Therefore, improvements in the data quality and quantity could be achieved by better defining the wave environment.

2. The duration of data records for the 81 and 86 metre vessels was 35.1 and 105.5 hours respectively from the delivery voyage, whilst there was 1.4 and 164.2 hours respectively from the service operations. However, of that data collected for the 81 and 86 metre vessels only 87% and 44% respectively could be used from the delivery voyage and 50% and 54% respectively could be used from service operations. Only if an increased amount of well defined sea directions were encountered could a greater proportion of the data be used for analysis.

3. Whilst long time frames were required to acquire sufficient data records, they were still limited to the speeds and wave headings that dominated the operational route of the vessel. However, data groups were formed from sufficient time records and averaged together for spectral analysis with useful outcomes.

4. Lower speeds tended to be associated with higher wave heights.

Vertical Accelerations

1. The accelerations at the bow were much higher than the transom and centre of gravity (CG), particularly in head sea waves. The acceleration only fell below 0.1g/m for speeds less than 12 knots and bow accelerations were up to 0.3g/m.

2. There were insufficient data records to use wave height as a variable for creating a data group, so the nonlinear effect of accelerations with wave height could not be considered in further detail. Thus a much longer measurement period would be required to obtain sufficient quantities to further investigate this variable.

3. It was found that varying the wave period affects accelerations as much as wave height. Acceleration per unit wave height tended to decrease with wave height for all speeds which may be attributed to the increasing wave periods of the larger waves. This was confirmed by the results that showed acceleration decreasing with increasing wave period.

4. The maximum spectral responses were generally between the dimensionless frequencies of 4 and 5, where most of the acceleration response energy was within the range of the dimensionless frequencies of 2 and 5. The vessel's natural acceleration response period clearly dominated over the wave peak period when looking at the vessel's maximum motion response. This indicates that the vessel filters the wave energy and limits the response to the range of frequencies corresponding with the vessel responsiveness.

5. The vessel response generally increased with speed, but not necessarily in a linear sense.

Transfer functions

1. Larger resonant magnitudes occurred with increasing speed. Resonance in the vessel's response was confirmed with some peak transfer functions reaching 2.5. This indicated that the motion control system modelled was probably undersized in relation to the level of damping possible.

2. The dimensionless frequency of maximum roll response tended to reduce with speed, which was generally between 3 and 4.

3. The vessel's response with wave height could not realistically be investigated outside the linear assumption but results obtained from another program BEAMSEA showed that vessel response was not linear with wave height (see also chapter 6).

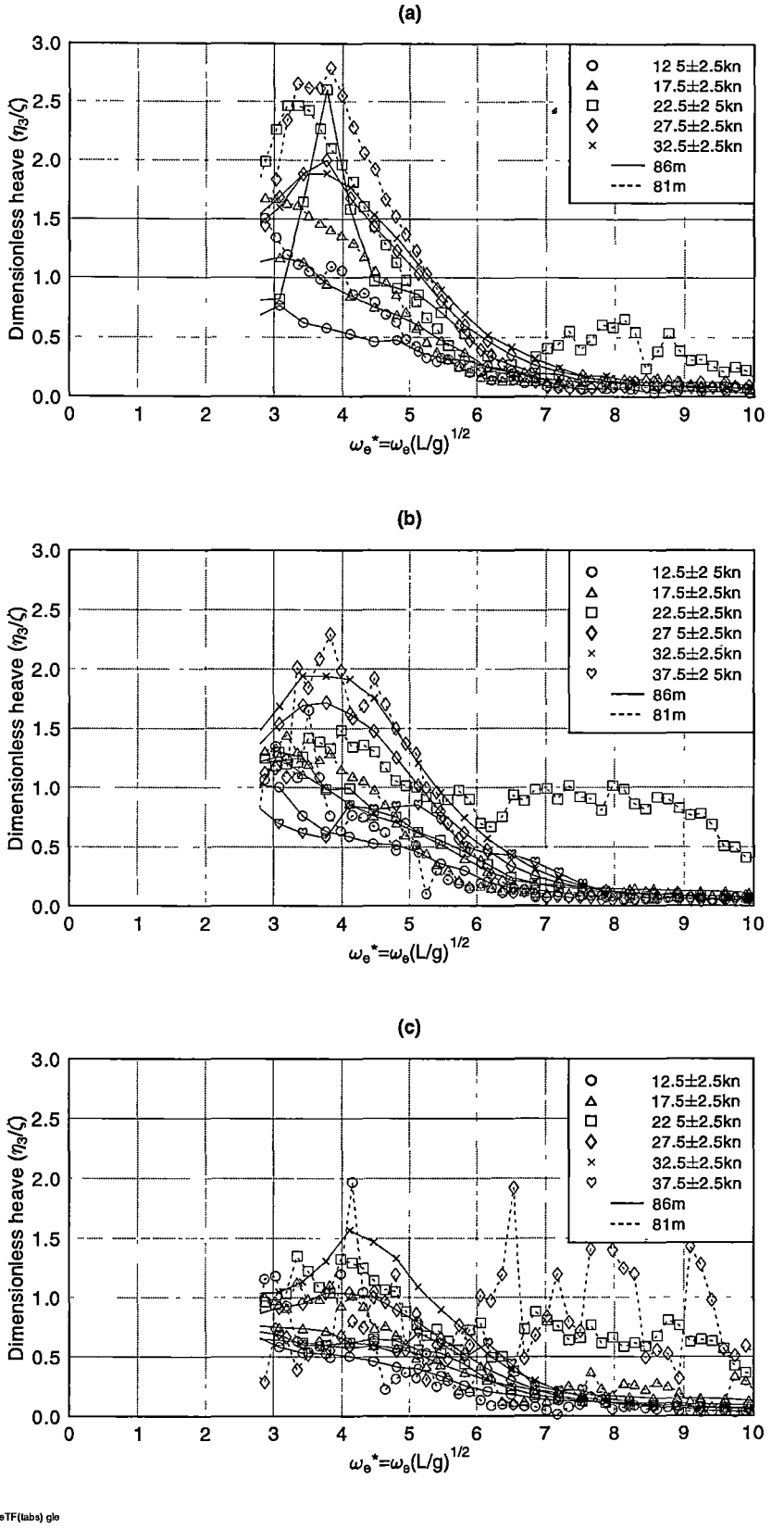

Figure 4.25: Measured heave displacement transfer functions (81 and 86m vessels, active tabs only). Observed wave heading sectors: (a) bow (180° ±22.5°), (b) bow-quarter (135° ±22.5°) and (c) beam (90° ±22.5°).

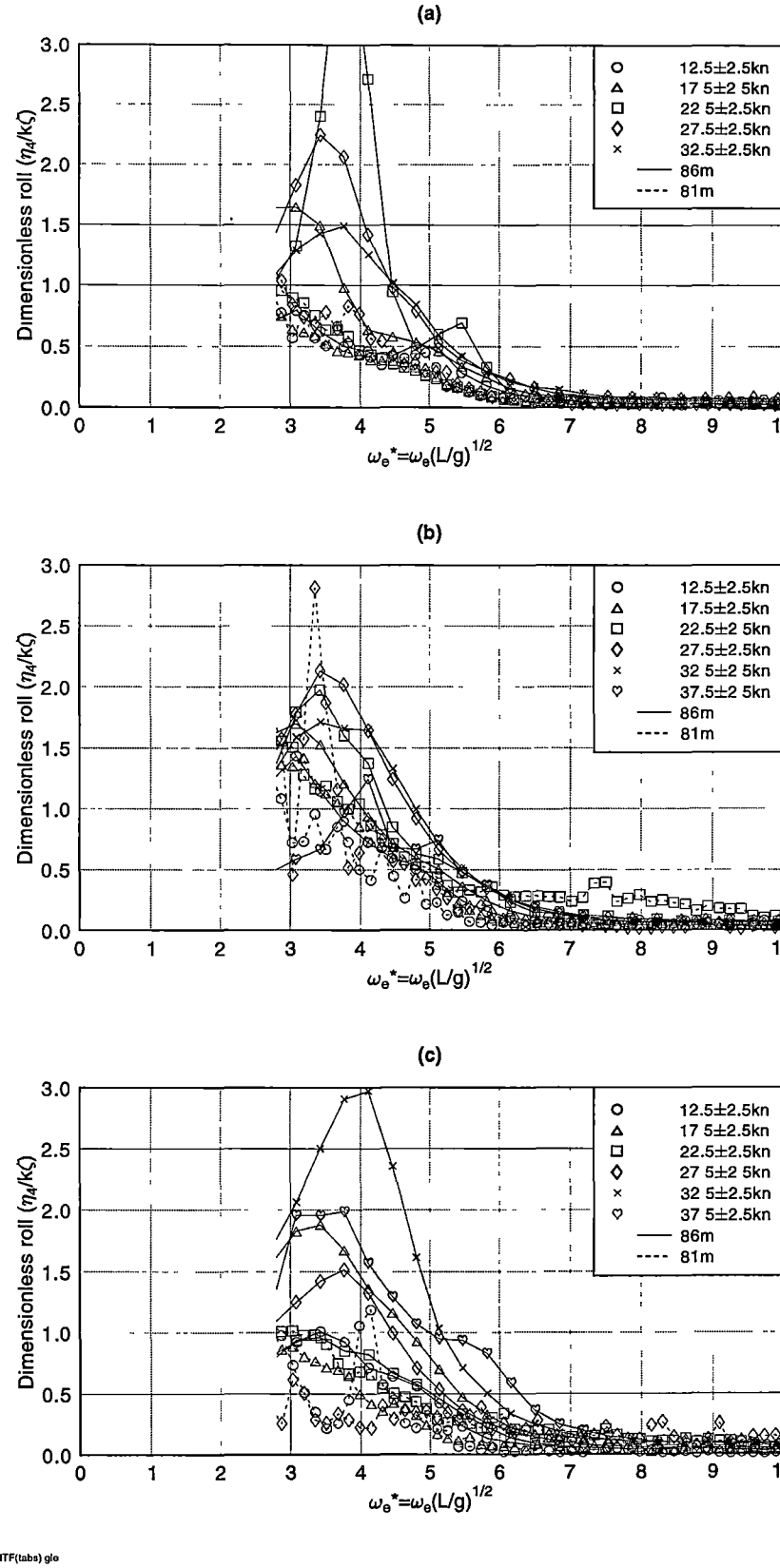

Figure 4.26: Measured roll displacement transfer functions (81 and 86m vessels, active tabs only). Observed wave heading sectors: (a) bow (180° ±22.5°), (b) bow-quarter (135° ±22.5°) and (c) beam (90° ±22.5°).

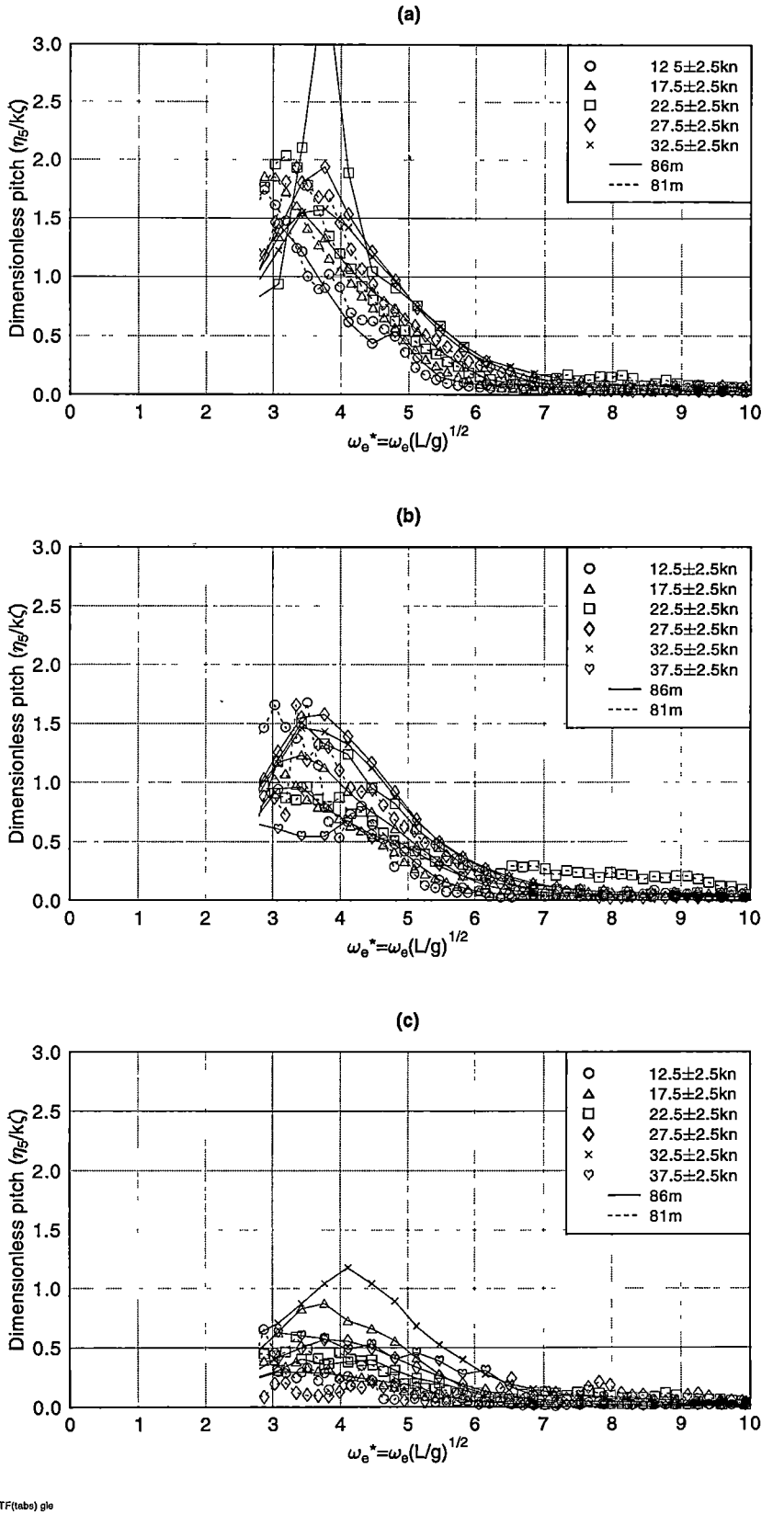

Figure 4.27: Measured pitch displacement transfer functions (81 and 86m vessels, active tabs only). Observed wave heading sectors: (a) bow (180° ±22.5°), (b) bow-quarter (135° ±22.5°) and (c) beam (90° ±22.5°).

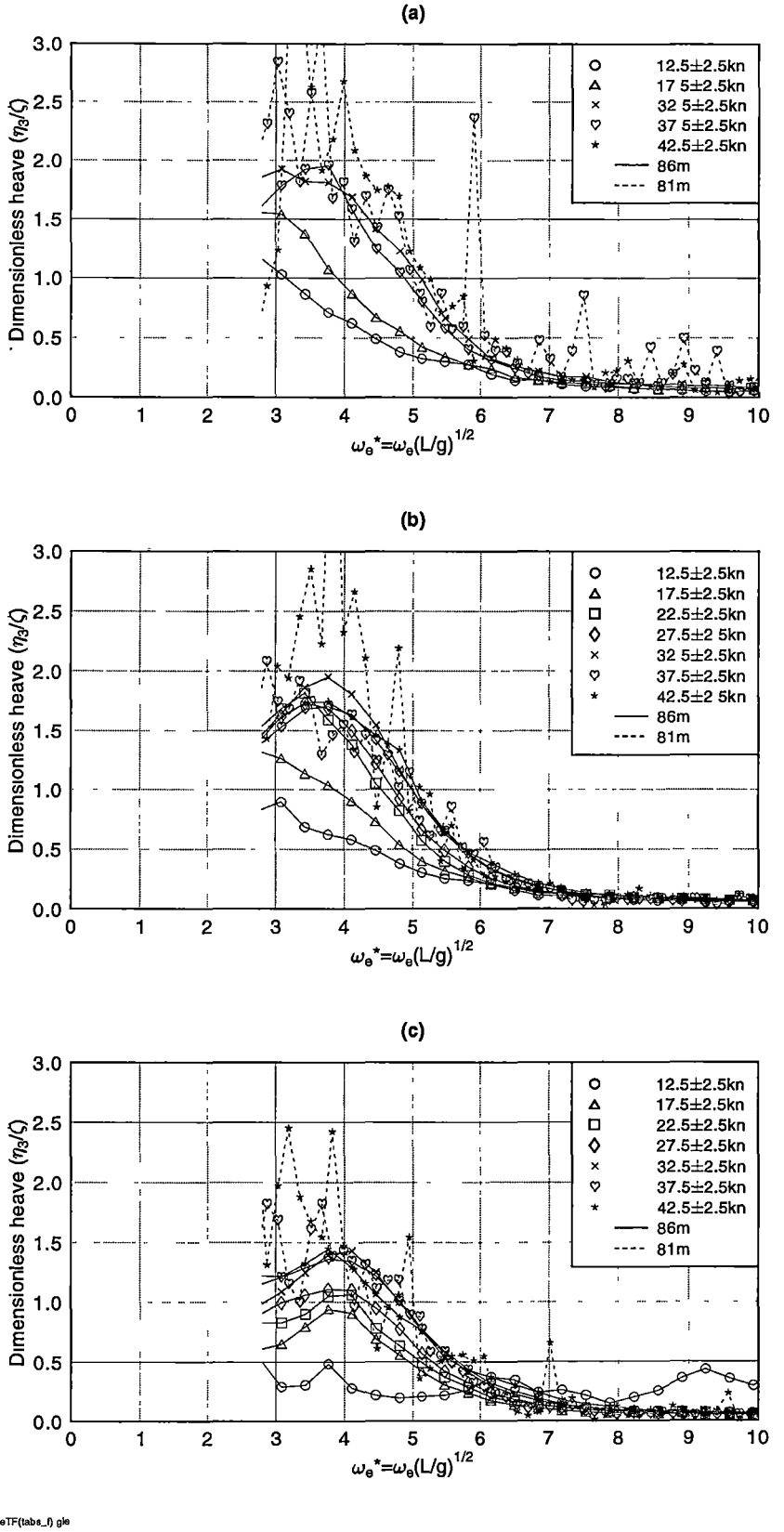

ref/plot_038-042_HeaveTF(tabs_f).gle

Figure 4.28: Measured heave displacement transfer functions (81 and 86m vessels, active tabs and T-foils). Observed wave heading sectors: (a) bow (180° ±22.5°), (b) bow-quarter (135° ±22.5°) and (c) beam (90° ±22.5°).

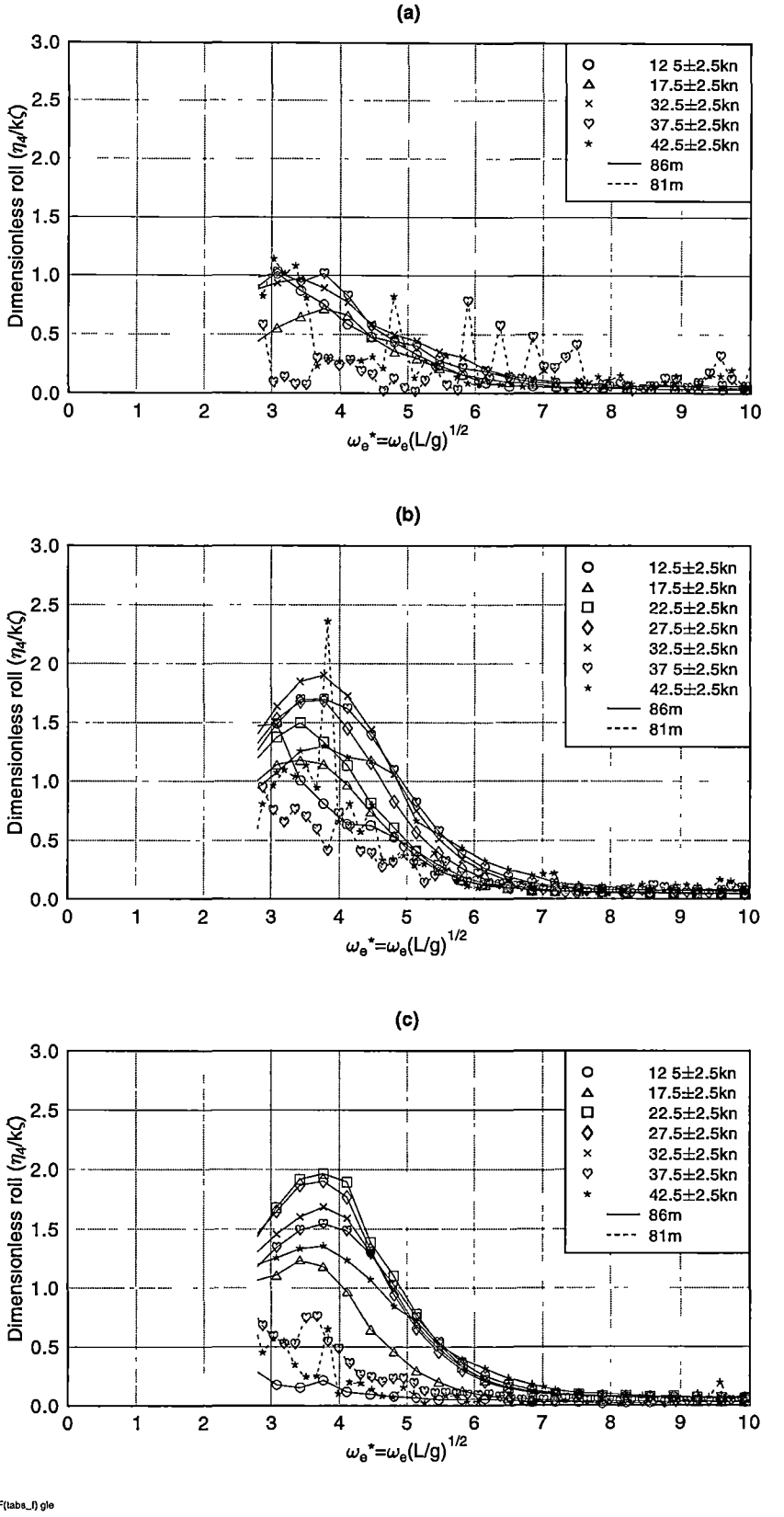

Figure 4.29: Measured roll displacement transfer functions (81 and 86m vessels, active tabs and T-foils). Observed wave heading sectors: (a) bow (180° ±22.5°), (b) bow-quarter (135° ±22.5°) and (c) beam (90° ±22.5°).

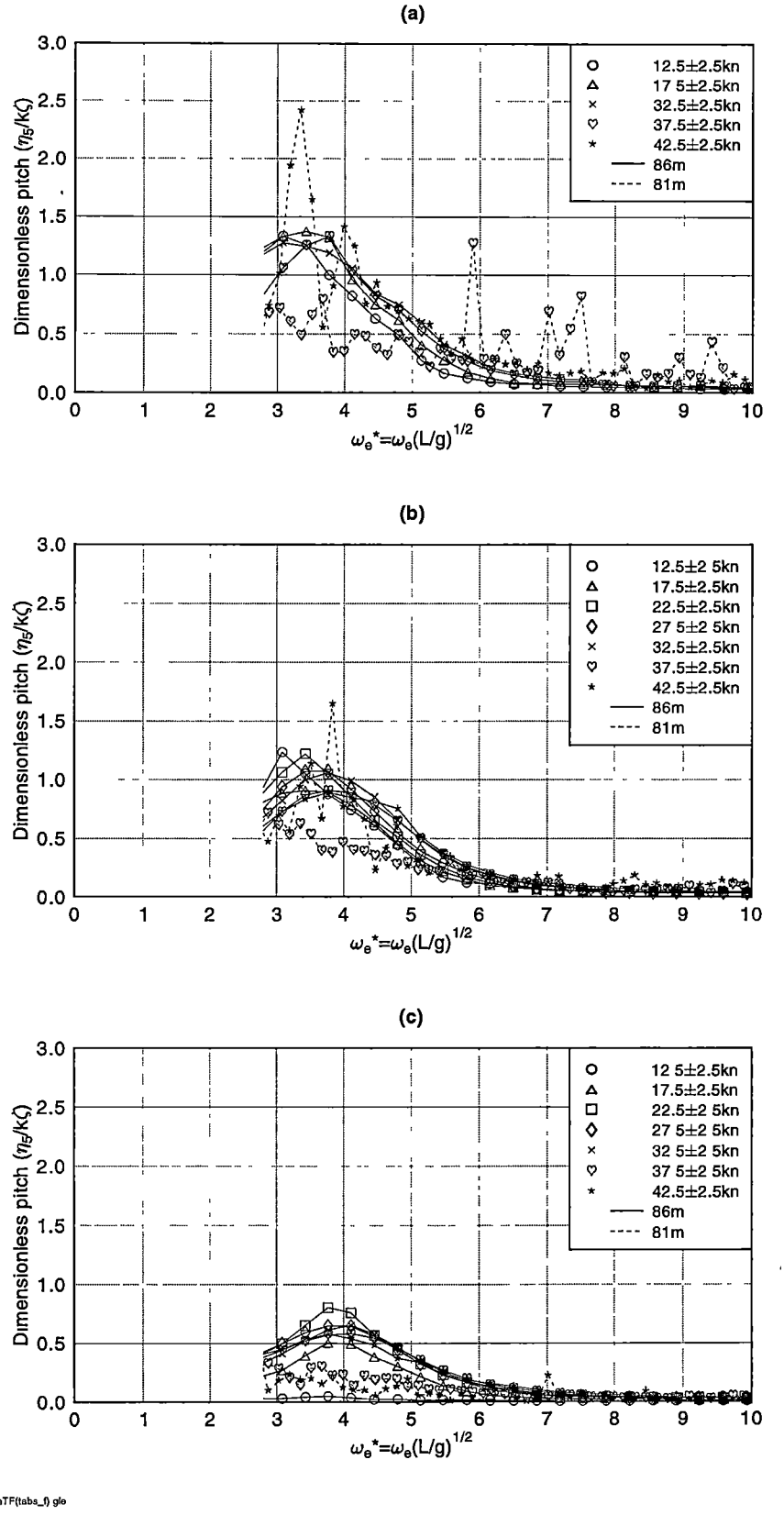

Figure 4.30: Measured pitch displacement transfer functions (81 and 86m vessels, active tabs and T-foils). Observed wave heading sectors: (a) bow (180° ±22.5°), (b) bow-quarter (135° ±22.5°) and (c) beam (90° ±22.5°).

Chapter 5

Predicted Motion Results

5.1 Introduction

The results presented in this chapter include those obtained with the numerical predictions of BESTSEA. These results whilst showing the end result of the methods presented in chapter 3, also form the basis for comparison with full-scale measurement results of chapter 4. With the nature of the experimental measurements being broad in their application it was not feasible to present all the measured and predicted results together in these chapters. This was firstly because the nature of the experiments relied on obtaining data in conditions that were not controlled and therefore broad assumptions and reasoning had to be made in the data reduction. This lead to an averaging of the data to form the final results. Secondly, the large amount of information presented within each plot made it more practical to segregate the two data sets of measured and predicted results. The predicted results will therefore be presented here and comparisons between the measured motion transfer functions and numerical predictions will be made in chapter 6.

5.2 Selection of Speed and Loading Conditions

With the accumulation of experimental motion records collected over an extended period of time it is reasonable to expect that the vessel loading condition was subject to change from day to day and voyage to voyage within a reasonable range. For practical reasons[1] it was not possible to digitally record the vessel loading condition for each voyage and furthermore this is not recorded during operations apart from the taking of draft marks. The distribution of vehicle loading can vary particularly when full capacity is not met giving the operator the choice on how the vehicles can be arranged to best trim the vessel to their advantage. This may imply that positioning as many vehicles toward the bow to give more bow down trim is desirable. Although the vessel displacement can be determined through the reading of draft marks the vessel radius of gyration in roll, pitch and yaw generally remains unknown for a particular voyage and cannot be determined unless the position and weight of every deadweight item made up of items such as cars, fuel and passengers is known. However, the range of possible loading conditions can be determined through analysis by looking at the range of possible loading scenarios to determine those that are governing the vessel's dynamic motion response once the vessel begins to encounter incident waves on its voyage. If the measured vessel response proves to be outside the predicted response then other

[1]This does not deminish the fact that it would certainly be useful to have the means to digitally record the loading condition variables.

variables such as wave height and wave period may need to be considered as the reason and may prove to be equally significant.

The variability of the vessel loading condition was investigated by creating weight estimates of the vessel for both the delivery voyage and for its operating conditions whilst in passenger service across the English Channel. This analysis sought only to consider these two very different operating conditions and determine how they affected the heave and pitch transfer functions and their frequency of maximum response. The results for the 81 and 86 metre vessels are shown in appendix A which shows the delivery departure and arrival conditions as well as the in service departure and arrival conditions for the vessels with a 50% and 100% load. Also shown for each condition is the change in hydrostatic conditions when the mass of the entrained water within the waterjet inlets is considered. Most hydrostatic analysis programs do not consider the effect of this additional mass in their normal computation for use in the analysis of vessel dynamics as the entrained water must be accounted for depending on the hull particulars being considered. For example, the mass of the entrained water is not included as part of the vessel displacement but conversely the inlets do not contribute to the vessel's buoyancy. This implies that the use of strip theory for motions analysis cannot resolve an equivalent displacement and position of the centre of gravity whilst also obtaining the correct draft. Generally, a strip theory calculation will not account for the weight of entrained water which can be over nine tonnes per jet. These vessels had two jets per hull so the entrained water consisted of approximately three to five percent of total vessel displacement. The entrained water is not part of the vessel's displacement but it is part of the vessel's moving mass and so was added to the displacement in the numerical model together with the modified centre of gravity and radius of gyration values. Table A.1 shows the delivery loading conditions for the 81 metre vessel whilst tables A.2 and A.3 show the 100% and 50% full loading conditions respectively for the vessel in operational service. The corresponding ranges of the radius of gyration for the vessel in roll, pitch and yaw are shown in table A.4 where the effect of the entrained water is also shown. Similarly, table A.6 shows the delivery loading conditions for the 86 metre vessel whilst tables A.7 and A.8 show the 100% and 50% full loading conditions respectively for the vessel in operational service. The corresponding ranges of the radius of gyration for the vessel in roll, pitch and yaw are shown in table A.9 where the effect of the entrained water is also shown. These loading conditions were selected because it was expected that the lightest and heaviest loading displacements would also create the broadest range of frequency response in the vessel. The half load condition was included to determine how this might effect the loading and in particular the radius of gyration when vehicles could be arranged in an uneven distribution on the vehicle deck.

After numerically modelling the vessels in all these loading conditions the heave and pitch response of each vessel at 32.5 knots without the influence of control surfaces is shown in figure 5.1 for the 81 metre vessel and in 5.2 for the 86 metre vessel. Only one speed was selected as it was expected that similar trends would also occur at other speeds and that the loading conditions that were governing the range of frequency responses at this speed would also be the governing conditions at the other speeds.

It can be seen in the figures that the magnitude and frequency of dominant response varied between the loading conditions in both heave and pitch. From these plots it can be seen that the broad range of predicted heave and pitch motions were essentially bounded by the "Service - full load departure" condition representing the lower dominant response frequency and the "Delivery - 10% arrival" condition representing the higher dominant response frequency. Whilst the former represented a heavy displace-

ment it also had a larger pitch radius of gyration compared with the latter which was of lighter displacement and lower pitch radius of gyration. By only using these loading conditions for the remainder of the results it should be possible to determine the maximum range of motions amplitudes possible for a modelled wave condition merely by presenting the results for these two loading conditions. All predicted motion results are therefore presented as either the "Service - full load departure" condition or the "Delivery - 10% arrival" condition and should not be confused with the measured data, which was collected during the delivery voyage where the vessel was fitted only with active transom tabs and during service operations where both active transom tabs and T-foils were installed. In either case the two numerically modelled loading conditions selected could be compared with the measured data obtained from either the delivery voyage or during service operations.

It can also be seen in these results that there were similar characteristics in the transfer functions between the 81 and 86 metre vessels so the results of the numerical predictions for the remainder of this chapter consist only of the 86 metre vessel to keep the computations to a practical level. Furthermore, the measured data for the 86 metre vessel contained in chapter 4 was of better quality because of its greater quantity and so would provide greater opportunity for comparison.

Numerically modelling the vessel at the speeds of 12.5 to 42.5 knots in increments of 5 knots was a logical step that came out of the experimental results, which were grouped according to speed in 5 knot increments from 10 to 45 knots. The speeds selected for numerical computation therefore represent the median of the speed ranges within each group of measured data.

We see from the results of figures 5.1 and 5.2 that when more heavily loaded the maximum heave response increased by about 60% and the frequency of maximum response reduces by about 15%. This is as would be expected where increased mass in any dynamic system tending to reduce its damping relative to critical damping and to lower its frequency of maximum response. However, the effect of loading changes on the pitch response is much smaller, the response maximum increasing by about 20% and its frequency reducing by only 5% at the higher displacement.

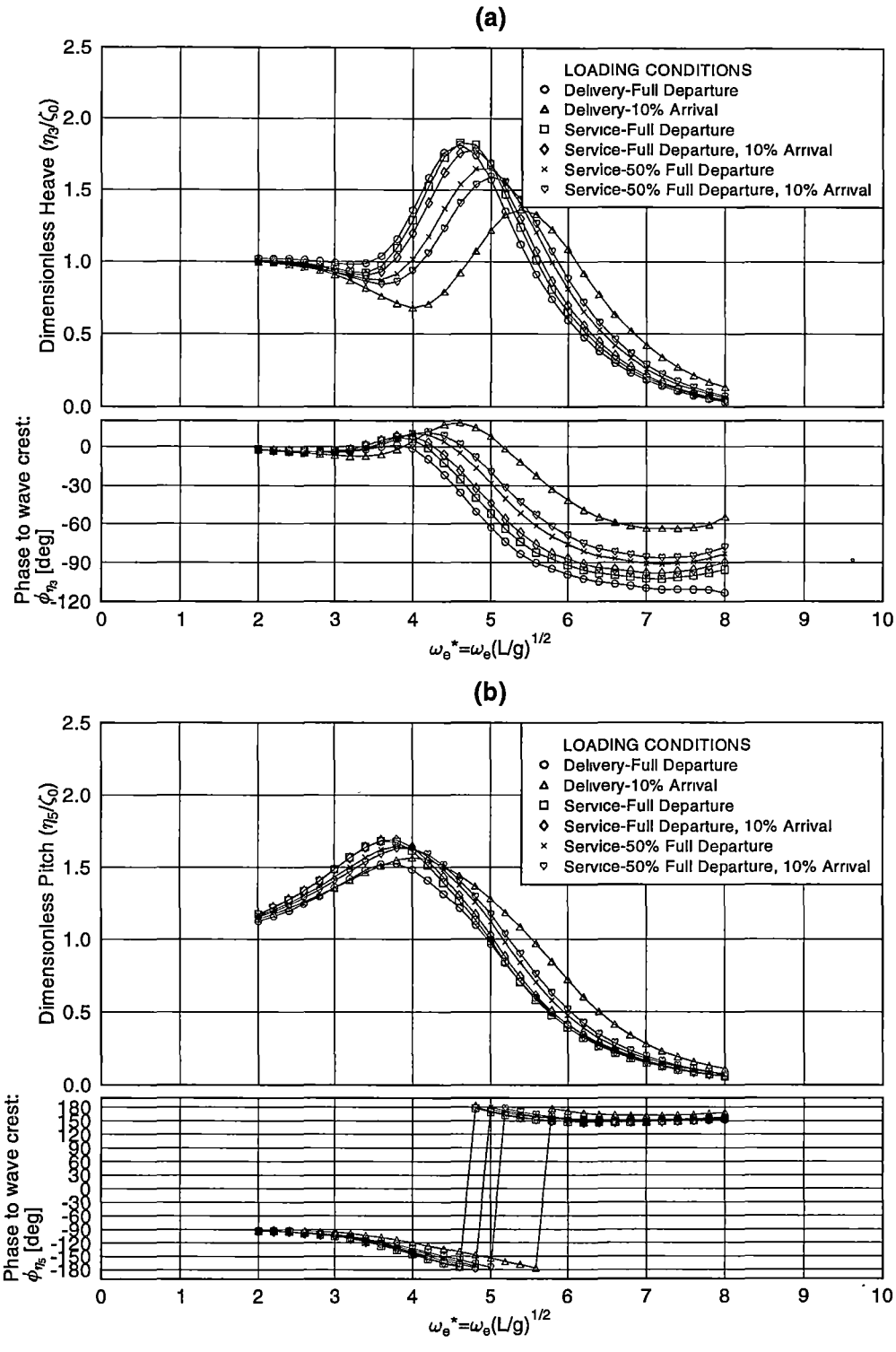

Figure 5.1: Transfer functions at various loading conditions (81m vessel, no control surfaces) in (a) heave and (b) pitch at 32.5kn.

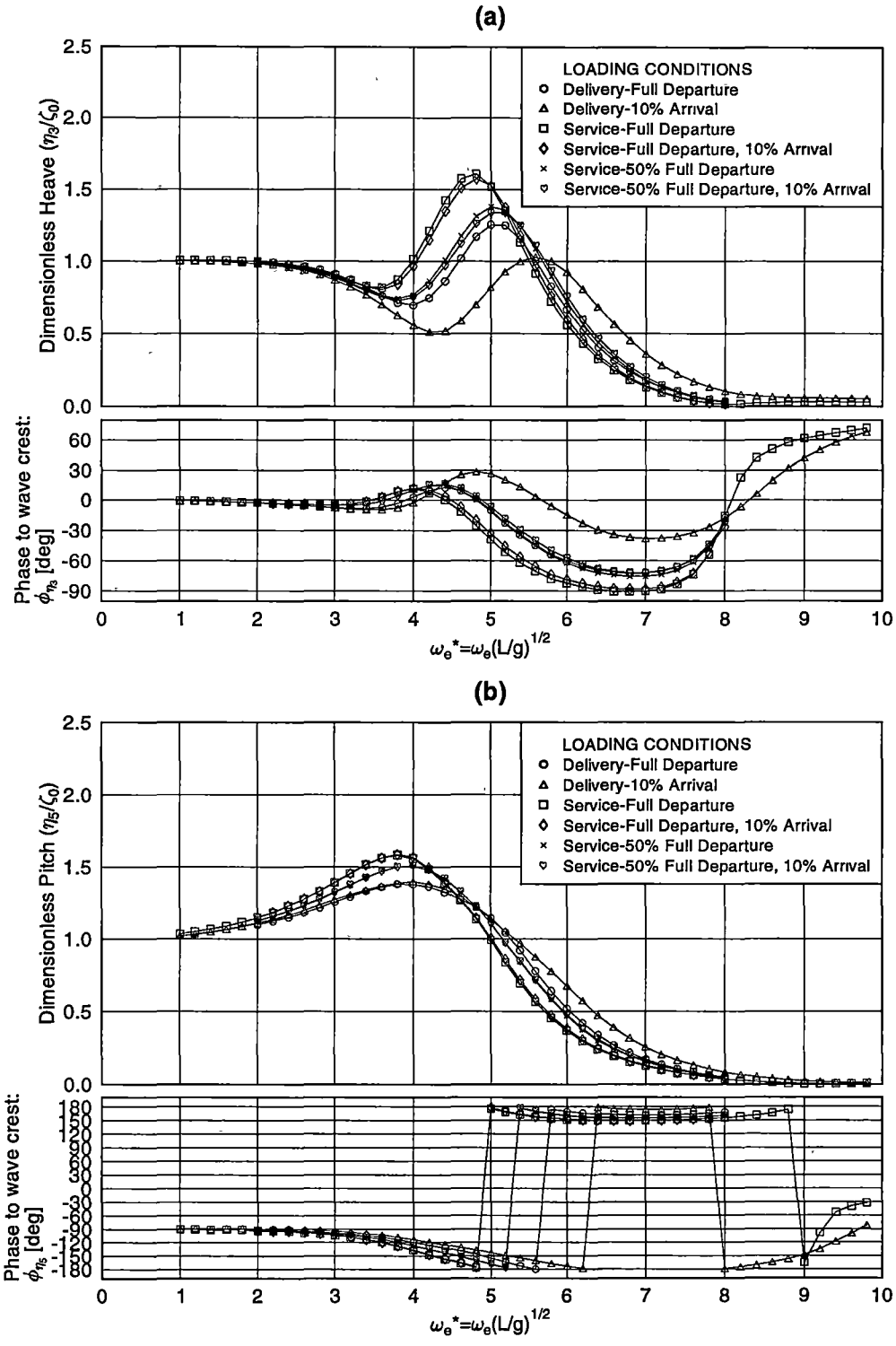

Figure 5.2: Transfer functions at various loading conditions (86m vessel, no control surfaces) in (a) heave and (b) pitch at 32.5kn.

5.3 Modelling of Sea Conditions and Motion Control System

5.3.1 Wave Period Selection

The procedure introduced in chapter 3 for determining the appropriate control gains for each motion control surface depend upon the wave spectrum and in particular the wave period of the spectrum. Whilst this procedure may be somewhat different to the control tuning method utilised in the commercial systems installed on the vessels, the predicted results are presented here at a single average wave period of 7 seconds. This period is lower than the average wave period (T_1) obtained from head sea measurement records for the 86 metre vessel, which ranged from an average of 8.9 to 12.8 seconds for the various speeds (see table 4.4). However, it is expected that at the average wave period of 7 seconds the vessel response per unit wave height should by comparison give a greater vessel response than for higher measured periods. This can be seen in the results of acceleration per unit wave height shown hereafter in the diagrams of figures 5.25 and 5.26 for the vessel with and without motion control surfaces. The selection of a shorter 7 second period for the computations also reflects the view that the route selected for the trials reported in chapter 4 was unusual in it exposure to incoming ocean swell thus giving rise to larger than usual average wave periods for a given condition of wave height.

5.3.2 Wave Height Selection and Spectrum

During the experimental measurements presented in chapter 4 it was found that the average wave heights measured in head seas for the 86 metre vessel ranged from 0.32 to 0.64 metres (RMS) or approximately 1.28 to 2.56 metres significant wave height (see table 4.4). On this basis the significant wave height was modelled in the computations at 2.5 metres[2] being closer to the upper side of this range and was based on the Bretschneider wave spectrum for that height. Its distribution with frequency is obviously somewhat different to the measured wave spectra presented in section 4.3.2. Using the measured average wave spectrum at each speed from the full-scale measurements instead of the idealised Bretschneider wave spectrum would have been entirely possible and would certainly be an ideal alternative, but the wave spectrum at each speed was generally different in terms of magnitude and distribution and at some speeds there was no data. More importantly, the measured average spectra reported in chapter 4 are in many cases clearly influenced by averaging across data obtained under significantly different sea conditions and therefore do not follow one of the well known spectral forms such as the Bretschneider spectrum. To maintain consistency between the wave spectra for the numerical computations a constant wave spectral shape was therefore used. This will create differences in the acceleration spectra and magnitudes in the comparison but these will need to be explained based on the differences in terms of the underlying wave spectra. The comparative Bretschneider wave spectra were shown in chapter 4, section 4.3.2 in figures 4.6 to 4.9. The Bretschneider wave spectra used in the predictions are shown in figure 5.3 for a range of wave periods. The first diagram shows the unidirectional wave spectra whilst the remaining diagrams below it show the same spectra modified to the encounter frequencies corresponding to the four speeds analysed with active control surfaces, these being 12.5, 22.5, 32.5 and 42.5 knots. The intermediate speeds of 17.5, 27.5 and 37.5 were excluded as they would not necessarily enhance the evidence of trends obtained from the other four speeds.

[2]This also corresponds to the top level of Sea State 4.

In some instances of wave spectra within the diagrams of figure 5.3, it can be seen that the wave encounter spectrum for $T_1 = 15$ seconds is slightly truncated at the minimum computed dimensionless wave encounter frequency of 1.0. This is not expected to significantly affect the calculations of the root mean square acceleration at this wave period which uses the area of the response spectrum. In particular, little significant acceleration response is expected at such low frequencies. Similarly, in some instances the wave encounter spectrum of $T_1 = 5$ seconds has been more severely truncated at the maximum computed dimensionless wave encounter frequency of 9.8. This also is not expected to significantly affect the calculations of the root mean square acceleration at this wave period because the heave and pitch transfer functions are very small at or above this frequency and so the response will also be small. Furthermore, the results presented are based on a 7 second average wave period[3], which in itself has small magnitudes at the higher frequencies and for which truncation errors are not significant.

5.3.3 Control Gain Settings with Active Controls

The implementation of active controls in the numerical prediction used the motion criterion defined in section 3.4.7.1 of chapter 3 as the basis for determining the motion reduction performance when modelling active controls. This criterion was based on the average acceleration spectrum taken between six longitudinal hull positions. The gains were selected according to the method given in chapter 3 by minimising the spectrum peak. The progressive reduction in the peak of the average acceleration spectrum can be seen in the results shown hereafter in section 5.5.2.

The control gains used to achieve the results with active control surfaces presented in this chapter were given in table 3.3 of chapter 3.

The motion control surfaces position and sizes are shown in table A.5 for the 81 metre vessel and table A.10 for the 86 metre vessel in appendix A although only the 86 metre vessel with active controls was modelled in this analysis.

[3]The vertical acceleration reponse spectra for the 86 metre vessel are presented in figures 5.16 to 5.19 for three longitudinal positions where it can be seen that low and high cut off frequencies are sufficient to capture the majority of the acceleration response bandwidth. These plots will be discussed in the following section.

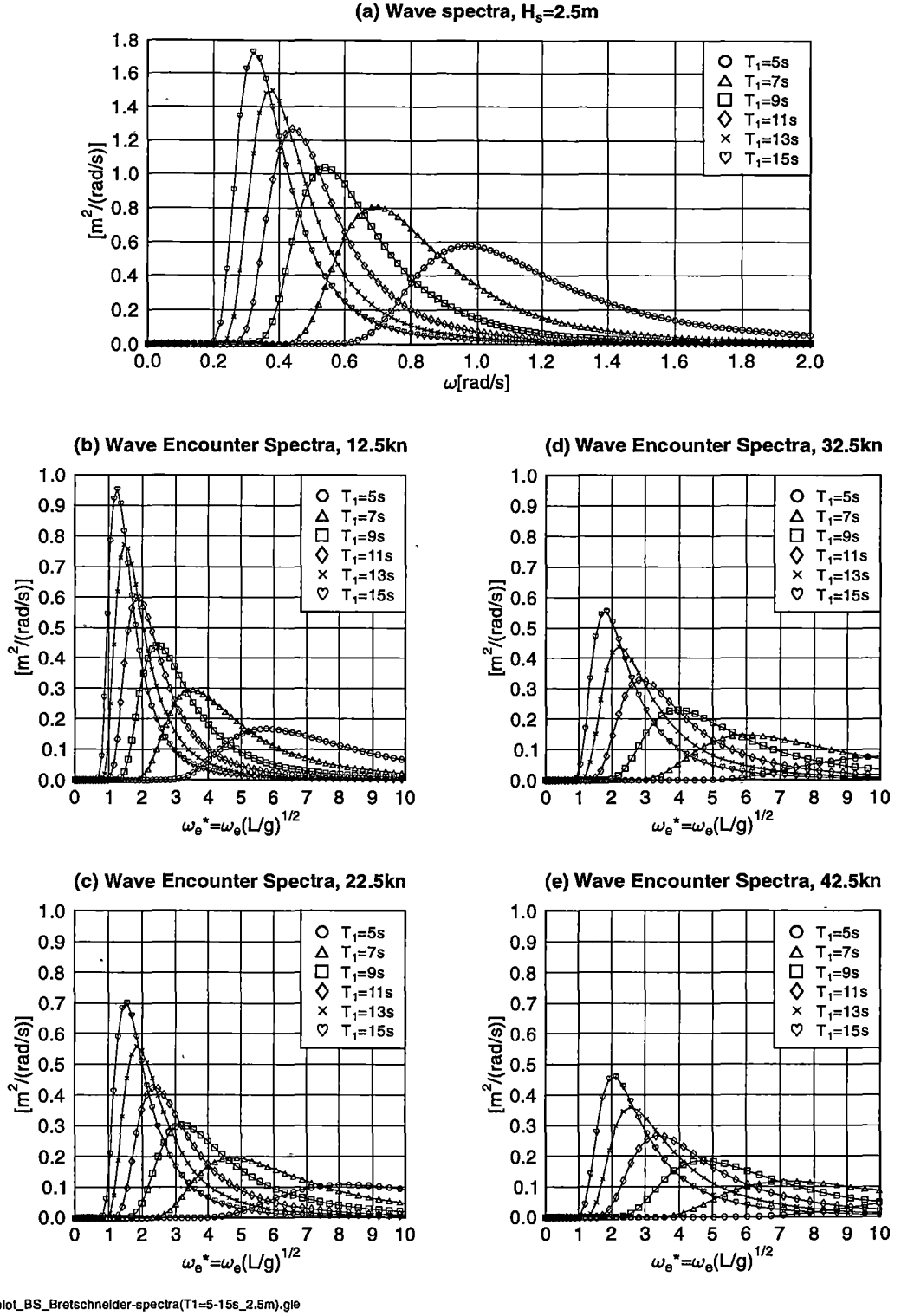

Figure 5.3: Bretschneider wave spectrum and corresponding head sea wave encounter spectra as used in computations ($H_s = 2.5$m, $T_1 = 7$s)

5.4 Effect of Speed on Transfer Functions

Results obtained from the BESTSEA numerical computations for the 86 metre vessel are presented as transfer functions from figures 5.4 to 5.15 for a range of speeds where the time series hydrodynamic solutions were computed in regular 0.5 metre waves to obtain a near linear solution at small wave height. In cases where active control surfaces were implemented, the computation scaled the control gains so as to obtain the maximum surface deflection in regular waves of 2.5 metres. The controls were optimized to reduce the average vessel acceleration in a Bretschneider wave spectrum of 2.5 metre significant wave height and 7 seconds average period. The hull configurations presented in this section include the two sets of motion control surfaces arranged in various combinations so that the incremental effects can be reviewed. These configurations consist of a

1. hull without control surfaces;
2. fixed transom tab and fixed T-foil;
3. active transom tab only (no T-foil);
4. active T-foil only (no transom tab);
5. active transom tab, fixed T-foil, and
6. active transom tab and active T-foil.

The first set of transfer functions in figures 5.4 and 5.5 show the effect of speed on the vessel for the two selected loading conditions. The first diagram (a) on each page shows the results at the "Service - Full departure" loading condition, which represents the heavier displacement whilst the second diagram (b) shows the results at the "Delivery - 10% arrival" loading condition, which represents the lighter displacement. As previously discussed, the former diagram has a lower frequency of response with a greater magnitude and the latter has a higher frequency of response of lower magnitude. It is clear from these diagrams that the vessel heave reduces significantly with speed, particularly at the resonant frequency whilst in pitch a reduction in speed has a similar effect. However, reduction of speed does not significantly alter the frequency of maximum heave response for speeds in the 22.5 to 42.5 knot range. At lower speeds the frequency of maximum heave response does reduce somewhat. For speeds less than about 20 knots the heave transfer function remains less than 1.0 at all frequencies, but continues to exhibit a clear maximum at the dimensionless frequency of about 4.8 (heavy loading condition) and 4.8 to 5.5 (light loading condition). The pitch response shows a more progressive reduction in frequency of the maximum transfer function as speed is reduced, and the maximum decreases more sharply at lower speeds. At the lowest speed (12.5kn) no maximum in the pitch transfer function is clear.

The magnitude of the peak of these transfer functions is of course influenced by the magnitude of the applied friction coefficient, which was explained in section 3.2.1.1 of chapter 3. All these results were obtained with a friction coefficient of 0.1 which in some cases may arguably be either too low or too high. However, the only effect of varying this parameter is to change the magnitude of the resonant peak of the transfer functions which may ultimately improve the correlation between the measured and computed responses.

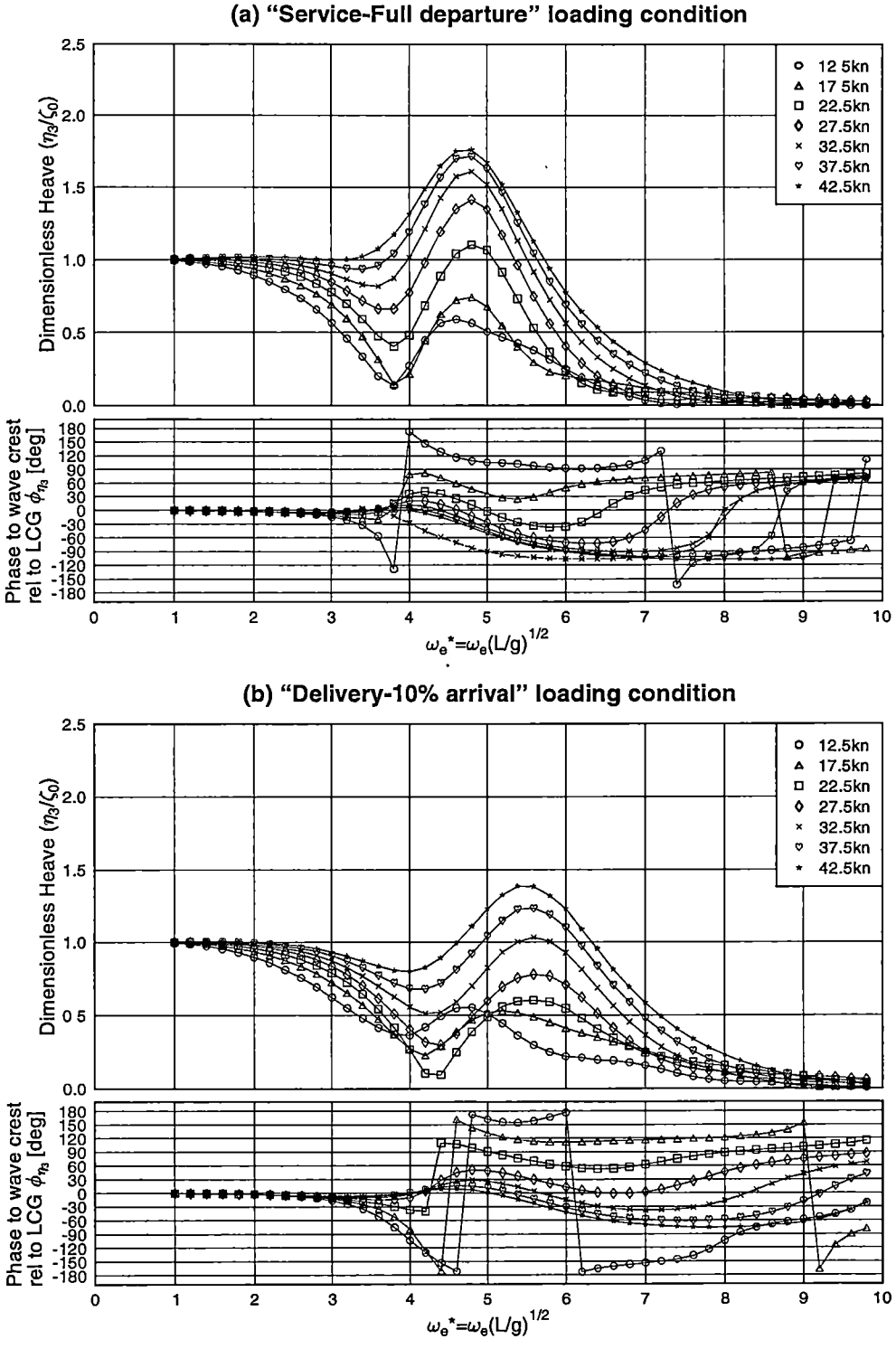

Figure 5.4: Predicted heave transfer functions (86m vessel, no control surfaces) at loading conditions of (a) "Service-full load departure" and (b) "Delivery-10% arrival" (Regular wave height of computation = 0.5m)

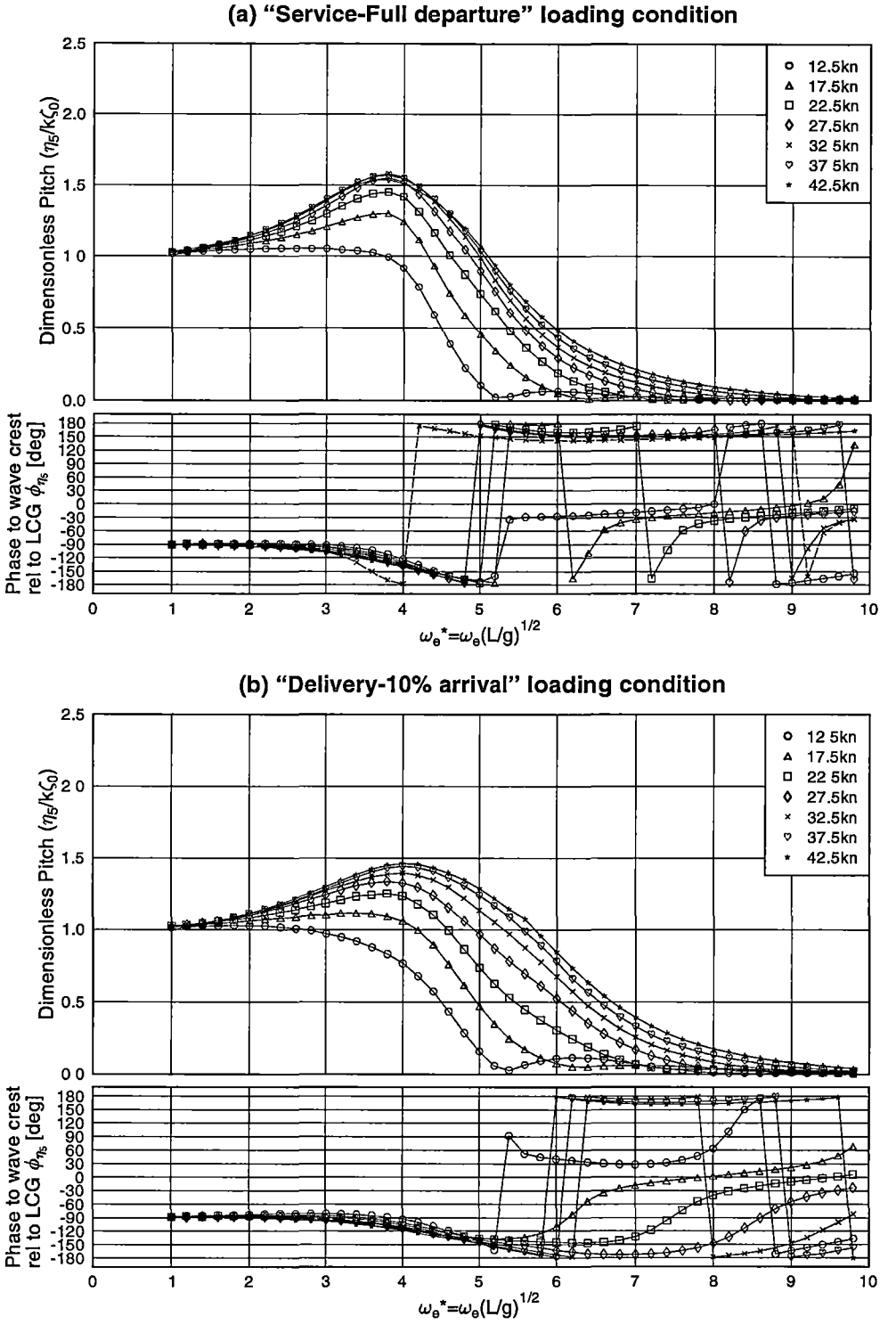

Figure 5.5: Predicted pitch transfer functions (86m vessel, no control surfaces) at loading conditions of (a) "Service-full load departure" and (b) "Delivery-10% arrival" (Regular wave height of computation = 0.5m)

5.4.1 With Fixed Motion Control Surfaces

With the addition of motion control surfaces to the hull there is first interest in obtaining a result that shows the damping effect of these surfaces without any active feedback from the control system. This result is shown in the diagrams of figures 5.6 and 5.7 whilst the previous result given for the hull without control surfaces is also shown. In this condition when the control surfaces are stationary relative to the hull, the transom tab only produces a steady lift force and does not produce a passive damping effect on the motion because the inflow angle of the fluid is assumed constant as the vessel heaves and pitches. In contrast, the T-foil is exposed to the free stream velocity and also assumed to be free from the influence of the hull by lying outside the region of reduced flow velocity due to the boundary layer and can generate a lift force as the free stream incidence angle changes in time due to the incident waves, the heave velocity, pitch displacement and pitch velocity.

It can be seen in these results that the motion reduction in both heave and pitch is greatest at the highest speed and the control effect steadily reduces with speed. This effect is to be expected as the lift force generated by the T-foil is proportional to the velocity squared and so a halving of the speed means a force reduction of 75%. At the lowest speed the effect of the fixed control surfaces is almost nonexistent. The damped natural frequency has also reduced as expected in both heave and pitch. It can be seen that the addition of the fixed T-foil has substantially damped the heave response at higher speeds, the maximum value reducing and the sharpness of the maximum decreasing. Similar effects occur at both loading conditions but are stronger at the light load. At light loading and high speed the fixed control surfaces have virtually eliminated the resonant maximum in heave response, which is always less than unity at all frequencies. The pitch shows smaller changes with the addition of the fixed surfaces presumably because the stern tab has no practical effect and the T-foil is closer to the centre of rotation in pitch. However, the fixed control surfaces do have an effect in increasing pitch damping at the higher speeds, the pitch reducing by about 20% at the highest speed.

5.4.2 With Active Transom Tabs Only

The benefit of using active transom tabs is shown through the numerical computation at the four speeds in figures 5.8 and 5.9. It can be seen that the benefit of these devices is relatively small, particularly at the lower speeds. The improvement in motion from these control surfaces appears greatest in reduced pitch by comparing the results in these two figures. The reduction in maximum heave at the top speed of 42.5 knots is about 5% for both loading conditions, whilst the pitch is reduced by about 20% at the top speed. These results raise serious issues about the benefit, or lack thereof, of fitting vessels only with transom tab motion controls. On the basis of these results it appears that such installations give relatively small benefit. This outcome is a direct result of the motion reduction objective which was to minimise the average vertical acceleration over the length of the hull. The transfer functions presented here are thus the result of that procedure where the reduction of pitch with the transom tab has the greatest benefit although heave was also slightly reduced.

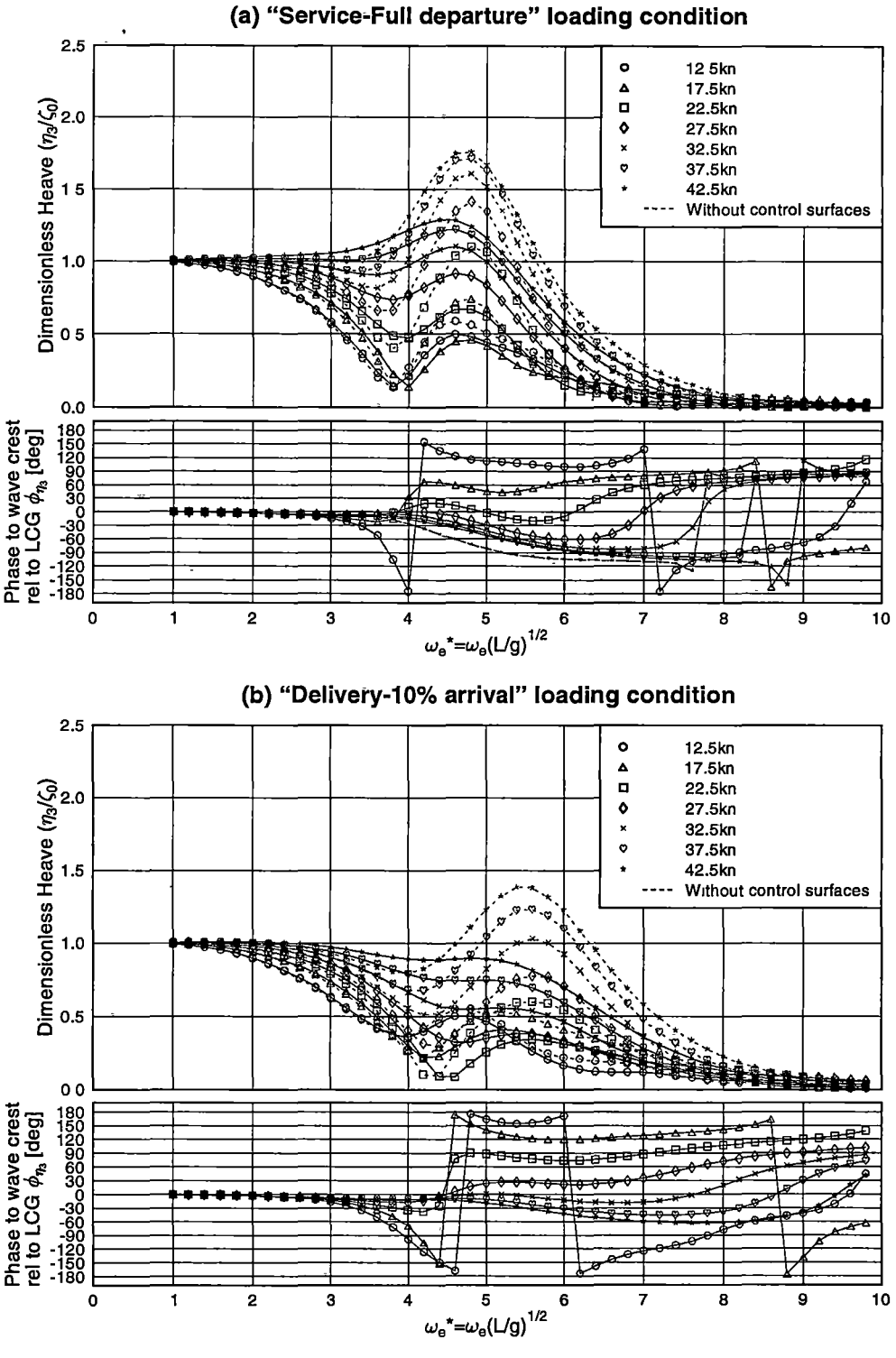

Figure 5.6: Predicted heave transfer functions (86m vessel, fixed tab and T-foil) at loading conditions of (a) "Service-full load departure" and (b) "Delivery-10% arrival" (Regular wave height of computation = 0.5m)

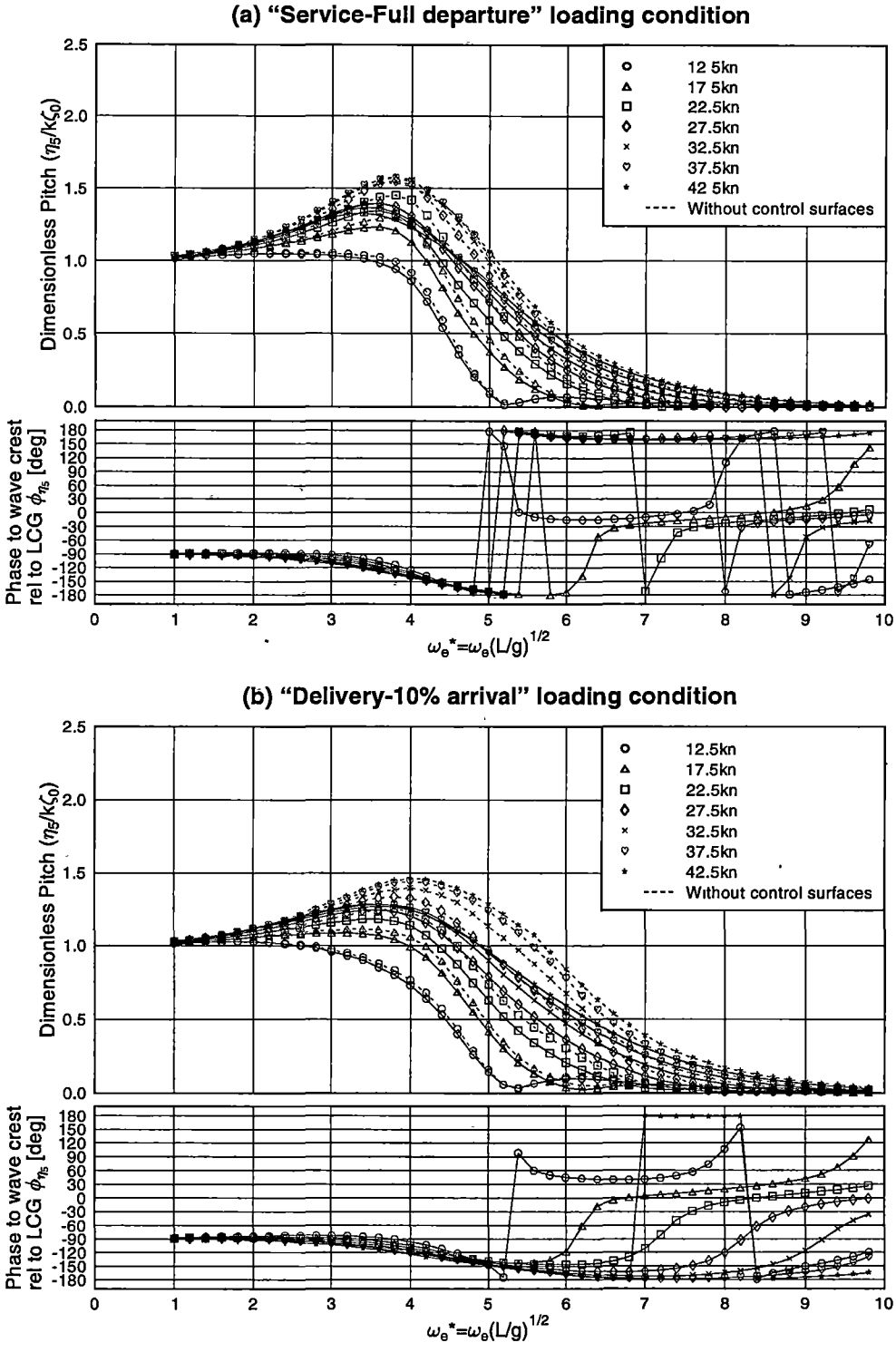

Figure 5.7: Predicted pitch transfer functions (86m vessel, fixed tab and T-foil) at loading conditions of (a) "Service-full load departure" and (b) "Delivery-10% arrival" (Regular wave height of computation = 0.5m)

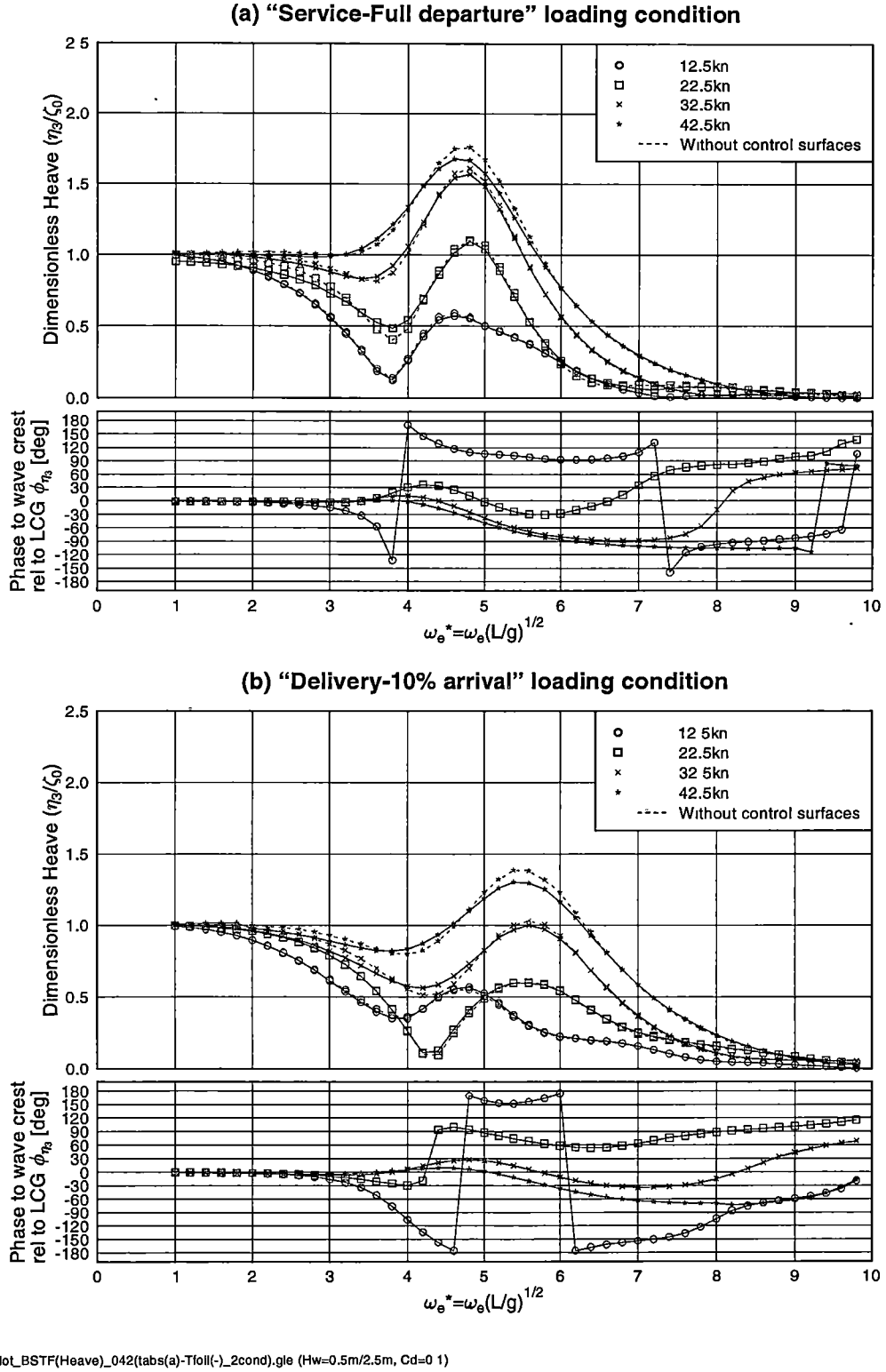

Figure 5.8: Predicted heave transfer functions (86m vessel, active tab only) at loading conditions of (a) "Service-full load departure" and (b) "Delivery-10% arrival" (Regular wave height of computation = 0.5m, Regular wave height of control surface maximum deflection = 2.5m, Control gains calculated with Bretschneider wave spectrum of H_s = 2.5m, T_1 = 7s)

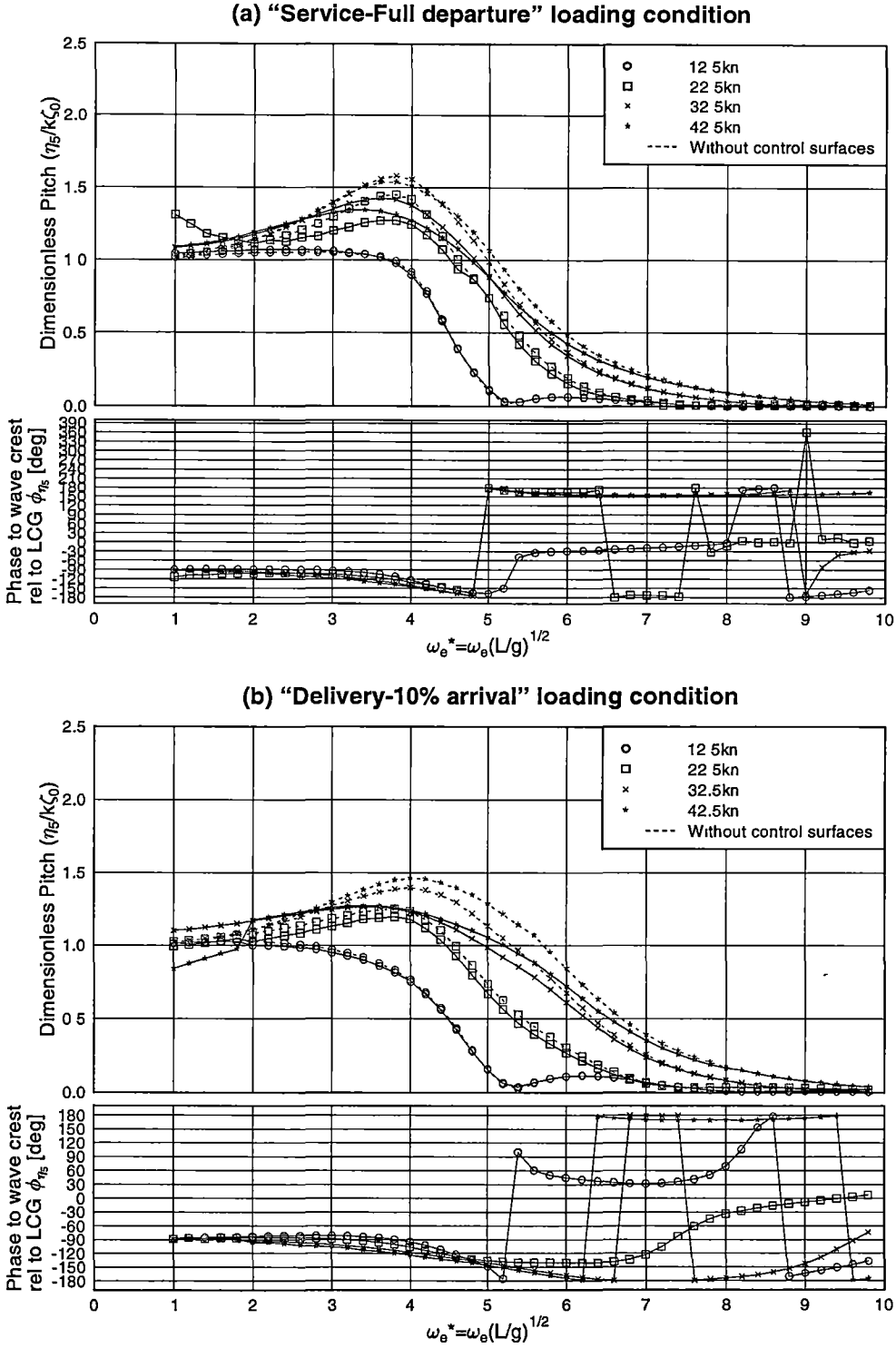

Figure 5.9: Predicted pitch transfer functions (86m vessel, active tab only) at loading conditions of (a) "Service-full load departure" and (b) "Delivery-10% arrival" (Regular wave height of computation = 0.5m, Regular wave height of control surface maximum deflection = 2.5m, Control gains calculated with Bretschneider wave spectrum of H_s = 2.5m, T_1 = 7s)

5.4.3 With Active Transom Tabs and Fixed T-foils

Adding fixed T-foils to the previous results whilst maintaining active transom tabs gave as expected only a slight improvement on the result obtained with fully fixed tabs and T-foils. This result is shown in figures 5.10 and 5.11 against the fully fixed configuration where a greater reduction in pitch than the heave can be seen. There is one anomaly in the results at 22.5 knots where the pitch transfer function has an irregular shape. This may in part be due to the time domain solution at some frequencies not reaching a steady periodic solution within the time frame nominated in the computation, thus introducing a small variation in the resolved magnitude. This irregular shape is clearly visible in the pitch transfer function of figure 5.11(b) for the "delivery - 10% arrival" loading condition but is not evident in the results obtained for the heavier loading condition and is not evident in the heave results.

The heave does not change significantly compared with the result from the fixed control surface configuration. The heave reduces by about 3% at the top speed only. In the lighter loading condition ("delivery - 10% arrival") the heave at the resonant frequency actually slightly increases whilst the pitch is reduced at all speeds. In the heavier loading condition the heave reduces slightly whilst the pitch is also reduced particularly at the higher speeds. Bearing in mind that the fixed transom tabs have no direct effect on the vessel dynamics, these results show that even if active the transom tab produce very little motion reduction. These results therefore reinforce the question regarding the suitability of transom tabs as motion control devices raised in section 5.4.2. As a consequence of these results it is suggested that there is a need to demonstrate the benefits of active transom tabs in sea trials.

Fitting transom tabs is a commonly adopted vessel configuration and yet these computations suggest strongly that active transom tabs have almost negligible effect on vessel motions. Clearly there is an issue here which needs resolution. However, it is recognised that their benefit as static trim control devices to improve vessel speed performance remains and therefore any suggestion of removing them completely can not be supported.

5.4.4 With Active T-foils Only

Based on the results presented for the fixed control surface configuration, it is clear that the T-foil even in the fixed configuration has significant effect in reducing the heave and pitch motions. The improvement due to the active control is shown to be less significant in figures 5.12 and 5.13 where the active T-foil result is displayed against the fixed control surface configuration result. The reduction in heave and pitch is about the same, which is a small improvement compared with the result from the fixed configuration. Once again there is a greater improvement at the higher speeds, with almost no improvement at the lowest speed of 12.5 knots. Once again these results raise serious issues concerning the benefits of active control systems at larger wave heights, the dominant effects of the motion controls being due to the passive action of the T-foils. However, the increased benefit that would result as the wave height is reduced cannot be overlooked and the fact that a T-foil of increased area or with a fully actuating control surface could also improve the result presented here.

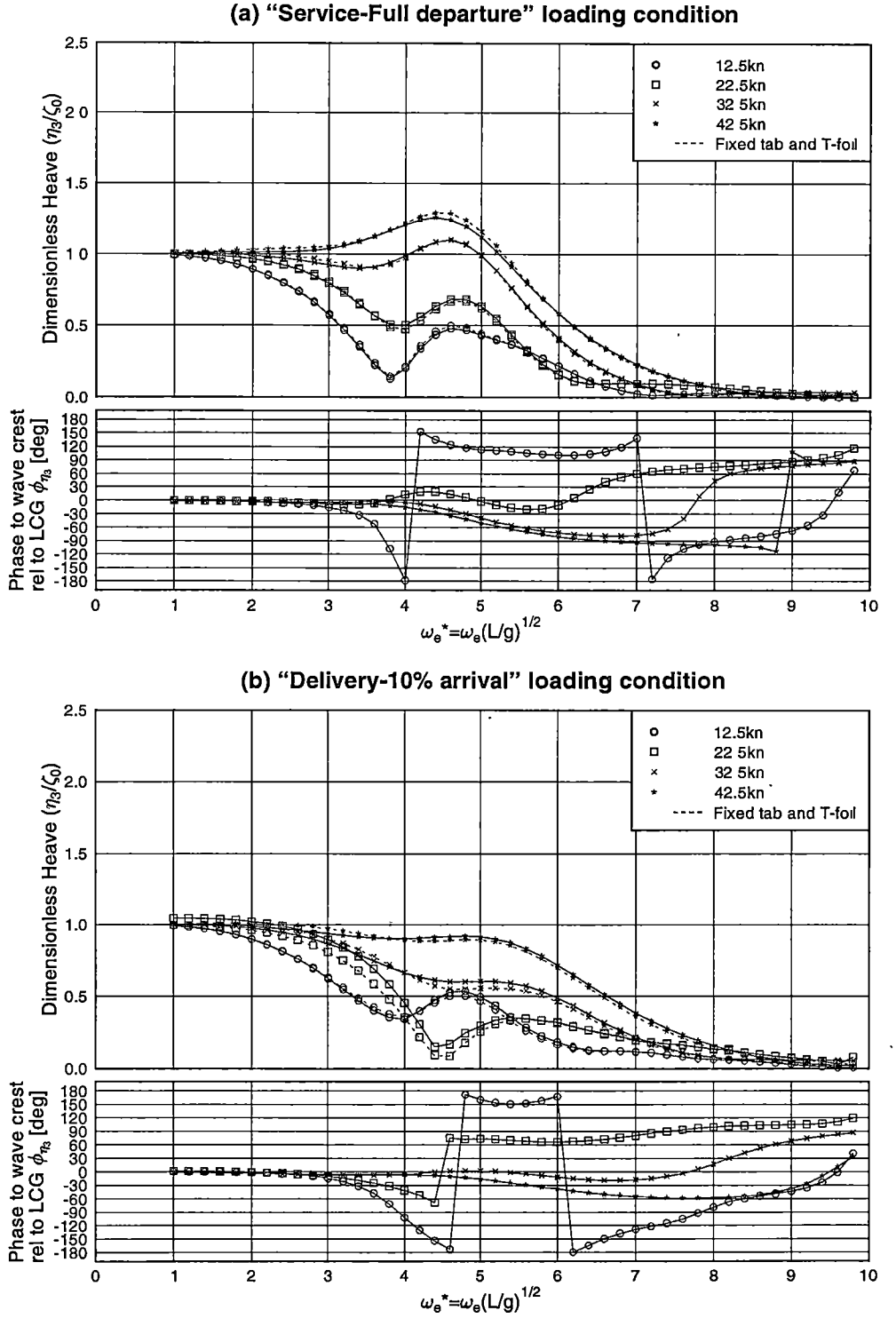

Figure 5.10: Predicted heave transfer functions (86m vessel, active tab, fixed T-foil) at loading conditions of (a) "Service-full load departure" and (b) "Delivery-10% arrival" (Regular wave height of computation = 0.5m, Regular wave height of control surface maximum deflection = 2.5m, Control gains calculated with Bretschneider wave spectrum of H_s = 2.5m, T_1 = 7s)

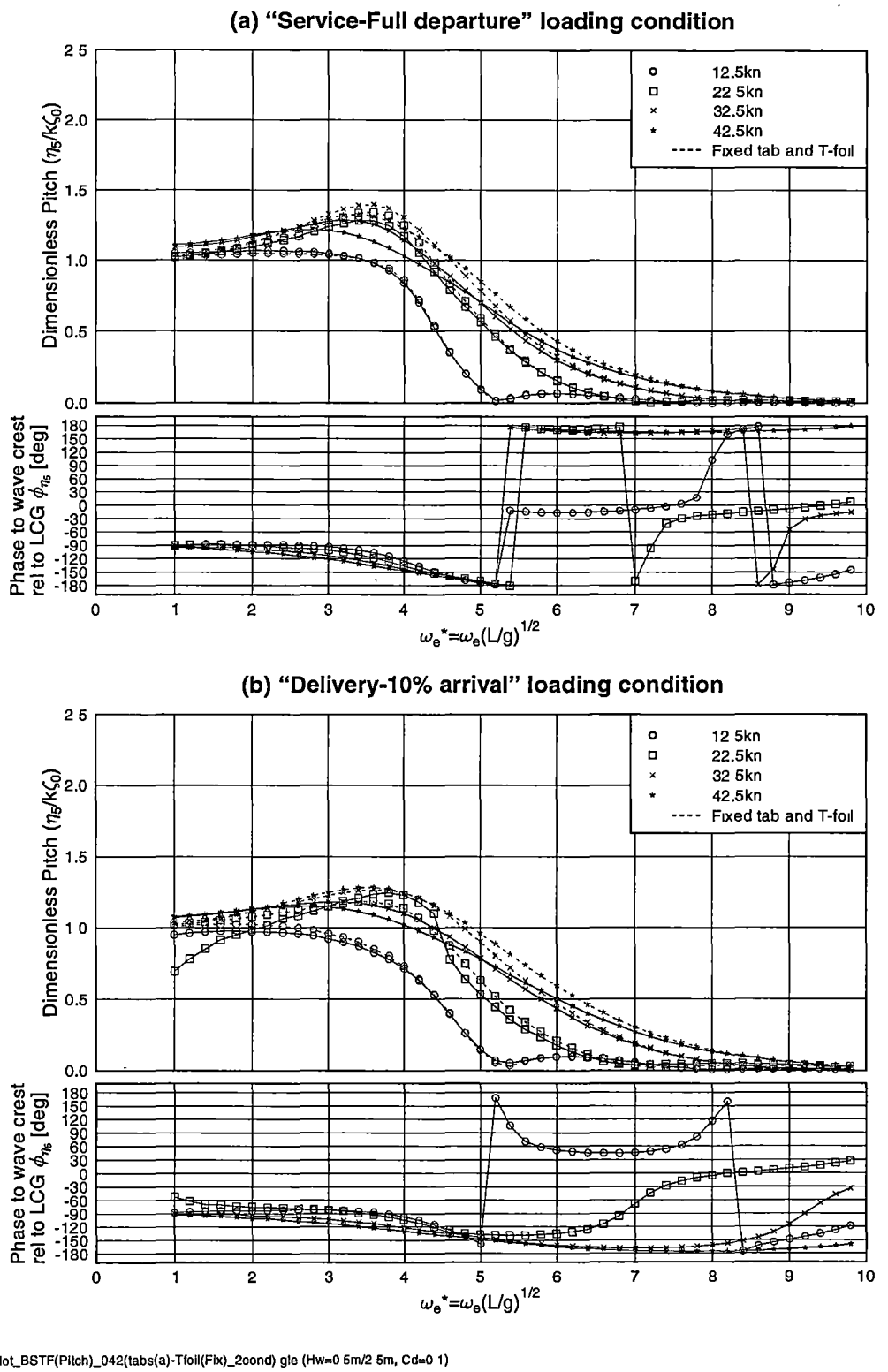

Figure 5.11: Predicted pitch transfer functions (86m vessel, active tab, fixed T-foil) at loading conditions of (a) "Service-full load departure" and (b) "Delivery-10% arrival" (Regular wave height of computation = 0.5m, Regular wave height of control surface maximum deflection = 2.5m, Control gains calculated with Bretschneider wave spectrum of H_s = 2.5m, T_1 = 7s)

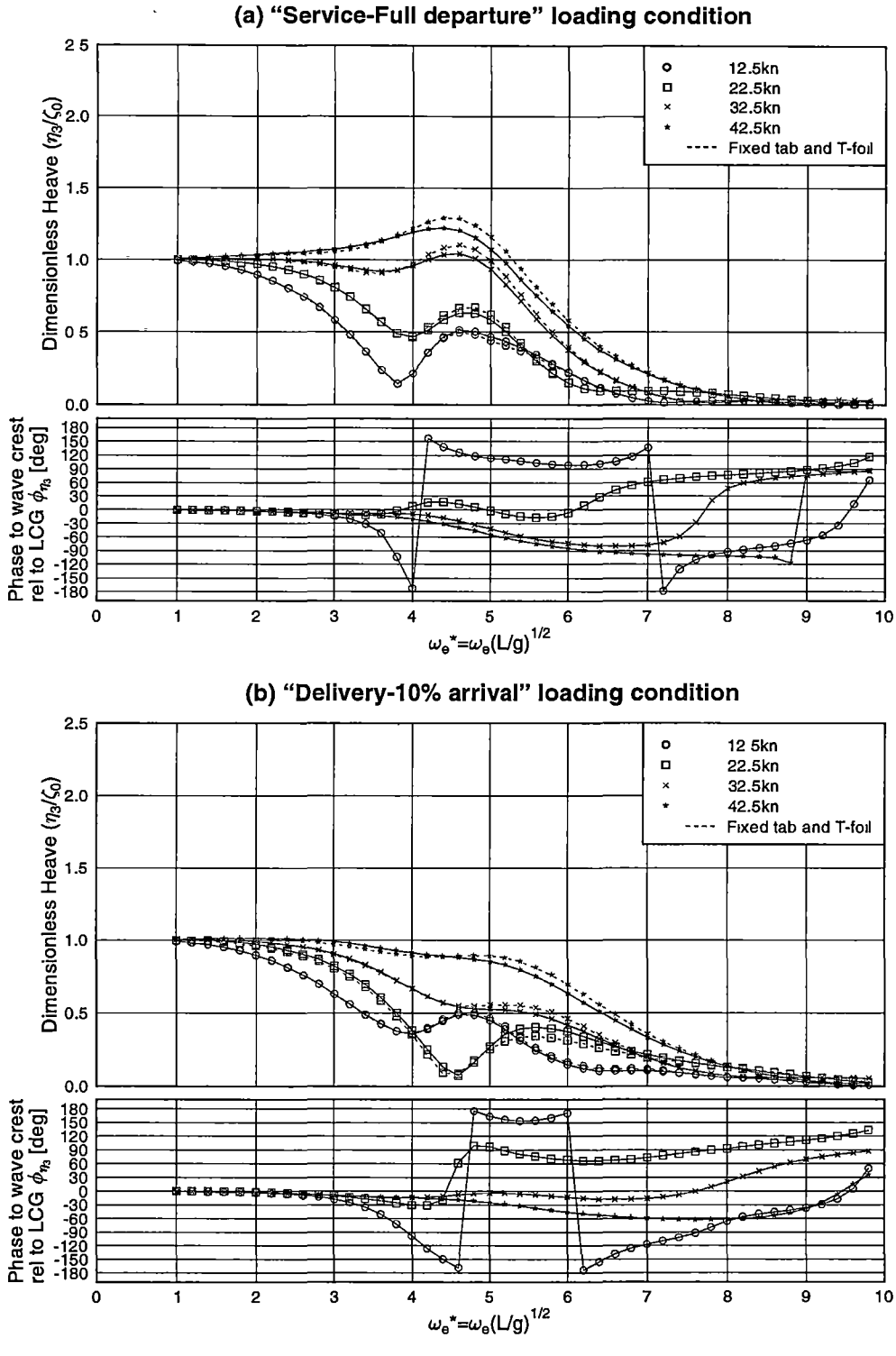

Figure 5.12: Predicted heave transfer functions (86m vessel, active T-foil only) at loading conditions of (a) "Service-full load departure" and (b) "Delivery-10% arrival" (Regular wave height of computation = 0.5m, Regular wave height of control surface maximum deflection = 2.5m, Control gains calculated with Bretschneider wave spectrum of $H_s = 2.5$m, $T_1 = 7$s)

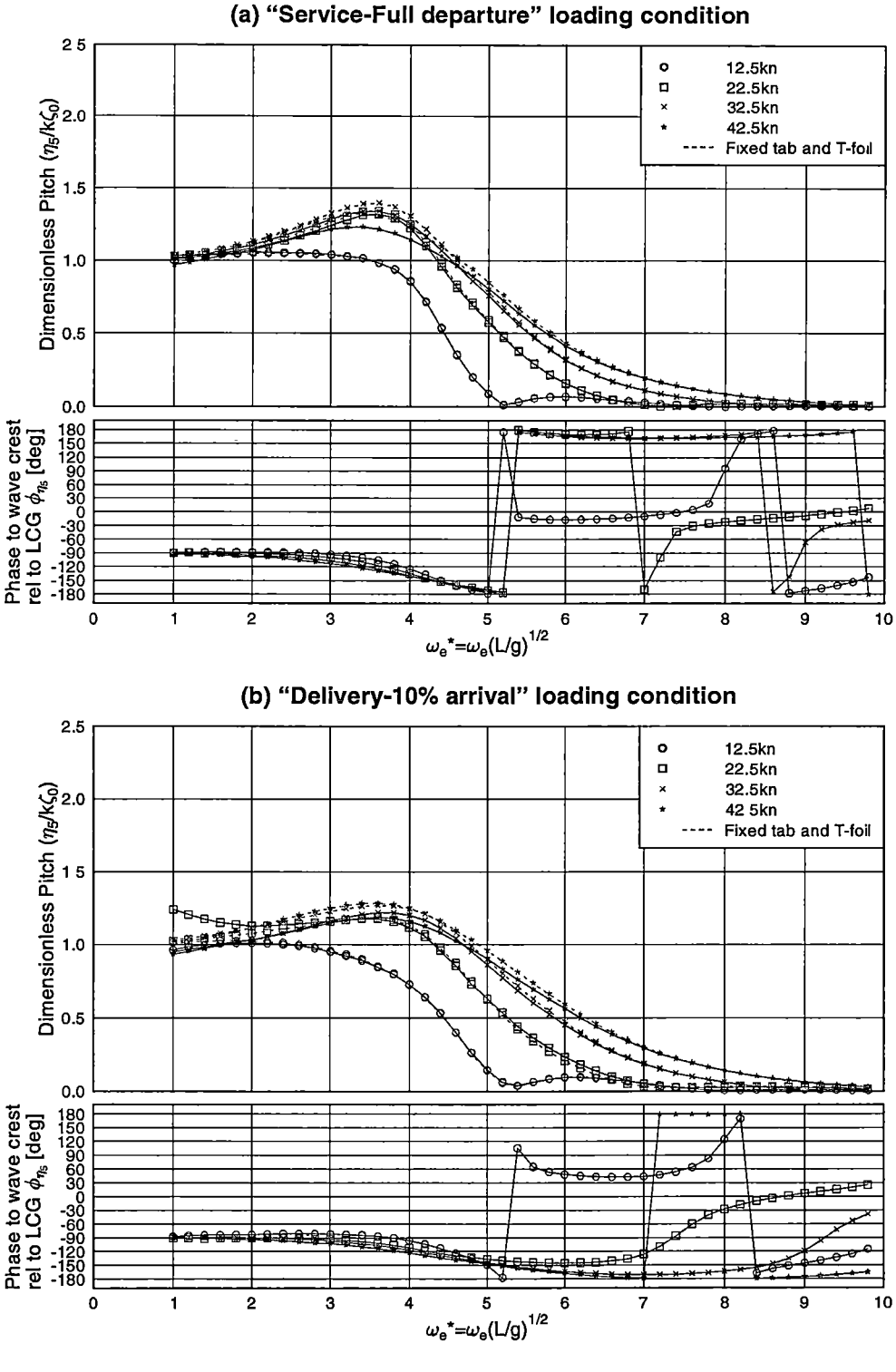

Figure 5.13: Predicted pitch transfer functions (86m vessel, active T-foil only) at loading conditions of (a) "Service-full load departure" and (b) "Delivery-10% arrival". (Regular wave height of computation = 0.5m, Regular wave height of control surface maximum deflection = 2.5m, Control gains calculated with Bretschneider wave spectrum of H_s = 2.5m, T_1 = 7s)

5.4.5 With Active Transom Tabs and T-foils

As expected the greatest improvement in the transfer functions of heave and pitch was obtained with active transom tabs and T-foils. This result is shown in figures 5.14 and 5.15, where the fixed control surface configuration results for the four speeds computed are also shown for comparison.

There was no improvement in the motions at the lower speed of 12.5 knots whilst the highest speed showed the greatest improvement. The irregular shaped pitch transfer function at 22.5 knots is again seen in figure 5.15(b) at the lighter displacement and is associated with the influence of the transom tab whose influence on the vessel caused the pitch motion solution to be unable to achieve a steady periodic solution within the allocated computation time.

The control gains selected for this solution were identical to those used for the devices when they were actively operated as independent surfaces. A table of these control gains was given in table 3.3 of chapter 3. These control gains were selected solely on the basis of minimising the average vertical acceleration over the hull length so the solution displayed by these transfer functions is the result of that procedure. This implies that the peak of the transfer function may not coincide with the frequency where the majority of the motion reduction is obtained but instead will be at the frequency of maximum average acceleration shown hereafter in the diagrams of figures 5.20 to 5.23. Whilst these results with both control surfaces active do show greater motion reduction due to the active control than for either surface in isolation, the active control feedback still has relatively modest effect and then only on the response at the higher speeds. At 42.5 knots the control feedback has reduced the heave transfer function maximum by 10% compared to the value with fixed surfaces and the pitch by about 5%. Active motion control is also seen to be more beneficial at the heavier loading condition.

5.4.6 Comparison of the Effect of Control Modes

It is clear from the transfer functions that the greatest influence of the control surfaces is obtained when active tabs are used in combination with the active T-foil whilst the effect of the T-foil alone exceeded the effect of the transom tab alone. This is a significant result as the force generated by the transom tab is greater than the T-foil as shown by figures in chapter 3 and leads to the conclusion that the location of the motion control surface may have a more significant effect on reducing motions than the force produced by the control surface. Further, it seems that the benefits of active feedback control on the motion control surfaces are relatively small. In general the control surfaces have very little effect in reducing motion at the lower vessel speeds. Overall the dominant contributory factor to motion reduction is the passive action of forward T-foils. No doubt this is due to the occurrence of the largest motions near the vessel bow and the location of the T-foil near that position. Moreover, it is clear from this outcome that the T-foil should not be mounted so close to the hull that its effect is reduced by shielding from relative motion of the hull and water. Finally, it should be stressed that in this section only the response amplitude has been considered. The beneficial effect of motion controls is more likely to be seen in the acceleration response to be discussed in the following sections. Also, the sea spectrum to which the vessel is exposed will have a significant influence in the assessment of motion control system effectiveness. It will be noted that for these computations the effectiveness of active feedback to the control surfaces is not very great in so far as the motion amplitudes are not greatly reduced by active control feedback. This is most likely due to the use of a relatively large wave height (2.5 metres) as the reference for computations. Under lower

wave height conditions larger control gains could be used without reaching the physical limit of control surface actuation and so the controls would be relatively more effective in reducing motion response functions. Operating in seas approaching the operational limit of 3 metres would present a considerable challenge to a motion control system with limited force capabilities.

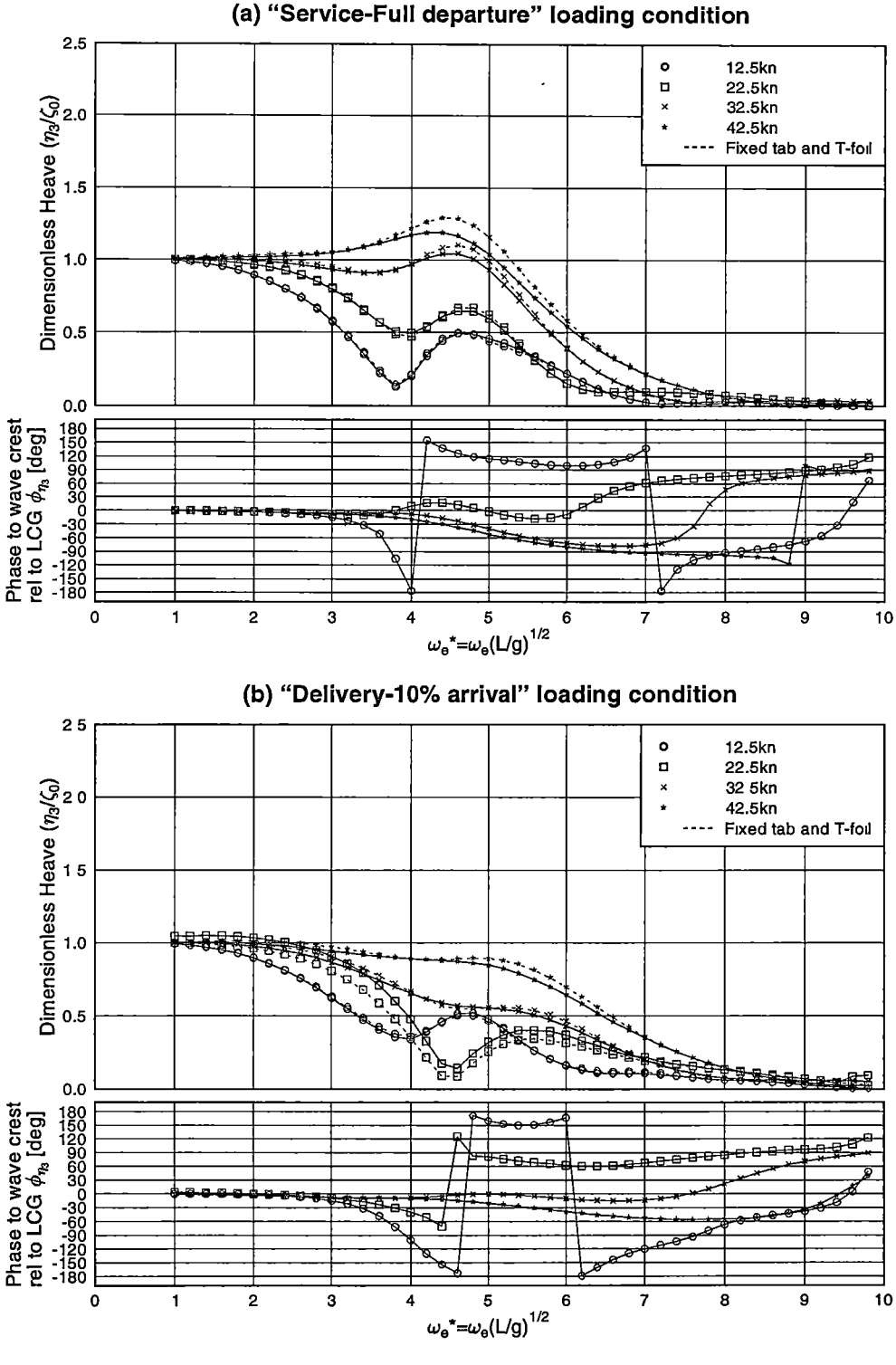

Figure 5.14: Predicted heave transfer functions (86m vessel, active tab and T-foil) at loading conditions of (a) "Service-full load departure" and (b) "Delivery-10% arrival" (Regular wave height of computation = 0.5m, Regular wave height of control surface maximum deflection = 2.5m, Control gains calculated with Bretschneider wave spectrum of $H_s = 2.5$m, $T_1 = 7$s)

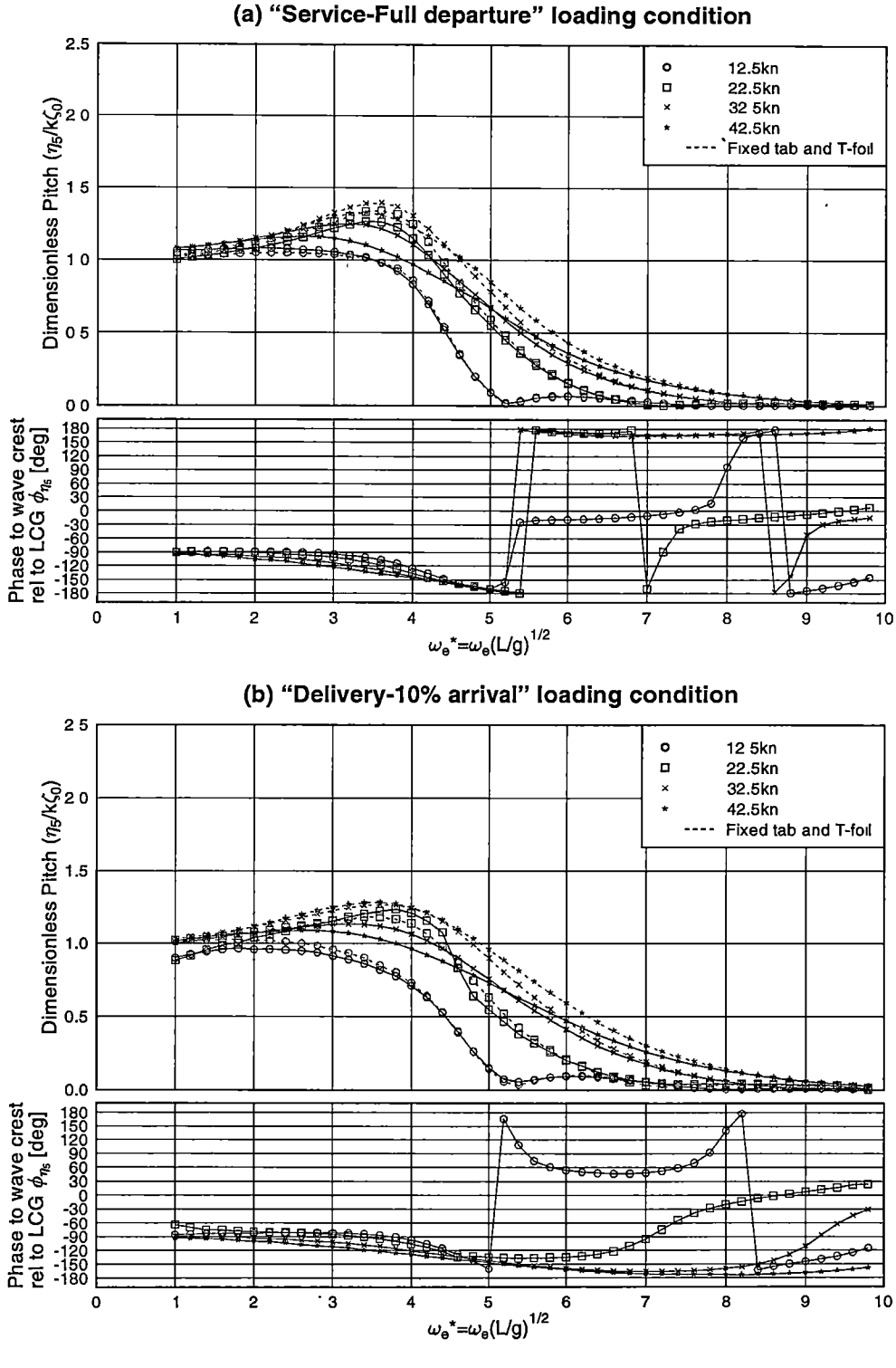

Figure 5.15: Predicted pitch transfer functions (86m vessel, active tab and T-foil) at loading conditions of (a) "Service-full load departure" and (b) "Delivery-10% arrival" (Regular wave height of computation = 0.5m, Regular wave height of control surface maximum deflection = 2.5m, Control gains calculated with Bretschneider wave spectrum of $H_s = 2.5$m, $T_1 = 7$s)

5.5 Vertical Accelerations

5.5.1 Effect of Position on Vessel on Vertical Acceleration Spectra

The vertical acceleration response spectra calculated for three longitudinal positions that include the aft perpendicular (AP), longitudinal centre of gravity (LCG) and forward perpendicular (FP) at two loading conditions are shown in figures 5.16 to 5.19. A variation in the shape of the response spectra between the AP, LCG and FP can be seen. Furthermore, the magnitude of the FP response values are much greater than the AP and considerably greater than the LCG, even with active controls operating, especially at low speed.

The response spectra at 12.5 and 22.5 knots have the notable distinction that the peak response of the AP and FP occur at a frequency that coincides with a reduction in heave response at the LCG, which indicates that at this frequency the local deck motions are predominantly due to the pitching motion. At these low speeds the heaving motion is not large as discussed in the previous section in terms of the motion transfer functions. At these two lowest speeds there is little effect of the motion controls on the motions, although the effect is greater at 22.5 knots than at 12.5 knots and there is little reduction of motion unless a forward T-foil is fitted.

The response at 22.5 knots for the "delivery - 10% arrival" loading condition (see figure 5.17) presented an irregular behaviour that was distinctively different to the results at the service loading condition or other speeds. The nature of this result shows that for frequencies lower than the selected frequency for calculating the gains (i.e. $\omega_e^* = 4.6$, see figure 5.21) for the active tab, fixed foil and active tab and active foil configurations, the gain selection was tending to increase the acceleration response at the AP and FP (see figure 5.21(b)). This suggests the problem was mainly due to the pitch excitation rather than heave, an assumption that was confirmed by the transfer functions of figures 5.10 and 5.11. It should be noted that the heave and pitch motions tend to be at 90° relative phasing and therefore adverse coupling can be induced, even through a damping algorithm based on heave and pitch velocities. The effect is present when the controls are made active and an increased pitch motion results due to coupling from the heave at lower frequencies. It is evident that making the motion controls active is not always beneficial at all positions.

These acceleration spectra also confirm that the effectiveness of the control surfaces increase with speed. It can also be seen that from acceleration spectra at the lower speeds of 12.5 and 22.5 knots, the LCG has two modes of excitation whereas the AP and FP generally only have one and at the frequency where the AP and FP are experiencing the greatest excitation the LCG has a reduced motion. However, as the speed increases the two modes seen at the lower speeds disappear and the shape of the spectra at the three positions start to contain similar characteristics that are predominately of one excitation mode. At higher speeds, it can be seen that the frequency of the resonant peaks coincide with the greatest response of the heave transfer functions together with their relative phases, rather than at the frequency where the greatest energy in the wave spectra is located. This would be expected for a resonant dynamic system, which effectively acts to filter and amplify the input spectrum.

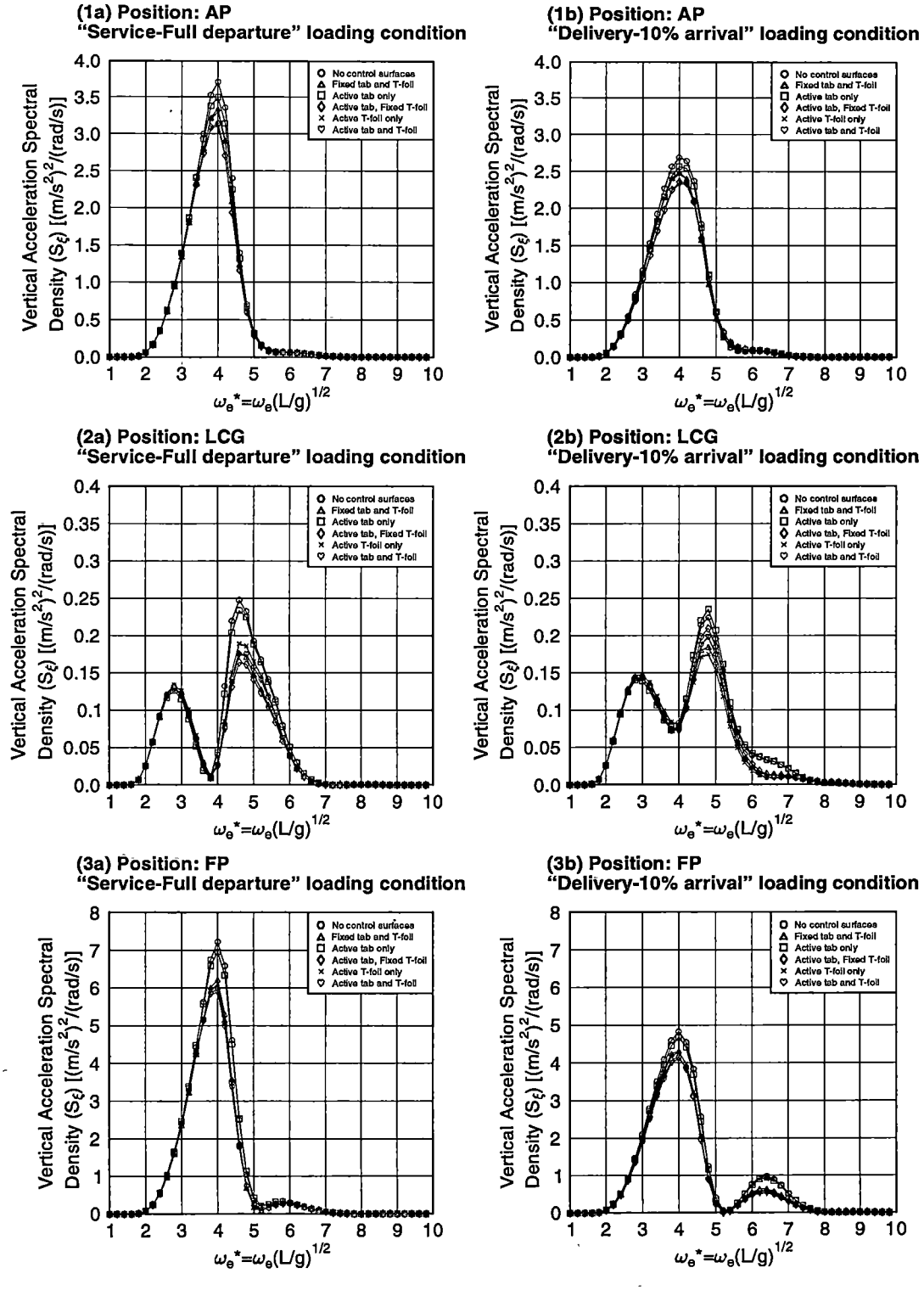

Figure 5.16: Predicted acceleration response spectral density (86m vessel, 12.5kn) at (1) aft perpendicular (AP), (2) longitudinal centre of gravity (LCG), (3) forward perpendicular (FP), for loading conditions of (a) "Service-full departure" and (b) "Delivery-10% arrival" (Regular wave height of computation = 0.5m, Regular wave height of control surface maximum deflection = 2.5m, Control gains calculated with Bretschneider wave spectrum of H_s = 2.5m, T_1 = 7s)

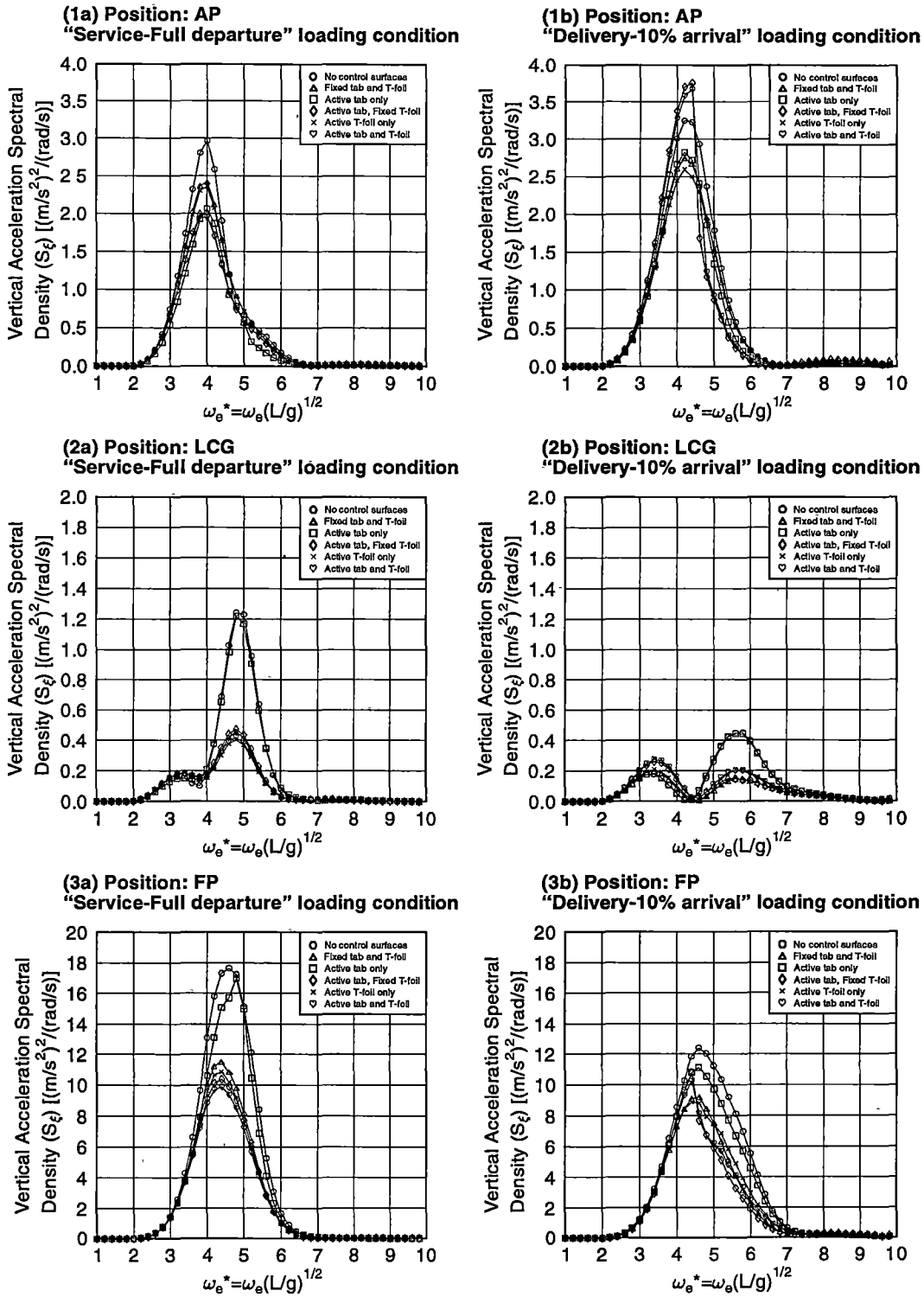

Figure 5.17: Predicted acceleration response spectral density (86m vessel, 22.5kn) at (1) aft perpendicular (AP), (2) longitudinal centre of gravity (LCG), (3) forward perpendicular (FP), for loading conditions of (a) "Service-full departure" and (b) "Delivery-10% arrival" (Regular wave height of computation = 0.5m, Regular wave height of control surface maximum deflection = 2.5m, Control gains calculated with Bretschneider wave spectrum of H_s = 2.5m, T_1 = 7s)

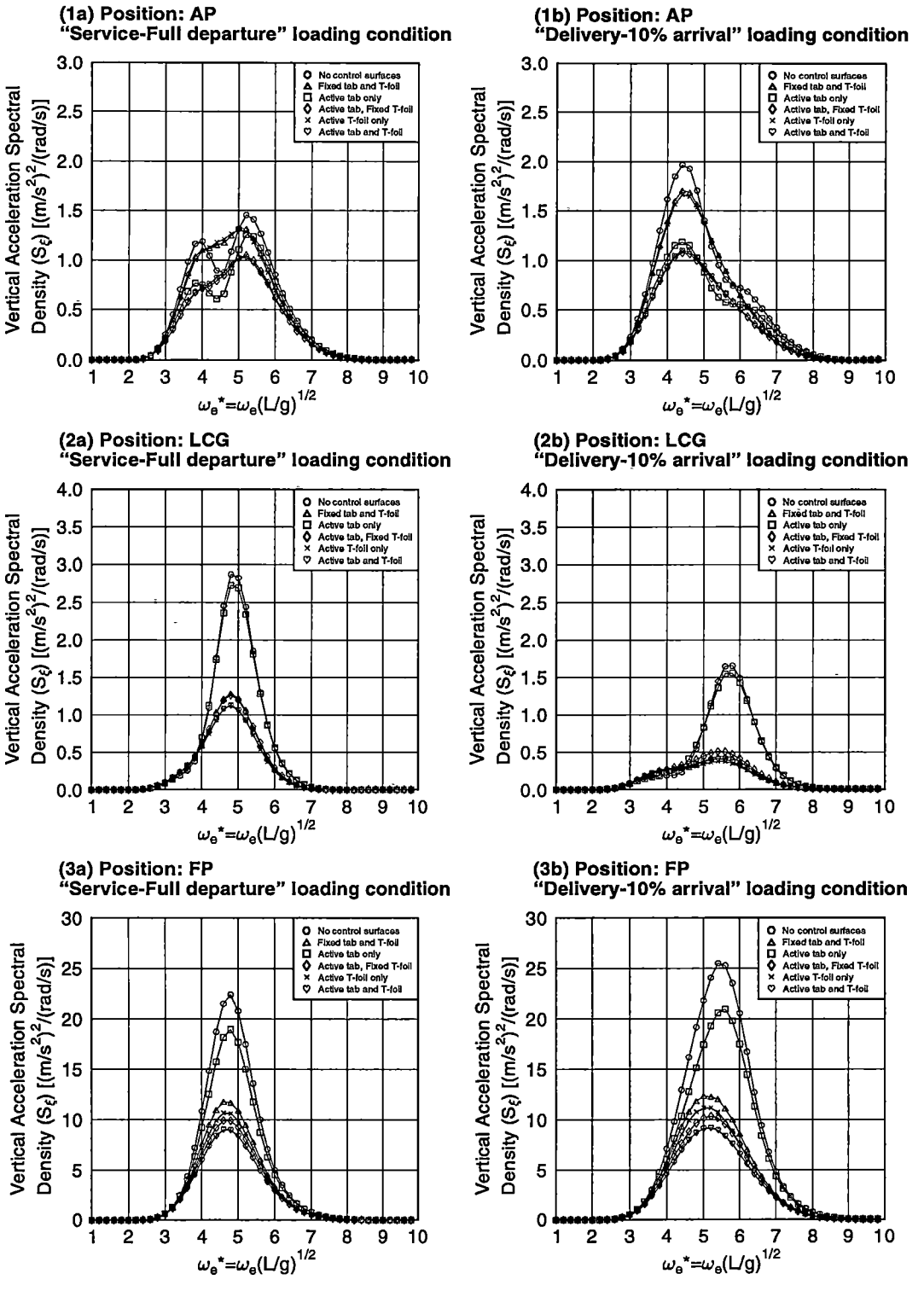

Figure 5.18: Predicted acceleration response spectral density (86m vessel, 32.5kn) at (1) aft perpendicular (AP), (2) longitudinal centre of gravity (LCG), (3) forward perpendicular (FP), for loading conditions of (a) "Service-full departure" and (b) "Delivery-10% arrival" (Regular wave height of computation = 0.5m, Regular wave height of control surface maximum deflection = 2.5m, Control gains calculated with Bretschneider wave spectrum of H_s = 2.5m, T_1 = 7s)

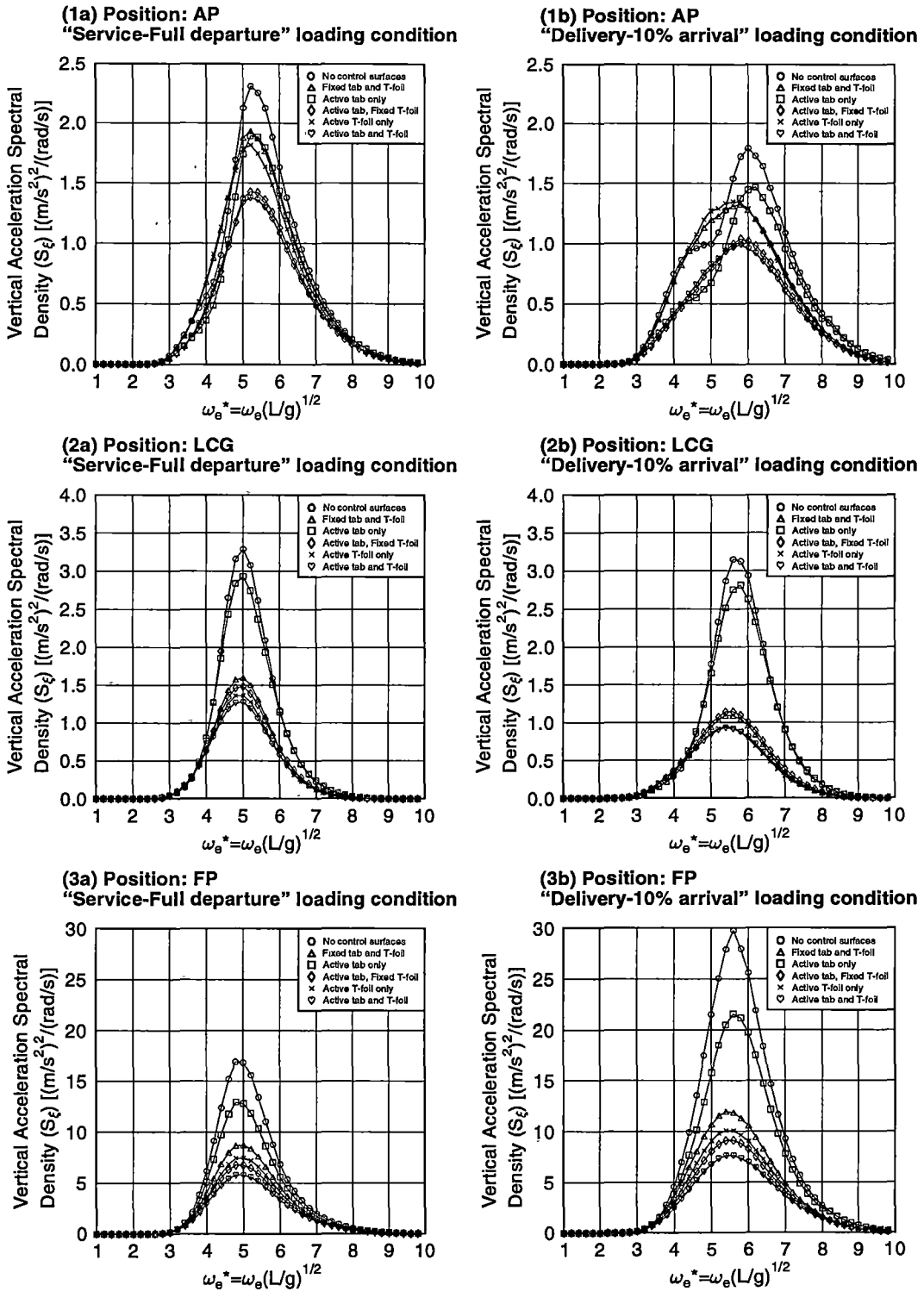

Figure 5.19: Predicted acceleration response spectral density (86m vessel, 42.5kn) at (1) aft perpendicular (AP), (2) longitudinal centre of gravity (LCG), (3) forward perpendicular (FP), for loading conditions of (a) "Service-full departure" and (b) "Delivery-10% arrival" (Regular wave height of computation = 0.5m, Regular wave height of control surface maximum deflection = 2.5m, Control gains calculated with Bretschneider wave spectrum of H_s = 2.5m, T_1 = 7s)

5.5.2 Effect of Speed on Average Acceleration Spectra

By implementing the procedure for selection of the appropriate control gains from section 3.4.7 of chapter 3, the average vertical acceleration response spectra in figures 5.20 to 5.23 for the 12.5, 22.5, 32.5 and 42.5 knots forward speeds were obtained. In these results the values at those positions along the vessel discussed in the previous section have been averaged so as to give a clearer comparison of the effect of control on the responses at different speeds and vessel loadings. All these figures generally show an improvement in the vertical acceleration as the various control surface configurations were implemented. A greater effect was obtained at the higher speeds, whilst at the lowest speed of 12.5 knots the improvement was only small. This is clearly due to the larger force the control surface is able to produce at the higher forward speeds. A greater improvement appeared to be obtained with the control surfaces when the vessel was in the lighter "delivery - 10% arrival" loading condition for which rather large average motions occurred without motion control surfaces (figure 5.23(b)). The uncontrolled hull had a larger spectral response magnitude in all cases.

These results show the effect of the control surfaces arising from the motion criterion used as the basis for selecting the gains as discussed previously in chapter 3. It is the frequency of the peak of these average spectra that was used as the basis for determining the gains for the motion control configuration based on the previously obtained solution. For example, the gains for the active tab configuration was based on the magnitude of the average acceleration obtained for the hull without control surfaces. This is consistent with the sequence set out in table 3.2 and the method described in section 3.4.7 to which the reader is directed for a full explanation, together with the gains selected that gave the results shown in this chapter. The averaged results show a useful although moderate benefit of using active tab (about 25% reduction at 42.5 knots when lightly loaded) and the strong effect of introducing fixed foils (62% reduction at 42.5 knots when lightly loaded). Overall the motion control system when fully active reduced motions by 74% when lightly loaded and by 64% when heavily loaded. A clearer view of the overall benefit of fitting motion control systems optimised according to the procedure of chapter 3 is thus obtained through these results where the average vertical accelerations on the vessel are used.

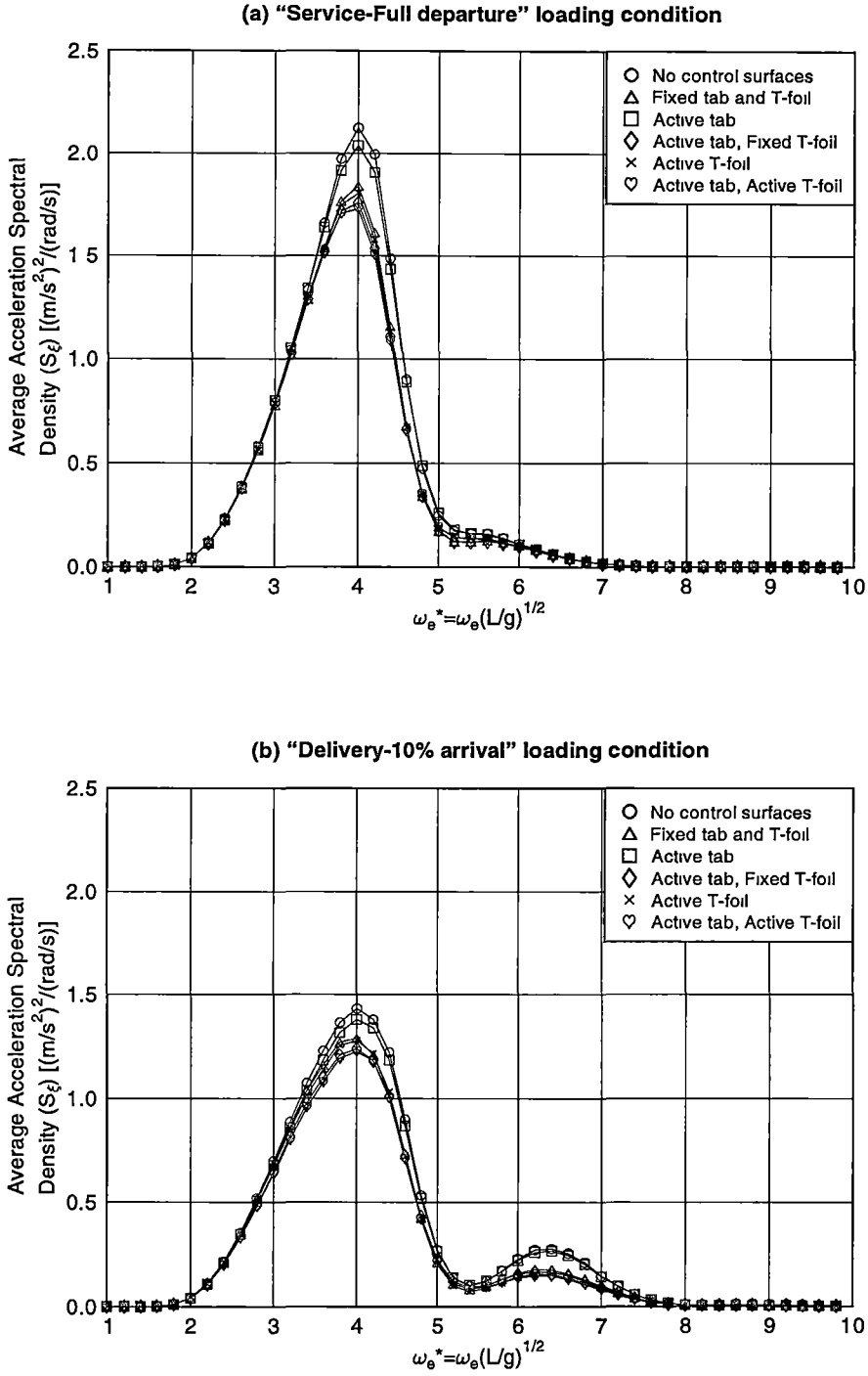

Figure 5.20: Predicted acceleration response spectral density (86m vessel, 12.5 knots, average between positions on vessel) for various motion control configurations and loading conditions of (a) "Service-full departure" and (b) "Delivery-10% arrival" (Regular wave height of computation = 0.5m, Regular wave height of control surface maximum deflection = 2.5m, Control gains calculated with Bretschneider wave spectrum of H_s = 2.5m, T_1 = 7s)

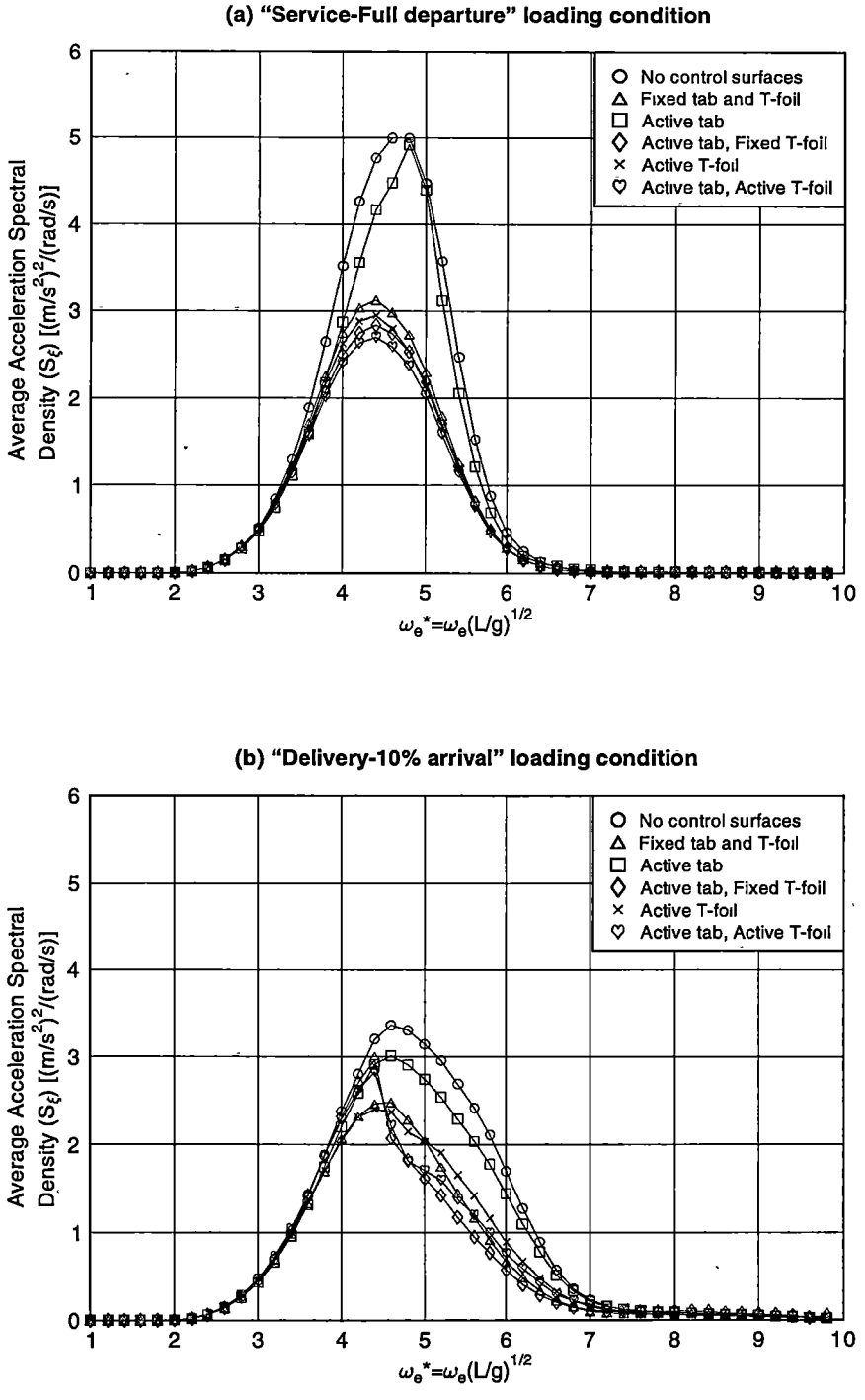

Figure 5.21: Predicted acceleration response spectral density (86m vessel, 22.5 knots, average between positions on vessel) for various motion control configurations and loading conditions of (a) "Service-full departure" and (b) "Delivery-10% arrival" (Regular wave height of computation = 0.5m, Regular wave height of control surface maximum deflection = 2.5m, Control gains calculated with Bretschneider wave spectrum of H_s = 2.5m, T_1 = 7s)

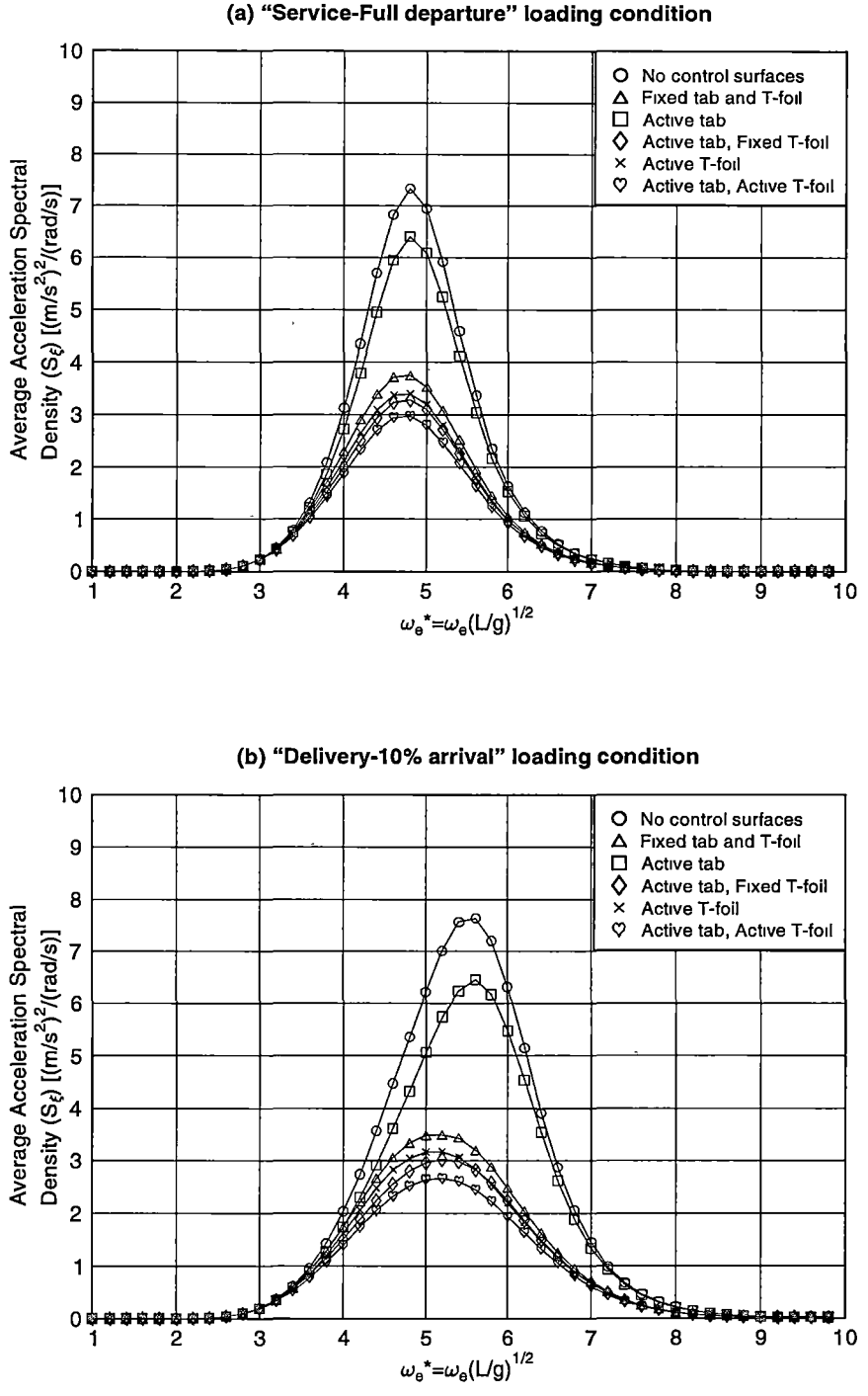

Figure 5.22: Predicted acceleration response spectral density (86m vessel, 32.5 knots, average between positions on vessel) for various motion control configurations and loading conditions of (a) "Service-full departure" and (b) "Delivery-10% arrival" (Regular wave height of computation = 0.5m, Regular wave height of control surface maximum deflection = 2.5m, Control gains calculated with Bretschneider wave spectrum of $H_s = 2.5$m, $T_1 = 7$s)

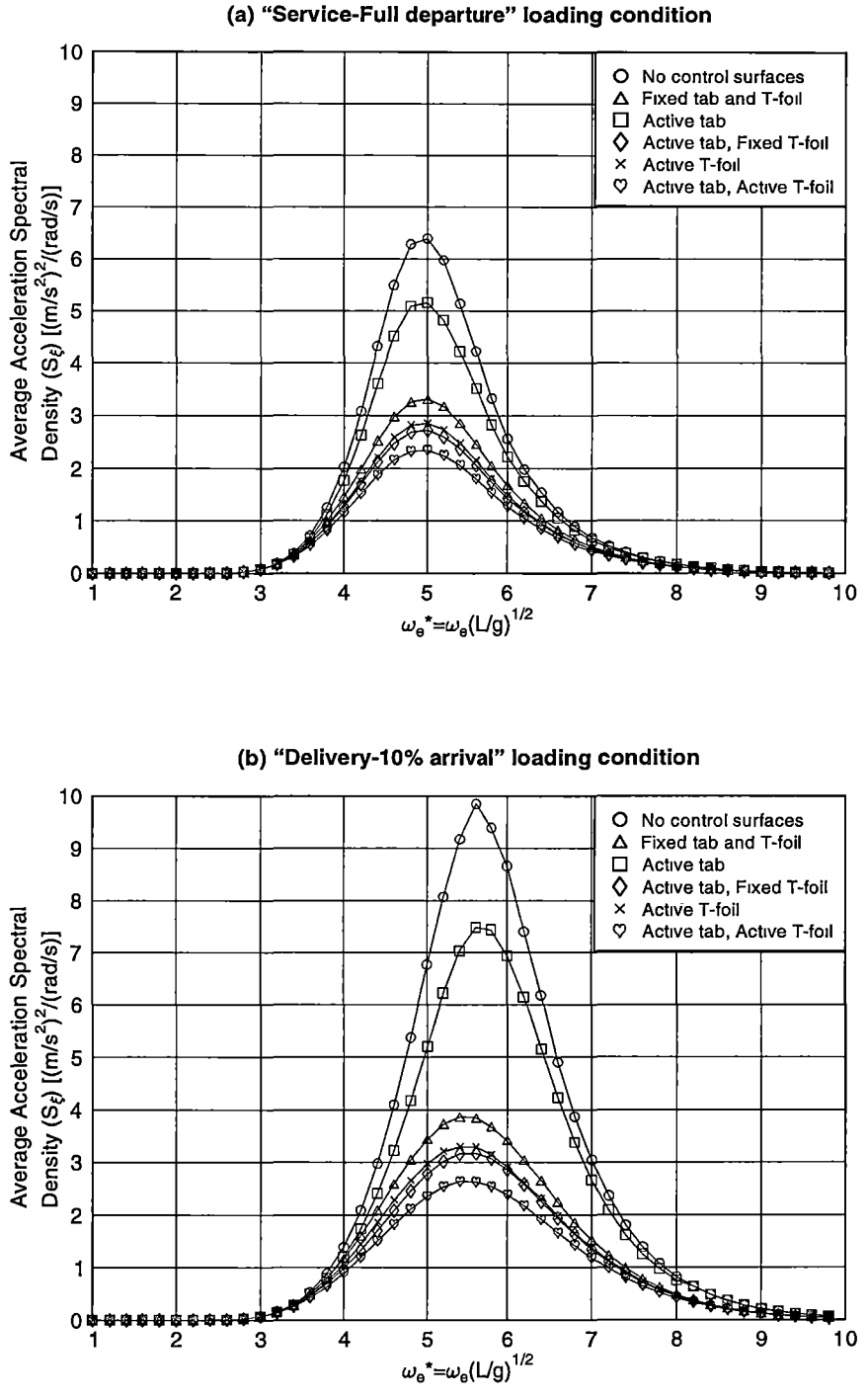

Figure 5.23: Predicted acceleration response spectral density (86m vessel, 42.5 knots, average between positions on vessel) for various motion control configurations and loading conditions of (a) "Service-full departure" and (b) "Delivery-10% arrival" (Regular wave height of computation = 0.5m, Regular wave height of control surface maximum deflection = 2.5m, Control gains calculated with Bretschneider wave spectrum of $H_s = 2.5$m, $T_1 = 7$s)

5.5.3 Effect of Speed on Acceleration Relative to Wave Height

From the acceleration spectra presented in the previous sections the root mean square (RMS) acceleration can be determined by integration of the spectra to obtain the RMS magnitude of acceleration based on the irregular wave Bretschneider spectrum. This was defined for these results with a significant wave height of 2.5 metres and an average period of 7 seconds. The observations made previously about the effectiveness of each control surface configuration is encapsulated by the results in the summary tables 5.1 and 5.2. These show the RMS acceleration for the positions of AP, LCG and FP corresponding to the spectra shown in figures 5.16 to 5.19 as well as the RMS acceleration based on the average spectra of figures 5.20 to 5.23. These results also confirm that the most effective control surface configuration is the active tab and T-foil combination as expected, with up to 32% improvement at 42.5 knots compared to the hull without control surfaces (bare hull) in the heavier loading condition ("service - full departure") and up to 40% improvement at 42.5 knots in the lighter loading condition ("delivery - 10% arrival"). The second best improvement was almost equal between using an active tab with fixed T-foil and the active T-foil only configurations. These were followed by the fixed (passive) control surface configuration (up to 22% and 30% improvement for the respective loading conditions) and then the active tab only configuration, which gave only a small improvement of up to 9% on the bare hull response.

These results have also been presented in figure 5.24 by plotting the vertical acceleration per unit wave height against the vessel speed. It can be seen that in some instances the acceleration at the forward perpendicular increases moderately as the speed decreases until the speed drops below 22.5 knots where it then decreases rapidly. Similarly, the acceleration at the aft perpendicular increases as the speed drops below 32.5 knots and continues to increase down to 12.5 knots. However, at the LCG position, the acceleration reduces moderately with speed. It is clearly evident in this figure also that the greatest reduction in vertical acceleration occurs at the highest speed where the difference between the solution with control surfaces and the solution without control surfaces is the greatest.

The two diagrams presented in figure 5.24 are at the heavy and light displacements. The characteristics of these vertical acceleration curves do vary to some extent between each other but it apparent that the heavier displacement generally has lower accelerations, which may have more to do with the larger radius of gyration than the extra mass involved. The trends at forward, LCG and aft positions indicate that whilst the relative acceleration increases steadily with speed at the centre of gravity, at the aft position lower speeds give rise to increased motion. From this it can be seen that the low speed motions are characterised by more severe pitching, whilst at high speed the combined effects of heaving and pitching to some extent reduce the aft motions as the heave (reflected in the motion at the LCG directly) increases. Figure 5.24 shows very clearly the increasing effectiveness of motion controls as the vessel speed increases.

		Service-Full departure condition							
Hull Configuration	Speed [kn]	Average acceleration [g/m RMS]	Reduction compared without control surfaces	AP [g/m RMS]	Reduction compared without control surfaces	LCG [g/m RMS]	Reduction compared without control surfaces	FP [g/m RMS]	Reduction compared without control surfaces
Without control surfaces	42.5	0.32	-	0.22	-	0.23	-	0.56	-
	37.5	0.31	-	0.21	-	0.22	-	0.59	-
	32.5	0.30	-	0.19	-	0.20	-	0.60	-
	27.5	0.28	-	0.19	-	0.17	-	0.59	-
	22.5	0.25	-	0.20	-	0.12	-	0.54	-
	17.5	0.20	-	0.23	-	0.08	-	0.43	-
	12.5	0.16	-	0.23	-	0.07	-	0.31	-
Fixed tab, fixed T-foil	42.5	0.25	22%	0.21	4%	0.17	25%	0.43	23%
	37.5	0.25	22%	0.20	3%	0.16	26%	0.45	23%
	32.5	0.24	22%	0.18	3%	0.15	27%	0.47	22%
	27.5	0.22	21%	0.18	3%	0.12	28%	0.47	21%
	22.5	0.20	19%	0.19	5%	0.09	29%	0.44	19%
	17.5	0.18	13%	0.22	5%	0.06	21%	0.38	13%
	12.5	0.15	7%	0.22	4%	0.06	9%	0.29	7%
Active tab	42.5	0.29	7%	0.20	9%	0.22	3%	0.50	11%
	32.5	0.29	5%	0.17	11%	0.20	1%	0.56	7%
	22.5	0.23	6%	0.17	16%	0.12	2%	0.51	6%
	12.5	0.16	1%	0.22	2%	0.07	1%	0.31	1%
Active T-foil	42.5	0.23	26%	0.21	6%	0.16	29%	0.41	28%
	32.5	0.23	25%	0.18	4%	0.14	30%	0.45	25%
	22.5	0.20	21%	0.19	6%	0.09	31%	0.43	21%
	12.5	0.15	6%	0.22	4%	0.06	7%	0.29	7%
Active tab, fixed T-foil	42.5	0.23	27%	0.19	17%	0.17	26%	0.39	30%
	32.5	0.23	26%	0.16	15%	0.15	26%	0.44	28%
	22.5	0.20	21%	0.18	13%	0.09	28%	0.43	22%
	12.5	0.15	8%	0.21	6%	0.06	12%	0.29	7%
Active tab, active T-foil	42.5	0.22	31%	0.18	17%	0.16	31%	0.37	35%
	32.5	0.22	29%	0.16	15%	0.14	29%	0.42	30%
	22.5	0.19	23%	0.18	13%	0.09	31%	0.42	23%
	12.5	0.15	8%	0.21	6%	0.06	9%	0.29	7%

C:\1Nigel\bs\042\report_results\Motion control reduction summary (042bs_RMSAccel-std).xls

Table 5.1: Acceleration per metre wave height (RMS) (86m vessel) (Regular wave height of computation = 0.5m, Regular wave height of control surface maximum deflection = 2.5m, Control gains calculated with Bretschneider wave spectrum of H_s = 2.5m, T_1 = 7s, Loading condition: "Service-full departure")

		Delivery-10% arrival condition							
Hull Configuration	Speed [kn]	Average acceleration [g/m RMS]	Reduction compared without control surfaces	AP [g/m RMS]	Reduction compared without control surfaces	LCG [g/m RMS]	Reduction compared without control surfaces	FP [g/m RMS]	Reduction compared without control surfaces
Without control surfaces	42.5	0.40	-	0.22	-	0.24	-	0.79	-
	37.5	0.38	-	0.21	-	0.21	-	0.77	-
	32.5	0.34	-	0.20	-	0.17	-	0.73	-
	27.5	0.29	-	0.22	-	0.12	-	0.64	-
	22.5	0.24	-	0.23	-	0.10	-	0.51	-
	17.5	0.19	-	0.24	-	0.09	-	0.39	-
	12.5	0.15	-	0.21	-	0.07	-	0.29	-
Fixed tab and T-foil	42.5	0.28	30%	0.20	9%	0.16	33%	0.55	30%
	37.5	0.27	29%	0.19	6%	0.14	34%	0.55	28%
	32.5	0.25	27%	0.19	5%	0.11	35%	0.54	26%
	27.5	0.22	23%	0.20	6%	0.08	33%	0.49	23%
	22.5	0.20	18%	0.22	6%	0.07	26%	0.42	18%
	17.5	0.17	10%	0.23	5%	0.07	14%	0.35	10%
	12.5	0.14	7%	0.21	3%	0.07	6%	0.27	7%
Active tab	42.5	0.36	9%	0.20	11%	0.23	3%	0.69	12%
	32.5	0.32	7%	0.17	18%	0.17	1%	0.67	8%
	22.5	0.23	5%	0.21	9%	0.10	0%	0.48	6%
	12.5	0.15	1%	0.21	1%	0.07	0%	0.29	2%
Active T-foil	42.5	0.27	34%	0.20	9%	0.15	37%	0.52	34%
	32.5	0.24	30%	0.19	6%	0.10	38%	0.51	30%
	22.5	0.20	16%	0.21	9%	0.08	19%	0.43	16%
	12.5	0.14	8%	0.20	4%	0.07	8%	0.27	8%
Active tab, fixed T-foil	42.5	0.26	34%	0.18	21%	0.17	32%	0.49	37%
	32.5	0.23	31%	0.16	21%	0.11	32%	0.50	32%
	22.5	0.20	18%	0.22	5%	0.08	18%	0.41	20%
	12.5	0.14	8%	0.20	5%	0.07	4%	0.27	9%
Active tab and T-foil	42.5	0.24	39%	0.17	22%	0.15	37%	0.46	42%
	32.5	0.22	35%	0.16	21%	0.11	37%	0.47	35%
	22.5	0.20	15%	0.22	4%	0.09	13%	0.42	18%
	12.5	0.14	9%	0.20	5%	0.07	7%	0.26	10%

C:\1Nigel\bs\042\report_results\Motion control reduction summary (042bs_RMSAccel-std).xls

Table 5.2: Acceleration per metre wave height (RMS) (86m vessel) (Regular wave height of computation = 0.5m, Regular wave height of control surface maximum deflection = 2.5m, Control gains calculated with Bretschneider wave spectrum of H_s = 2.5m, T_1 = 7s, Loading condition: "Delivery-10% arrival")

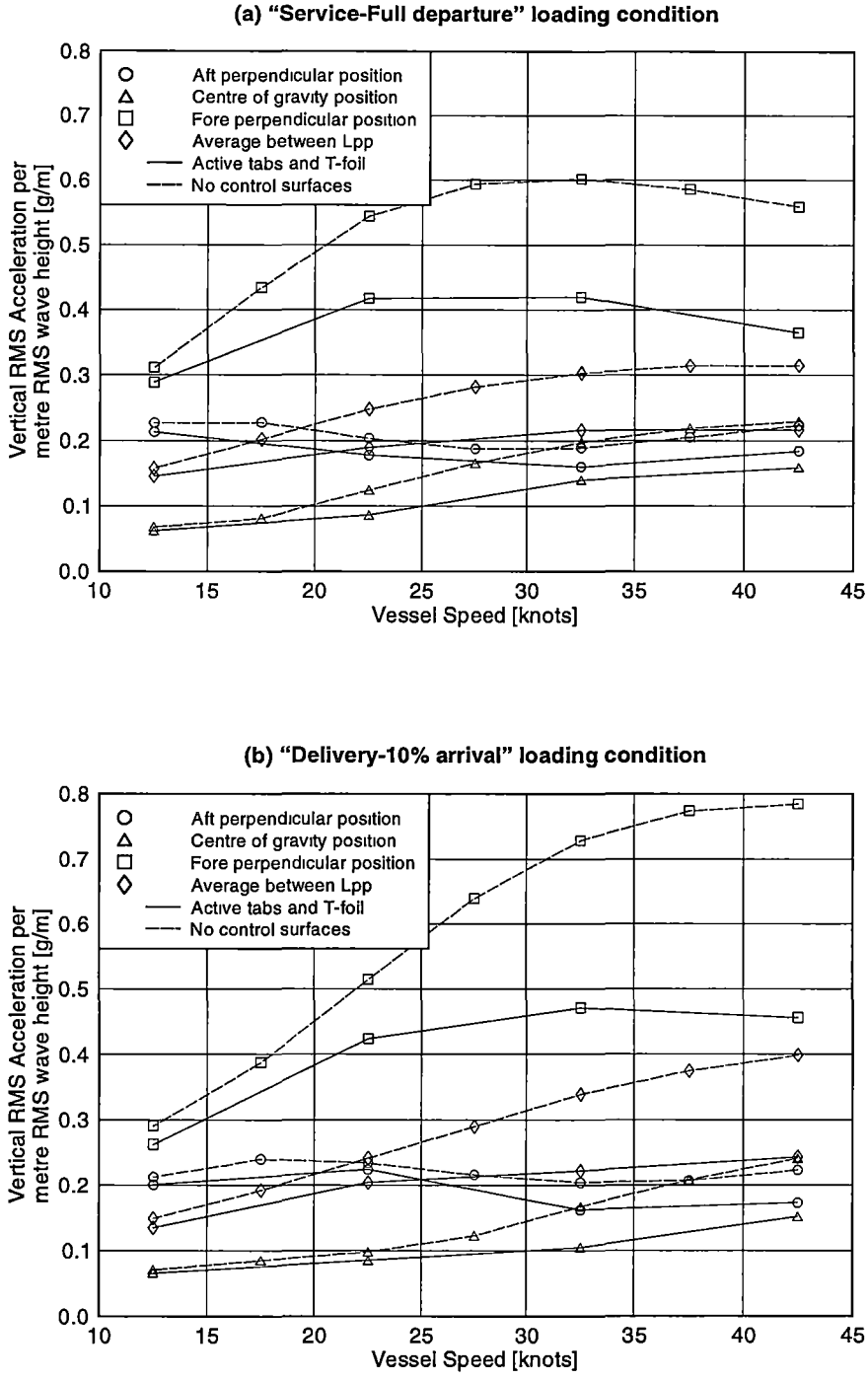

Figure 5.24: Predicted vertical RMS acceleration per metre RMS wave height (86m vessel) for various speeds at the aft perpendicular (AP), longitudinal centre of gravity (LCG), forward perpendicular (FP), for loading conditions of (a) "Service-full departure" and (b) "Delivery-10% arrival" (Regular wave height of computation = 0.5m, Regular wave height of control surface full deflection = 2.5m, Control gains calculated with Bretschneider wave spectrum of $H_s = 2.5$m, $T_1 = 7$s)

5.5.4 Effect of Wave Period on Accelerations

In chapter 3 a method to determine suitable control gains was outlined, which relied on the selection of a motion criterion. Against this criterion suitable gains were selected that minimised the average acceleration over the longitudinal extent of the hull between perpendiculars where the acceleration was averaged between five equi-distant positions in addition to the plane of the LCG. Whilst this criterion was equally suited for application with any wave height and period, only one wave height and period is presented in the analysis of previous sections to place a practical limit on the number of computations required. However, when there are no active control surfaces modelled and linearity with wave height is assumed, then only one transfer function is required to calculate the vertical acceleration response of the 86 metre vessel for a range of wave periods. Alternatively if there are active controls to be considered then the procedure presented for selecting the gains is based on a unique wave height and period. Thus to calculate the root mean square (RMS) acceleration response for a range of wave periods requires the gains to be determined at each variation of wave height and period. Although this may be entirely practical, only one wave height and period was solved in this analysis for cases with active controls at four speeds from 12.5 to 42.5 knots. Therefore, the results in figure 5.25 show the RMS vertical acceleration of the hull without control surfaces and with active tabs. The solution without control surfaces is valid for all periods displayed. However, although the solution with active tabs is also shown for a range of wave periods, the gains were only solved at the 7 second period and so the results at all other periods are based on gains that were not ideally suited for that period. The results in figure 5.26 show the RMS vertical acceleration of the hull with fixed control surfaces and with active tabs and T-foils. The solution without control surfaces is valid for all periods displayed. Once again, the solution with active tabs and T-foils is shown for a range of periods, although the gains were only solved at the 7 second period and so the results at all other periods are based on gains that were not ideally suited for that period. This implies that the result could be improved at the other periods if appropriate gains were selected for each of those periods.

The diagrams presented in figures 5.25 and 5.26 show that for both control surface configurations there is a maximum vertical acceleration response at approximately 7 seconds average wave period at the higher speeds. As the speed reduces the period of maximum response also decreased. This would be expected as the maximum response corresponds with the frequency of maximum excitation as the speed reduces and therefore so also will the resonant period.

It is immediately obvious from these results that the motions in the bow are significantly greater than at the LCG and transom. This is not unexpected as most conventional hull forms display this phenomenon and has been evident in the discussion of the preceding sections. The results without control surfaces in figure 5.25 show that as the speed of the vessel decreases the bow accelerations decrease the most out of the three positions. Also, for wave periods around 9 seconds in the heavier loading condition (see 3a) there is an increase in motions as the speed decreases down to about 22.5 knots before the motions also start to decrease. At even lower periods a reduction in speed will actually increase the accelerations (see figure 5.25(3a)). For example, in a 5 second wave period the acceleration per unit wave height will increase from 0.25g/m to 0.35g/m if the speed is reduced from 42.5 knots to 32.5 knots. Furthermore, for wave periods less than 8 seconds, motions at the transom (AP) also increase as speed is reduced down to 12.5 knots (see figure 5.25(1a)). The motions at the LCG decrease with speed for all wave periods. These characteristics are not as prominent when the vessel displacement is lighter as shown in the corresponding diagrams on the right side

(see figure 5.25(1b), (2b) and (3b)).

The results of figures 5.25 and 5.26 emphasise the importance of wave period, which has a very strong effect on the vessel motion. It is evident that a period of 6 to 7 seconds gives the maximum motion. This corresponds closely with the estimates made of the most likely wave period for the vessel to encounter in service, which was the basis of the computations in preceding sections. However, it should be noted that the operational measurements reported on the Channel Island route and on delivery voyages almost always showed significantly longer wave periods for which the motion response would not be as great. Thus it can be seen that the selection of wave period for the purpose of predicting motions on a particular service route is a critical issue.

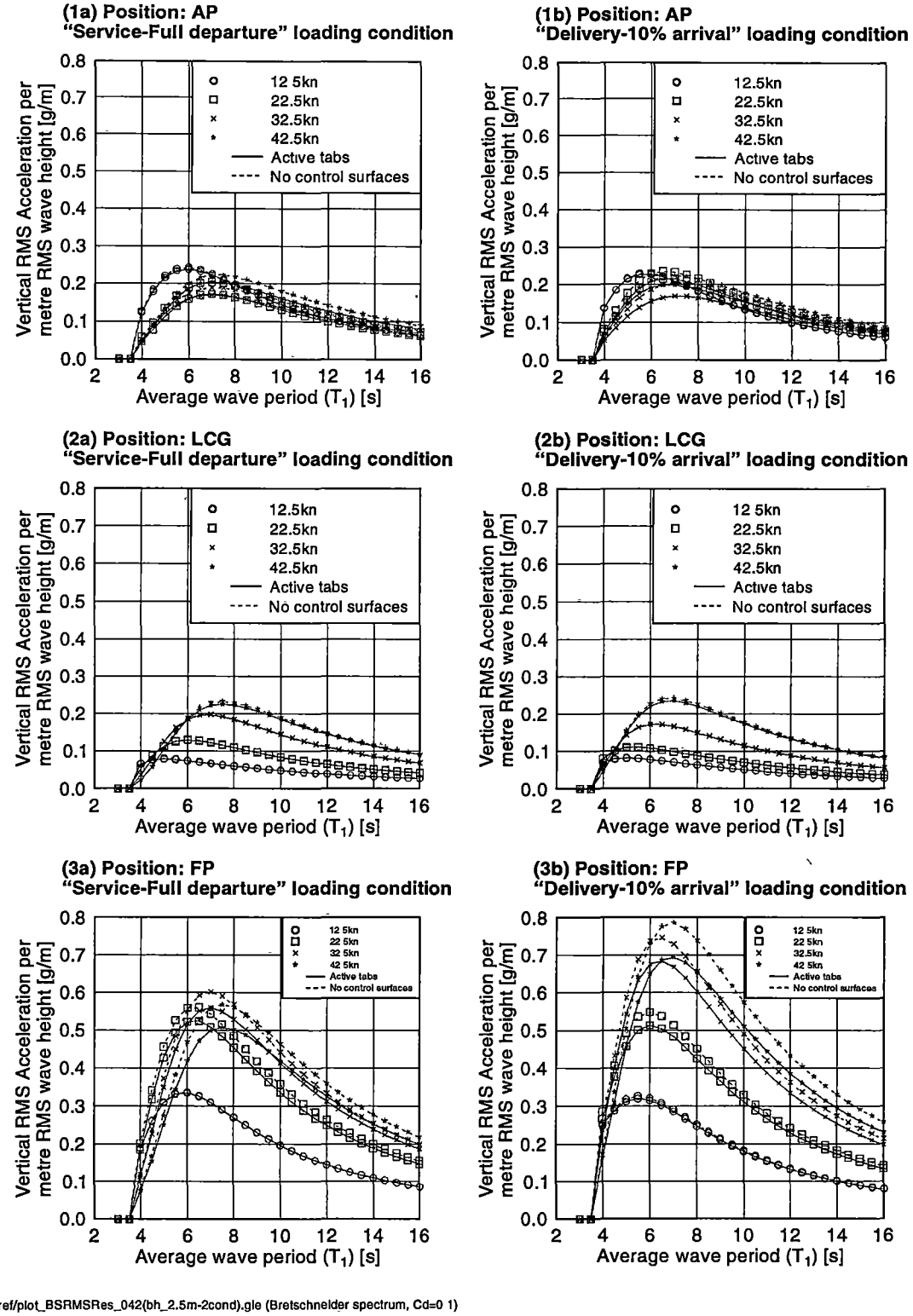

Figure 5.25: Predicted vertical acceleration (86m vessel, without control surfaces) at (1) aft perpendicular (AP), (2) longitudinal centre of gravity (LCG), (3) forward perpendicular (FP), for loading conditions of (a) "Service-full departure" and (b) "Delivery-10% arrival" (Regular wave height of computation = 0.5m, Bretschneider wave spectrum of $H_s = 2.5$m)

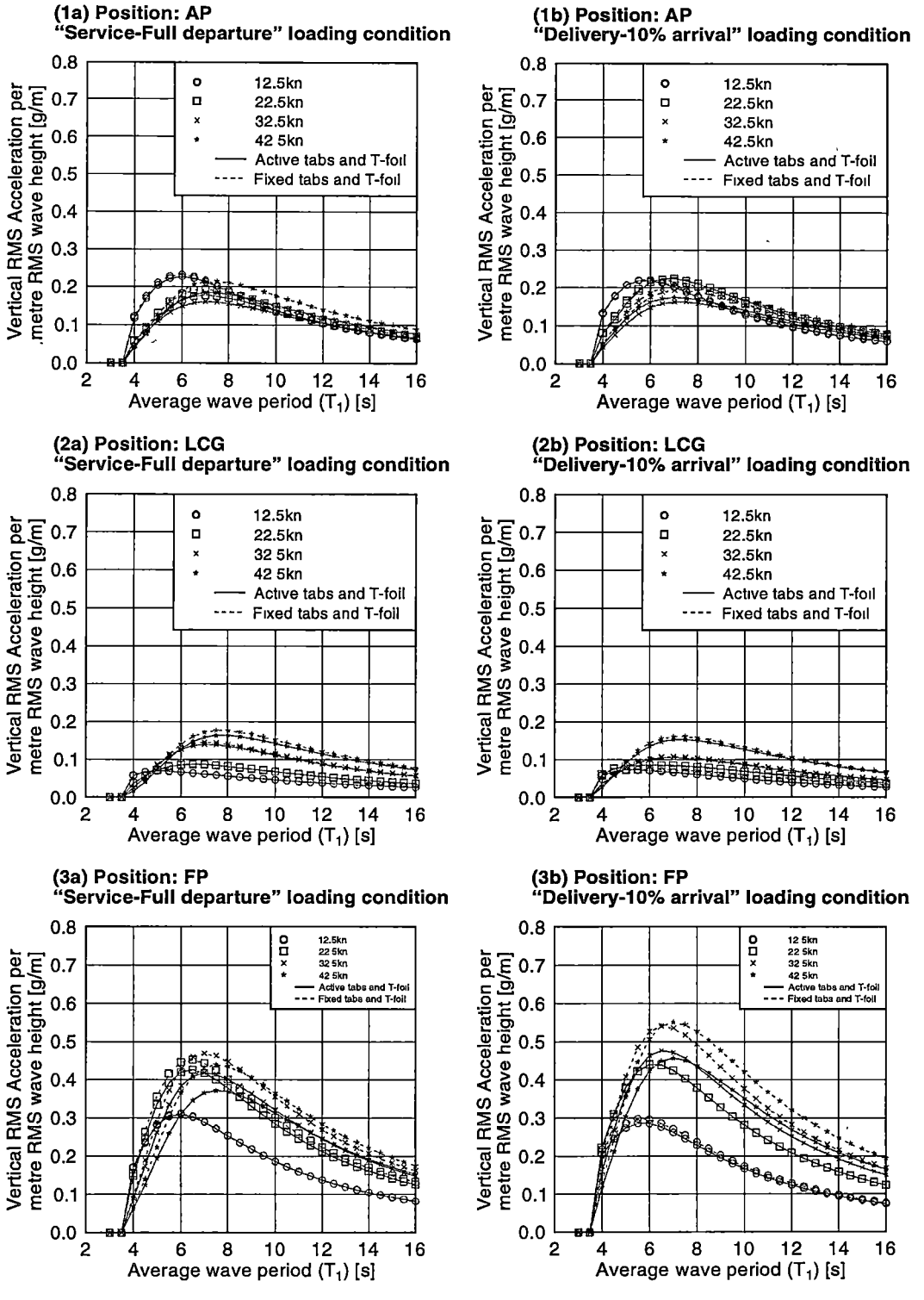

Figure 5.26: Predicted vertical acceleration (RMS) (86m vessel, fixed tab and T-foil) at (1) aft perpendicular (AP), (2) longitudinal centre of gravity (LCG), (3) forward perpendicular (FP), for loading conditions of (a) "Service-full departure" and (b) "Delivery-10% arrival" (Regular wave height of computation = 0.5m, Bretschneider wave spectrum of $H_s = 2.5$m)

5.5.5 Effect of Position and Controls on Acceleration Relative to Wave Height

The longitudinal distribution of RMS acceleration determined at the six vessel positions are shown in figure 5.27 for a variety of motion control configurations and speeds. These results are computed for the standard wave period of 7 seconds and a 2.5 metre significant wave height, which is considered to be the most severe condition based on the results of the previous figures 5.25 and 5.26. It can be seen that positions near the longitudinal centre of gravity (LCG) present the lowest acceleration at any speed, whilst the bow consistently has the highest. However, the greatest improvement with active control surfaces is always at the bow, which achieved a minimum acceleration of approximately 0.25g/m at 12.5 knots whilst much smaller improvements are made at the LCG position, which achieved a minimum acceleration of approximately 0.06g/m also at 12.5 knots. Relative accelerations at the bow lie in the range 0.25 to 0.8g/m, those at the LCG in the range 0.06 to 0.19g/m and at the stern in the range 0.14 to 0.23g/m. Relative acceleration is a parameter often used in design practice as an overall indicator of seakeeping behaviour, but it is based on the pre-supposition of linear response and should therefore be interpreted with caution.

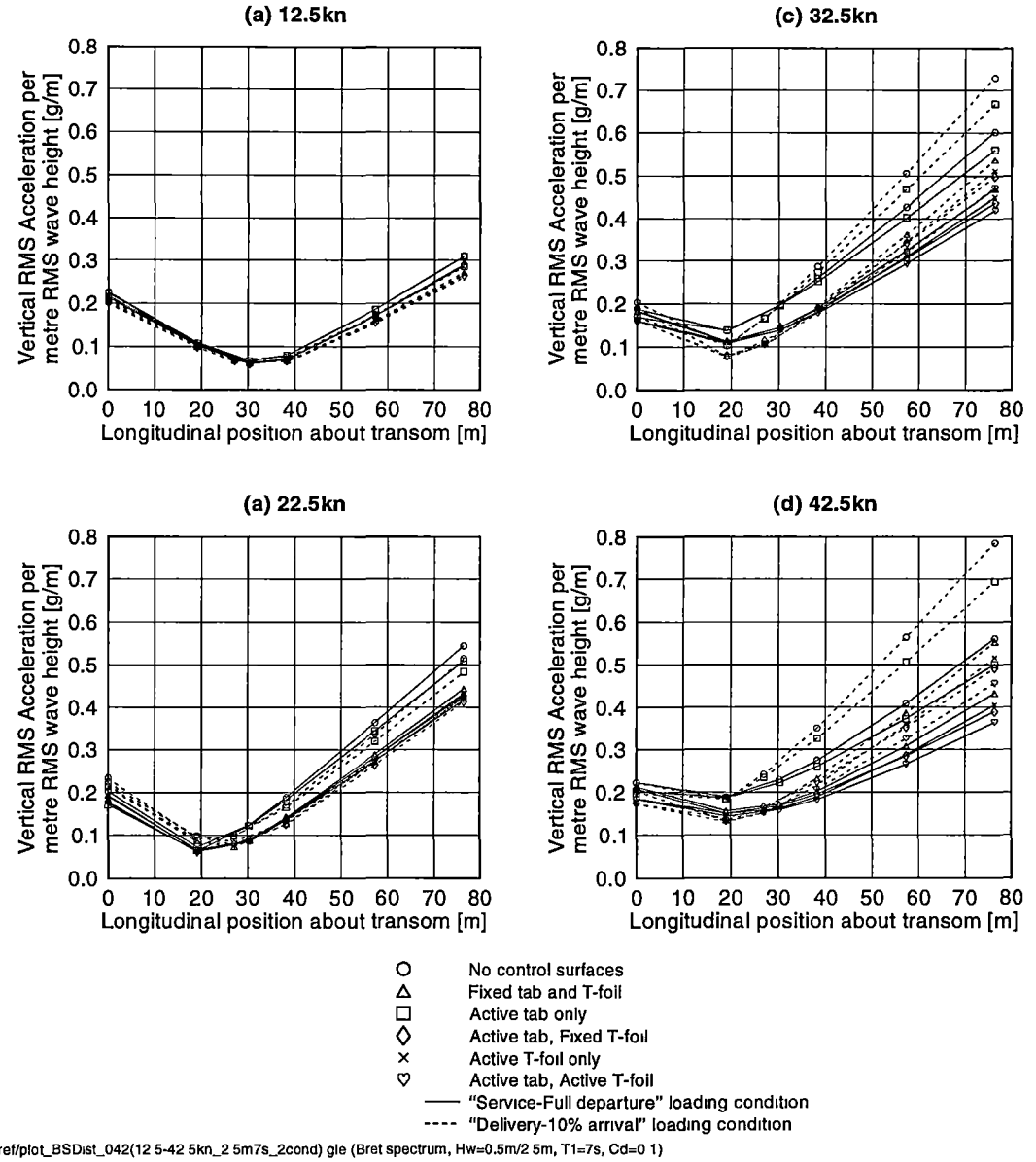

Figure 5.27: Predicted vertical acceleration response distribution (86m vessel, 12.5 - 42.5kn). (Regular wave height of computation = 0.5m, Regular wave height of control surface maximum deflection = 2.5m, Control gains calculated with Bretschneider wave spectrum of H_s = 2.5m, T_1 = 7s)

5.6 Effect of Regular Wave Height on Transfer Functions and Accelerations

The assumption of a hull response that is linear wave height has been the basis on which the previous results in this chapter have been presented, where the regular wave height of computation was 0.5 metres. In cases where control surfaces were implemented the wave height of maximum control surface deflection in most instances were set at the regular wave height of 2.5 metres, which corresponded to the significant wave height at which the vessel responses were to be determined. The 0.5 metre computation wave height was small enough to avoid introducing the effects of hull shape and large wave force magnitudes that are associated with large amplitude motions into the numerical computation. The handling of the free surface by the time domain theory of BESTSEA permits it to account in the fluid domain, the instantaneous fully immersed hull section in the body boundary condition. With this in mind, additional results were obtained in which higher regular wave heights were implemented in the computation to determine the effect of wave height on the vessel heave and pitch. The regular wave height was increased to 2.5 metres, as this was within the range of wave heights that were observed during the full-scale measurements. Furthermore, the computations for active controls assumed the wave height of maximum control surface deflection was 2.5 metres and the wave spectrum had a significant wave height of 2.5 metres. Both of these assumptions remained the same as for previous computations using the regular wave height of 0.5 metres.

The transfer functions for the hull without motion control surfaces for a range of speeds are shown in figure 5.28 for heave and pitch together with the computational solutions for the 0.5 metre regular wave height (discussed previously in figures 5.4 and 5.5). It can be clearly seen that the transfer functions generally show a reduction in the frequency of maximum response for both heave and pitch whilst the heave increases in magnitude at the frequency of maximum response. The pitch transfer functions also increase in magnitude at the lower speeds to the point where they exceed the magnitude of the higher speeds. Their shape also becomes more peaked about a lower frequency. It is obvious that the shape of these transfer functions at some points do not take on a smooth and regular form as those obtained from the smaller regular wave height of 0.5 metres. This change in shape of the transfer functions is perhaps a reflection of the increased unsteady wave forces acting on the hull, particularly near the bow as it emerges and re-enters the free surface leading to greater difficulty in obtaining a regular periodic solution in the computation. The lower speeds of 12.5 and 22.5 knots show a large increase in maximum response for a narrow band of frequencies until at the higher speeds the shape takes on a smoother appearance of lower maximum response. Not only does the shape in the transfer function change but there are shifts at some frequencies in the phase, some of which are more significant than others and these will influence the magnitude of accelerations calculated at positions about the vessel centre of gravity.

The transfer functions computed at the regular wave height of 2.5 metres (as opposed to the transfer functions previously computed at the nominal wave height of 0.5 metres) with fixed motion control surfaces are shown in figure 5.29 for heave and pitch together with the solution without control surfaces[4]. It can be seen that the change in the shape of the transfer functions (calculated in regular waves of 2.5 metres) with fixed

[4]This same solution without control surfaces and computed at the regular wave height of 2.5m was also used in the previous figure 5.28 for comparison with a computation at the regular wave height of 0.5 metres.

control surfaces show a reduction in frequency of maximum response compared with the transfer functions calculated in regular waves of 0.5 metres shown in the previous figure 5.28. Compared with the solution without control surfaces (shown in the same figure) there has been a reduction in response magnitude without any real change in the frequency of maximum response. The increased damping of the fixed control surfaces has created curves that are smoother and have a more regular shape at the higher speeds of 22.5 to 42.5 knots. Although the results in figure 5.29 represent a reduction in motions compared with the hull without control surfaces, the magnitude of response for all speeds at the dimensionless frequency of 4 are almost similar, being a value just below 1.5 for both heave and pitch. Another observation is that the reduction in response with fixed control surfaces at 12.5 knots is greater than that seen in figures 5.6 and 5.7 where the regular wave height of computation was 0.5 metres. This indicates that fixed control surfaces may appear more effective in computations with a larger regular wave height than in computations that adopt a smaller regular wave height.

These substantial changes in the characteristic of the transfer functions will most certainly have a significant effect on the degree of correlation that one can obtain with measurements and these will be referred to again in the discussion of the following chapter 6 where computed and measured responses are compared in detail.

An additional set of transfer functions at 32.5 knots forward speed are shown in figure 5.30. These compare the effect on heave and pitch for computations using regular wave heights of 0.5 and 2.5 metres for a range of motion control configurations. These include the hull without control surfaces, with fixed tab and T-foil, with active tab only and with active tab and T-foil configurations. The transfer functions computed at the higher wave height have the characteristics previously discussed of a lower frequency of maximum response and the reductions in response due to the implementation of control surfaces are of a similar magnitude but the absolute magnitudes have increased. This is to be expected as the increase in wave height has produced an increase in the proportional response of the vessel. Such properties indicate that hull response to waves is not necessarily linear.

Combining the transfer functions derived through computation at the regular wave height of 2.5 metres with a Bretschneider wave spectrum of 2.5 metres significant wave height and 7 second average period, one obtains the acceleration response spectra of figure 5.31. It is clear from these results that the spectra generally have reduced the frequency of maximum response a small amount when implementing the higher 2.5 metre regular waves in the computation. At the LCG the magnitude of response has increased (see figure 5.31(1b)). The bow motion has actually reduced substantially in magnitude at the larger wave height (see figure 5.31(1c)) whilst the stern has increased in magnitude at some frequencies and reduced at others (see figure 5.31(1a)).

Taking the average of the acceleration spectra between six longitudinal positions the diagram of average acceleration spectra shown in figure 5.31(2) is obtained. In this result the average spectra has been reduced in magnitude and the peak of maximum response has been reduced in frequency at the larger wave height.

There is no reason to believe that similar results would not be obtained if larger wave heights were also applied to the hull configured with active control surfaces. It would appear from the results presented thus far that computing the vessel accelerations at the smaller wave height of 0.5 metres may over predict the vessel acceleration at larger wave heights whilst also increasing the frequency of maximum response to a higher value than should otherwise be the case.

Solving the acceleration response for a range of wave periods with the Bretschneider wave spectrum of 2.5 metre significant wave height and integrating the results, one

obtains the relative RMS acceleration for a range of wave periods. These results have been shown once again for the hull without and with fixed control surfaces (i.e. fixed tab and T-foil) in figure 5.32. The outcome shows that for the acceleration spectra at one wave period as in the previous figure 5.31, the increased regular wave height of computation of 2.5 metres has decreased the RMS acceleration at the bow. No significant change is seen at the stern. At the LCG the RMS acceleration has slightly increased for periods above 6 seconds, whilst slightly decreasing at periods below 6 seconds. All these results were computed at the heavier "service-full departure" loading condition so the frequency of maximum response shown in these results represent the lowest that could be attained by varying the vessel displacement in the computation. Overall the effect of using a regular wave height in the computation that is closer to the significant wave height of interest, tends to show a lower average RMS acceleration over the length of the vessel. Therefore, the computation based on the regular wave height of 0.5 metres would tend to over predict the accelerations for a wave spectrum of 2.5 metres significant wave height.

The results obtained in this section from a computation with regular waves at 2.5 metres at this stage are an unsubstantiated outcome from the numerical method. As far as the author is aware no fundamental comparisons have been made using this theory in large wave heights from model tests or previously published work that would add more experimental verification of the transfer functions obtained here. However, they are added as their nature is consistent with the theoretical application of the body boundary conditions and in some cases the results seem plausible based on the results obtained from full-scale measurements discussed in chapter 4 and brought together with these results in chapter 6.

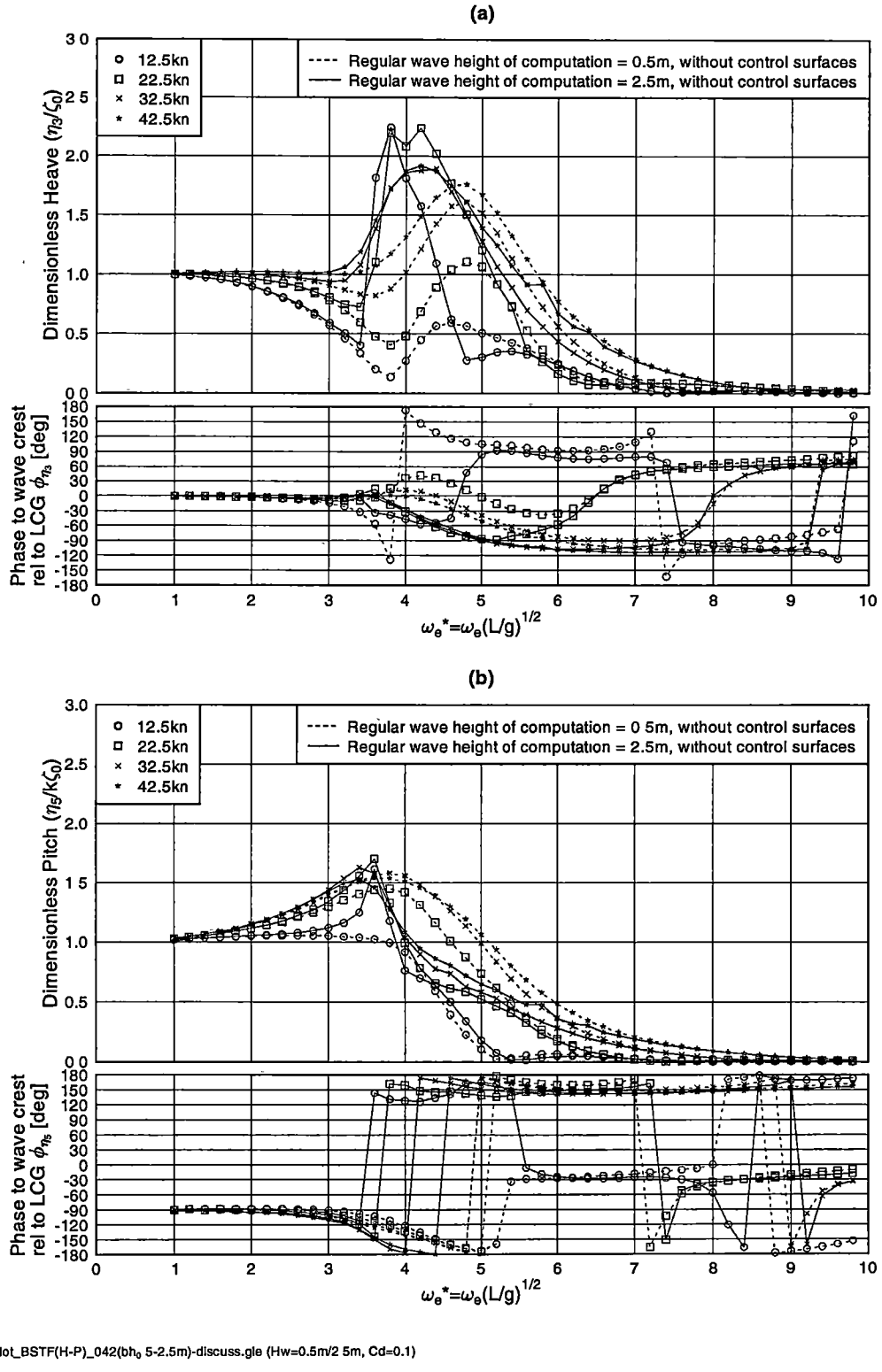

Figure 5.28: Predicted heave and pitch transfer functions (86m vessel, 32.5kn, without control surfaces). Comparison of computations at the regular wave heights of 0.5 and 2.5 metres (Loading condition: "Service-full departure")

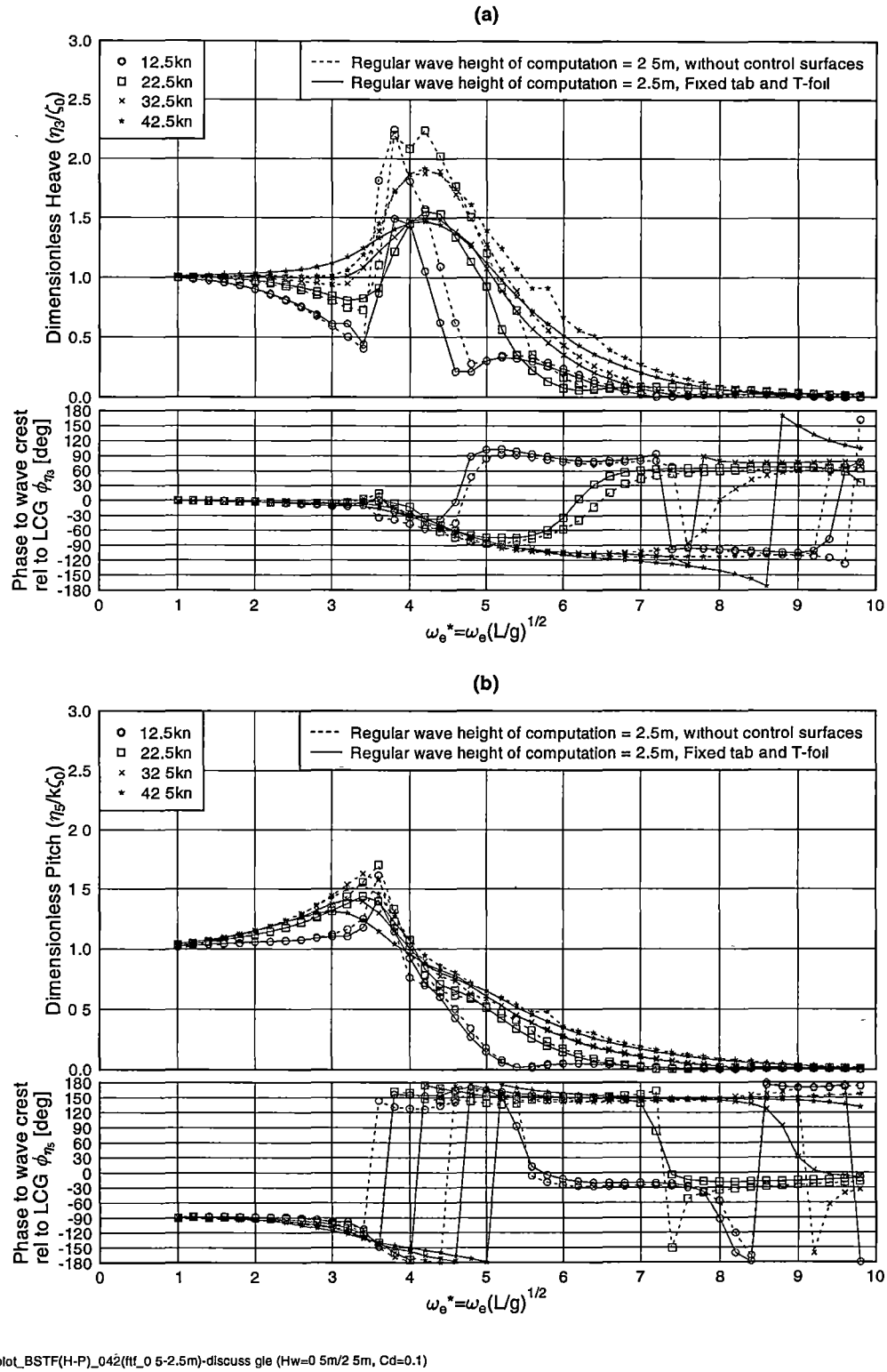

ref/plot_BSTF(H-P)_042(ftf_0 5-2.5m)-discuss gle (Hw=0 5m/2 5m, Cd=0.1)

Figure 5.29: Predicted heave and pitch transfer functions (86m vessel, 32.5kn). Comparison of hull without control surfaces to hull with fixed tab and T-foil. Computation only at 2.5 metre regular wave height (Loading condition: "Service-full departure")

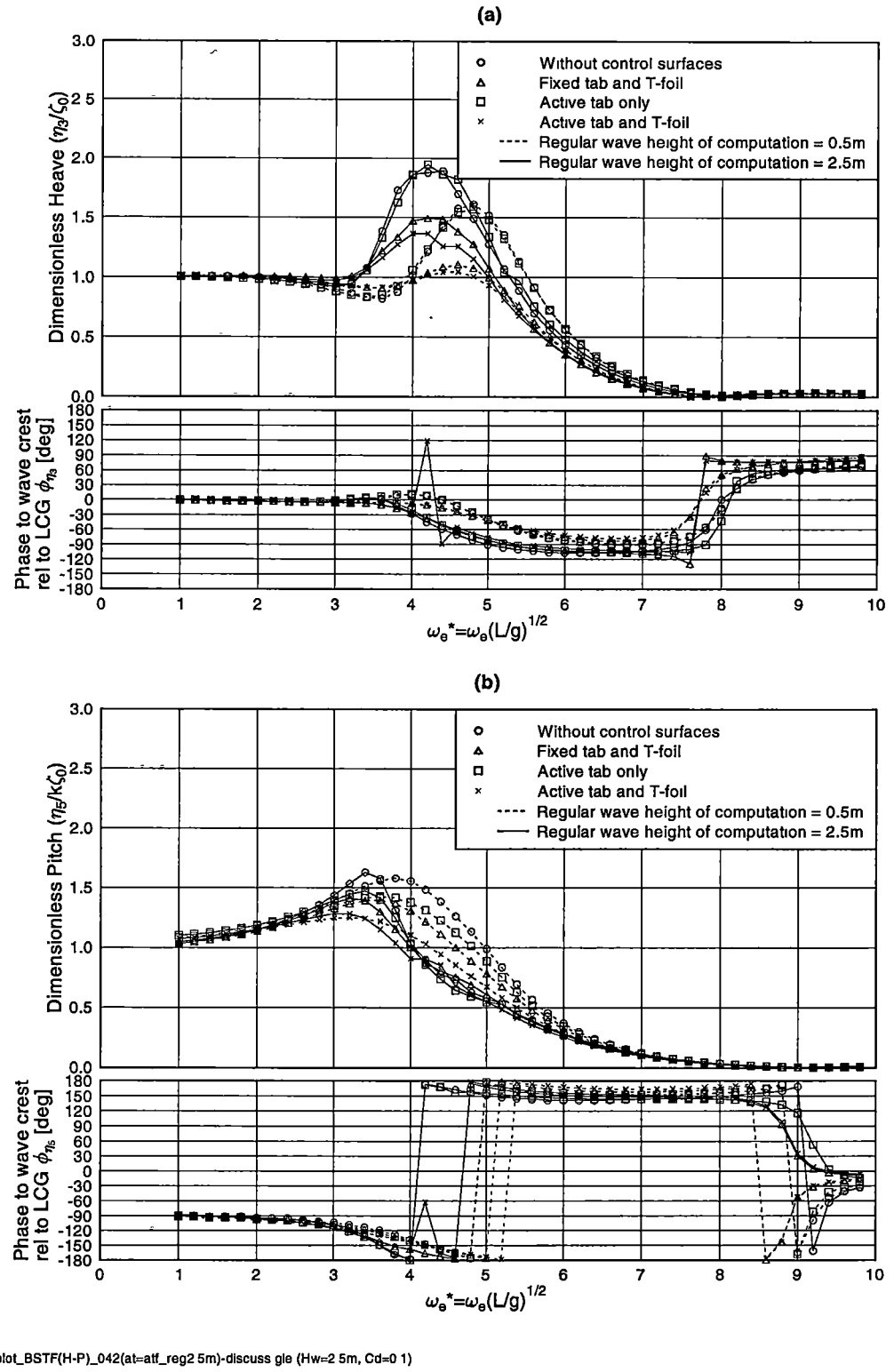

ref/plot_BSTF(H-P)_042(at=atf_reg2 5m)-discuss gle (Hw=2 5m, Cd=0 1)

Figure 5.30: Predicted heave and pitch transfer functions (86m vessel, 32.5kn, various configurations) comparing computations at 0.5 and 2.5 metre regular wave height (Loading condition: "Service-full departure")

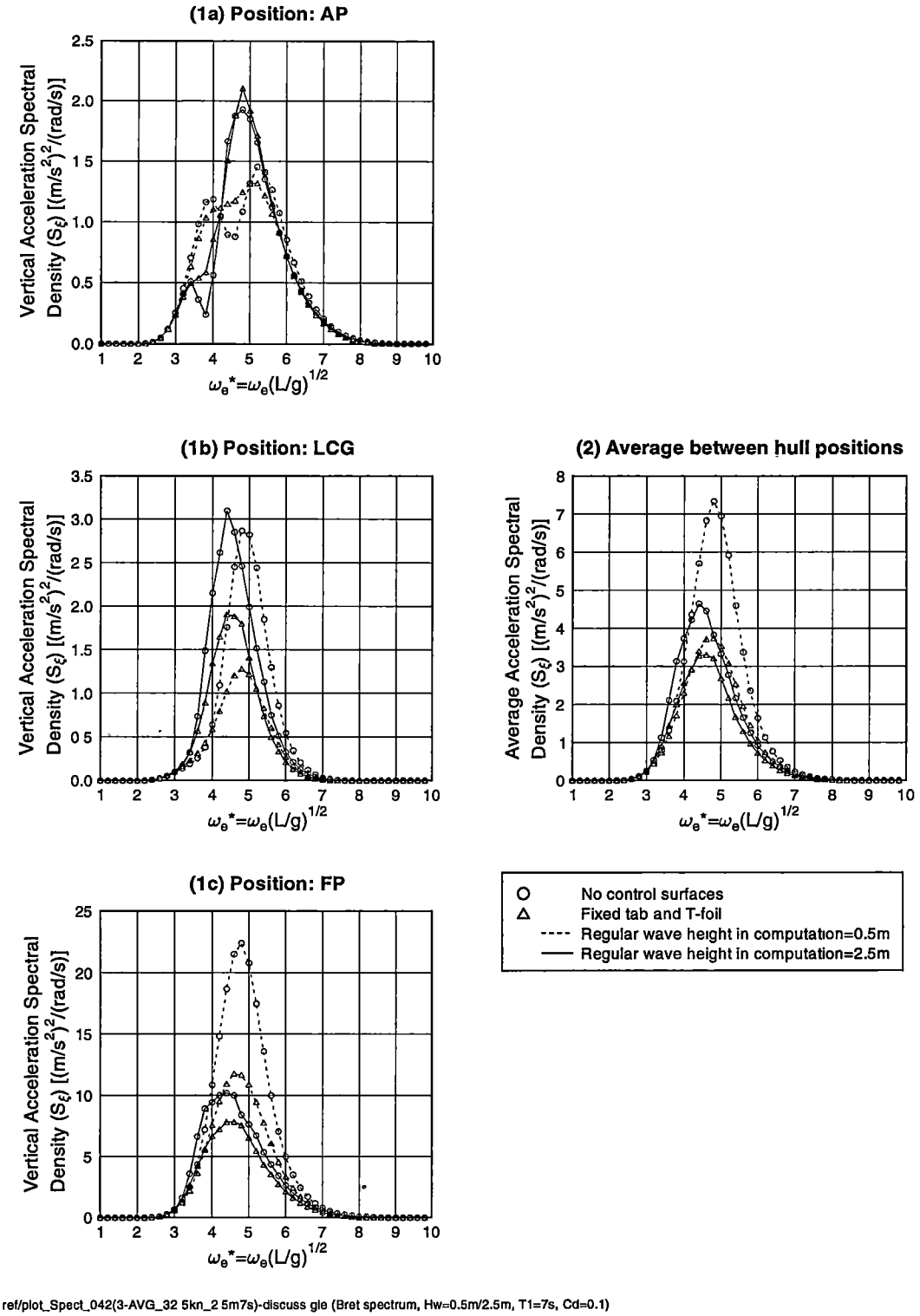

Figure 5.31: Predicted acceleration response spectra (86m vessel, 32.5kn) for computations at 0.5 and 2.5 metre regular wave heights. (1a) aft perpendicular (AP), (1b) longitudinal centre of gravity (LCG), (1c) forward perpendicular (FP) and (2) averaged between hull positions (Loading condition: "Service-full departure")

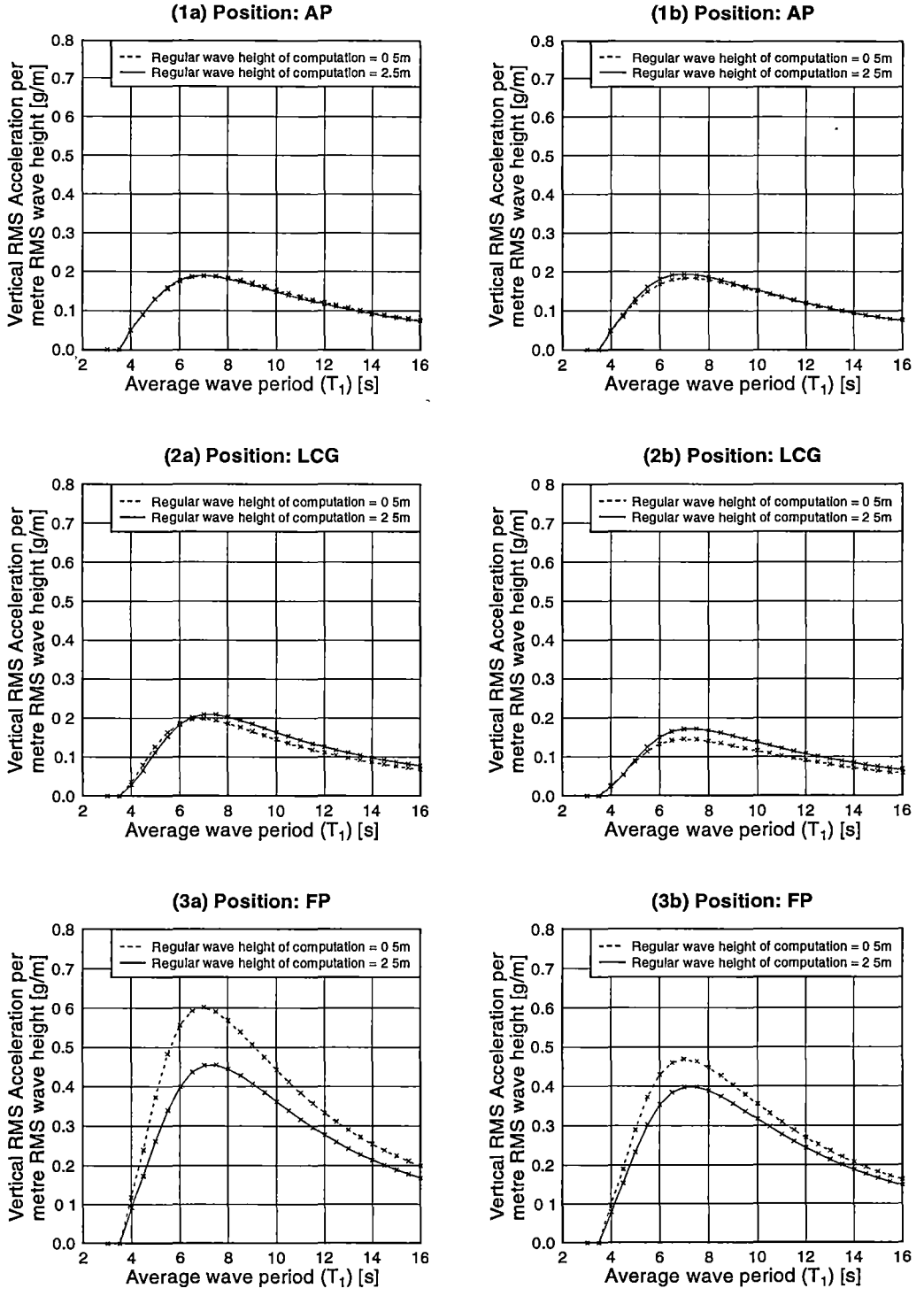

Figure 5.32: Predicted vertical acceleration (86m vessel, 32.5kn) for computations at 0.5 and 2.5 metre regular wave heights. (1) aft perpendicular (AP), (2) longitudinal centre of gravity (LCG), (3) forward perpendicular (FP) and (a) without control surfaces, (b) fixed tab and T-foil (Loading condition: "Service-full departure", Bretschneider wave spectrum of $H_s = 2.5$m)

5.7 Effect of MCS Target Wave Height on Acceleration Relative to Wave Height

In prior sections the vessel response with control surfaces has been computed with regular waves of 0.5 metres and the control surfaces have been set up to obtain full deflection at the regular wave height of 2.5 metres through appropriate selection of the control gains, which also corresponds with the significant wave height of the wave spectrum. The transfer functions were then combined with a 7 second average period wave spectrum. In this section two additional solutions are obtained where the wave height of full control surface deflection is changed to regular wave heights of 1.25 and 1.56 metres instead of the previous solution that used 2.5 metres. In effect this results in selection of higher control system gain settings. These additional wave heights for control limitation corresponded to half the significant wave height and the average wave height of a 2.5 metre Bretschneider wave spectrum. The root mean square (RMS) of the acceleration response obtained from this approach is shown in tables 5.3 and 5.4 for the "service - full departure" loading condition and at three hull positions. These results can be directly compared with the results of table 5.1.

		Service-Full departure condition							
Hull Configuration	Speed [kn]	Average [g/m]	Reduction	AP [g/m-RMS]	Reduction	LCG [g/m-RMS]	Reduction	FP [g/m-RMS]	Reduction
Without control surfaces	32.5	0.30	-	0.19	-	0.20	-	0.60	-
Fixed tab, fixed T-foil	32.5	0.24	22%	0.18	3%	0.15	27%	0.47	22%
Active tab	32.5	0.28	9%	0.16	17%	0.20	1%	0.53	12%
Active T-foil	32.5	0.22	27%	0.18	4%	0.13	33%	0.43	28%
Active tab, fixed T-foil	32.5	0.22	29%	0.15	22%	0.15	26%	0.41	32%
Active tab, active T-foil	32.5	0.20	33%	0.15	22%	0.14	31%	0.38	37%

C:\1Nigel\bs\042\report_results\Motion control reduction summary (042bs_RMSAccel-std).xls

Table 5.3: Acceleration per metre wave height (RMS) (86m vessel, 32.5kn, Regular wave height of computation = 0.5m, Regular wave height of control surface maximum deflection = 1.25m, Control gains calculated with Bretschneider wave spectrum of H_s = 2.5m, T_1 = 7s, Loading condition: "Service-full departure"; For comparison with table 5.1 where the wave height of maximum control surface deflection is altered)

The combined results from these three tables are shown in figure 5.33 where the RMS acceleration response at the aft perpendicular (AP), longitudinal centre of gravity (LCG) and forward perpendicular (FP) have been plotted against regular wave height for control limitation or the regular wave height for maximum control deflection.

It can be seen in figure 5.33 that the majority of the RMS acceleration responses are constant with wave height, indicating that the RMS acceleration is not particularly sensitive to the regular wave height at which the control surfaces reach full deflection. However, the result at the FP does show some sensitivity to the selection of wave height for full control deflection because the RMS acceleration per unit wave height is not entire constant as the regular wave height of maximum control deflection increases. These results show that using the same wave height (i.e. 2.5 metres) as defined by

		Service-Full departure condition							
Hull Configuration	Speed [kn]	Average [g/m]	Reduction	AP [g/m-RMS]	Reduction	LCG [g/m-RMS]	Reduction	FP [g/m-RMS]	Reduction
Without control surfaces	32.5	0.30	-	0.19	-	0.20	-	0.60	-
Fixed tab, fixed T-foil	32.5	0.24	22%	0.18	3%	0.15	27%	0.47	22%
Active tab	32.5	0.28	7%	0.16	14%	0.20	1%	0.54	10%
Active T-foil	32.5	0.24	22%	0.18	3%	0.15	27%	0.47	22%
Active tab, fixed T-foil	32.5	0.22	27%	0.14	24%	0.14	29%	0.44	27%
Active tab, active T-foil	32.5	0.21	32%	0.15	20%	0.14	31%	0.39	35%

C:\1Nigel\bs\042\report_results\Motion control reduction summary (042bs_RMSAccel-std).xls

Table 5.4: Acceleration per metre wave height (RMS) (86m vessel, 32.5kn, Regular wave height of computation = 0.5m, Regular wave height of control surface maximum deflection = 1.56m, Control gains calculated with Bretschneider wave spectrum of H_s = 2.5m, T_1 = 7s, Loading condition: "Service-full departure"; For comparison with table 5.1 where the wave height of maximum control surface deflection is altered)

the wave spectrum for achieving full deflection may not significantly alter the RMS acceleration per unit wave height.

The solutions in figure 5.33 without control surfaces appear as expected as lines of constant acceleration in all the diagrams. This is because these results are not influenced by controls and so do not change in relation to the wave height and the linear assumption applies.

The reason for the lack of sensitivity of the relative motions to the wave height at which the control dynamic movement was limited can be seen in the results of previous sections where control activity has a relatively small effect in reducing motions compared to motions with inactive fixed control surfaces. However, even these modest reductions due to control dynamic activity were confined to frequencies near the motion resonance. The consequence of this is that control activity has a very small effect on the overall response to a random sea as seen in figure 5.33. Once again it is apparent that in relatively large seas the control surfaces are severely limited by the maximum unsteady forces which they can produce as the control surfaces incidence is varied by the control system.

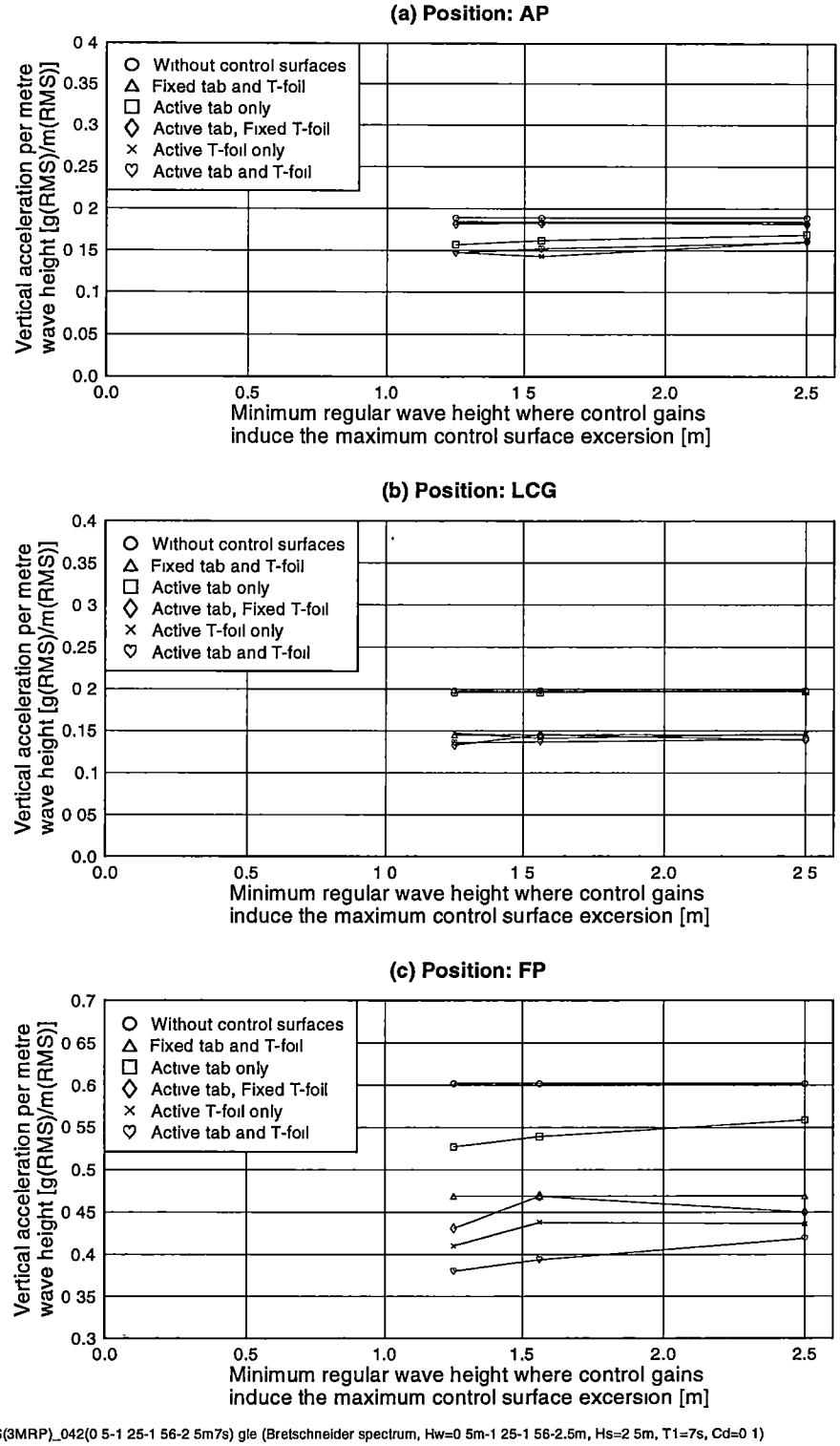

Figure 5.33: Predicted change in RMS acceleration (86m vessel, 32.5kn, "Service-Full departure" loading condition) due to variation in the targetted regular wave height of control surface maximum deflection. (a) aft perpendicular (AP), (b) longitudinal centre of gravity (LCG), (c) forward perpendicular (FP) (Regular wave height of computation = 0.5m; Bretschneider wave spectrum $H_s = 2.5$m, $T_1 = 7$s)

5.8 Effect of Vessel Acceleration on Human Tolerance

Discussion that considers the vessel accelerations also implies that the human tolerance to vessel motions is an important component that regulates what defines a severe acceleration. This is a broad subject that is outside the scope of this analysis and will only be briefly considered to place in perspective the accelerations levels. One of the ways that vertical accelerations have been defined in relation to the likelihood of a person experiencing motion sickness is from the experiments of McCauley et al. (1976). Whilst this method is not conclusive in its own right, it provides a measure of comparison that is founded on regular frequencies and their relationship to human tolerance to vertical accelerations over finite time intervals.

5.8.1 Motion Sickness Incidence

The calculation of motion sickness incidence (MSI) according to the method of McCauley et al. (1976) for a 2 hour period was calculated for the vessel at various speeds without motion control surfaces and with active tabs and T-foils at various longitudinal passenger positions. These results are shown in figure 5.34 where the MSI levels tend to follow the acceleration distribution as expected. The lowest level achieved at the 2.5 metre significant wave height and 7 second period with active controls occurred at the LCG in the heavier ("service - full departure") loading condition at the lowest speed of 12.5 knots where the MSI was approximately 3%. The lowest MSI value at the bow was 46% at the speed of 42.5 knots whilst the lowest value at the stern was 12%, also occurring at the highest speed of 42.5 knots in the heavy loading condition.

The highest level of MSI at the stern with active controls occurred at the lower speeds reaching about 40%. The medium speeds had the highest MSI at the bow of about 60%. The highest level of MSI at the LCG was about 15%.

These figures clearly indicate that on vessels with this hull form the most comfortable position is near the LCG position. Depending on the speed of the vessel, this optimal location will move forward somewhat at the lower speeds and move aft at the higher speeds. However, in general positions near the LCG are most comfortable for all the cases considered.

Table 5.5 shows the average MSI over the length of the vessel without control surfaces and with active tab and T-foil. The outcome is similar to the acceleration without control surfaces where a reduction in speed also reduces the MSI but with active tab and T-foil the MSI initially increases before reducing. Furthermore, the average reduction with controls is not much improved, even at the lowest speed of 12.5 knots. However, the average MSI improved by up to 38% with active control surfaces fitted at the highest speed of 42.5 knots.

It can be seen from these results that the vessel in 2.5 metre, 7 second seas has MSI levels that vary significantly from bow to stern and can change significantly with speed and the level of control activity. However, the computations in the present work have necessarily been confined to the head sea conditions within the capacity of the program BESTSEA. Therefore, it was not considered appropriate to attempt further detailed investigation of MSI.

5.9 Summary

This chapter presented the predicted results for the 81 and 86 metre vessels considered in the present analysis at two loading conditions, representing a range of motion responses. Key findings from these results include:

Hull Configuration	Speed [kn]	Service-Full departure loading condition		Delivery-10% arrival loading condition	
		MSI (%) (average)	Reduction compared without control surface	MSI (%) (average)	Reduction compared without control surface
Without control surfaces	12.5	25.6	-	22.7	-
	22.5	34.0	-	30.0	-
	32.5	38.0	-	34.9	-
	42.5	37.7	-	37.7	-
Active tab and T-foil	12.5	23.9	6.8%	20.9	18.4%
	22.5	27.1	20.4%	27.4	19.5%
	32.5	27.8	26.9%	24.6	35.2%
	42.5	24.9	33.9%	23.4	37.9%

Table 5.5: Average MSI over length of vessel computed in head seas at two loading conditions (Control gains calculated with Bretschneider wave spectrum of $H_s = 2.5$m, $T_1 = 7$s; see also figure 5.34)

1. The vessels heave and pitch magnitudes reduced with speed.

2. A change in speed did not significantly alter the frequency of maximum response, except at speeds below 20 knots where larger variations were evident.

3. Active transom tabs reduced pitch motion more than heave motion, where at the highest speed, heave was reduced by 5% compared to pitch at 20%. Therefore vessels fitted only with transom tabs receive only a modest benefit.

4. The fixed T-foil alone had a significant effect in reducing the heave and pitch motions. The majority of the benefit occurred with the passive action of the device as opposed to the effect of active controls. This has yet to be substantiated against full-scale tests.

5. The influence of the T-foil was greater than the transom tab. This is significant in the sense that the position of the control surface was more important than the control force, as in this analysis the transom tab had a greater force potential than the T-foil.

6. Control surfaces have a decreasing benefit of motion reduction at low speed. They also have a reduced benefit as the wave height increases such that the size of motion control system would be severely challenged to provide sufficient force at the vessel's operating limit of 3 metres significant wave height.

7. Wave period had a major effect on the vessel motions where accelerations generally reduced with increasing period over approximately 7 seconds. The minimum acceleration predicted for the 86 metre vessel with a wave spectrum of 2.5m significant wave height and 7 seconds average period was 0.06g/m, located near the longitudinal centre of gravity.

8. The use of larger regular wave heights in the computation resulted in smaller acceleration levels. The acceleration levels per unit wave height were not significantly sensitive to the regular wave height selected for maximum control surface deflection. The most effective control inputs in this analysis used both pitch and heave for the head sea computation.

9. The Motion Sickness Incidence (MSI) in head sea waves with active motion controls ranged from 20% to 25%. This was an improvement of up to 34% on the hull without control surfaces. However, the MSI levels remained high.

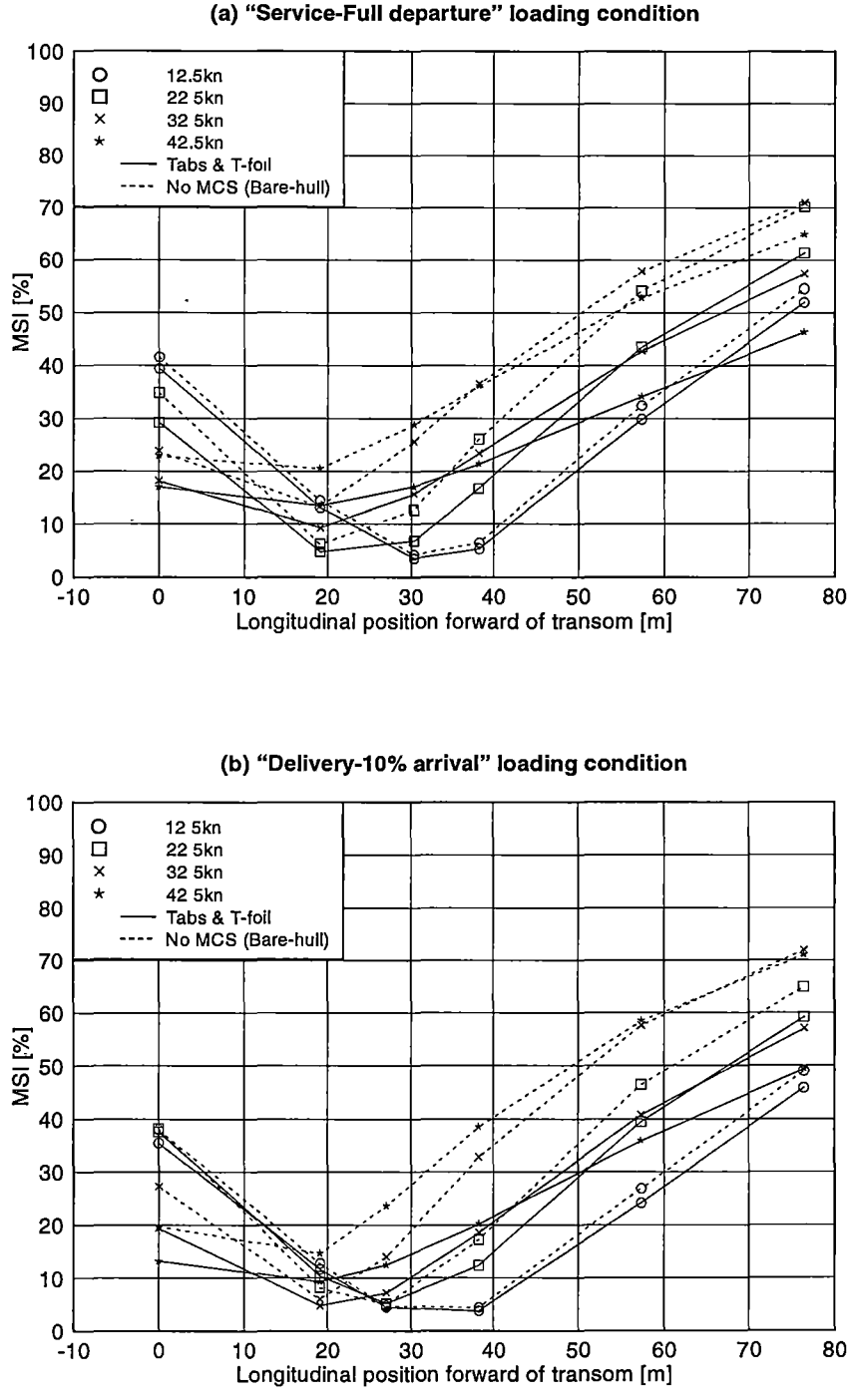

Figure 5.34: Predicted motion sickness incidence (MSI) over 2-hours exposure duration (McCauley et al. (1976)) (86m vessel) at loading conditions of (a) "Service-full departure" and (b) "Delivery-10% arrival" (Regular wave height of computation = 0.5m, Regular wave height of control surface maximum deflection = 2.5m, Control gains calculated with Bretschneider wave spectrum of H_s = 2.5m, T_1 = 7s; see also table 5.5)

Chapter 6

Comparison of computed and measured responses

6.1 Introduction

The results of full-scale experiments and numerical analysis have been presented in chapters 4 and 5 respectively where transfer functions were presented for heave, pitch and roll from measurements and for heave and pitch from head sea numerical predictions. In addition, the vertical accelerations per unit wave height were presented as distributions and magnitudes. The two sets of results were presented independently and now some of these results will be combined for comparison in this chapter to form the basis of a discussion on both the measurements and predictions.

Where possible data from the numerical and predicted results will be presented in this chapter but in some cases chapters 4 and 5 may be referred to in support of some discussions.

6.2 Comparison of Transfer Functions

Most of the computed results of this work made the broad assumption that a linear solution would provide a reasonable prediction of transfer functions and a foundation from which the vessel accelerations could be determined. Comparison of the predicted transfer functions (see chapter 5) derived in small wave heights with derived transfer functions from full-scale measurements (see chapter 4) in head seas showed a disparity between the two that was particularly apparent with the frequency of maximum response. In particular, the measured transfer functions had a lower frequency of response than predicted through numerical computations at small wave height. Data records obtained from full-scale measurements in head seas and presented in chapter 4 are represented here with the predicted transfer functions. The available speeds from the delivery voyage of the 86 metre vessel include 12.5, 17.5, 22.5, 27.5 and 32.5 knots whilst available speeds from service operations on the English Channel include 12.5, 17.5, 32.5 and 37.5 knots. From the delivery voyage data only the speeds of 12.5 and 32.5 knots are used for comparison as they are representative of both the low and high speeds and showing the intermediate results would not necessarily add to the discussion. Furthermore, with the low quantity of data obtained at 22.5 knots the result was not consistent with the results obtained at other speeds. Similarly, from the data obtained during service operations only the speeds of 12.5 and 32.5 knots will be used for comparison as the other speeds represented only an approximate interpolation on

these speeds and their characteristics were not substantially different so they would not contribute significantly to the comparison.

The comparisons in head seas for the 86 metre vessel are shown in figures 6.1 and 6.2 for the delivery voyage measurements and in figures 6.3 and 6.4 for the measurements during service operations. The delivery voyage measurement of course only include the hull configuration with active transom tabs whilst the measurements made during service operations include active tabs and T-foils in the hull control surface configuration.

6.2.1 Delivery Voyage Transfer Function Comparison

Figure 6.1 shows the delivery voyage measured comparison with predictions at 12.5 knots for heave and pitch. It can be seen that in heave (figure 6.1(a)) the measured result was close to the prediction using the regular wave height of 0.5 metres for computation. The amount of data making up the measured result consisted of approximately 10 minutes of data (see table 4.2) but the result is consistent with other low speed results from measurement. No predicted results were obtained using the 2.5 metre regular wave height because the low speed and low force produced by the transom tab in wave conditions this high meant that a reliable periodic solution could not be achieved in the gain finding routine. Table 4.8 shows that the average RMS wave height for these measurements was 0.64 metres (i.e. about 2.56 metre significant wave height) but the bandwidth parameter shows (see table 4.6) that the seas were broadband, which suggests that multidirectional wave conditions may have influenced the measured vessel response sufficiently to create the difference in outcome when compared with the computed results.

It can be seen that in pitch (figure 6.1(b)) that the measured result has a peak at the dimensionless frequency of 3.0 that may be the result of insufficient data to form a smooth spectral shape rather than representing a true spectral peak. Furthermore, the predicted results did not display any type of peak. However, the reducing magnitude at the higher frequencies is of similar form and magnitude to the predicted results.

On reflection one would expect these comparisons at the low speed of 12.5 knots to be relatively straightforward because there is no significant resonant character in the response functions to consider as the vessel is much less dynamically responsive at low speed. Thus one would expect the predicted and measured results to be generally quite similar. The fact that there were some small differences leads one to suspect that the wave environment had significant directional spreading thus altering the result from what would be predicted for long crested head seas waves at 12.5 knots.

The comparison of the measured transfer function at 32.5 knots for the delivery voyage with predictions are shown in figure 6.2 for heave and pitch. In heave, it can be seen that the frequency of maximum response is lower than all the predictions but that the prediction for 2.5 metre regular waves in the computation is closer to the measured result both in terms of frequency and magnitude. This larger wave height prediction also used the heavier vessel displacement and showed the lowest frequency of maximum response of all the displacements. It is evident therefore that the prediction was only moderately successful in duplicating the result of the heave transfer function obtained from measurements. This does not necessarily mean that the numerical method is deficient since the environment in which the measurements were conducted would have involved seas which were somewhat variable in direction. At dimensionless frequencies above 5.3 there was better agreement between the measured and predicted results.

The comparison in pitch showed that the predicted result at the heavier displacement ("service-full departure") using the 0.5 metre regular waves in the computation showed much greater similarities with the measured result. The only difference was in

the magnitude of the peaks, which differed by about 0.2. Otherwise the slope away from the maximum were almost identical. Although the quantity of data used to generate this result was identical to that used for the heave, the pitch result showed better agreement. The pitch computation at the regular wave height of 2.5 metres did not compare as well as the computations using the 0.5 metre regular waves. Also, the results for the light displacement did not compare as favourably as the heavy displacement, primarily due to the increase of the frequency of maximum heave. This aspect will be discussed further in the following section.

6.2.2 Service Operations Transfer Function Comparison

Figure 6.3 shows the delivery voyage comparison of measured with predicted results at 12.5 knots for heave and pitch. It can be seen that in heave (figure 6.3(a)) the measured result was closer to the predicted result using the regular wave height of 0.5 metres at dimensionless frequencies above 5, but elsewhere there is a departure between the two. The amount of data making up the measured result consisted of approximately 27 minutes of data (see table 4.2), which was satisfactory and the result is consistent with other low speed results from measurement. Table 4.8 shows that the average RMS wave height for these measurements was 0.85 metres (i.e. about 3.4 metre significant wave height) and the bandwidth parameter shows (see table 4.6) that the seas were broadband. These sea conditions encountered during the measurements may once again be the main reason that no resonance is seen in the measured results as can be seen in the prediction. Whilst the duration of the measured data may appear to be adequate (27 minutes) this does not guarantee that there is adequate spectral energy in all frequency bands of interest.

It can be seen that in pitch (figure 6.3(b)) the outcome of the results closely resemble those discussed previously for the 12.5 knot delivery voyage case (with transom tabs only). The peak response and frequency are very similar and the computed responses show no real differences. Accordingly, the measured response is higher at the dimensionless frequencies greater than 4.0 and its downward slope as the frequency increases is lower than all predictions. Below the dimensionless frequency of 4, the only prediction that showed any excitation greater than unity is the prediction that used 2.5 metre regular waves, but the frequency of maximum response was higher than measured.

The comparison of the measured and predicted transfer functions at 32.5 knots for service operations where the hull had tab and T-foil active control surfaces are shown in figure 6.4 for heave and pitch. In heave, it can be seen that the measured frequency of maximum response is again lower than all the predictions but the prediction using 2.5 metre regular waves is the closest to the measured result. There was agreement in the magnitude of the transfer function toward the higher frequencies, where there is a generally good comparison. At dimensionless frequencies greater than 6, the measurements were higher than predicted right up to a dimensionless frequency of 10. Below a dimensionless frequency of 4.5 the measured results continued to increase and showed signs of peaking at the frequency of 3 just before the frequency of truncation. By comparison the predicted results had closely approached unity at this point resulting in a larger difference between the magnitudes of the measured and predicted results.

The comparison in pitch showed that the predicted result at the heavier displacement ("service-full departure") using the 0.5 metre regular wave height in the computation showed best agreement with the measured result in both magnitude and form. This outcome is slightly better than the result obtained previously at 32.5 knots for the delivery voyage comparison (see figure 6.2(b)). The peaks were in agreement as well as

the roll off with increasing frequency. The quantity of data used to generate this result was identical to that used for the heave and consisted of over 40 minutes of recording time in an average wave height of 0.44 metres RMS (i.e. about 1.76 metres significant wave height). The computation in a regular wave height of 2.5 metres did not compare as well as the computations using smaller regular waves and the light displacement did not have a shape that compared as favourably as the heavy displacement. However, the variation between these predictions and the measured results suggest that the computation is not particularly sensitive to the loading or wave conditions, which may be why a good agreement was obtained.

6.2.3 Effect of Wave Height on Transfer Functions with a More Recent Prediction Program

At the time that the computations were carried out which formed the basis of investigation into the effects of displacement, speed and control surface action, the program BESTSEA was the only version of the time domain method available. As discussed in previous sections of this chapter in addition to chapter 5 (see section 5.6), this program was used to compute motion solutions with regular head sea waves of 0.5 and 2.5 metres. It was found that the increased wave height produced a reduction in the frequency of maximum response as well as an increase in the magnitude. Using this program in its current format limited computational work to head sea waves as alteration of the program to include secondary hulls, oblique wave directions and some motion degrees of freedom was necessarily placed outside the scope of this project. Thus the effect of wave interaction between the hulls of the twin-hull vessels was neglected in addition to effects of surge, sway, roll and yaw motions. More recently a later version of BESTSEA was developed in which the modelling of multi-hull designs in oblique seas could be considered with improved solution stability at large wave heights. This program (labelled BEAMSEA) has been used by Davis and Holloway (2003b) to investigate the effects of wave height. Of particular relevance here are results generated using BEAMSEA in head waves of various heights that support some trends found with BESTSEA. Figure 6.5 shows the resulting transfer functions for the 86 metre vessel with wave heights of between 0.5 and 4.0 metres for the speed of 37.5 knots. It can be seen that there is a progressive reduction in the frequency of maximum response as the wave height increases. This supports the finding discussed in previous sections of this chapter and in chapter 5 (see section 5.6) where the regular wave height of computation was increased from 0.5 to 2.5 metres.

One difference that can be seen in the heave transfer function of figure 6.5 to the heave transfer functions computed in this work is that the maximum response of the transfer function tends to decrease with wave height. This is different to the outcome obtained with BESTSEA where the maximum response tended to increase with wave height. The reason for this variation is not fully understood and requires further investigation where similar hull parameters used in the analysis of this work can be better reflected in the computation to assess the source of these notable differences. It could be argued that at larger wave height there is significant hull emergence at the bow and stern, which reduces the natural frequency of response due to waterplane area reductions that also reduce the forcing effect of the encountered waves. This would indicate that a decrease in maximum amplitude is more likely as shown by the BEAMSEA results. In addition, it is possible that the effect is due to hull interference effects, not represented in BESTSEA. Despite this difference in the response magnitude with speed it is sufficient to observe that there is a reduction in the frequency of maximum response even with a solution obtained from a more advanced program that

considers additional hydrodynamic effects.

On the basis of that, these BEAMSEA results which support some characteristics seen with the BESTSEA results, there is further evidence that a major contributory factor in the relatively high frequency of predicted maximum heave discussed in preceding sections is the use of small wave heights in the computations.

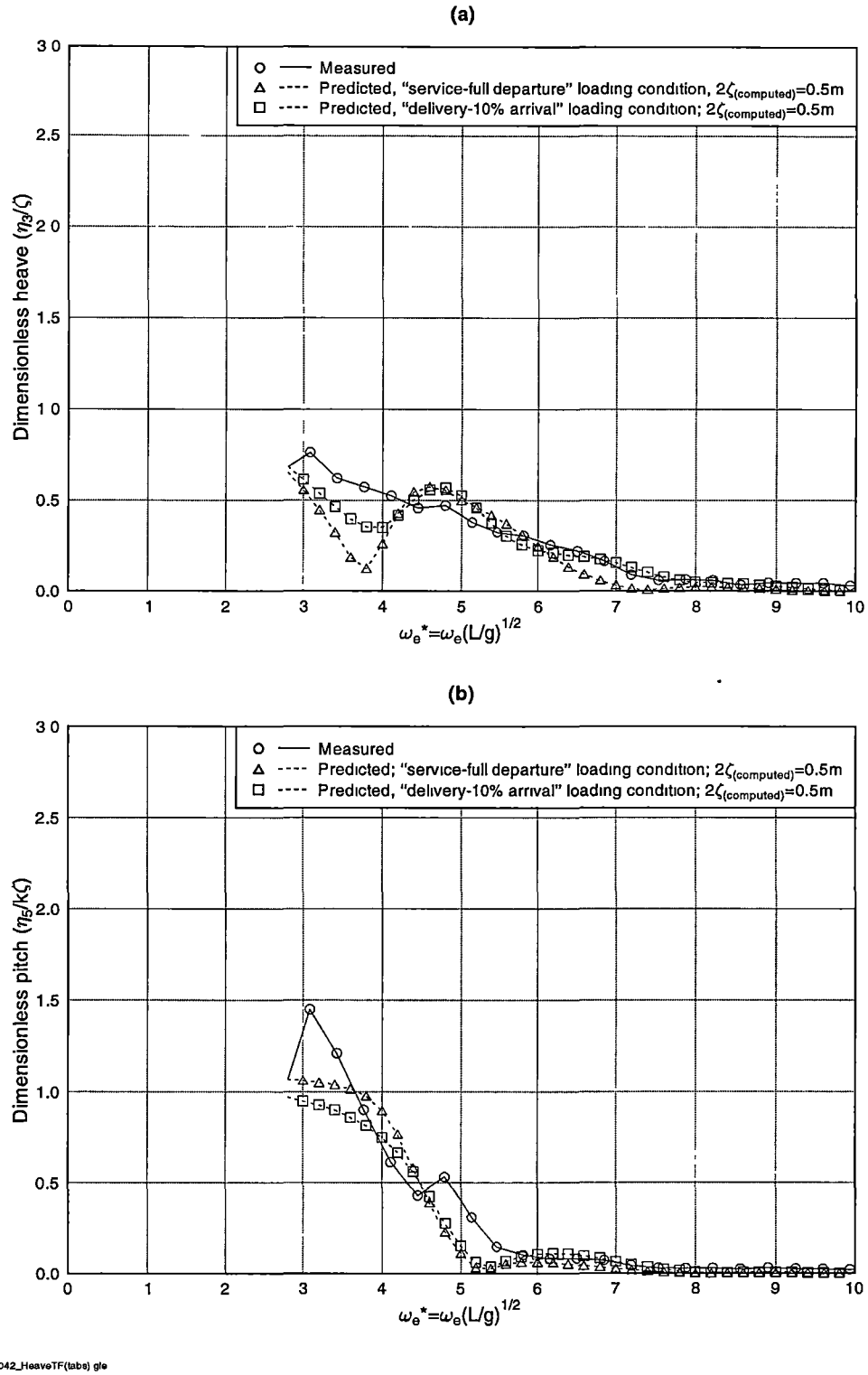

Figure 6.1: Transfer function comparison in (a) heave and (b) pitch (86m vessel, 12.5kn, active tabs only)

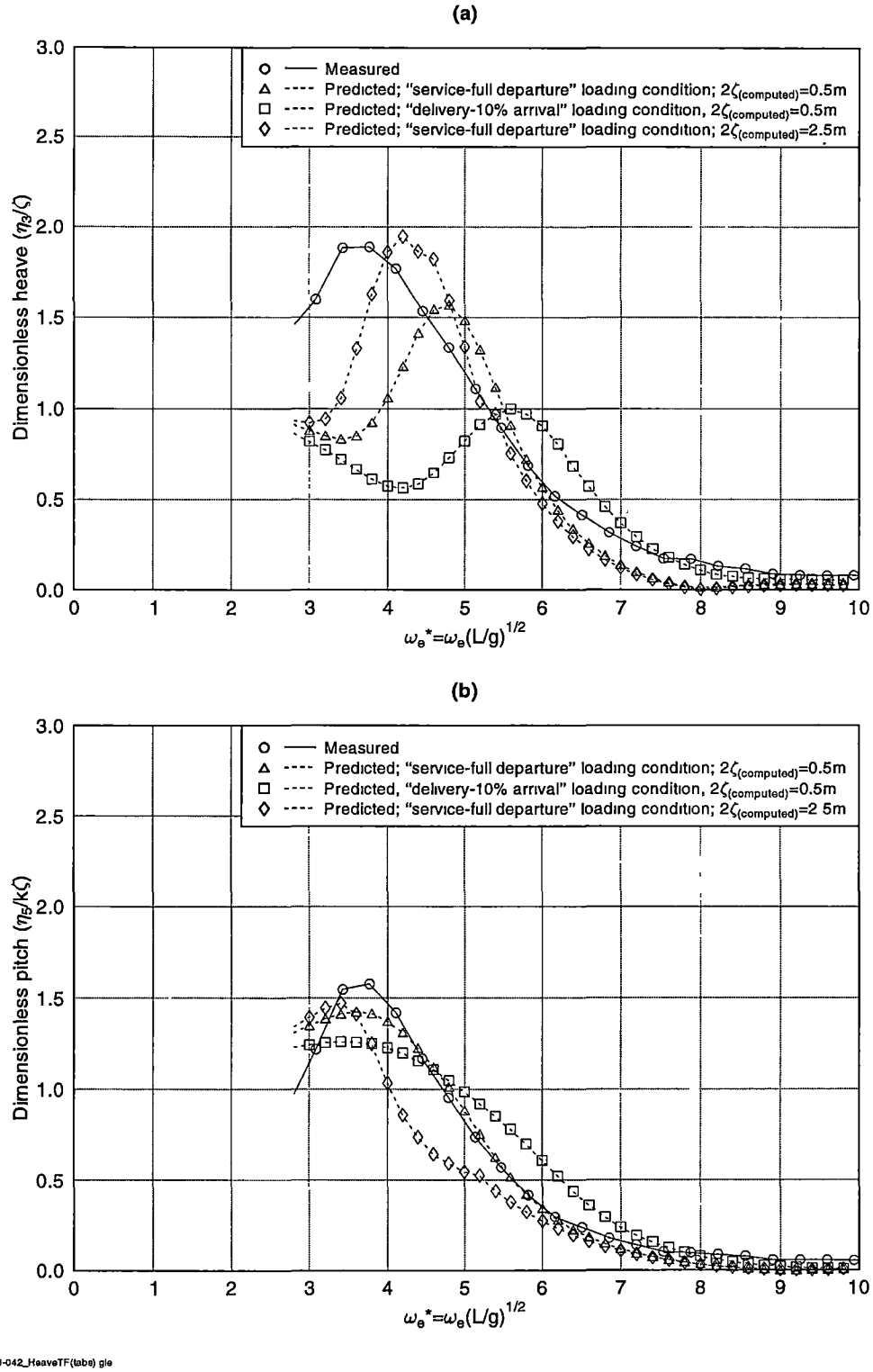

Figure 6.2: Transfer function comparison in (a) heave and (b) pitch (86m vessel, 32.5kn, active tabs only)

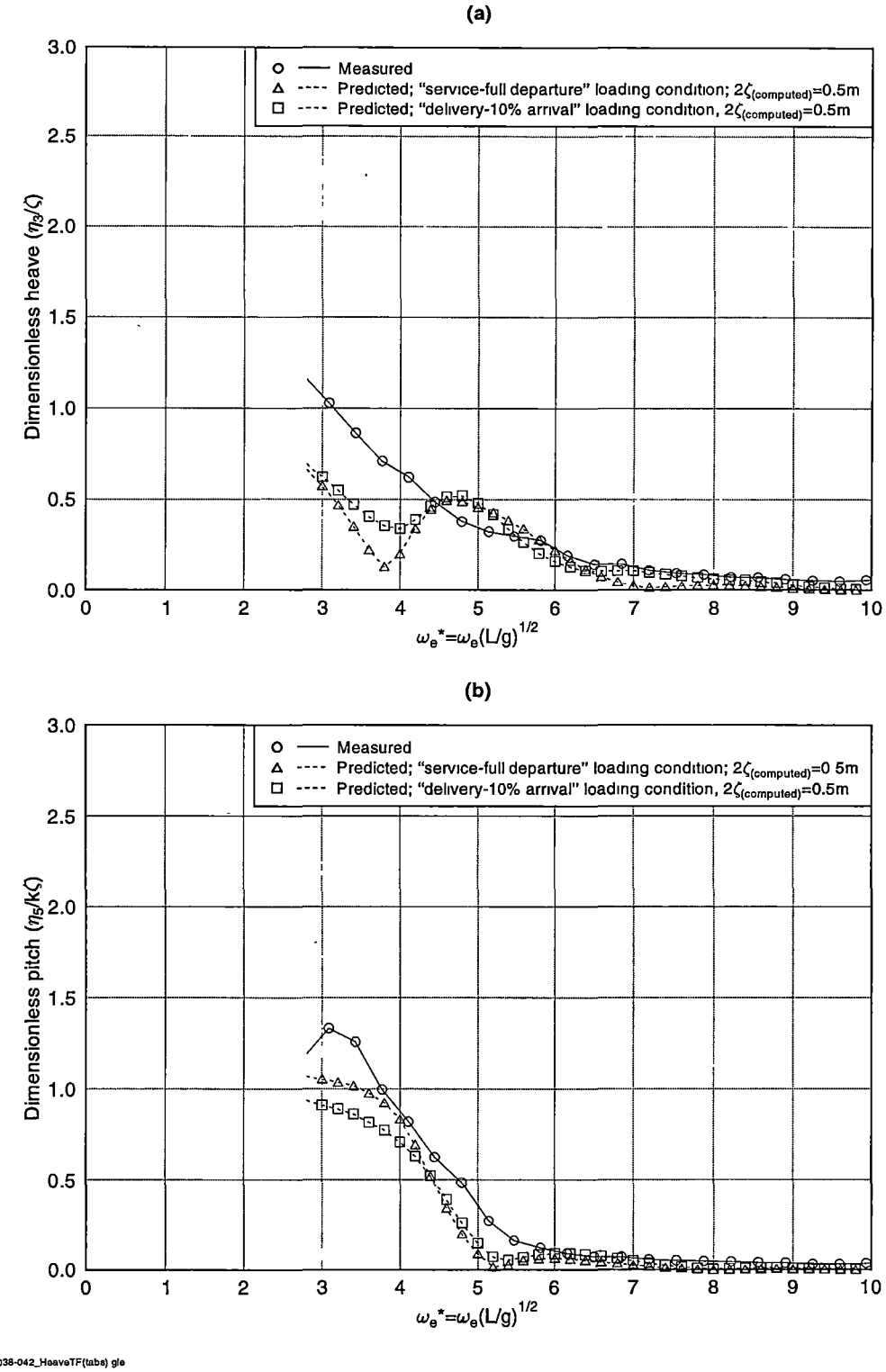

Figure 6.3: Transfer function comparison in (a) heave and (b) pitch (86m vessel, 12.5kn, active tabs and T-foils)

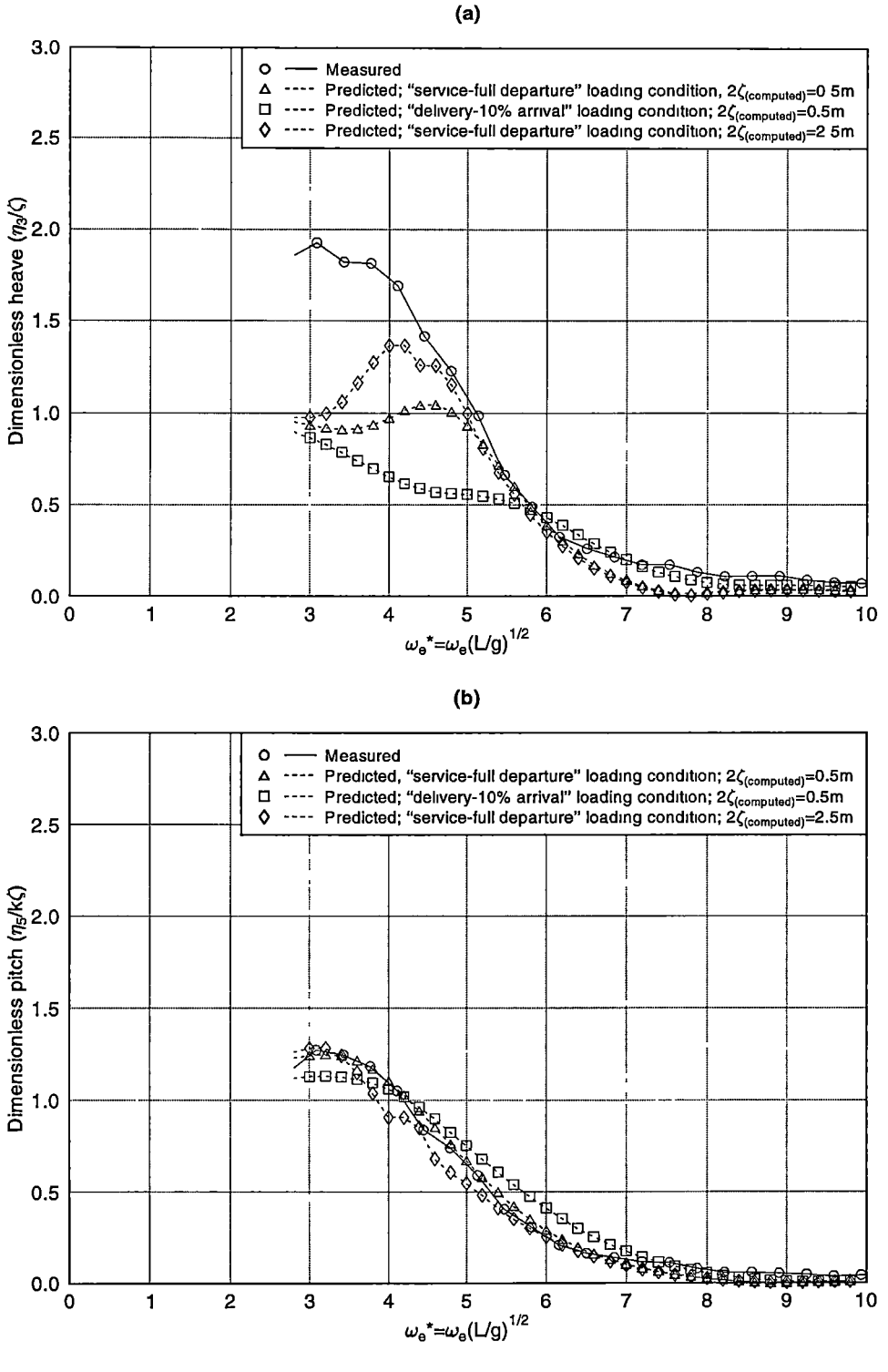

Figure 6.4: Transfer function comparison in (a) heave and (b) pitch (86m vessel, 32.5kn, active tabs and T-foils)

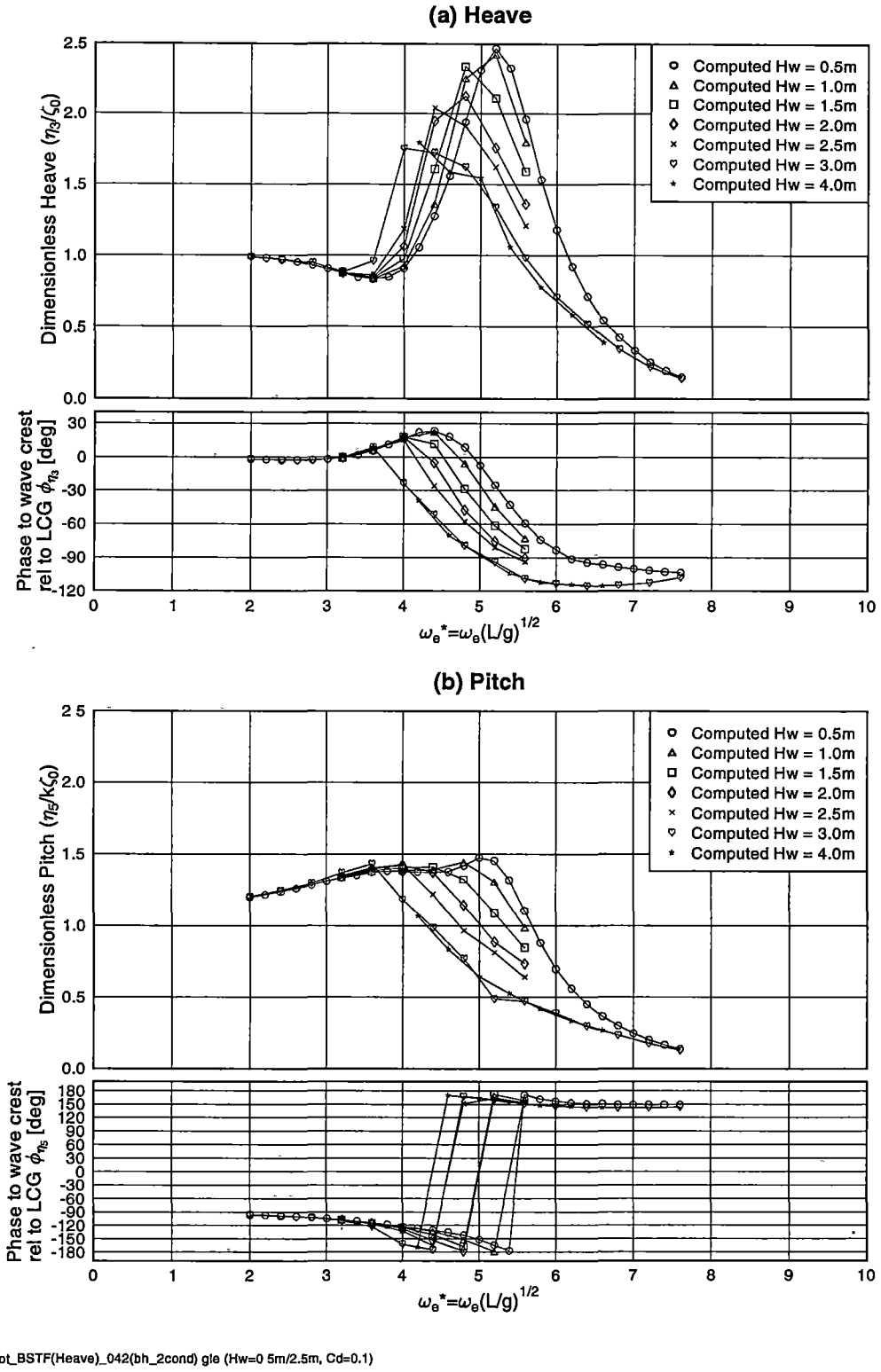

ref/plot_BSTF(Heave)_042(bh_2cond) gle (Hw=0 5m/2.5m, Cd=0.1)

Figure 6.5: Transfer functions in (a) Heave and (b) Pitch using BEAMSEA with computations at various wave heights (86m vessel, 37.5kn, Hull loading condition not available)

6.3 Comparison of Accelerations Relative to Wave Height

6.3.1 Variation of Relative Acceleration with Wave Period

The results obtained from full-scale measurements and predictions in head seas of accelerations per unit wave height (RMS) are shown in figure 6.6 for hull configurations that include active tabs that reflect the delivery voyage records and active tabs and T-foils that reflect the data records obtained during service operations. All data obtained from measurements are displayed in these diagrams that include the speeds between 12.5 and 32.5 knots in increments of 5 knots for the active tab configuration and the speeds of 12.5, 17.5, 32.5 and 37.5 knots for the active tab and T-foil configuration. The predictions in the former set show the 12.5, 22.5 and 32.5 knot results whilst the later set show the predictions for 12.5 and 32.5 knots only as these are sufficient for comparative purposes.

It is clear in these results that the measured data produced higher accelerations at the LCG than the predictions suggest at all periods shown. However, for wave periods over 7 seconds both the measured and predicted results show that the acceleration magnitude decreases with increasing wave period. Furthermore, both the predicted and the measured results show that the accelerations decrease with speed. The differences between the results may be due to the spread of wave directions present at the time of full-scale measurements that increased the acceleration above what would normally be the case with long crested waves, which were used in the numerical computation for the predicted results. The computed results are based on the relatively narrow band Bretschneider wave spectrum (see sections 4.3.2, 5.3.2 and appendix E) whereas the measured data was obtained in conditions that were quite variable and therefore had a broader spread of wave energy from various directions for a range of encounter frequencies.

Differences of up to 5.2 metres are known to exist between the assumed LCG location for measurements (32.2m forward of transom) and computations (27.035m to 30.324m forward of transom), which may contribute to the differences in acceleration. This is expected to be small but not necessarily insignificant (see also section 6.3.2). Therefore the differences seen between the measured and predicted results are to be expected. This is also supported by evidence seen in the previously compared transfer functions of section 6.2 that showed differences consistent with these acceleration results.

6.3.2 Variation of Acceleration with Longitudinal Position

The accelerations per unit wave height over the length of the vessel on the hull centreline are shown in figure 6.7 for both measured and predicted results. In the measurements only the results corresponding to the locations of the vertical accelerometers are shown whilst the predicted results show the accelerations per unit wave height at the six longitudinal positions (i.e. AP, 0.25Lpp, LCG, 0.5Lpp, 0.75Lpp, FP). The predicted results are based on a Bretschneider wave spectrum of 2.5 metre significant wave height, which may be slightly higher than the average wave height for which the measured data was obtained. As discussed in the previous section it is known that there is a difference between the spectrum assumed for predictions and the wave energy spectrum for which the measurements were obtained. This in itself could lead to the appreciable variation in the relative accelerations determined here.

The results in some cases show reasonable agreement between the measured and predicted data in figure 6.7(a), which shows the configuration with only transom tabs.

In particular the result at 22.5 knots has quite good agreement simultaneously over the length of the vessel whilst the 12.5 knots case has good agreement in the bow and LCG but not at the aft end. Furthermore, the 32.5 knot case has good agreement in the aft end and at the LCG but not at the bow.

The results in figure 6.7(b) show the configuration with tabs and T-foils. The predictions at the bow over estimate the acceleration at 12.5 knots but under estimate relative acceleration at 32.5 knots. The predicted outcome in the stern at 12.5 and 17.5 knots are unusually small.

Overall the general shape of the longitudinal distributions are consistent between measured and predicted data, although there are variations at some speeds and positions. However, based on the results discussed in preceding sections one would expect the agreement between measured and predicted not to be exact. As discussed, the most likely contributory factors are differences between encountered wave energy spectra for measured and predicted responses, variability of sea direction for the measured data, wave amplitude effects on the transfer functions and consequent derivation between predicted and measured encounter frequency of maximum response transfer function.

6.4 Summary

This chapter has presented selected comparisons between the measured and predicted results for the 86 metre vessel considered in the present analysis. Key findings from these results include:

Transfer function comparisons

1. The 12.5 knot results showed the closest prediction to measured data. To obtain better comparisons at this and other speeds, other unknown variables may need to be isolated, such as wave directional spreading and wave height. In general, the comparisons had the potential to be better than those obtained but the variability of the wave environment was the greatest factor in the discrepancies between measured and predicted results. Wave height non-linearity may also contribute to the variations seen.

2. Further results using a more recent program for computational hydrodynamic solutions support the finding that there is a reduction in the frequency of maximum response as the regular wave height increases. Also, the maximum response of the transfer function tend to decrease with regular wave height. This remains a topic for further investigation.

3. The pitch motion was generally in better agreement than the heave results and was less sensitive to variations in loading condition.

Accelerations relative to wave height

1. The measured accelerations were higher than the predicted accelerations however, in both cases the acceleration decreased with increasing periods over 7 seconds and in both cases the accelerations decreased with speed.

2. Differences seen in the transfer functions are also evident in the acceleration comparisons but trends of acceleration decreasing with increasing wave period over 7 seconds remained similar between the measurements and predictions. Also, the accelerations generally decreased with speed.

3. The trends in the vertical acceleration with longitudinal distribution showed similarities. Although there were some variations, the general shape of the longitudinal distributions was consistent between the measured and predicted data.

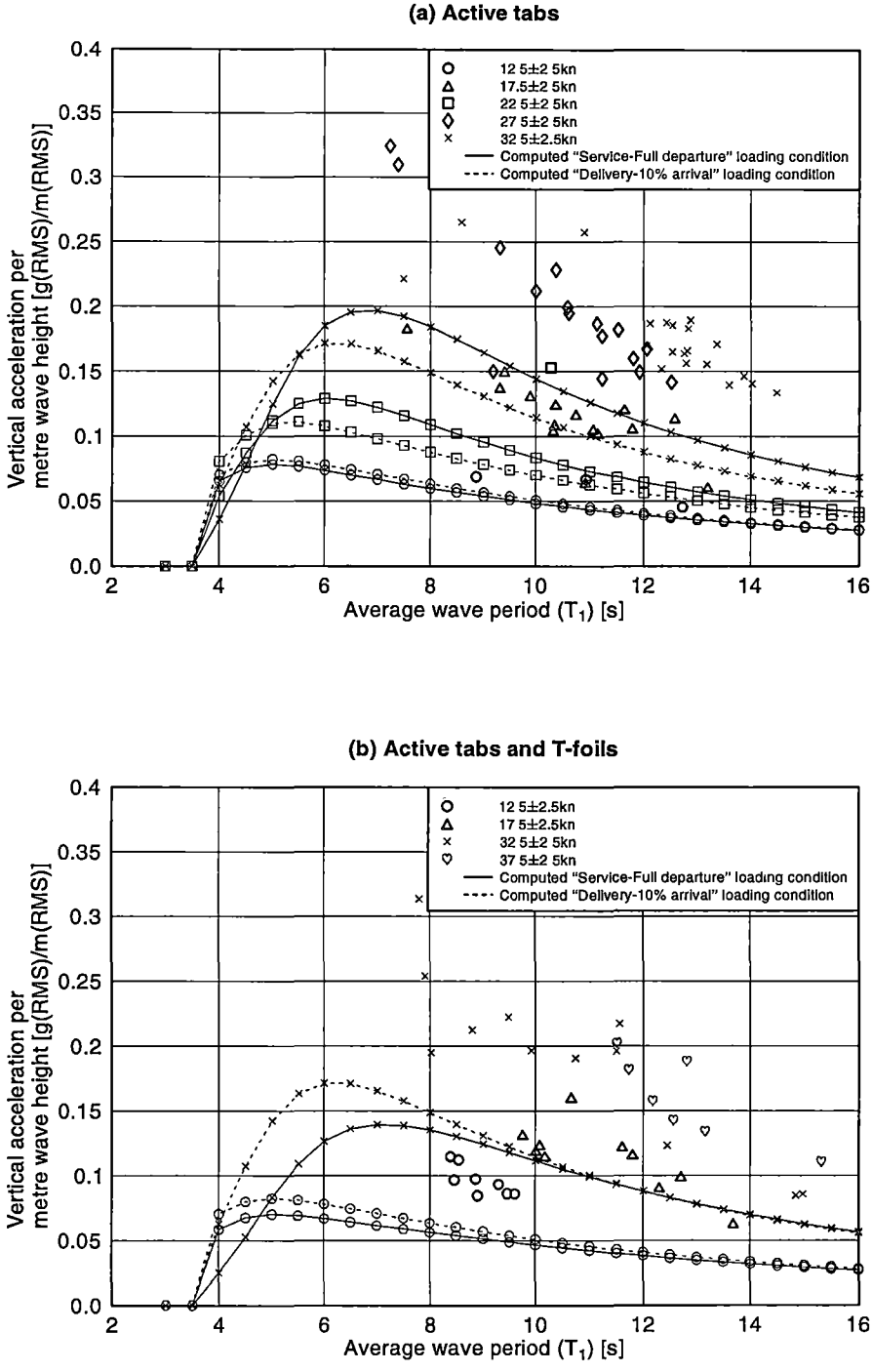

Figure 6.6: Comparison between computed and measured acceleration per unit wave height (RMS) at LCG in head seas for (a) active tabs and (b) Active tabs and T-foils (86 metre vessel. Note: data points laying on the lines are computed results; other points are measured results)

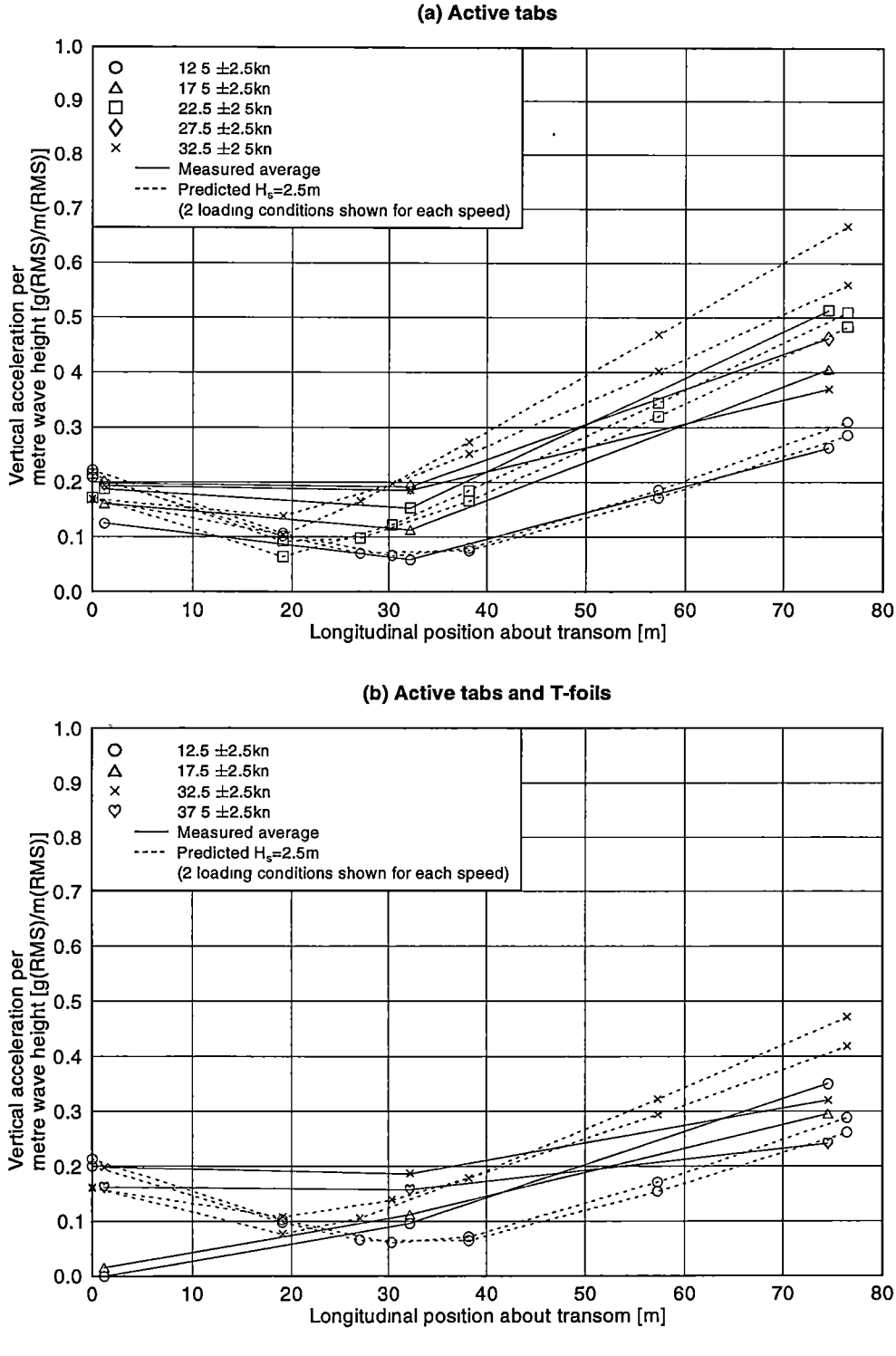

Figure 6.7: Comparison of predicted and measured distribution of acceleration per unit wave height (RMS) in head seas for (a) active tabs and (b) Active tabs and T-foils (86 metre vessel. Predicted results show both the "Service-full departure" and the "Delivery-10% arrival" loading conditions, although no distinction is made between the two)

Chapter 7

Discussion and Conclusions

7.1 Introduction

The objective of this thesis was to implement full-scale measurements of hull motions for two high Froude number vessels. By accounting for the effects of the wave environment and the motion control system, the motion responses could be reconciled to show that the numerical computation could model the vessel motions with reasonable accuracy according to results extracted from full-scale measurements.

The wave environment was measured with the use of a ship mounted one-dimensional microwave proximity radar that measured the sea surface profile. Through using the vessel as the means of determining the primary wave direction, spectral analysis was able to show similar characteristics between full-scale measurements and numerical predictions.

7.2 Overall Conduct of the Sea Trials Program

The sea trials conducted as described in chapter 2 essentially laid the ground work to provide the outcomes of this analysis and as such were perhaps the most important aspect of the investigation. It is clear that for a trials program to be successful it must contain clear objectives and processes for the data records to be utilised in the most efficient manner and for significant outcomes to be achieved. One of the major difficulties in this process is the cost of instrumentation from which basic motion data can be extracted with the greatest amount of accuracy and least amount of noise contamination. At the time of these experiments the cost of instrumentation to measure six degrees of freedom was considerable and so the measurements had to rely on the use of linear accelerometers when the ship system motion sensors were not available. This was not such a severe limitation in the measurement procedure because by comparison the measurement of the wave environment was the more complex and technically difficult area of measurement based on the available instrumentation. Measurement of the ship motion was however of great importance together with the wave measurement as it was required to resolve the vessel response and transfer functions.

An uncertain aspect of full-scale measurements is the amount of data that might be returned as the result of deployment of instrumentation on a vessel. This in some respects could be better planned with access to historical wave data should the vessel be operating on a known route, but in the case where the operating route is not well known or defined then having the flexibility to leave instrumentation on a vessel for a significant amount of time was the only alternative approach around this issue. This would then maximise the quantity of data collected during a given duration of the

measurement program, but there will always be the uncertainty of the precise sea conditions encountered and the impact of this on the final results of the investigation. Given the generally high cost of installation of the instrumentation it would make more sense where possible, for the instrumentation to form part of the essential ship equipment that would be on the vessel permanently. This would include equipment that forms part of a comprehensive motion control system that remains with the vessel for the duration of its operational life. There is then every expectation that over the duration of several years enough data could be collected for analysis for a variety of sea conditions and vessel speeds. In the present work even though the vessels were exposed to a range of different geographical areas in various oceans during the delivery voyage and during the course of normal operations most of the data for the 86 metre vessel was collected on the route in the English Channel. The range of wave periods and wave heights were not such a problem as obtaining enough wave headings relative to the forward speed of the vessel. In particular, rather limited quantities of data were obtained in head seas. Furthermore, the reality that the vessel was operationally limited because of wave height restrictions meant that quantities of data from the vessel in large wave height conditions was simply not available. However, more low wave height data could have been obtained with a lower setting on the automatic data acquisition trigger level. At the commencement of the investigation selection of the acquisition trigger level presented a difficult decision, balancing the storage capacity of the on board computer against the intervals at which it could be accessed. The overwhelming dominance of the bow quartering and beam seas in the results obtained in this analysis demonstrate that the wave headings were severely limited by the set nature of the operating route. Although the large amount of data from these headings were beneficial, the bow headings data was severely limited.

The procedure for wave measurement used in this work precluded the wave direction determination directly from the onboard instrumentation. More advanced equipment such as wave radar that could determine the statistics of the three-dimensional environment surrounding the ship was not available. Ideally the entire wave climate surrounding the vessel would be measured to create an accurate and comprehensive understanding of the wave environment, including its directional and frequency components in a moving frame of reference on the vessel with the ability to convert this information to a stationary frame of reference. However, in the circumstance where such instrumentation was not available, then the method of determining the wave direction through analysis of the ship motions has been shown for twin-hull vessels to be a practical means of determining the average wave direction and can provide essential but general average information about a critical variable for the analysis of ship motions. In this case the primary wave directions became clearly evident from the data but unfortunately it was not possible to determine the range of wave directional components that contributed to each wave spectrum. This was particularly evident in the data where roll did not reduce to zero in the head sea data because of the directional wave components that always lie outside the primary wave direction.

The development of transfer functions relies primarily on the quality and quantity of wave data, the ship motions data and the ability to sort the data into subsets based on the operating variables. These include the wave period, wave direction, vessel speed, vessel loading condition, motion control surface configuration and where possible wave height. It was of course essential to obtain a sufficient duration of data for subsequent spectral analysis within each of the subsets of data. In the present work, even after collecting data for more than a year of regular operations, it was only possible to analyse data in subsets defined by two parameters only, the vessel speed and sea direction.

The transfer functions, despite the detailed differences between measured and predicted outcomes, show that the magnitude of maximum response generally decreases with speed. Also the measured results showed that a reduction in speed did not always give a reduction in vessel accelerations. However, the roll actually increased as the speed reduced and did not begin to decrease until the speed was less than 22.5 knots.

It is apparent from the wave conditions measured on each vessel that the wave height and period in the operating environment can vary significantly as they did in these measurements, but this may not always be the case. Wave conditions very much depend on the operational route of the vessel, which leads one to believe that during the design of a vessel, the wave environment in which it is to operate should be considered. Even within the wave height limitations placed on the vessels considered in this analysis, the average wave periods varied between 6 and 20 seconds. With the vessel encountering bow quartering, beam and stern quartering wave directions for the majority of the time it make sense that the design of the vessel for this route should be considered in combination with these factors. They are the governing conditions, which in combination with the vessel response to those conditions will ultimately influence the passenger comfort. One therefore must appreciate that the vessel design for motion comfort could ultimately be driven according to a range of motion criteria, such as motion sickness incidence (MSI) where based on a definition of acceptable motion levels the hull shape and motion control system is considered with respect of the wave environment in which the vessel is to operate. On this premise, there is no reason the owner or operator of the vessel could not commence operations based on a well planned set of outcomes that will meet pre-determined target expectations. However, whilst certain sea conditions may predominate, such as the relatively long period bow quartering seas on the service route in the present investigation, there will always be perhaps rare occasions where encountered conditions will deviate from the most common. Thus the selection of a vessel will ultimately depend on achieving an appropriate balance between the most common and rather uncommon sea conditions. However, close matching of a vessel design to a particular route (as in the case of the SWATH form HSS for example) may result in consideration of a vessel that is not flexible with regard to the routes that it can service and which is therefore of limited value to its various owners.

Based on results obtained from full-scale measurements there was no conclusive evidence that the vessel speed was limited by wave height. However, there was stronger support for the proposition that the speed of the vessel as operated is strongly influenced by the wave slope, which is a function of wave height. This evidence is not supported by the beam sea results but it was quite strongly supported for the bow and bow quartering wave directions.

7.3 Computational Investigation of Response

The computations undertaken for the 86 metre vessel provided transfer functions, acceleration spectra and accelerations per unit wave height for hull configurations that included active motion control surfaces for the head sea wave direction only. These results indicate that at larger displacements the motions of the vessel improved because there was an increase in mass and radius of gyration, both of which increased the hull inertia. These effects reduced the frequency of maximum response and thus also reduced the accelerations, which reduce with the square of the frequency. This outcome is evident in both the transfer functions and the acceleration magnitudes.

Some computations using higher computed regular wave heights of 2.5 metres

showed that there were nonlinear effects in the motion response per unit wave height that should be considered. These effects were particularly evident in the transfer functions where there was a reduction in the frequency of maximum response as well as a general change in the shape or magnitude of response with frequency.

The method introduced to determine the gains for the active control surfaces proved to be useful but had limitations in the range of wave heights and speeds at which the gains could be successfully determined. This excluded combinations of low speeds and higher wave heights where the force of the control surface was small in proportion to the overall wave force on the hull. This was evident where either a regular periodic solution could not be achieved or the effect of the control surface on the vessel was so small that it was not possible to determine a set of gains that minimised the motions.

It is clear that in cases where resonance is identified in the transfer functions, the vessel is not critically damped and there remains some scope for the size of the motion control surfaces to be increased[1]. This was particularly evident in transfer functions obtained from both measurement and prediction. An increase in the size of the control surfaces would increase their damping force capability and thus their effectiveness in higher wave heights. The computations showed that the existing arrangement of active control surfaces that included a transom tab and T-foil in a head sea of significant wave height of 2.5 metres, the average acceleration over the length of the vessel could be reduced by up to 39% compared with the hull without control surfaces. This improvement with active control surfaces was increased at the light vessel displacement compared with the heavy displacement.

It was clear in the head sea computations that a reduction in speed did not necessarily mean a reduction in accelerations at specific positions on the vessel particularly the forward and aft perpendiculars. However, on average the accelerations did tend to reduce with speed.

The motion sickness incidence (MSI) computed at the regular wave height of 0.5 metres and combined with a Bretschneider wave spectrum of 2.5 metres showed that the MSI (expressed as a percentage of the total passenger population) was reduced from 38% to 23% with active control surfaces fitted (a reduction of 39%). This reduction was of similar magnitude to the reduction achieved in accelerations, which is not unexpected.

7.4 Comparison of Measured and Computed Motions

It is clear from the computed and measured results in head sea waves that the computed motions did not accurately predict the outcomes obtained from measurement. This was still the case even when the numerical computation used the higher regular wave height, which had a lower maximum heave response frequency than that achieved with

[1]Whilst outside the scope of the present study, this issue requires further research and is an aspect of motion control systems that refers to the motion on vessels in relation to the size of the selected control surfaces. They usually remain undersized in terms of their potential to reduce the motions of a vessel in a given wave height, because of other practical constraints on the vessel's performance, such as resistance.

The performance of control surfaces (or other devices) depends on the selected motion criterion. In the present study this consisted of the average vertical acceleration taken over the hull length. If for some reason the criterion is based on the reduction of roll or pitch displacement only, then the true effectiveness of the devices may be over stated in relation to the improvement felt by the crew or passengers. The vertical and lateral accelerations primarily contribute to passenger comfort. So whilst a comprehensive set of criteria may consider the motions of the rigid body in all six degrees of freedom, a minimum criterion set should at least consider the degrees of freedom affecting the vertical and lateral planes.

computation using a lower regular wave height. This indicated that the differences may have been the result of factors other than wave height nonlinearity or loading condition. Furthermore, it suggests that the measured wave environment was not sufficiently well defined for the numerical predictions to show close agreement with the measured data, particularly at the higher speeds. Had the wave conditions been better defined and thus better modelled in the computation, particularly with regard to direction, one would have expected the measured transfer functions to have fallen within the band of the predicted results obtained for the heavy and light loading conditions (i.e. "service-full departure" and the "delivery-10% arrival" loading conditions respectively).

The unknown factor in these comparisons is the characteristics of the wave environment that was discussed in chapter 4 with respect to the variability of the directional wave spreading and thus very broad banded nature that seems to be typical of the measured wave environment. By comparison, the predictions are calculated in regular waves of constant wave height and generally must assume linearity. What arises from the comparison of results is that it is difficult to make a determination whether the variations between computed and measured results are because of the wave environment not being well defined during the course of measurements or whether the nonlinear behaviour in the vessel motion response occurred with the increased wave height. It seems most likely that the outcomes are a result of both these influences. However, one must suspect that because the predictions at the higher regular wave height were unsuccessful in fully resolving the differences between the measurements and the predictions, the general nature of the measured wave environment was not well enough defined for it to be adequately represented in the computations. This also raises the possibility that if the numerical prediction is doing a reasonable job, which previous publications suggest is the case, then the deficiency may rest in how well the wave environment is defined and whether the nonlinear behaviour of the vessel at higher wave heights makes comparison in the frequency domain with full-scale measurements an exercise that indeed requires much greater detail regarding these variables.

Compared with the measured data of the 86 metre vessel response in bow quartering seas, which had over 29 hours of data during the delivery voyage and over 45 hours during service operations, the quantity of head sea data was significantly less, containing approximately 2 to 3 hours for all speeds combined. The most data allocated to any one speed only reached 75 minutes on the delivery voyage and 41 minutes in service operations. This ultimately results in measured data of lesser quality and this can be seen by comparing the various measured transfer functions of these two wave headings shown in figures 4.25 to 4.30 of chapter 4. It can be seen that the transfer functions at the wave heading of 135 degrees have much smoother and better regularity than the head sea (180 degree) diagrams, which are used for comparison with the predicted head sea data in this chapter. Despite these irregularities there is not any evidence that the measured results in head seas were producing any significant error, as the transfer functions in bow quartering seas also have a comparatively low frequency of maximum response and were not greatly different from the results in the head sea measurements.

There are of course other questions that are not revealed in the details of the data that may have influenced the results. Table 4.4 shows the average wave height for each data group defined by speed, hull configuration and wave heading and showed that the average significant wave height varied between 1.32 and 2.56 metres. In the light of the large amplitude computations described in chapters 5 and 6 it seems that this wave height is greater than that which might reasonably be expected to produce a linear result based on the actual hull shape. The non-linearity with wave height however, is likely to have a lesser effect than the influence of a confused measured sea state with

a broad spread of wave directions as the comparisons with numerical predictions have indicted in previous discussion.

The full-scale vessel also had the influence of steered waterjets that may in general impose a variable horizontal and vertical component of thrust at the aft end of the hull. One would assume that these forces are approximately constant and would tend to trim and sink the hull by some constant amount. In most instances this could be counteracted by the trimming offset imposed on the transom tabs. However, the force of the water jet inlets seems unlikely to be sufficient to cause substantial irregular and unsteady heave and pitch forces that could influence the motion response in waves. This can not be verified within the scope of this investigation without knowing the variation in the thrust vector produced by the waterjets when the vessel is oscillating in waves.

The full-scale vessel also had a centre bow that was not modelled in the computation but was nevertheless present on the full-scale vessel. However, the centre bow has a relatively fine deadrise angle from its keel and is significantly displaced above the still water line. Its effect is therefore expected to be small except in relatively large seas in which tunnel or wetdeck slamming may occur. The operational limitation of 3 metre significant wave height for the data records collected during service operations thus precludes significant forces arising on the centre bow at least for this set of data records.

It is obvious that for the predictions to compare favourably with the measurements the frequency of maximum response must coincide as also must the magnitude. If the frequency of maximum response and the shape of the transfer function are already well predicted, then it is a relatively easy exercise to adjust the peak by tuning the levels of damping applied in the numerical predictions. However, if the frequency of maximum response does not coincide and in addition the shape of the transfer function does not resemble the measured outcome then adjustment of damping in the computed solution will not resolve the issue. One therefore must suspect that the variations between measured and predicted outcomes may be merely influenced by the one-dimensional wave assumption of the predicted results and non-linear wave height effects.

7.5 Specific Outcomes of the Investigation

The research program conducted here has involved the combination of an extensive program of sea trials involving installation of instrumentation on two vessels and data collection over a total period of approximately two years. This has been complemented with a computational investigation of various aspects of the motion response of the vessels. The overall outcomes of the work are as follows:

1. **Determination of sea direction from ship motions records:** A method for determining the primary direction of the encountered sea by analysis of the ship motions record has been successfully implemented. The method has some limitations in that it relies on the well defined pitch and roll motions of a catamaran configuration, and in its present implementation it is essentially founded on the dominance of relatively long wavelength seas for which there is unit response to encountered waves. The latter aspect could be refined by developing the method to incorporate the effects of less than unit response for short seas if necessary. However, notwithstanding these limitations the method has formed an adequate basis for data records to be assigned to broad directional sets and it has therefore met the requirements of this first investigation undertaken anywhere along these lines.

2. **Selection of ride control algorithm parameters:** A computational method has been developed for the optimal determination of motion control system algorithm parameters and has been shown to be effective in maximising motion reductions. Whilst it must be recognised that the computational method available here has limitations, in particular that the program BESTSEA had only the capability of resolving head sea motions, the method clearly shows promise. The method has potential for future development to optimise parameter selection for a range of sea directions using the very recently developed program BEAMSEA, which was not available at the time of the present investigation.

3. **Nature of encountered sea conditions:** The data collected from the two vessels in the present investigation has give insight into aspects of encountered sea conditions. Whilst more severe conditions of wave height were encountered on the delivery cruises, the service operations being restricted to 3 metres maximum significant wave height, it is clear that sea conditions on particular routes will present very individual features, which should be considered when assessing vessel suitability. In the case of the two measured vessels of this investigation it is particularly evident that the operational route presented primarily bow quartering seas and that the wave periods were relatively long due to exposure to incoming ocean swells. Even though this route is well known and experienced crew might have been able to give a general indication of these aspects when the vessels were first put into service, it is true to say that the route sea conditions were not known by the author to this level of detail prior to the conduct of this investigation. It is however, fair to say that such information may have been available from oceanographic institutions such as the United Kingdom Meteorological Office (UK Met Office) prior to the measurements but is usually often associated with considerable expense and therefore not readily available. No doubt similar limitations regarding the detailed character of sea conditions on other routes would also exist. Indeed, there may in many cases be excessive reliance placed on the use of more general sea condition data, such as generalised relations between wave height and wave period of the type developed by Darbyshire and Draper (1963.). The present results show that a direct application of such general data to this particular operating route is inappropriate since wave periods are greatly increased by the contribution of ocean swells. This may be a more common feature of coastal ferry routes than is often realised.

4. **Vertical accelerations on board vessels:** There has been a generally good correlation between measured and predicted on board accelerations. These are very strongly influenced by the response of the vessel and acceleration spectra are generally quite sharply peaked in form. Also it is clear from both measured and computed data that motions towards the bow are much more severe. This is almost an inevitable feature of this type of vessel and can only be circumvented by SWATH designs, such as the Stena HSS. However, SWATH designs are very prone to deck diving in following seas and have been subjected to significant bow damage as a result. Therefore extreme caution has to be taken when operating a SWATH vessel in following seas. Whilst the present vessels do have wave piercing bow forms, it is clear form the present work that their response is nearer to that of a conventional vessel than to a SWATH. Moreover, the adoption of an elevated centre bow present on the full-scale vessels but absent in these computations confers an increased measure of seaworthiness to the vessels in more severe and following seas and makes them generally more versatile and better suited to new

spheres of freight or military operation. However, in passenger service it is clear that passenger accommodation should be strongly concentrated towards the stern so as to minimise passenger discomfort.

5. **Vessel motion response transfer functions:** The investigation has found a good measure of agreement between measured and computed transfer functions with regard to the effect of vessel speed and wave encounter frequency. However the present investigation has necessarily been limited to head sea comparisons, and it is evident that further investigation of the effects of sea direction and wave height is needed. In particular some computations with BESTSEA and further preliminary investigations using the more recently developed program BEAMSEA has shown that nonlinear wave height related effects seem likely to go some way towards resolving the issue of the frequency and magnitude of maximum motions.

7.6 Implications of Research

The results of this study show that the methods employed here to model full-scale vessels can reasonably well reproduce the motion characteristics of full-scale vessels. With the ability to conduct further experiments with a greater range of recorded variables it should be possible to determine a vessel's characteristics more accurately in all wave environments. The data analysis might then be extended to also show the non-linear characteristics of vessel response with wave height and wave period. Furthermore, it is clear from the results that given the inevitable limitation of measurement time frame and opportunity, full-scale measurements may not provide the full range of conditions required. This would leave model tests as the only alternative. The reason for this is two fold. Firstly, as the wave increase in size or the vessel motions become uncomfortable, the first reaction from the crew will be to slow the vessel or to change course. This will almost always be done with the same regularity making measurement of extreme vessel responses rare or unattainable during normal operations. Secondly, the route and timing of the vessel operations during the measurement period may not provide the vessel with a full range of wave heights, directions and periods. Even if the range of available wave heights and periods are exceptional then the opportunities to have measurements made at every wave heading may not occur.

A natural extension of this research is the option for all vessels to not only be fitted with monitoring equipment but also to have extended capacity for the data to be analysed on a regular basis. Given that installation of a motion control system necessarily demands installation of motion sensors, it seems that the additional items required for a long term measurement programme are provision of data storage capabilities and also installation of a wave sensor. Provision of data storage facilities need not be a particularly demanding requirement given advances made in this area in recent years. However, a more economic wave sensing system that the TSK radar would be needed if more extensive data collection involving a number of vessels is to be contemplated.

7.7 Other Matters for Future Investigation

There are various directions of study that could be pursued in future in relation to full-scale measurements and obtaining verification with numerical prediction methods. These areas include:

- further study into the use of wave measurement from the platform of a moving vessel and obtaining three dimensional wave spectra;

- conduct of model tests for comparison with full-scale measurements to determine the extent that full-scale phenomena can be duplicated at model scale;
- through collection of an increased amount of data it may be possible to add the category of wave height to the data collected and thus conduct a more rigorous analysis of the full-scale vessel response to a wave system is more accurately described;
- numerical modelling in this analysis was based on the superposition of regular waves and on the basic assumption that the linearity exists in the computations. Furthermore, the wave environment was based on a wave spectrum that assumed all waves came from one primary wave direction. If a better three-dimensional model of the measured wave environment could be captured then duplication in the numerical prediction may produce better comparisons;
- the motion control systems on full-scale vessels operate in an irregular wave environment. It is unknown therefore whether the modelling of control surfaces in the frequency domain according to the method of this analysis does reflect the operation of these systems in irregular waves. A natural extension of modelling is therefore to give the numerical method the ability to compute directly the response to irregular waves, thus allowing the ship based control algorithm to be implemented directly in the numerical prediction. However, in proposing this option, it must be said that suppliers of motion control systems are understandably reluctant to release full details of their control algorithms and strategies. This issue could be partly overcome by data logging the control surface deflections. Numerical modelling using irregular waves directly may be a means of making a better comparison between measurements and numerical predictions. This would then place the subsequent data analysis from both measurements and numerical predictions on an identical basis and the same spectral analysis would then be performed on both sets of results. Thus the comparison would be more direct than has been possible here.

Bibliography

Adams, J. (1994). Condor, *Fast Ferry International* pp. 17–23. May.

Adams, J. D. (1996). Advances in Motion Control of High Speed Ferries, *International Cruise and Ferry Review* **Spring/Summer**: 143–145.

Akers, R. (1999). Motion Control, *Professional Boat Builder* pp. 82–95. October/November.

Aksu, S., Sanford, D., Hammond, L. and Cannon, S. (2002). Evaluation of Seakeeping and Motion Characteristics of the Royal Australian Navy Wave-Piercing Catamaran HMAS Jervis Bay, *in* L. Prandolini (ed.), *Proceedings of Pacific 2002 International Maritime Conference*, pp. 88–97. see also The Australian Naval Architect, 6(1) pp. 23-28.

Anonymous (1999). Navigation and other systems - hybrid anti-rolling system, Shipbuilding and Marine Engineering in Japan (JSEA). Advertisement from Ishikawajima-Harima Heavy Industries Co.

Australian Standard, AS 2670.3 (1990). Evaluation of Human Exposure to Whole-Body Vibration, Part 3: Evaluation of Exposure to Whole-Body Z-Axis Vertical Vibration in the Frequency Range 0.1 to 0.63 Hz, Standards Australia. ISBN: 0 7262 6342 7.

Australian/New Zealand Standard, AS/NZS 4476 (1997). Acoustics: Octave-Band and Fractional-Octave-Band Filters, Published jointly by Standards Australia and Standards New Zealand.

Bachman, R. J., Lai, R. J. and Foley, E. W. (1987). Directional Wave Measurements for Application to Ship Trial Analysis, *in* R. F. Messalle (ed.), *Proceedings of the Twenty-First American Towing Tank Conference*, David W. Taylor Naval Ship Research and Development Center, Bethesda, Maryland, National Academy Press, Washington, D.C., pp. 399–405.

Barber, N. F. (1954). Finding the Direction of Travel of Sea Waves, *Nature* **174**: 1048–1050.

Beauchamp, K. G. and Yuen, C. K. (1979). *Digital Methods for Signal Analysis*, George Allen and Unwin Ltd., chapter 4 - Spectral Analysis; 5 - Correlation Analysis, pp. 131–211.

Beaumont, J. G. and Robinson, D. W. (1991). Classification Aspects of Ship Flexibility, *Philosophical Transactions of The Royal Society of London, Series A - Physical Sciences and Engineering* **334**(1634): 371–389.

Beck, R. F. (1994). Time-Domain Computations for Floating Bodies, *Applied Ocean Research* **16**: 267–282.

Beck, R. F., Cao, Y. and Lee, T.-H. (1993). Fully Nonlinear Water Wave Computations Using the Desingularized Method, *Sixth International Conference on Numberical Ship Hydrodynamics, The University of Iowa* .

Beck, R. F., Cao, Y., Scorpio, S. M. and Schultz, W. W. (1994). Nonlinear Ship Motion Computations Using the Disingularized Method, *Twentieth Symposium on Naval Hydrodynamics, Santa Barbara, California.*

Bendat, J. S. and Piersol, A. G. (1980). *Engineering Applications of Correlation and Spectral Analysis*, Wiley-Interscience Publication, John Wiley & Sons, Inc. ISBN: 0-471-05887-4.

Boulton, C. (1999). The AMD Wavepiercing Catamaran - Seakeeping Excellence, World Wide Web: http://www.amd.com.au/papers/350se/350se.html.

British Standards, BS 6841 (1987). British Standard Guide to Measurement and Evaluation of Human Exposure to Whole-Body Mechanical Vibration and Repeated Shock.

Brown, J. C., Clarke, J. D., Dow, R. S., Jones, G. L. and Smith, C. S. (1991). Measurement of wave-induced loads in ships at sea, *Philosophical Transactions of The Royal Society of London, Series A - Physical Sciences and Engineering* **334**(1634): 293–306.

Brown, P. W. (1971). An experimental and theoretical study of planing surfaces with trim flaps, *Davidson Laboratory Report 1463*, Stevens Institute of Technology.

Burns, R. S. (1990). A New Approach to Optimising Fuel Economy for Ships in a Seaway, *in* M. M. A. Pourzanjani and G. N. Roberts (eds), *Proceedings of the International Conference on Modelling and Control of Marine Craft, Exeter, UK,*, Polytechnic South West, Plymouth, U.K., Elsevier Applied Science, pp. 372–381.

Callahan, J. T. (1991). Marine Grade Aluminium Alloys for High-Speed Craft Construction, *IMAS 91 - High Speed Marine Transportation*, number 13, Marine Management (Holdings), pp. 111–122. Paper 13.

Cannon, S. and Mutton, P. (1997). The Integrated Hull Condition Monitoring System Project, *AME'97 - Turning Research Into Reality*, Australian Maritime Engineering Cooperative Research Centre. Thursday 1 May 1997 - Session 2, AME Research Showcase.

Cartwright, D. E. (1956). On Determining the Directions of Waves from a Ship at Sea, *Proceedings of the Royal Society, Series A, London* **234**: 382–387.

Clauss, G. F., Crossland, P., Soares, C. G., Hong, S.-W., Kishev, R., Kyozuka, Y., Stansberg, C. T., Kriebel, D. L. and Wolfram, J. (1999). The Specialist Committe on Environmental Modeling - Final Report and Recommendations to the 22nd ITTC, *Procedings of the 22nd International Towing Tank Conference (ITTC'99)*, ITTC.

Coggeshall, I. S. (1985). Oceanic Engineering: The Making of an IEEE Society, *IEEE Journal of Oceanic Engineering* **OE-10**(2): 63–83. see section "The Passing Scene".

Colwell, J. L. (1994). Motion Sickness Habituation in the Naval Environment, *DREA TECHNICAL MEMORANDUM 94/211*, National Defence, Research and Development Branch, Defence Research Establishment Atlantic.

Coyle, J. (2000). Sitting Pretty, *Yachting* pp. 108–111.

Darbyshire, M. and Draper, L. (1963.). Wind Generated Sea Waves, *Engineering* pp. 482–483. 5 April.

Davis, M. and Holloway, D. (2003a). Effect of Sea, Ride Controls, Hull Form and Spacing on Motion and Sickness Incidence for High Speed Catamarans, *Proceedings of the Seventh International Conference on Fast Sea Transportation (FAST'03)* . Submitted for Publishing.

Davis, M. R. and Holloway, D. S. (2003b). Nonlinear Effect of Wave Amplitude on Motion and Global Loads for INCAT Hull 042 in Headseas, *Confidential project report, INCAT-UTAS ARC SPIRT project*, University of Tasmania (UTAS). July.

Davis, M. R., Watson, N. L. and Holloway, D. S. (2003). Wave Response of an 86m High Speed Catamaran, *International Journal of Maritime Engineering* . Submitted for publishing.

Dipper, Jr, M. J. (1987). Techniques in Directional Wave Spectral Analysis with Applications for the Seakeeping Basin, *in* R. F. Messalle (ed.), *Proceedings of the Twenty-First American Towing Tank Conference*, David W. Taylor Naval Ship Research and Development Center, Code 1562, Special Ship and Ocean Systems Dynamics Branch, National Academy Press, Washington, D.C., pp. 385–397.

Dipper, Jr, M. J. (1997). Ship-Borne Wave Height Measurements, *Marine Technology* **34**(4): 267–275.

Dogliani, M. and Bondini, F. (1999). Full-Scale Measurements on a Last Generation HSC, *HSMV conference* .

Dorey, A. (1990). High Speed Small Craft, *Royal Institution of Naval Architects (RINA)* **132**: 191–200.

Duffy, E. (1999). Interceptor Outdates Transom Flaps, *Speed at Sea* **5**(6): 15. December.

Dussert-Vidalet, R., Gaudin, C., Galtier, B. and Adams, J. (1995). Optimization and Contractual Validation of the Seakeeping Performance of the New Fast Ferry Ship for SNCM, *in* C. F. L. Kruppa (ed.), *Proceedings of the Third International Conference on Fast Sea Transportation (FAST'95)*, Schiffbautechnische Gesellschaft, pp. 271–293.

Ericson, T. O. (2002). *Trim Tabs versus Interceptors for Ride Control*, Bachalor of engineering thesis, School of Mechanical and Manufacturing Engineering, The University of New South Wales.

Faltinsen, O. M. (1993). On Sea-Keeping of Conventional and High-Speed Vessels, *Journal of Ship Research* **37**(2): 87–101. Fifteenth Georg Weinblum Memorial Lecture.

Faltinsen, O. and Zhao, R. (1991). Numerical Predictions of Ship Motions at High Forward Speed, *Philosophical Transactions of The Royal Society of London, Series A - Physical Sciences and Engineering* **334**(1634): 241–252.

Fossen, T. I. (1994). *Guidance and Control of Ocean Vehicles*, John Wiley & Sons.

Froude, W. (1861). On the Rolling of Ships, *Transactions of the Institution of Naval Architects, London, England (INA)* pp. 180–229.

Gaillarde, G. (2002). Behaviour of Motoryachts at Sea, *The Yacht Report* pp. 101–105. November/December.

Geller, W. (1940). Die Seekrankheit und Ihre Behandlung, *Klinische Wochenschrift, Jahrg* **19**(51): 1310–1313.

Glauert, H. (1959). *The Elements of Aerofoil and Airscrew Theory*, second edn, Cambridge University press.

Gong, D. S., Hong, S. Y., Hong, S. W., Kim, B. S., Yoo, S. Y. and Han, D. H. (1994). Seakeeping Analysis of a 80-M Class High Speed Catamaran, *Proceedings of the Forth (1994) International Offshore and Polar Engineering Conference, Osaka, Japan*, The International Society of Offshore and Polar Engineers, pp. 603–607. ISBN: 1-880653-10-9 (Set); ISBN: 1-880653-14-1 (Vol. 4).

Goodwin, G. C., Perez, T., Seron, M. and Tzeng, C.-Y. (2000). On Fundamental Limitations for Rudder Roll Stabilization of Ships, *Control and Decision Conference, Sydney, Australia*, pp. 4705–4710.

Haywood, A. J. (1995). Motion Control Systems, *AquaMarine '95*, Australian Maritime Engineering Cooperative Research Centre Limited (AMECRC), pp. 50–56.

Haywood, A. J. and Duncan, A. J. (1997). Experiences Using System Identification Techniques on High Speed Ferries, *Fourth International Conference on Fast Sea Transportation (FAST'97)*, Baird Publications Ltd, Hong Kong, pp. 797–803.

Haywood, A. J., Duncan, A. J., Klaka, K. P. and Bennett, J. (1994). The Role of Simulation in the Development of a Ride Control System for Fast Ferries., *International Conference on Manoeuvring and Control of Marine Craft (MCMC'94)*, Australian Maritime Engineering Cooperative Reserch Centre (AMECRC). Report AMECRC C 94/1.

Haywood, A. J., Duncan, A. J., Klaka, K. P. and Bennett, J. (1995). The Development of a Ride Control System for Fast Ferries, *Control Engineering Practice* **3**(5): 695–702.

Hearn, G. E. (1991). Seakeeping Theories: Spoilt for Choice?, *The North East Coast Institution of Engineers and Shipbuilders* **107**: 45–66.

Hercus, P. C. (1988). Beyond 2001, *High-Speed Surface Craft* pp. 25–30.

Hercus, P. C., Armstrong, N. A. and Egan, B. K. (1991). The Seakeeping Comfort of Large Fast Catamarans, *IMAS 91 - High Speed Marine Transportation*, number 1, Marine Management (Holdings), pp. 5–11. Paper 1.

Hoerner, S. F. and Borst, H. V. (1975). *Fluid-Dynamic Lift*, Mrs Liselotte A. Hoerner.

Holloway, D. S. (1998). *A High Froude Number Time Domain Strip Theory Applied to the Seakeeping of Semi-SWATHs*, PhD thesis, University of Tasmania.

Holloway, D. S. and Davis, M. R. (1997). Seakeeping Response of a Family of Semi-SWATH Hull Forms, *in* A. Jeffs (ed.), *Fourth International Conference on Fast Sea Transportation (FAST'97)*, University of Tasmania, Baird Publications Ltd, Hong Kong, pp. 43–49.

Holloway, D. S. and Davis, M. R. (1998). Private communication, School of Engineering, University of Tasmania.

Holloway, D. S. and Davis, M. R. (2001a). Computation of Ship Motion by a High Froude Number Time Domain Strip Theory, *Internal report SERR08/01*, The University of Tasmania.

Holloway, D. S. and Davis, M. R. (2001b). Green Function Solutions for the Transient Motion of Water Sections, *Internal report SERR07/01*, The University of Tasmania.

Holloway, D. S. and Davis, M. R. (2002a). Green Function Solutions for the Transient Motion of Water Sections, *Journal of Ship Research* **46**(2): 99–120.

Holloway, D. S. and Davis, M. R. (2002b). Seakeeping Computations for Semi-SWATHs at High Froude Number, *Transactions of the Royal Institution of Naval Architects (RINA)* **paper W303.**

Hua, J. and Palmquist, M. (1995). Wave Estimation Through Ship Motion Measurements - A Practical Approach, *International Conference on Seakeeping and Weather in Association with the Nautical Institute*, The Royal Institution of Naval Architects (RINA). Paper 6.

Hudson, D. A., Price, W. G. and Temarel, P. (1995). Seakeeping Performance of High Speed Displacement Craft, *in* C. F. L. Kruppa (ed.), *Proceedings of the Third International Conference on Fast Sea Transportation (FAST'95)*, Schiffbautechnische Gesellschaft, pp. 877–892.

Hutchison, B. L. (1990). Seakeeping Studies: A Status Report, *SNAME Transactions* **98**: 263–317.

Hynds, P. (1997). Channel Islands Services Overcome Setbacks, *Speed at Sea* **3**(5): 9–12. Nov/Dec.

International Organisation for Standardisation, ISO 2631/3 (1985). Evaluation of Human Exposure to Whole Body Vibration, Part 3: Evaluation to Whole Body Z-Axis Vertical Vibration in the Frequency Range 0.1 to 0.63 Hz.

Ito, H., Shibasaki, K., Matsuo, M., Mizuta, A. and Sugimoto, H. (1997). Cavitation Erosion Tests of High Tensile Stainless Steels for Techno-Superliner (TSL-F) Hulls, *Fourth International Conference on Fast Sea Transportation (FAST'97)*, Baird Publications Ltd, Hong Kong, pp. 553–557.

Jacobs, W. R. (1958). The Analytical Calculation of Ship Bending Moments in Regular Waves, *Journal of Ship Research* **2**(1): 20–28.

Kang, C.-G. and Gong, I.-Y. (1995). Time domain simulation of the motion of a high speed twinhull with control planes in waves, *in* C. F. L. Kruppa (ed.), *Proceedings of the Third International Conference on Fast Sea Transportation (FAST'95)*, Schiffbautechnische Gesellschaft, pp. 1031–1041.

Kashiwagi, M. (1997). Numerical Seakeeping Calculations Based on the Slender Ship Theory, *Ship Technology Research* **44**(4): 167–192.

Kent, J. L. (1924). The Effect of Wind and Waves on the Propulsion of Ships, *Transactions of the Institution of Naval Architects, London, England (INA)* **66**: 188–213. and plates 11 and 12.

Kent, J. L. (1927). Propulsion of Ships under Different Weather Conditions, *Transactions of the Institution of Naval Architects, London, England (INA)* **69**: 145–163.

Klaka, K. (1997). Ocean Leveller, *AME'97 - Turning Research Into Reality*, Australian Maritime Engineering Cooperative Research Centre. Thursday, 1 May 1997 - Session 2, AME Research Showcase.

Klaka, K. P. and Webb, G. A. (1992). The Motions of Ships in Shallow Water, *11th Australasian Fluid Mechanics Conference, University of Tasmania, Hobart, Australia*, AMECRC Curtin University; CMST, Curtin University, pp. 359–362.

Knaggs(ed.), T. (2000). New Technique to Counter the Dangers of Parametric Roll, *The Naval Architect - International Journal of The Royal Institution of Naval Architects* p. 50.

Kohlmoos, A. and Schellin, T. E. (2002). Motion Prediction and Sea Trial Measurements for Comfort Rating of a Catamaran, *High Speed Craft* .

Korvin-Kroukovsky, B. V. (1955). Investigation of Ship Motions in Regular Waves, *Transactions of The Society of Naval Architects and Marine Engineers* pp. 386–435.

Korvin-Kroukovsky, B. V. (1961). *Theory of Seakeeping*, The society of Naval Architects and Marine Engineers (SNAME), 74 Trinity Place, New York 6, N.Y.

Korvin-Kroukovsky, B. V. and Jacobs, W. R. (1957). Pitching and Heaving Motions of a Ship in Regular Waves, *Transactions of The Society of Naval Architects and Marine Engineers* pp. 590–632.

Korvin-Kroukovsky, B. V. and Lewis, E. V. (1955). Ship Motions in Regular and Irregular Seas, *International Ship Building Progress* **2**(6): 81–95.

Kriloff, A. (1896). A New Theory of the Pitching Motion of Ships on Waves and of the Stresses Produced by This Motion, *Transactions of the Institution of Naval Architects, London, England (INA)* pp. 135–196. Read at the 39th session of the Institution of Naval Architects.

Kriloff, A. (1898). A General Theory of the Oscillations of a Ship on Waves, *Transactions of the Institution of Naval Architects, London, England (INA)* pp. 135–196.

Kubinec, J. (2001). Analysis Evaluates Ride Quality Cost Benefits, *Speed at Sea* **7**(2): 30–31. April.

Kvalsvold, J., Loseth, R. and Falkenthall, H. (1999). Effect of Motion Control on High-Speed Craft Operability, *5th Symposium on High Speed Marine Vehicles*, HSMV.

Kvalsvold, J., Svensen, T. and Braathen, A. (1995). Comfort Assessment of Large High-Speed Catamarans, *International Symposium on High Speed Vessels for Transport and Defence*, The Royal Institution of Naval Architects. 2nd paper.

Lawther, A. (1983). A Survey of Motion Sickness on a Passenger Ship, *Paper Presented at the United Kingdom Informal Group Meeting on Human Response to Vibration Held at NIAE, Silsoe*, Vol. 2, p. 15 pages.

Lawther, A. and Griffin, M. J. (1980). Measurement of Ship Motion, *in* D. J. Oborne and J. A. Levis (eds), *Human Factors in Transport Research, International Conference on Ergonomics and Transport, Volume 2, User Factors: Comfort, The Environment and Behaviour*, Vol. 2, The Ergonomics Society, Academic Press, pp. 131–139.

Lawther, A. and Griffin, M. J. (1987). Prediction of the Incidence of Motion Sickness from the Magnitude, Frequency, and Duration of Vertical Oscillation, *Journal of Acoustical Society of America* **82**(3): 957–966.

Lawther, A. and Griffin, M. J. (1988). Motion Sickness and Motion Characteristics of Vessels at Sea, *Ergonomics* **31**(10): 1373–1394.

Lee, C. M. and Curphey, R. M. (1977). Prediction of Motion, Stability, and Wave Load of Small-Waterplane-Area, Twin-Hull Ships, *Transactions of the Society of Naval Architects and Marine Engineers* **85**: 94–130. Presented at the annual meeting, New York, NJ., 10-12 November, 1977.

Lee, C. M., Lee, S. J. and Kim, Y. G. (1997). Effect of Free Surface on Lift Characteristics of Fins Attached to a Strut, *in* A. Jeffs (ed.), *Fourth International Conference on Fast Sea Transportation (FAST'97)*, Baird Publications Ltd, Hong Kong, pp. 139–144.

Lewis, E. V. (ed.) (1988a). *Principles of Naval Architecture - Motions in Waves and Controllability*, Vol. 1, second edn, The Society of Naval Architects and Marine Engineers, 601 Pavonia Avenue, Jersey City, NJ.

Lewis, E. V. (ed.) (1988b). *Principles of Naval Architecture - Resistance, Propulsion and Vibration*, Vol. 2, second edn, The Society of Naval Architects and Marine Engineers, 601 Pavonia Avenue, Jersey City, NJ.

Lewis, E. V. (ed.) (1989). *Principles of Naval Architecture - Stability and Strength*, Vol. 3, second edn, The Society of Naval Architects and Marine Engineers, 601 Pavonia Avenue, Jersey City, NJ.

Lloyd, A. R. J. M. (1989). *Seakeeping: Ship Behaviour in Rough Weather*, Ellis Horwood Series in Marine Technology, Ellis Horwood Limited, Market Cross House, Cooper Street, Chichester, West Sussex, PO19 1EB, England. Original hard back copy.

Marks, W. (1967). Determination of the Wave Spectrum from Observed Motions of a Vehicle in a Seaway, *Journal of Ship Research* .

McCauley, M. E., Royal, J. W., Wylie, C. D., O'Hanlon, J. F. and Mackie, R. R. (1976). Motion Sickness Incidence: Exploratory Studies of Habituation, Pitch and Roll, and the Refinement of a Mathematical Model, *Technical Report 1733-2*, Human Factors Research, Incorporated, 6780 Cortona Drive, Goleta, California, 93017. Prepared for Medical and Dental Sciences, Biological Sciences Division, Office of Naval Research, Department of the Navy; Contract N00014-73-C-0040; Task No. NR 105-841;.

Michel, W. H. (1999). Sea Spectra Revisited, *Marine Technology* **36**(4): 211–227.

Moan, T., Skallerud, B. and Skjastad, O. (1991). Structural Analysis and Design of Hydrofoils and Struts, *in* K. O. Holden, O. Faltinsen and T. Moan (eds), *Proceedings from the First International Conference on Fast Sea Transportation (FAST'91)*, Vol. 1, Tapir Publishers, Tronheim, Norway, pp. 743–764.

Nakos, D. and Sclavounos, P. (1991). Ship Motions by a Three-Dimensional Rankine Panel Method, *Eighteenth Symposium on Naval Hydrodynamics, Ann Arbor*, National Academy Press Washington, D.C., pp. 21–40.

Newman, J. N. (1977). *Marine Hydrodynamics*, The Massachusetts Intitute of Technology (The MIT Press), Cambridge, Massachusetts and London England. ISBN: 0-262-14026-8.

Newman, J. N. (1978). The Theory of Ship Motions, *Advances in Applied Mechanics*, chapter 18, pp. 221–283.

Newman, J. N. (1991). The Quest for a Three-Dimensional Theory of Ship-Wave Interactions, *Philosophical Transactions of The Royal Society of London, Series A - Physical Sciences and Engineering* **334**(1634): 213–227.

Newman, J. N. and Sclavounos, P. (1980). The Unified Theory of Ship Motions, *Thirteenth Symposium on Naval Hydrodynamics, Tokyo*, Tokyo, pp. 373–394.

Nordenstrøm, N., Faltinsen, O. and Perdersen, B. (1971). Prediction of Wave-Induced Motions and Loads for Catamarans, *Third Annual Offshore Technology Conference, Dallas, Texas*, Vol. 2, Offshore Technology Conference, pp. 13–58. Vol 2; Paper Number: OTC 1418.

Ogilvie, T. F. (1964). Recent Progress Toward the Understanding and Prediction of Ship Motions, *Fifth Symposium on Naval Hydrodynamics, Bergen, Norway*, Office of Naval Research, Department of the Navy, Washington D.C., pp. 3–79.

Ogilvie, T. F. and Tuck, E. O. (1969). A Rational Strip Theory of Ship Motions: Part 1, *Technical Report 013*, Department of Naval Architecture, The University of Michigan College of Engineering.

O'Hanlon, J. F. and McCauley, M. E. (1974). Motion Sickness Incidence as a Function of the Frequency and Acceleration of Vertical Sinusoidal Motion, *Aerospace Medicine* **45**(4): 366–369.

Ohtsubo, H. and Kubota, A. (1991). Vertical Motions and Wave Loads of Large High-Speed Ships with Hydrofoils, *in* K. O. Holden, O. Faltinsen and T. Moan (eds), *Proceedings from the First International Conference on Fast Sea Transportation (FAST'91)*, Tapir Publishers, Tronheim, Norway, pp. 829–844. Volume 2; Session 17: Wave Loads.

Othfors, D. and Ljungström, H. (2003). Great Ocean Liners, http://www.greatoceanliners.net/index2.html.

Perez, T., Tzeng, C.-Y. and Goodwin, G. C. (2000). Model Predictive Rudder Roll Stabilization Control for Ships, *Maneuvring and Control of Marine Craft (MCMC'2000), Alboug, Denmark*, IFAC, pp. 45–50.

Phelps, B. P. (1997). Determination of Wave Loads for Ship Structural Analysis, *Technical Report DSTO-RR-0116*, Department of Defence - Defence Science and Technology Organisation.

Pierce, R. D. (1992). Run Length and Statistical Error Estimation for Seakeeping Tests and Trials, *Twenty Third American Towing Tank Conference*, Carderock Division, Naval Surface Warfare Center, USA, pp. 73–84.

Pike, D. (2003). Interceptors Also Effective on Smaller Fast Craft, *Speed at Sea* **9**(1): 44–45. February.

Pitts, W. C., Nielson, J. N. and Kaattari, G. E. (1959). Lift and Center of Pressure of Wing-Body-Tail Combinations at Subsonic, Transonic, and Supersonic Speeds, *NACA report 1307*, NACA.

Ponomarev, A. V. (1991). New Method for Improvement of Performance and Seakeeping Characteristics of High-Speed Craft, *Fast'95*, pp. 1029–1037.

Ponomarev, A. V., Sadovnikov, D. Y. and Sadovnikov, Y. M. (1995). New Approaches to Improvement of Propulsive Performance and Seakeeping Qualities of High-Speed Vessels, *Fast'95*, pp. 1169–1180.

Rantanen, A., Holmberg, J. and Karppinen, T. (1995). Measurement of Encountered Waves and Ship Motions During Full Scale Seakeeping Trials, *International Conference on Seakeeping and Weather in Association with The Nautical Institute*, The Royal Institution of Naval Architects (RINA). Paper 7.

Reason, J. T. and Brand, J. J. (1975). *Motion Sickness*, Academic Press. Copied from a book from the Clinical library.

Redmayne(ed.), M. H. (2003). The Great White - Oceanfast and the Aussie Rules, *The Yacht Report* **51**: 52–63. January/February.

Rodriguez, G., Soares, C. G. and Machado, U. (1999). Uncertainty of the Sea State Parameters Resulting from the Methods of Spectral Estimation, *Ocean Engineering* **26**: 991–1002.

Salvesen, N., Tuck, E. O. and Faltinsen, O. (1970). Ship Motions and Sea Loads, *Transactions of The Society of Naval Architects and Marine Engineers* **78**: 250–287.

Saul, G. C. (1946). *The Gyroscope and Its Applications*, Hutchinson's Scientific and Technical Publications, chapter 8, pp. 129–133.

Saunders, H. E. (Second printing 1982). *Hydrodynamics in Ship Design*, The Sociey of Naval Architects and Marine Engineers (SNAME), One World Trade Center, Suite 1369, New York, N.Y. 10048.

Savitsky, D. and Brown, P. W. (1976). Procedures for Hydrodynamic Evaluation of Planing Hulls in Smooth and Rough Water, *Marine Technology* **13**(4): 381–400. October.

Scarborough, J. B. (1958). *The Gyroscope Theory and Applications*, New York: Interscience Publishers Inc., chapter 8, pp. 187–214.

Schellin, T. E. and Papanikolaou, A. (1991). Prediction of Seakeeping Performance of a Swath Ship and Comparison with Measurements, *in* K. O. Holden, O. Faltinsen and T. Moan (eds), *Proceedings from the First International Conference on Fast Sea Transportation (FAST'91)*, Tapir Publishers, Tronheim, Norway, pp. 811–827. Volume 2; Session 17: Wave loads.

Schellin, T. E. and Rathje, H. (1995). A Panel Method Applied to Hydrodynamic Analysis of Twin-Hull Ships, *in* C. F. L. Kruppa (ed.), *Proceedings of the Third International Conference on Fast Sea Transportation (FAST'95)*, Schiffbautechnische Gesellschaft, pp. 905–916.

Shaw, O. J. (1954). On the Dynamics of Motion Sickness in a Seaway, *The Scientific Monthly* **78**(2): 110–116. February.

Shock, R. A. and Thiagarajan, K. (1998). Feasibility of Lift Dumping Foils for High Speed Ferries, *AME'98*, Australian Maritime Engineering CRC Ltd.

Slotwinski, A. R., Goodwin, F. E. and Simonson, D. L. (1989). Utilizing GaAlAs Laser Diodes as a Source for Frequency Modulated Continuous Wave (FMCW) Coherent Laser Radars, *SPIE Laser Diode Technology and Applications* **1043**: 245–251.

Smith, R. C. (1995). Motion Sickness on High Speed Vessels, *First AMECRC Postgraduate Student Conference*, Australian Maritime Engineering Cooperative Research Centre (AMECRC).

Smith, R. C. (1997). The Development of a Mathematical Measure to Continuously Assess the Severity and Incidence of Motion Sickness, *AME'97 - Postgraduate Conference*, Australian Maratime Engineering Cooperative Research Centre (AMECRC).

Smith, R. C. and Koss, L. L. (1995). Motion Sickness Incidence Study on Rottnest Island High Speed Ferries, *in* C. F. L. Kruppa (ed.), *Proceedings of the Third International Conference on Fast Sea Transportation (FAST'95)*, Schiffbautechnische Gesellschaft, pp. 417–428.

Smith, R. C. and Koss, L. L. (1997). Motion Sickness Study on Wavepiercing Catamarans, *Fourth International Conference on Fast Sea Transportation (FAST'97)*, Baird Publications Ltd, Hong Kong, pp. 791–795.

St. Denis, M. (1957). On the Reduction of Motion Data from Model Tests in Confused Seas, *Proceedings, Symposium on the Behaviour of Shp in a Seaway, 25th Anniversary of the Netherlands Model Basin, Wageningen, Final Two Volume Edition. (NSMB)*, pp. 133–144, 870–872.

St Denis, M. and Pierson, W. J. (1953). On the Motions of Ships in Confused Seas, *Transactions of the Society of Naval Architects and Marine Engineers* pp. 280–357.

Steinmann, P., Fach, K. and Menon, B. (1999). Global and Slamming Sea Loads Acting on an 86m High Speed Catamaran Ferry, *Fifth International Conference on Fast Sea Transportation (FAST'99)*, The Society of Naval Architects and Marine Engineers (SNAME), pp. 709–718.

Swanton, C., Haywood, A. and Schaub, B. (1999). Simulation - An Essential Tool in the Design of Motion Control Systems, *Fifth International Conference on Fast Sea Transportation (FAST'99)*, The Society of Naval Architects and Marine Engineers (SNAME), pp. 73–81.

Thompson, J. L. (1979). Ship Motion Measurements Made on an Attack Class Patrol Boat (HMAS Bombard), *RANRL REPORT 6/78 AR-001-029*, Department of Defence, Defence Science and Technology Organisation, R.A.N. Research Laboratory, Edgecliff, NSW.

Tornblad, J. (1987). Marine Propellors and Propulsion of Ships, *Compendium textbook R-394-E*, Marine Laboratory, KaMeWa AB, PO Box 1010, S-681 01 Kristinehamn, Sweden. Translation of the Swedish version "Fartygspropellrar och fartygs framdrift" 1985, with additions.

Treakle, T. W. (1998). *A Time-Domain Numerical Study of Passive and Active Anti-Roll Tanks to Reduce Ship Motions*, Master of science in ocean engineering, Virginia Polytechnic Institute and State University.

TSK (2003). Tsurumi Seiki Co., Ltd. (TSK) - Shipborne Wave Height Meter, http://tsk-jp.com/.

TSKA, I. (1993). *TSK Remote Wave Height Meter - Operating Manual*, TSKA, Inc.

Tucker, M. J. (1952). A Wave Recorder for Use in Ships, *Nature* **170**: 657.

Tucker, M. J. (1956). A Shipborne Wave Recorder, *Intitution of Naval Architects* **98**: 236–250.

Tucker, M. J. (1991). *Waves in Ocean Engineering: Measurement, Analysis, Interpretation*, Ellis Horwood Series in Marine Science, Ellis Horwood, Market Cross House, Cooper Street, Chichester, West Sussex, PO19 1EB, England.

Vulovich, R., Hirayama, T., Toki, N. and Mizuno, H. (1989). Characteristics of Hull Stresses Measured on a Large Containership in Rough Seas, *Transactions of the Society of Naval Architects and Marine Engineers (SNAME)* **97**: 397–428.

Wadlin, K. L. and Christopher, K. W. (1958). A Method for Calculation of Hydrodynamic Lift for Submerged and Planing Rectangular Lifting Surfaces, *Technical Report Technical Note 4168*, National Advisory Committee for Aeronautics.

Walree, F. V. (1997). A New Computational Method for the Hydrodynamic Performance of Hydrofoil Craft, *in* A. Jeffs (ed.), *Fourth International Conference on Fast Sea Transportation (FAST'97)*, Baird Publications Ltd, Hong Kong, pp. 291–297.

Wang, Z., Folso, R., Bondini, F. and Pedersen, T. (1999). Linear and Non-Linear Numerical Seakeeping Evaluation of a Fast Monohull Ferry Compared to Full Scale Measurements, *Fifth International Conference on Fast Sea Transportation (FAST'99)*, The Society of Naval Architects and Marine Engineers (SNAME), pp. 443–456.

Wehausen, J. V. and Laitone, E. V. (1960). Surface Waves, *in* S. Flügge (ed.), *Handbuch der Physik*, Vol. 9 of *Stromunesmechanik III*, Springer-Verlag, Berlin, chapter 9, pp. 445–814.

Welch, P. D. (1967). The Use of Fast Fourier Transform for the Estimation of Power Spectra: A Method Based on Time Averaging Over Short, Modified Periodograms, *IEEE Transactions on Audio and Electroacoustics* **AU-15**(2): 70–73.

Wellicome, J. F., Temarel, P., Molland, A. F. and Couser, P. R. (1995). Experimental Measurements of the Seakeeping Characteristics of Fast Displacement Catamarans in Long-Crested Seas, *Technical Report 89*, Universiy of Southampton, Department of Ship Science, Faculty of Engineering and Applied Science.

Widmark, C. (2001). Interceptor steering offers gains in efficiency, *Speed at Sea* **7**(2): 28–29. April.

Wilson(ed.), T. (2000). Trade-Off Needed Between Tabs and Interceptors, *Speed at Sea* **6**(6): 28–30. December, Content sourced from Maritime Dynamics Incorporated.

Witmer, D. J. and Lewis, J. W. (1994). Operational and Scientific Hull Structure Monitoring on TAPS Trade Tanders, *Transactions of The Society of Naval Architects and Marine Engineers (SNAME)* **102**: 501–533.

Witmer, D. J. and Lewis, J. W. (1995). The BP Oil Tanker Structural Monitoring System, *Marine Technology* **32**(4): 277–296.

Yasuda, A., Kuwashima, S. and Kanai, Y. (1985). A Shipborne-Type Wave-Height Meter for Oceangoing Vessels, Using Microwave Doppler Radar, *IEEE Journal of Oceanic Engineering* **OE-10**(2): 138–143.

Yeung, R. W. and Kim, S.-H. (1981). Radiation Forces on Ships with Forward Speed, *Proceedings Third International Conference on Numerical Ship Hydrodynamics*, pp. 499–515.

Yeung, R. W. and Kim, S. H. (1984). A New Development in the Theory of Oscillating and Translating Slender Ships, *Fifteenth Symposium on Naval Hydrodynamics*, pp. 195–218.

Yoo, W.-J., Park, J.-H., Lee, T.-Y. and Oh, I.-G. (1997). Prediction of the Effects of Control Surfaces on the Motion of a Catamaran, *Proceedings of the Seventh International Offshore and Polar Engineering Conference*, Vol. 4, Samsung Heavy Industries Co., Ltd., Daejon, Korea, The International Society of Offshore and Polar Engineers, pp. 729–735. ISBN: 1-880653-28-1 (set); ISBN: 1-880653-32-X (Vol 4).

Yum, D.-J., Min, K.-S., Song, K.-J. and Lee, H.-Y. (1995). Theoretical Prediction of Seakeeping Performance and Comparison with Sea Trial Results for High-Speed Foil Catamaran Ship, *in* C. F. L. Kruppa (ed.), *Proceedings of the Third International Conference on Fast Sea Transportation (FAST'95)*, Schiffbautechnische Gesellschaft, pp. 1053–1063.

Zhao, R. and Aarsnes, J. V. (1995). Numerical and Experimental Studies of Nonlinear Motions and Loads of a High Speed Catamaran, *in* C. F. L. Kruppa (ed.), *Proceedings of the Third International Conference on Fast Sea Transportation (FAST'95)*, Schiffbautechnische Gesellschaft, pp. 1017–1030.

Zhu, D. X. and Katory, M. (1995). 3-D Time Domain Numerical Model for the Prediction of Ship Motions in Random Seas, *International Journal of Offshore and Polar Engineering* **5**(2): 120–126. June.

Zhu, D. X. and Katory, M. (1998). A Time-Domain Prediction Method of Ship Motions, *Ocean Engineering* **25**(9): 781–791. June.

Appendix A

Hull particulars

A.1 81 metre Vessel (Hull 038)

The hydrostatics for the 81 metre vessel in the delivery load, service full load and service half load conditions are given in tables A.1, A.2, A.3 respectively. These conditions essentially encapsulate the range of loading conditions throughout the duration of experimental measurements. Figure A.1 is a representation of the hull fitted with motion control system comprised of transom mounted trim tabs and forward mounted T-foils, which are located at the positions given in table A.5.

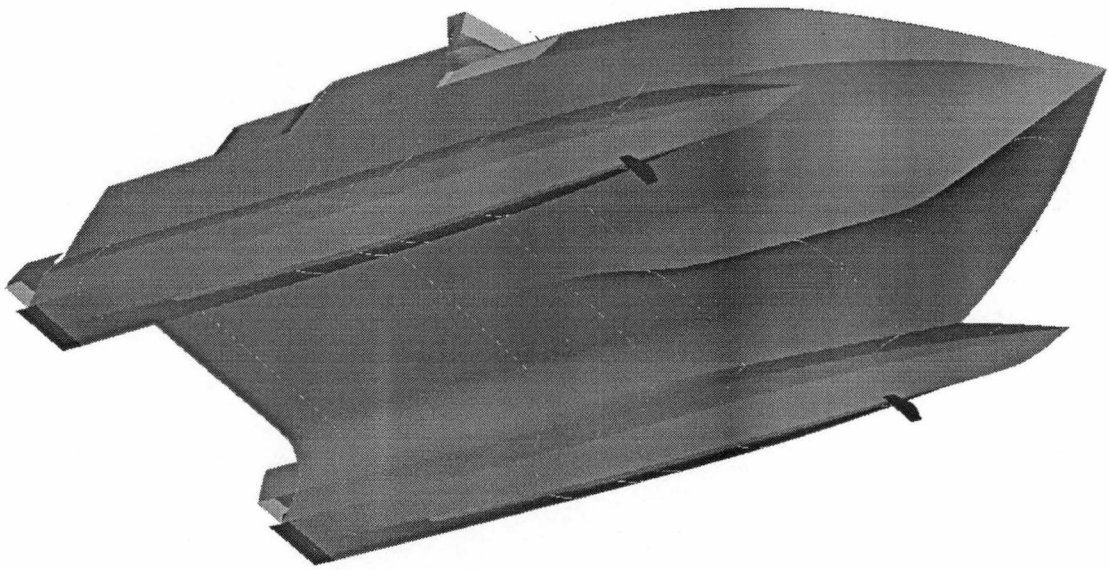

Figure A.1: Full motion control configuration with transom tabs and forward mounted T-foils (81 metre vessel, Hull 038) .

	81 metre (Hull 038) Load condition		Delivery - Lightship		Delivery - Full Departure		Delivery - Full, 10% arrival	
	Jet Inlet calculation method		Non-Buoyant	As tanks	Non-Buoyant	As tanks	Non-Buoyant	As tanks
1	Draft Amidships	[m]	2 916	2 916	3 836	3 836	3 142	3 142
2	Displacement	[t]	754	785	1178	1209	861	892
3	Heel to Starboard	[degree]	0	0	-0.05	-0.05	0.04	0 04
4	Draft at FP	[m]	2.393	2.392	3.914	3.912	2.68	2.68
5	Draft at AP	[m]	3 438	3 44	3 758	3 76	3 604	3 604
6	Draft at LCF	[m]	2.997	3	3.826	3.826	3.207	3.207
7	Trim (+ve by stern)	[m]	1 045	1 049	-0.156	-0 153	0.924	0 924
8	LWL	[m]	66.514	66.506	66.654	66.66	66.137	66.136
9	BWL	[m]	25.995	25.996	25 989	25 988	26	26
10	LWL/BWL	-	15.5	15.5	15.5	15.5	15.5	15.5
11	LWL/draft amidships	-	22 8	22 8	17.4	17.4	21.0	21 0
12	Wetted Area	[m2]	816.356	816.419	1065.696	1065.624	876.898	876.887
13	Waterplane Area	[m2]	474 946	477 726	492.205	492.252	485 983	486 065
14	Prismatic Coefficient	-	0.649	0.676	0.75	0.77	0.684	0.709
15	Block Coefficient	-	0.484	0 504	0 612	0 628	0 513	0.532
16	Midship Area Coefficient	-	0.978	0.978	0.817	0.817	0.975	0.975
17	Waterplane Area Coefficient	-	0 828	0.833	0 856	0 856	0.846	0 846
18	LCB to zero pt	[m]	24.386	23.464	28.261	27.556	25.169	24.33
19	LCF to zero pt	[m]	28.025	27 856	28 845	28 848	28 498	28.493
20	KB	[m]	2.154	2.163	2.591	2.586	2.267	2.271
21	KGf	[m]	6 57	6 403	6.34	6.237	7 048	6 884
22	BMt	[m]	76.699	74.062	50.812	49.498	68.725	66.322
23	BML	[m]	179 083	174 805	126 479	123 234	166 618	160 841
24	GMt	[m]	72 282	69.822	47.063	45.847	63 944	61.709
25	GML	[m]	174 667	170.565	122.73	119 582	161 836	156 227
26	KMt	[m]	78.853	76.225	53.403	52 084	70.992	68.593
27	KML	[m]	181.237	176.968	129 071	125 82	168 885	163 112
28	TPc	[t/cm]	4.869	4.898	5 046	5.047	4.982	4.983
29	MTc	[t.m]	19 86	20 201	21 8	21 806	21 015	21 025
30	RM at 1deg = GMt Disp sin(1)	[t m]	950.988	956.866	967.264	967.35	960.766	960.94
34	LOA	[m]	81 61	81 61	81.61	81 61	81 61	81 61
35	BOA	[m]	26	26	26	26	26	26
36	Lpp	[m]	66 3	66 3	66 3	66 3	66 3	66 3
37	Lpp/2	[m]	33.15	33.15	33.15	33.15	33.15	33.15
38	Demi-hull length	[m]	67 3	67 3	67 3	67.3	67.3	67 3
39	Demi-hull beam	[m]	4.33	4.33	4.33	4.33	4.33	4.33
40	AP (from zero)	[m]	0	0	0	0	0	0
41	Amidships (from zero)	[m]	33.15	33.15	33.15	33.15	33.15	33.15
42	Transom (from zero)	[m]	0	0	0	0	0	0
43	Amidships (from transom)	[m]	33.15	33.15	33.15	33.15	33.15	33.15
44	LCG (from zero)	[m]	24.453	23 529	28 251	27 552	25.230	24 390
45	LCG (from AP)	[m]	24.453	23.529	28.251	27.552	25.23	24.39
46	LCG (from amidships)	[m]	8.697	9 621	4.899	5 598	7 92	8 76
47	LCG (from transom)	[m]	24.453	23.529	28.251	27.552	25.23	24.39
48	Bow (from zero)	[m]	76 8	76 8	76.8	76.8	76 8	76 8

Table A.1: Principle hull particulars (81m vessel) for delivery loading conditions (Note: table contains light displacement (Delivery - Full, 10% arrival) condition as used in numerical predictions)

	81 metre (Hull 038) Load condition		Service - Lightship		Service - Full Departure		Service - Full, 10% arrival	
	Jet Inlet calculation method		Non-Buoyant	As tanks	Non-Buoyant	As tanks	Non-Buoyant	As tanks
1	Draft Amidships	[m]	2.943	2 943	3.679	3 679	3.596	3 596
2	Displacement	[t]	762	794	1107	1138	1066	1097
3	Heel to Starboard	[degree]	0	0	-0 05	-0.05	0.04	0.04
4	Draft at FP	[m]	2.488	2.486	3.614	3.613	3.506	3.505
5	Draft at AP	[m]	3 398	3.401	3 745	3.745	3.685	3.686
6	Draft at LCF	[m]	3.01	3.014	3.687	3.687	3.607	3.607
7	Trim (+ve by stern)	[m]	0 909	0.915	0.131	0 132	0.18	0.181
8	LWL	[m]	66.784	66.772	67.181	67.181	67.066	67.065
9	BWL	[m]	25.994	25.994	26.011	26 011	26 008	26.008
10	LWL/BWL	-	15.5	15.5	15.5	15.5	15.5	15.5
11	LWL/draft amidships	-	22.7	22 7	18.3	18.3	18.7	18.6
12	Wetted Area	[m2]	823.216	823.832	1022.003	1021.968	999.424	999.406
13	Waterplane Area	[m2]	476.72	480.242	497.911	497.908	497.094	497 103
14	Prismatic Coefficient	-	0.669	0.696	0.741	0.762	0.736	0.758
15	Block Coefficient	-	0.491	0.511	0 594	0.611	0.585	0.603
16	Midship Area Coefficient	-	0.749	0.749	0.807	0.807	0.804	0.804
17	Waterplane Area Coefficient	-	0.831	0.837	0.865	0 865	0.864	0.864
18	LCB to zero pt	[m]	24.791	23.862	27.615	26 888	27.452	26.702
19	LCF to zero pt.	[m]	28 266	28 051	29.122	29.122	29 084	29 083
20	KB	[m]	2.158	2.167	2.517	2.513	2.473	2.471
21	KGf	[m]	6.51	6.347	7.223	7 089	7 419	7 275
22	BMt	[m]	76.147	73.674	54.766	53.259	56.792	55.168
23	BML	[m]	179.039	175.621	138.329	134 52	143.116	139.029
24	GMt	[m]	71.795	69.493	50.06	48.682	51.846	50.364
25	GML	[m]	174.686	171 44	133 623	129.944	138.171	134.225
26	KMt	[m]	78.305	75.841	57.283	55.772	59.265	57.639
27	KML	[m]	181.197	177.788	140 846	137 033	145.59	141.5
28	TPc	[t/cm]	4.887	4.923	5.105	5.105	5.096	5.096
29	MTc	[t m]	20.081	20.52	22.309	22 308	22.21	22.211
30	RM at 1deg = GMt.Disp.sin(1)	[t m]	954.978	962.428	967.059	967.055	964.29	964.308
34	LOA	[m]	81 61	81.61	81.61	81 61	81.61	81.61
35	BOA	[m]	26	26	26	26	26	26
36	Lpp	[m]	66.3	66.3	66.3	66 3	66 3	66.3
37	Lpp/2	[m]	33.15	33.15	33.15	33.15	33.15	33.15
38	Demi-hull length	[m]	67.3	67.3	67.3	67 3	67.3	67.3
39	Demi-hull beam	[m]	4.33	4.33	4.33	4.33	4.33	4.33
40	AP (from zero)	[m]	0	0	0	0	0	0
41	Amidships (from zero)	[m]	33.15	33.15	33.15	33.15	33.15	33.15
42	Transom (from zero)	[m]	0	0	0	0	0	0
43	Amidships (from transom)	[m]	33.15	33.15	33.15	33.15	33.15	33.15
44	LCG (from zero)	[m]	24.850	23.920	27.625	26.901	27.464	26.717
45	LCG (from AP)	[m]	24.85	23.92	27.625	26.901	27.464	26.717
46	LCG (from amidships)	[m]	8.3	9.23	5.525	6.249	5.686	6.433
47	LCG (from transom)	[m]	24.85	23.92	27.625	26.901	27.464	26.717
48	Bow (from zero)	[m]	76.8	76 8	76 8	76.8	76 8	76 8

Table A.2: Principle hull particulars (81m vessel) for in service 100% load conditions (Note: table contains heavy displacement (Service - Full departure) condition as used in numerical predictions)

	81 metre (Hull 038) Load condition		Service - 50% Full Departure		Service - 50% Full, 10% Arrival	
	Jet Inlet calculation method		Non-Buoyant	As tanks	Non-Buoyant	As tanks
1	Draft Amidships	[m]	3.433	3 433	3.349	3.349
2	Displacement	[t]	983	1014	942	973
3	Heel to Starboard	[degree]	-0.05	-0.05	0.04	0.04
4	Draft at FP	[m]	3.348	3.348	3.237	3.237
5	Draft at AP	[m]	3.518	3.519	3.46	3.461
6	Draft at LCF	[m]	3.443	3.444	3.362	3.363
7	Trim (+ve by stern)	[m]	0.17	0.171	0.223	0.223
8	LWL	[m]	67.528	67.524	67.577	67.575
9	BWL	[m]	26.001	26.001	25.998	25.998
10	LWL/BWL	-	15.5	15.5	15.5	15.5
11	LWL/draft amidships	-	19.7	19 7	20.2	20.2
12	Wetted Area	[m2]	957.441	957.46	934.502	934.605
13	Waterplane Area	[m2]	494 449	495.741	493 407	495.895
14	Prismatic Coefficient	-	0.727	0.751	0.721	0.745
15	Block Coefficient	-	0 571	0.589	0.561	0.58
16	Midship Area Coefficient	-	0.793	0.793	0.789	0.789
17	Waterplane Area Coefficient	-	0.861	0.863	0.859	0 864
18	LCB to zero pt.	[m]	27.337	26.531	27.133	26.306
19	LCF to zero pt.	[m]	29.081	29.004	29 023	28.877
20	KB	[m]	2.384	2.384	2.34	2.342
21	KGf	[m]	6.979	6 837	7.191	7.036
22	BMt	[m]	61.254	59.513	63.793	62.046
23	BML	[m]	153.242	149.618	159.225	156.327
24	GMt	[m]	56.659	55.06	58.943	57.352
25	GML	[m]	148.647	145.166	154.375	151 633
26	KMt	[m]	63.638	61.897	66.133	64.387
27	KML	[m]	155.626	152 002	161.565	158 668
28	TPc	[t/cm]	5.069	5.082	5.058	5.084
29	MTc	[t m]	22.034	22.206	21.926	22.254
30	RM at 1deg = GMt.Disp.sin(1)	[t.m]	971.817	974.548	968.677	973.939
34	LOA	[m]	81 61	81.61	81.61	81.61
35	BOA	[m]	26	26	26	26
36	Lpp	[m]	66.3	66.3	66.3	66.3
37	Lpp/2	[m]	33.15	33.15	33.15	33.15
38	Demi-hull length	[m]	67 3	67.3	67.3	67.3
39	Demi-hull beam	[m]	4.33	4.33	4.33	4.33
40	AP (from zero)	[m]	0	0	0	0
41	Amidships (from zero)	[m]	33.15	33.15	33.15	33.15
42	Transom (from zero)	[m]	0	0	0	0
43	Amidships (from transom)	[m]	33.15	33.15	33.15	33.15
44	LCG (from zero)	[m]	27.348	26.543	27.153	26.321
45	LCG (from AP)	[m]	27.348	26.543	27.153	26.321
46	LCG (from amidships)	[m]	5.802	6.607	5.997	6.829
47	LCG (from transom)	[m]	27.348	26.543	27.153	26.321
48	Bow (from zero)	[m]	76.8	76.8	76.8	76.8

Table A.3: Principle hull particulars (81m vessel) for in service 50% load conditions

	Entrained water included?	ROLL		PITCH		YAW	
		% of BOA	[m]	% of Lpp	[m]	% of Lpp	[m]
Delivery - Lightship	excl.	37.7%	9.813	27.7%	21.135	26.8%	20.476
	incl.	38.1%	9.917	27.9%	21.283	27.2%	20.811
Delivery - Full Departure	excl.	38.0%	9.891	23.4%	17.897	23.4%	17.871
	incl.	38.3%	9.946	23.9%	18.282	24.0%	18.360
Delivery - Full, 10% arrival	excl.	37.0%	9.626	26.3%	20.092	25.4%	19.420
	incl.	37.4%	9.724	26.6%	20.311	25.9%	19.813
Service - Lightship	excl.	37.9%	9.846	27.9%	21.347	27.1%	20.744
	incl.	38.3%	9.945	28.1%	21.504	27.6%	21.079
Service - Full Departure	excl.	35.2%	9.164	27.0%	20.601	25.1%	19.215
	incl.	35.7%	9.272	27.3%	20.847	25.7%	19.638
Service - Full, 10% arrival	excl.	34.7%	9.022	27.5%	21.010	25.5%	19.452
	incl.	35.2%	9.145	27.8%	21.242	26.0%	19.875
Service - 50% Full Departure	excl.	34.7%	9.022	27.5%	21.010	25.5%	19.452
	incl.	35.2%	9.145	27.8%	21.242	26.0%	19.875
Service - 50% Full, 10% arrival	excl.	34.7%	9.022	27.5%	21.010	25.5%	19.452
	incl.	35.2%	9.145	27.8%	21.242	26.0%	19.875

Table A.4: Radius of gyration values (81m vessel) for a range of delivery and in service loading conditions

	Leading edge CL position						
Description	Longitudinal	Offset	Height	Mean chord	Span	Area	Longitudinal centre of force
	(+ve fwd of transom) [m]	(about hull centreline) [m]	(above baseline) [m]	[m]	[m]	[m2]	(+ve fwd of transom) [m]
Transom tab	0.612	10.834	1.400	2.000	4.000	8.000	1.012
T-foil	56.400	10.834	0.600	1.216	2.395	2.912	55.792

Table A.5: Motion control surface positions and sizes (81m vessel)

A.2 86 metre Vessel (Hull 042)

The hydrostatics for the 86 metre vessel in the delivery load, service full load and service half load conditions are given in tables A.6, A.7, A.8 respectively. These conditions essentially encapsulate the range of loading conditions throughout the duration of experimental measurements. Figure A.2 is a representation of the hull fitted with motion control system comprised of transom mounted trim tabs and forward mounted T-foils, which are located at the positions given in table A.10.

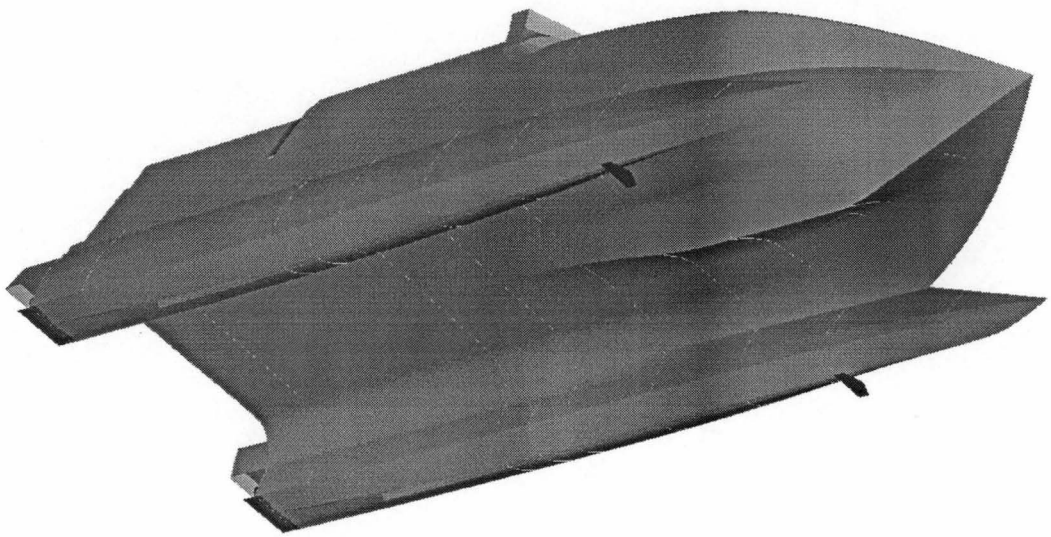

Figure A.2: Full motion control configuration with transom tabs and forward mounted T-foils (86 metre vessel, Hull 042)

	86 metre (Hull 042) Load Condition		Delivery - Lightship		Delivery - Full Departure		Delivery - Full, 10% arrival	
	Jet Inlet calculation method		Non-Buoyant	As tanks	Non-Buoyant	As tanks	Non-Buoyant	As tanks
1	Draft Amidships	[m]	2.693	2 695	3.449	3 45	2 815	2.816
2	Displacement	[t]	825	863	1209	1247	887	925
3	Heel to Starboard	[degree]	0	0	-0 05	-0.05	0 04	0.04
4	Draft at FP	[m]	2.302	2.281	3.396	3.395	2.457	2.446
5	Draft at AP	[m]	3.084	3 108	3.503	3.504	3.173	3 187
6	Draft at LCF	[m]	2.761	2.776	3.458	3.458	2.876	2.887
7	Trim (+ve by stern)	[m]	0.782	0.826	0.108	0.108	0.715	0.742
8	LWL	[m]	76.702	76.669	77.08	77.077	76.964	76.949
9	BWL	[m]	25 984	25.985	26	26	25 99	25.99
10	LWL/BWL	[m2]	17.7	17.7	17.7	17.7	17.7	17.7
11	LWL/draft amidships	[m2]	28.5	28.4	22.3	22.3	27.3	27.3
12	Wetted Area	-	902.776	903.833	1144.203	1144.227	941.944	942.758
13	Waterplane Area	-	516.443	529 801	544.509	546.223	523.707	534 956
14	Prismatic Coefficient	-	0.613	0.636	0.693	0.714	0.626	0.649
15	Block Coefficient	-	0 41	0.427	0 506	0 521	0.425	0.442
16	Midship Area Coefficient	[m]	0.722	0.724	0.773	0.773	0.73	0.73
17	Waterplane Area Coefficient	[m]	0.783	0 803	0 822	0 825	0.793	0.81
18	LCB to zero pt	[m]	27.586	26.461	30.433	29.576	28.047	26.989
19	LCF to zero pt.	[m]	31.5	30 646	32.273	32 17	31.687	30 991
20	KB	[m]	1.909	1.924	2.282	2.282	1.971	1.982
21	KGf	[m]	7 199	6 986	6.552	6 424	7 558	7.345
22	BMt	[m]	76.15	74.741	54.801	53.328	71.829	70.409
23	BML	[m]	218.812	224.72	173.063	169.375	211.393	215.24
24	GMt	[m]	70.86	69.678	50.531	49.186	66.241	65.046
25	GML	[m]	213.522	219 657	168 793	165.233	205.806	209 878
26	KMt	[m]	78.059	76.665	57.083	55.61	73.799	72.391
27	KML	[m]	220.721	226 644	175.345	171 657	213.364	217.223
28	TPc	[t/cm]	5.295	5.432	5.582	5.6	5.369	5.484
29	MTc	[t.m]	23 064	24.798	26.714	26 956	23.901	25.397
30	RM at 1deg = GMt.Disp.sin(1)	[t.m]	1020.713	1049.013	1066.472	1070.097	1025.902	1049.668
34	LOA	[m]	86 412	86 412	86.412	86.412	86 412	86.412
35	BOA	[m]	26	26	26	26	26	26
36	Lpp	[m]	76.412	76 412	76 412	76.412	76 412	76.412
37	Lpp/2	[m]	38.206	38.206	38.206	38.206	38.206	38.206
38	Demi-hull length	[m]	76.709	76.709	76.709	76 709	76.709	76.709
39	Demi-hull beam	[m]	4.33	4.33	4.33	4.33	4 33	4.33
40	AP (from zero)	[m]	0	0	0	0	0	0
41	Amidships (from zero)	[m]	38.206	38.206	38.206	38.206	38.206	38.206
42	Transom (from zero)	[m]	0	0	0	0	0	0
43	Amidships (from transom)	[m]	38.206	38.206	38.206	38.206	38.206	38.206
44	LCG (from zero)	[m]	27 633	26 515	30.438	29 580	28.097	27 035
45	LCG (from AP)	[m]	27.633	26.515	30.438	29 58	28.097	27.035
46	LCG (from amidships)	[m]	10 573	11.691	7.768	8.626	10 109	11.171
47	LCG (from transom)	[m]	27.633	26.515	30.438	29.58	28.097	27.035
48	Bow (from zero)	[m]	81 6	81 6	81 6	81.6	81 6	81 6

Table A.6: Principle hull particulars (86m vessel) for delivery loading conditions (Note: table contains light displacement (Delivery - Full, 10% arrival) condition as used in numerical predictions)

	86 metre (Hull 042) Load Condition		Service - Lightship		Service - Full Departure		Service - Full, 10% arrival	
	Jet Inlet calculation method		Non-Buoyant	As tanks	Non-Buoyant	As tanks	Non-Buoyant	As tanks
1	Draft Amidships	[m]	2 717	2 72	3.483	3 484	3 401	3 402
2	Displacement	[t]	834	871	1213	1251	1167	1204
3	Heel to Starboard	[degree]	0	0	-0.05	-0 05	0.04	0.04
4	Draft at FP	[m]	2.378	2.358	3.602	3.6	3.525	3.521
5	Draft at AP	[m]	3 056	3 082	3.364	3.368	3 276	3.283
6	Draft at LCF	[m]	2.775	2.79	3.465	3.465	3.382	3.383
7	Trim (+ve by stern)	[m]	0 678	0 724	-0.237	-0.232	-0.249	-0.237
8	LWL	[m]	76.827	76.795	77.77	77.756	78.024	77.984
9	BWL	[m]	25 984	25 985	26	26	26	26
10	LWL/BWL	[m2]	17.7	17.7	17.7	17.7	17.7	17.7
11	LWL/draft amidships	[m2]	28 3	28 2	22 3	22 3	22.9	22 9
12	Wetted Area	-	909.759	911.07	1150.826	1151.207	1122.42	1122 998
13	Waterplane Area	-	518 049	532 153	544 788	549 839	542 652	550.633
14	Prismatic Coefficient	-	0 619	0.642	0.707	0.728	0.703	0.725
15	Block Coefficient	-	0 416	0 432	0.519	0 534	0 512	0 527
16	Midship Area Coefficient	[m]	0.722	0.723	0.806	0.806	0.801	0.802
17	Waterplane Area Coefficient	[m]	0 785	0.807	0.823	0 83	0 82	0 832
18	LCB to zero pt	[m]	27.92	26.802	31.216	30.342	31.196	30.289
19	LCF to zero pt	[m]	31 662	30 77	32 399	32 097	32 454	31 977
20	KB	[m]	1.914	1 929	2.287	2.286	2.242	2.243
21	KGf	[m]	7.138	6 93	7 726	7 564	7 952	7 776
22	BMt	[m]	75.632	74.357	54.651	53.511	56.597	55.647
23	BML	[m]	218 729	225 545	172.927	172.158	177 933	179.585
24	GMt	[m]	70.408	69.356	49.212	48.233	50.887	50.113
25	GML	[m]	213.505	220 544	167 487	166 88	172 222	174.051
26	KMt	[m]	77.546	76.286	56.938	55.797	58.839	57.89
27	KML	[m]	220 643	227 474	175 214	174.444	180 174	181 828
28	TPc	[t/cm]	5.311	5.456	5.585	5.637	5.563	5.645
29	MTc	[t m]	23.292	25.137	26 593	27 311	26 302	27 43
30	RM at 1deg = GMt Disp.sin(1)	[t m]	1024.336	1054.207	1042.006	1052.681	1036.363	1053.233
34	LOA	[m]	86 412	86 412	86.412	86 412	86 412	86 412
35	BOA	[m]	26	26	26	26	26	26
36	Lpp	[m]	76 412	76.412	76.412	76.412	76 412	76 412
37	Lpp/2	[m]	38.206	38.206	38.206	38 206	38.206	38 206
38	Demi-hull length	[m]	76.709	76 709	76 709	76 709	76 709	76 709
39	Demi-hull beam	[m]	4.33	4.33	4.33	4.33	4.33	4.33
40	AP (from zero)	[m]	0	0	0	0	0	0
41	Amidships (from zero)	[m]	38.206	38.206	38.206	38.206	38.206	38.206
42	Transom (from zero)	[m]	0	0	0	0	0	0
43	Amidships (from transom)	[m]	38.206	38.206	38.206	38.206	38 206	38.206
44	LCG (from zero)	[m]	27.964	26 842	31 202	30 324	31 178	30 267
45	LCG (from AP)	[m]	27.964	26 842	31.202	30 324	31.178	30 267
46	LCG (from amidships)	[m]	10 242	11 364	7 004	7 882	7 028	7.939
47	LCG (from transom)	[m]	27.964	26.842	31.202	30.324	31 178	30.267
48	Bow (from zero)	[m]	81 6	81 6	81 6	81 6	81 6	81 6

Table A.7: Principle hull particulars (86m vessel) for in service 100% load conditions (Note: table contains heavy displacement (Service - Full departure) condition as used in numerical predictions)

	86 metre (Hull 042) Load Condition		Service - 50% Full Departure		Service - 50% Full, 10% Arrival	
	Jet Inlet calculation method		Non-Buoyant	As tanks	Non-Buoyant	As tanks
1	Draft Amidships	[m]	3 212	3.214	3.128	3 132
2	Displacement	[t]	1067	1104	1021	1058
3	Heel to Starboard	[degree]	-0.05	-0 05	0.04	0.04
4	Draft at FP	[m]	3.28	3.267	3.203	3.184
5	Draft at AP	[m]	3.144	3.161	3.054	3.079
6	Draft at LCF	[m]	3.202	3.205	3.117	3.123
7	Trim (+ve by stern)	[m]	-0.136	-0.106	-0.149	-0.105
8	LWL	[m]	78.021	78.005	77.927	77.904
9	BWL	[m]	25.997	25.997	25.994	25.994
10	LWL/BWL	[m2]	17.7	17.7	17.7	17.7
11	LWL/draft amidships	[m2]	24.3	24.3	24.9	24.9
12	Wetted Area	-	1061.615	1062.634	1034.514	1035.969
13	Waterplane Area	-	537.077	549.291	534.312	548 608
14	Prismatic Coefficient	-	0.69	0.712	0.686	0.707
15	Block Coefficient	-	0.49	0.506	0.483	0 498
16	Midship Area Coefficient	[m]	0.763	0.758	0.764	0.752
17	Waterplane Area Coefficient	[m]	0.812	0.83	0.808	0.83
18	LCB to zero pt.	[m]	30.79	29.81	30.743	29.724
19	LCF to zero pt.	[m]	32 516	31.778	32 563	31.695
20	KB	[m]	2.143	2.147	2.097	2.102
21	KGf	[m]	7.515	7.338	7.763	7.57
22	BMt	[m]	61.265	60.536	63.709	63.105
23	BML	[m]	189.239	194 711	195.211	202.723
24	GMt	[m]	55.893	55.345	58.042	57.637
25	GML	[m]	183 867	189 52	189.545	197.255
26	KMt	[m]	63.408	62.683	65.805	65.207
27	KML	[m]	191 382	196 857	197.308	204.825
28	TPc	[t/cm]	5.506	5.631	5.478	5.624
29	MTc	[t.m]	25 675	27 388	25.319	27.312
30	RM at 1deg = GMt.Disp.sin(1)	[t m]	1040.816	1066.622	1033.957	1064.24
34	LOA	[m]	86.412	86.412	86.412	86.412
35	BOA	[m]	26	26	26	26
36	Lpp	[m]	76.412	76.412	76.412	76.412
37	Lpp/2	[m]	38.206	38.206	38.206	38.206
38	Demi-hull length	[m]	76.709	76.709	76.709	76.709
39	Demi-hull beam	[m]	4.33	4.33	4.33	4.33
40	AP (from zero)	[m]	0	0	0	0
41	Amidships (from zero)	[m]	38.206	38.206	38.206	38.206
42	Transom (from zero)	[m]	0	0	0	0
43	Amidships (from transom)	[m]	38.206	38.206	38.206	38.206
44	LCG (from zero)	[m]	30.782	29.802	30 736	29.715
45	LCG (from AP)	[m]	30.782	29.802	30.736	29.715
46	LCG (from amidships)	[m]	7 424	8.404	7.47	8 491
47	LCG (from transom)	[m]	30.782	29.802	30.736	29.715
48	Bow (from zero)	[m]	81 6	81.6	81.6	81.6

Table A.8: Principle hull particulars (86m vessel) for in service 50% load conditions

	Entrained water?	ROLL		PITCH		YAW	
		% of BOA	[m]	% of Lpp	[m]	% of Lpp	[m]
Delivery - Lightship	excluded	39.0%	10.137	29.3%	22.386	28.2%	21.517
	included	39.3%	10.220	29.5%	22.530	28.6%	21.834
Delivery - Full Departure	excluded	40.4%	10.508	25.2%	19.238	25.2%	19.294
	included	40.5%	10.540	25.6%	19.575	25.8%	19.721
Delivery - Full, 10% arrival	excluded	39.5%	10.268	28.5%	21.768	27.6%	21.086
	included	39.7%	10.335	28.7%	21.954	28.0%	21.427
Service - Lightship	excluded	39.1%	10.163	29.5%	22.519	28.4%	21.699
	included	39.4%	10.243	29.7%	22.671	28.8%	22.019
Service - Full Departure	excluded	36.3%	9.425	29.3%	22.352	27.3%	20.847
	included	36.6%	9.518	29.6%	22.585	27.8%	21.239
Service - Full, 10% arrival	excluded	35.7%	9.290	29.8%	22.786	27.6%	21.117
	included	36.1%	9.395	30.1%	23.009	28.2%	21.510
Service - 50% Full Departure	excluded	37.5%	9.762	29.4%	22.441	27.7%	21.195
	included	37.9%	9.848	29.7%	22.681	28.3%	21.596
Service - 50% Full, 10% arrival	excluded	37.1%	9.634	30.0%	22.938	28.2%	21.515
	included	37.4%	9.733	30.3%	23.163	28.7%	21.915

Table A.9: Radius of gyration values (86m vessel) for a range of delivery and in service loading conditions

	Leading edge CL position						
Description	Longitudinal (+ve fwd of transom) [m]	Offset (about hull centreline) [m]	Height (above baseline) [m]	Mean chord [m]	Span [m]	Area [m2]	Longitudinal centre of force (+ve fwd of transom) [m]
Transom tab	0.600	10.834	1.296	2.000	4.000	8.000	1.000
T-foil	61.800	10.834	0.200	1.216	2.395	2.912	61.192

Table A.10: Motion control surface positions and sizes (86m vessel)

Appendix B

Experimental Instrumentation and Data

B.1 Instrumentation on the 81 metre Vessel (Hull 038)

The 81 metre vessel instrumentation consisted of

1. TSK wave meter with analog outputs were connected to the A/D board of the "Daqbook";
2. Notebook computer with data acquisition software;
3. "IOtech Daqbook 112" A/D conversion module;
4. "IOtech DBK 43" strain gauge module;
5. 8 structurally mounted strain gauges with a direct cable connection to the junction box mounted in the bridge;
6. Global positioning system (GPS) data cable between the GPS to the serial port of Notebook computer;
7. Connection to the "Maritime Dynamics" (MDI) motions control system A/D board of the "Daqbook".

A junction box mounted on the port side of the bridge terminated all ship connections prior to connection with the data acquisition system.

B.1.1 TSK Wave Meter

The TSK unit measures ocean wave amplitudes and periods by mounting it directly over the free surface at the bow of the vessel. The data signals are returned to a processor that calculates running averages of the wave height and period whilst also providing the surface profile using the relative distance from the sensor to the free surface and the acceleration signal. The significant wave height, bow vertical displacement, relative wave height (sensor to free surface) and wave profile outputs were obtained from BNC analog output connectors located on the units' processor. Alternatively, real time wave height time series data was available in digital RS232. The reader is directed to the TSK wave height meter operators manual (TSKA (1993)) for further information about the operation of this unit. Some of these details have been reproduced here. The calculated data was also displayed for viewing on the processor unit.

Specification

- Wave Height Range: ±14.5 meters
- Wave Height Resolution: 1.4 cm
- Wave Height Accuracy: 10% of measured wave height
- Wave period range: 0-20 seconds
- Power requirements: 0.6 amp, 110VAC (240V adaptor)
- Operating temperature range: 0-40deg C

B.1.1.1 Bow Mounted Sensor

The Sensor unit contains a Gunn oscillator, two detector diodes, a microwave horn and two amplifiers. X-band microwave radar emissions are emitted vertically downward at the moving sea surface. Reflected microwaves which have undergone a Doppler shift caused by the moving sea surface undergo a change in frequency. The returned signal are mixed with the original microwave signal in the sensor wave guide. The resulting interference pattern is detected by the diodes and used to calculate the relative vertical wave velocity. Through integration of this signal, the relative wave displacement is calculated.

Specification

- Output frequency: 10.525 GHz
- Output power: 10mW
- Antenna Gain: 19dB
- Microwave beam angle: 13 degrees
- Weight: 11kg
- Size: 260mm diameter by 350mm high
- Operating temperature range: -20°C to 50°C
- Maximum ship roll: ±15 degrees

B.1.1.2 TSK Accelerometer

A single accelerometer mounted adjacent to the microwave sensor was used to measure the bow vertical acceleration. The accelerometer was located inside an oil filled case and used a servo amplifier to output a signal representing the force imposed on the seismic mass under acceleration.

Vertical motion only is required for the wave height calculation. The vertical motions are measured by use of a gimbal mounting system to ensure the accelerometer is kept vertical to remove the measurement of accelerations in other directions. A viscous fluid level is maintained in the case to dampen the motion for the sensor.

Specification

- Range: $\pm 2g$ (2V/g)
- Accuracy: $\pm 0.5\%$ full scale
- Weight: 7.5 kg
- Size: 170mm x 170mm x 140mm
- Oil: Silicon, KF96, with kinematic viscosity of 5000 centistoke = 5000 scm/s

B.1.1.3 Fore-peak Junction Box

Signals from the TSK sea surface transducer and accelerometer were connected to a junction box mounted in the forward hull compartment which supplied the transducers with ± 15 VDC of power. The junction box was connected to the TSK processor unit mounted in the bridge. Waterproof connectors were used to allow easy removal of the junction box at the conclusion of the measurements. (See Farnell catalogue Amphenol free socket 5 way 14S5S MS 3106A Farnell 617-120; also cable cleanup and bush 97-3057-1007-1, Farnell 151-627)

The maximum distance permitted between the accelerometer or microwave sensor and the junction box was 20 metres whilst the maximum distance between the signal processor and the junction box was 50 metres.

Junction Box Specification

- Weight: 4kg
- Size: 290x150x290mm

System Cable Specification Outer insulation and shielding:

- Outside diameter: 10.5 mm
- Outside sheath: Black PVC, 10.5 mm OD, 1.1 mm thick
- Inner sheath: Black PVC, 7.7 mm OD, 1.0 mm thick
- Shielding: Steel braided armor, 8.3 mm OD

Conductors:

- Quantity: 6 conductors
- Composition: 20/0.18TA, 0.9 mm OD
- Diameter: 0.5 mm^2
- Insulation: PVC, 1.9 mm OD, 0.5 mm thick
- Insulation resistance: >10 MOhm/km
- Conductor resistance: <39.4 Ohm/km

B.1.1.4 TSK Signal Processor Display Unit

The signal processor unit mounted on the bridge received the raw data signals from the accelerometer and the sea surface transducer from which it calculated the running wave statistics. It achieved this by taking data from the microwave sensor and passing it through a phase discriminator which determined whether the wave motion was up or down. Since the Doppler data measured wave velocity, the signal was integrated to calculate the wave surface displacement. Likewise, the accelerometer data was double integrated in time to calculate the vertical bow displacement in time. The accelerometer displacement signal was subtracted from the microwave sensor to sea surface relative distance data to calculate the wave height in time which was passed to the significant wave height and mean period calculation circuits. The sensor data output rate was switch selectable and was set at 10 Hertz.

Specifications

- Weight: 6.5 kg
- Size: 480x99x127mm

Analog Data Output The maximum range of all five analog channels was ±15 volts. The maximum output range of the TSK unit was ±5 volts (20 metres wave height) which was compatible with the ±5 volt range of the Daqbook containing the A/D card.

Abbreviation	Channel	Conversion	Range (V)	Range
SD	Ship Displacement	$SD = 10$ m/V $\times V$	-1 to +1	±10 m
RWH	Relative Wave Height	$RWH = 10$ m/V $\times V$	-1 to +1	±10 m
WH	Wave Height	$WH = 2$ m/V $\times V$	-5 to +5	±10 m
SWH	Significant Wave Height	$SWH = 4$ m/V $\times V$	0 to +2.5	0 to +10 m
AWP	Average Wave Period	$AWP = 4$ sec/V $\times V$	0 to +5	0 to +20 sec

Table B.1: Calibration values for wave meter

B.1.1.5 Processor Unit Calibration

Calibration of the unit was an electrical factory calibration where an oscillator and dummy generator replaced the microwave sensor and input signal to the processor. The oscillator frequency is compared to the processor output and calibration made with potentiometers to obtain agreement between the two.

B.1.1.6 Significant Wave Height

The TSK processor unit calculated the significant wave height according to the procedure given by Tucker (1991) (see p94) which assumes the sea surface to be a random Gaussian process. The real time wave data is passed through a rectifier circuit, then through an averager, which uses the last 6 minutes of data. The significant wave height is calculated 5.01 times the average rectified wave height.

The average encounter period was calculated by counting the number of times the wave height passes downward through the average sea level. The counts were added for the latest twenty minutes of data and the period was then calculated with the formula (20 minutes)/(number of counts).

B.1.2 Analog to Digital Conversion Module

The analog to digital conversion model was a commercially available IOtech Daqbook 112 device that connected to the computer through the parallel port and a 12V power supply. It contained a screw terminal card to which the analog input signals were connected that included the TSK wave meter and the ship motion transducers.

The Daqbook had a 12 bit acquisition card corresponding to 4096 levels. The full range of the card was $\pm 5V$ giving a $2.441mV$ $(\frac{10V}{4096})$ resolution when the gain was set to unity.

B.1.3 GPS Connection

Connection to the ship Global Positioning System (GPS) consisted of a ground and signal connected to the 9 pin serial port of the computer. The GPS output was an industry standard interface NMEA 0183.

B.1.4 Motion Instrumentation Output

Motion measurements were made using the existing ship transducers to obtain the vertical accelerations on the hull centreline at the bow, centre of gravity and aft locations. The accelerometers contained a 2-pole low pass filter with a 5 Hz cut off frequency. Pitch and roll measurements were recorded from rate gyros located near the hull centre of gravity. There were a total of six outputs from the motion instrumentation system made up from 3 twisted pairs which are summarized in table B.2.

No.	Motion output wire	Signal	Signal range	Voltage	Voltage after voltage divider
1	Black	Pitch	$\pm 10°$	0 to 5	0 to 5
2	Blue	Roll	$\pm 10°$	0 to 5	0 to 5
3	Red	Bow accelerometer	$\pm 2g$	± 10	± 5
4	Orange	LCG accelerometer	$\pm 2g$	± 10	± 5
5	White	Aft vertical accel.	$\pm 2g$	± 10	± 5
6	Green	Common	$\pm 2g$	± 10	± 5

Table B.2: Motions calibration (81m vessel)

B.1.5 Data Output

Data acquisition commenced initially with Daqview software until the implementation of the custom written Labview software. These files were recorded in one storage folder of the computer designated 038data1 whilst all subsequent files acquired with Labview were recorded in the storage folders 038data2 to 038data10. The different folders represent new file formats as alterations and improvements were made.

All connections to the PC were made through the screw terminal card mounted in the A/D module. The channel connections made to the screw terminal card are listed in table B.4. This table also shows the format of the data files within the various storage folders. Where more than one input was used on a particular channel, all variations are shown. Variations of the input type only affected the wave meter inputs.

		Acquisition subgroups					
		try1data\ try2data\ 038data2\ 038data3\ 038data4\		038data5\		038data6\ 038data7\ 038data8\ - poor 038data9a\ - poor 038data9b\ - poor 038data10\ - poor	
***.cor file column index**	**Signal Channel**	**Corresponding file headers**	***.cor file units**	**Corresponding file headers**	***.cor file units**	**Corresponding file headers**	***.cor file units**
1	1	Bow accelerometer	g	>same		>same	
2	2	LCG accelerometer	g	>same		>same	
3	3	Roll gyro	deg.	>same		>same	
4	4	Pitch gyro	deg.	>same		>same	
Not in file	5	Ultrasonic wave detector	V	>same		>same	
5	6	Port transom tab	V	>same		>same	
6	7	Stbd transom tab	V	>same		>same	
7	8	TSK - SD*	m	>same		>same	
8	9	TSK - WH*	m	>same		TSK - RWH*	m
9	10	TSK - SWH*	m	>same		TSK - WH*	m
10	11	TSK - AWP*	sec	TSK - RWH*	m	TSK - SWH*	m
11	16	S.G.-16	MPa	>same		>same	
12	17	S.G.-17	MPa	>same		>same	
13	18	S.G.-18	MPa	>same		>same	
14	19	S.G.-19	MPa	>same		>same	
15	20	S.G.-20	MPa	>same		>same	
Not in file	21	S.G.-21	MPa	>same		>same	
16	22	S.G.-22	MPa	>same		>same	
17	23	S.G.-23	MPa	>same		>same	

*

TSK - SD	Vertical displacement as measured by the TSK unit
TSK - WH	Sea surface displacement as measured by the TSK unit
TSK - SWH	Significant wave height as measured by the TSK unit
TSK - AWP	Average wave period as measured by the TSK unit
TSK - RWH	Relative wave height as measured by the TSK unit

ref/ c:\1Nigel\038DATA\038\Data information\038 data summary

Table B.3: Channel configuration and header list for *.cor files (81m vessel)

*.cor file column index	Signal Channel	Units	Item	Location Description	Longitudinal [m]	Transverse [m]	Vertical [m]
1	1	g	Bow vertical accelerometer (+ve up)	Fwd of forward peak bulkhead, near vessesl CL, frame 59	70.800	0.000	10.652
2	2	g	LCG vertical accelerometer (+ve up)	Aft side of frame 22 under main car deck, on vessel CL	26.000	0.000	6.200
3	3	deg	Roll (+ve stbd down)	Aft side of frame 22 under main car deck, on vessel CL	26.000	0.000	6.200
4	4	deg	Pitch (+ve bow up)	Aft side of frame 22 under main car deck, on vessel CL	26.000	0.000	6.200
-	5	m	Ultrasonic relative wave height	Port bow	74.4	-1.8	10.652
5	6	V	Port tab	Port jet room	0.600	-10.834	1.400
6	7	V	Starboard tab	Starboard jet room	0.600	10.834	1.400
7	8	V	Ship displacement (SD - TSK output)	On platform in FP compartment, on vessel CL, frame 62	74.000	0.000	10.300
8	9	m	(WH or RWH - TSK output)	Taken at transducer mount, frame 62	74.400	-1.800	10.652
9	10	m	(SWH or WH - TSK output)	Taken at transducer mount, frame 62	-	-	-
10	11	s, m	(AWP, RWH or SWH - TSK output)	Taken at transducer mount, frame 62	-	-	-
11	16	MPa	Strain gauge 16 (Al)	Port portal top aft, Fr 10	12	-11.5	11.2
12	17	MPa	Strain gauge 17 (Al)	Port port top midship, mid fr 24-25	28.8	-11.5	11.2
13	18	MPa	Strain gauge 18 (Al)	Keel plate port midship, mid fr 24-25	28.8	-10.834	0.892
14	19	MPa	Strain gauge 19 (Al)	Port portal top fwd, mid fr 32-33	38.4	-11.5	11.2
15	20	MPa	Strain gauge 20 (Al)	Steel vertical support, port face at top, fr	40.8	0	10.35
-	21	MPa	Strain gauge 21 (Al)	B/H fr 34 vessel centreline - Vertical DNE	40.8	0	10.35
16	22	MPa	Strain gauge 22 (Al)	B/H fr 34 vessel centreline - Horizontal	40.8	0	10.35
17	23	MPa	Strain gauge 23 (Al)	B/H fr 34 vessel centreline - 45 deg	40.8	0	10.35

ref/ c:\1Nigel\038DATA\038\Data information\038 data summary

Table B.4: Instrumentation positions, channel configuration and header list for *.cor files (81m vessel)

B.2 Instrumentation on the 86 metre Vessel (Hull 042)

The hardware installation on the 86 metre vessel had some unique differences to the 81 metre vessel in the arrangement of the strain gauges and an expansion of the amount of recorded data. An extra accelerometer mounted aft in the hull was included and extra GPS string outputs such as vessel heading were included. The following gives an overview of the hardware installed on the vessel where it remained for the delivery voyage and the following twelve months.

1. TSK wave meter with analog outputs connected via the Daqbook;
2. Notebook computer with DAQ software;
3. IOtech Daqbook 112 A/D conversion module;
4. IOtech DBK 43 strain gauge module;
5. 8 structurally mounted strain gauges with appropriate cable connection to the bridge junction box;
6. GPS data cable from GPS to serial port of Notebook computer;
7. Connection to the bridge motions control board with a data cable, and
8. 10 Channel Analog Optoisolater with in built voltage divider for mounting between the Daqbook and the MDI motion control panel.

A junction box mounted on the port side of the bridge terminated all ship connections prior to connection with the data acquisition system. For details of the TSK wave meter, notebook computer, analog to digital conversion and GPS connection, the reader is referred to the notes for the 81 metre vessel.

B.2.1 Motion Instrumentation

Motion measurements were made using accelerometers positioned at the bow, centre of gravity (CG), on the port side adjacent to the CG and in the aft end. The accelerometers from the ship mounted motion control system contained a 2-pole, unity gain, 50 Hertz low pass filter. There were a total of six outputs from the motion instrumentation system made up from 3 twisted pairs which are summarized in table B.5.

No.	Motion control system output conections	Signal	Signal range	Voltage range	Voltage after optical iscolator
1	White	Bow vertical accel.	$\pm 2g$	± 10	± 5
2	Black (white associated)	LCG vertical accel.	$\pm 2g$	± 10	± 5
3	Red	Aft vertical accel.	$\pm 2g$	± 10	± 5
4	Black (red associated)	Common	$\pm 2g$	± 10	± 5
5	Green	Pitch (unassigned)	$\pm 10°$	0 to +5	0 to +5
6	Black (green associated)	Roll (unassigned)	$\pm 10°$	0 to +5	0 to +5

Table B.5: Motions channel calibrations (86m vessel)

B.2.1.1 Optical Isolator

The Optical isolator unit was connected between the Daqbook A/D input module and the ship's motion control system to prevent ground loops between the data acquisition system and the ship's motion control system (MCS).

B.2.2 Ship Electrical Junction Boxes

Electrical junction boxes were placed in the bow for the wave meter and accelerometer which was connected to a junction box on the port side of the vehicle deck which was connected to a bridge junction box by a 32 core cable. It was from this junction box that connections were made to the Daqbook containing the A/D card.

B.2.3 Data Output

Data acquisition made use of custom written Labview software to acquire the data. These files were recorded in the four storage folders. The different folders represented new file formats as alterations and improvements were made. All connections to the PC were made through the screw terminal card mounted in the A/D module. The channel connections made to the screw terminal card are listed in table B.6. This table also shows the format of the data files.

*.cor file column index	Signal Channel	Units	Item	Location Description	Longitudinal [m]	Transverse [m]	Vertical [m]
1	1	g	Bow vertical accelerometer (+ve up)	Fwd of forward peak bulkhead, near vessesl CL, Fr 62	74.5	0	11
2	2	g	LCG vertical accelerometer (+ve up)	Aft side of frame 27 under main car deck, on vessel CL	32.2	0	6.6
3	3	g	Aft vertical accelerometer (+ve up)	Near frame 1 under main car deck, on vessel CL	1.2	0	6.6
4	4	degrees	Pitch (+ve bow up)	Aft side of frame 27 under car deck, on vessel CL	-	-	-
5	5	degrees	Roll (+ve stbd down)	Aft side of frame 27 under car deck, on vessel CL	-	-	-
6	6	metres	Ship displacement (SD - TSK output) (+ve up)	On platform just behind frame 63, fwd of FP bulkhead, on vessel CL	75	0	10.5
7	7	metres	Relative surface displacement (RWH - TSK output)	Taken at transducer mount, frame 66	79.2	-2.5	10.8
8	8	metres	Sea surface displacement (WH - TSK output)	Taken at transducer mount, frame 66	-	-	-
9	9	metres	Derived sea surface displacement (WH_derived)	Taken at transducer mount, frame 66	-	-	-
10	10	metres	Significant wave height (WH - TSK output)	Taken at transducer mount, frame 66	-	-	-
11	16	MPa	Strain gauge 16 (on steel)	Aft port steel Chevron brace fwd of frame 1, underside face near vessel CL	1.5	-0.5	11
12	17	MPa	Strain gauge 17 (on steel)	Aft stbd steel Chevron brace fwd of frame 1, underside face near vessel CL	1.5	0.5	11
13	18	MPa	Strain gauge 18 (on aluminium)	Transverse square section girder at frame 14, on topside side, on vessel CL	16.8	0	12
14	19	MPa	Strain gauge 19 (on aluminium)	Transverse square section girder at frame 14, on bottom side, on vessel CL	16.8	0	10.5
15	20	MPa	Strain gauge 20 (on aluminium)	Inner bat cross structure side, aft face, fwd of frame 14	17.5	-2	10.5
16	21	MPa	Strain gauge 21 (on aluminium)	Outer bat cross structure side, aft face, fwd of frame 14	17.5	-6	10.5
17	22	MPa	Strain gauge 22 (on aluminium)	Longitudinal beams, 4300 off centre, top face of beam flange, frame 24.5	29.4	-4.3	11
18	23	MPa	Strain gauge 23 (on aluminium)	Port portal top, top mid face of web, frame 24.5	29.4	-11	10.7
19	24	MPa	Strain gauge 24 (on aluminium)	Longitudinal member 4300 off centre, top face of beam flange, frame 32	38.4	-4.3	11
20	25	MPa	Strain gauge 25 (on aluminium)	Transverse horizontal girder over vehicle deck, lower web aft face, frame 35	42	0	10
21	26	MPa	Strain gauge 26 (on aluminium)	Keel plate, frame 24.5	29.4	-10.834	0.5
22	27	MPa	Strain gauge 27 (on aluminium)	Keel plate, frame 35.5	42.6	-10.834	0.8
23	28	MPa	Strain gauge 28 (on aluminium)	Keel plate, frame 41.5	49.8	-10.834	0.9
24	29	MPa	Strain gauge 29 (on steel)	Port steel column, aft face, mid height, frame 54	64.8	-3.8	9.6
25	30	MPa	Strain gauge 30 (on steel)	Stbd steel column, aft face, mid height, frame 54	64.8	3.8	9.6
26	31	MPa	Strain gauge 31 (on aluminium)	Tunnel structure under car deck, fwd face, lower web, frame 26	31.43	0	6.4
27	11	g	Port mounted accelerometer	Mounted over electrical junction box on port side of main vehicle deck, frame 27	32.4	-10.834	8.625

ref/ c:\1Nigel\042DATA\042\Data information\042_channel_description(thesis).xls

Table B.6: Instrumentation positions, channel configuration and header list for *.cor files (86m vessel). Roll and pitch although not directly recorded were post calculated and reentered back into the *.cor data file

Appendix C

Bestsea Hull Geometry Definition

The time domain program Bestsea required a geometry file that defined the hull shape to contain a number of regularly spaced sections along the ship length. Each section was defined by a series of offsets defined by x (horizontal) and y (vertical) coordinates. Table C.1 shows the required format of this file.

n_s		:number of sections
n_{p1}		:No. points in section 1 (2nd after the zero section at bow)
x_1	y_1	:highest vertical coordinate of section 1
x_2	y_2	.
.	.	.
x_{np1}	y_{np1}	:coordinate at the keel of section 1
n_{p2}		:No. points in section 2
x_1	y_1	:highest vertical coordinate of section 2
x_2	y_2	.
.	.	.
x_{np2}	y_{np2}	:coordinate at the keel of section 2
n_{p1}		:No. points in section i
x_1	y_1	:highest vertical coordinate of section i
x_2	y_2	.
.	.	.
x_{npi}	y_{npi}	:coordinate at the keel of section i
$n_{p(n_s)}$		:No. points in section ns (stern)
x_1	y_1	:highest vertical coordinate of section ns
x_2	y_2	.
.	.	.
$x_{np(n_s)}$	$y_{np(n_s)}$	:coordinate at the keel of section ns

Table C.1: Bestsea program geometry input file format

Appendix D

Labview program listing

The front screen of the computer programs written to create BESTSEA input files and to post process the BESTSEA output data are shown in figures D.1 and D.2 respectively. Other programs used in the analysis are shown in figures D.3 and D.4.

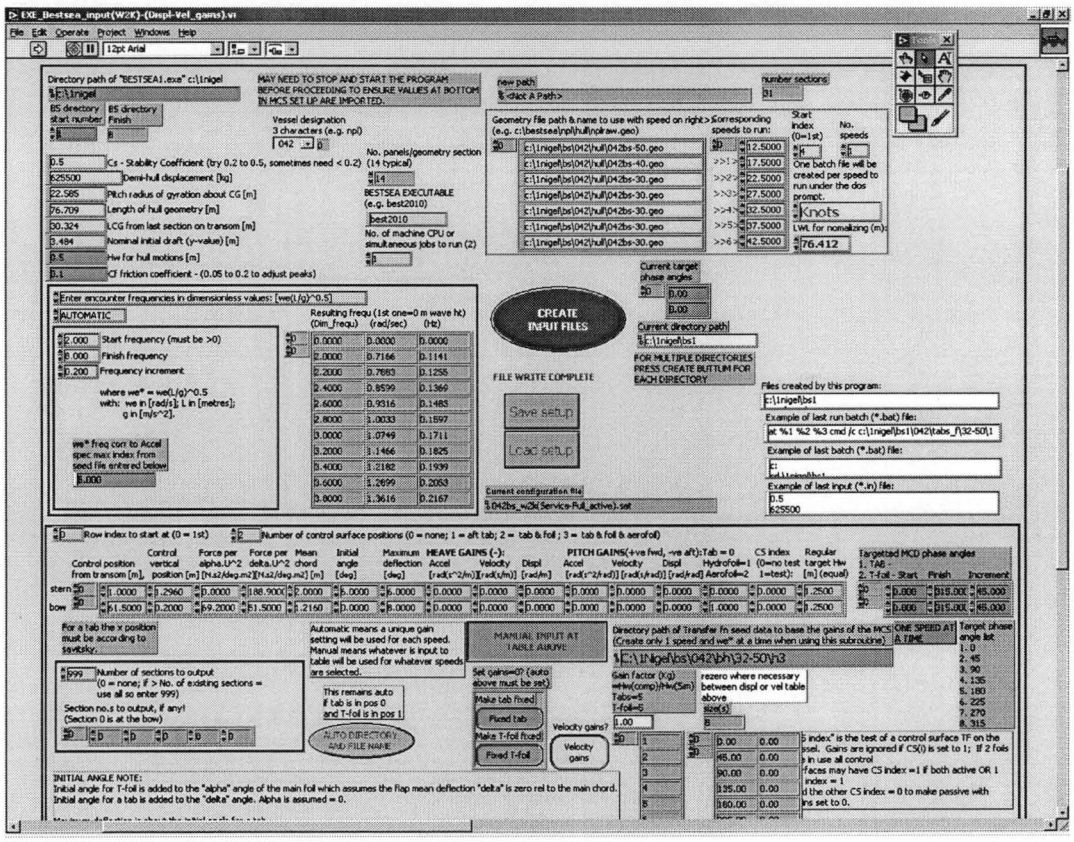

Figure D.1: BESTSEA time domain computation input configuration program

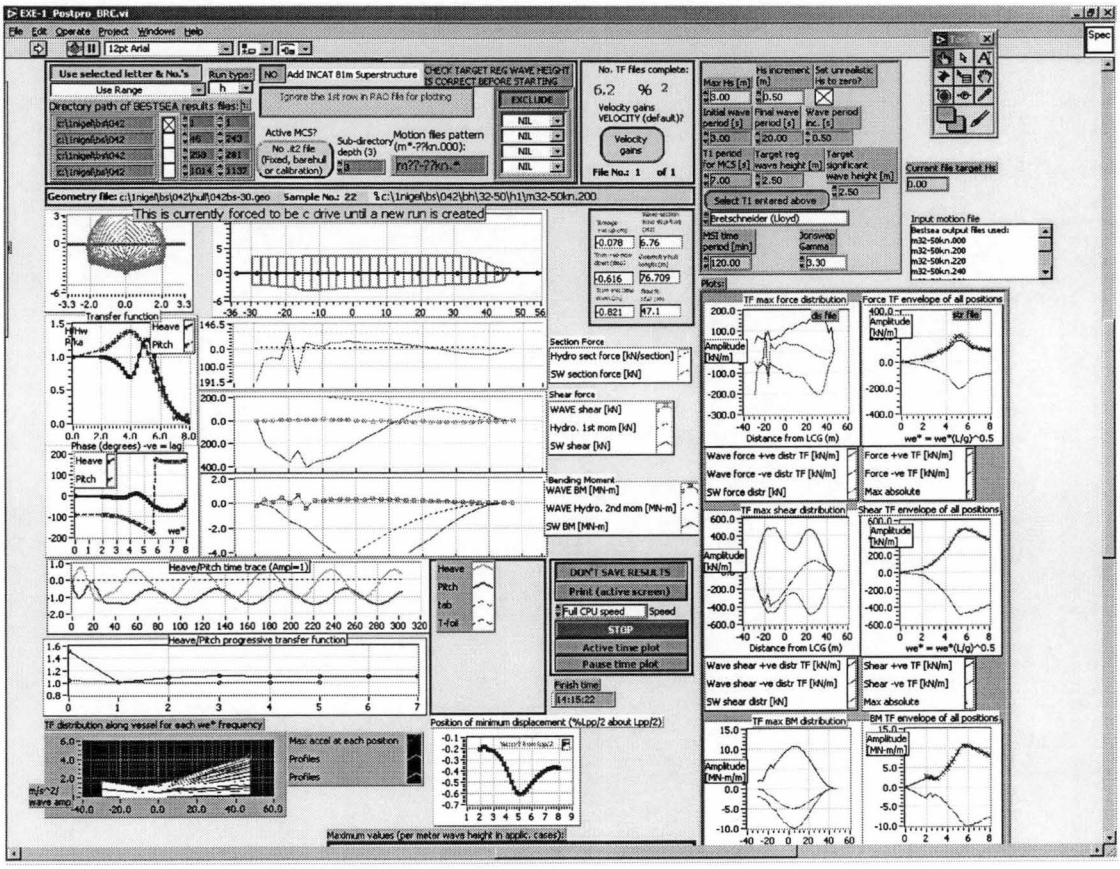

Figure D.2: BESTSEA time domain numerical computation post analysis program

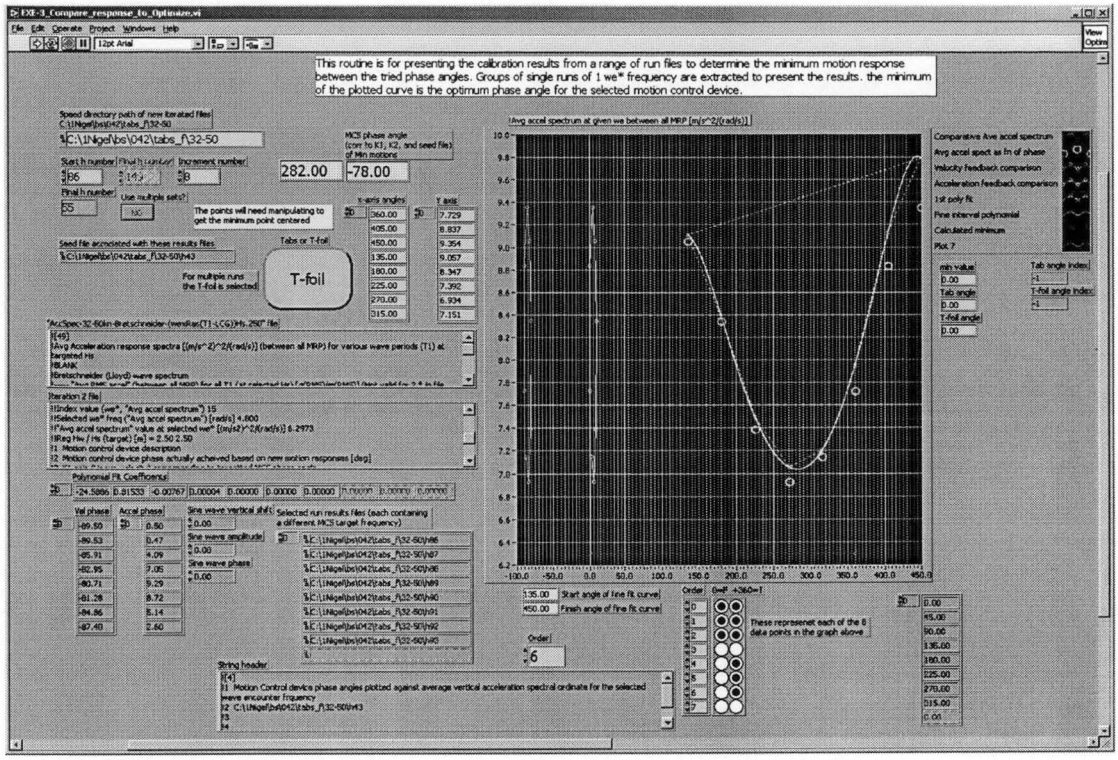

Figure D.3: Motion control system phase optimization plotting program for extracting the minimum phase angle.

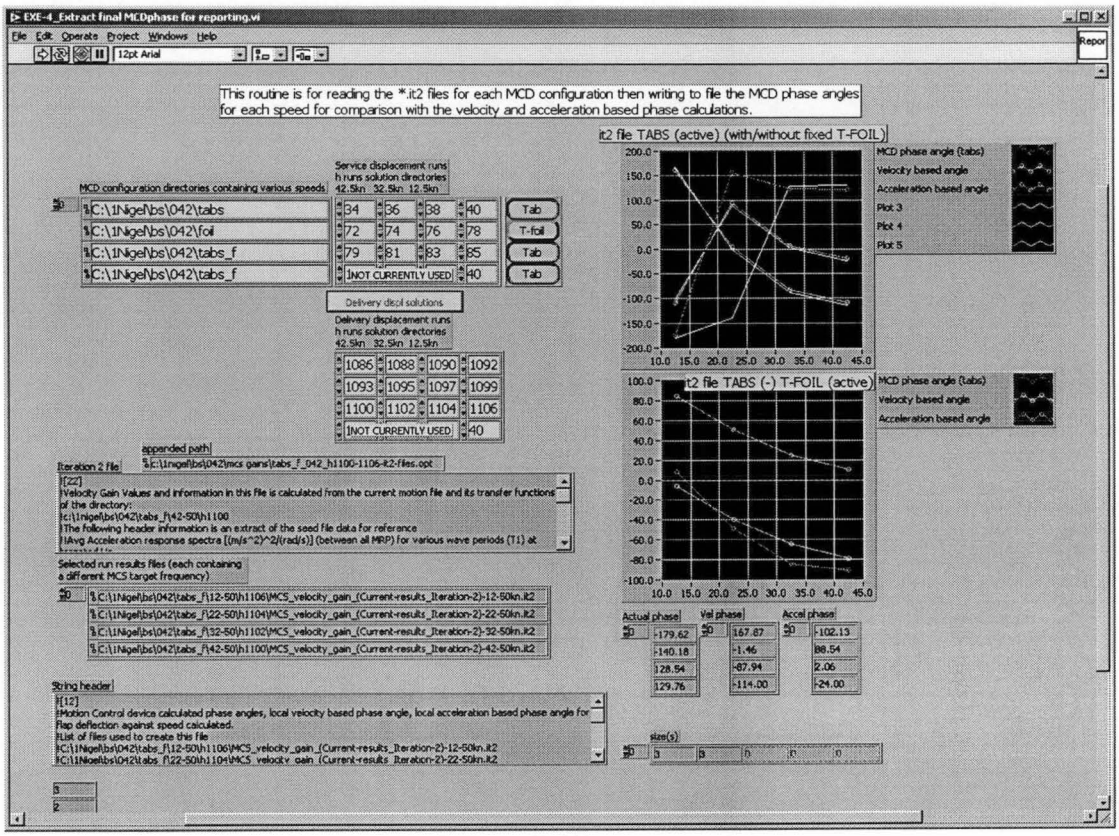

Figure D.4: Routine for extracting the phase angles for reporting

Appendix E

The Bretschneider Wave Spectrum

The Generalized or Modified Pierson-Moskowitz wave spectrum Tucker (1991) Pp107-108 also known as the Bretschneider, ITTC or ISSC wave spectrum provided the basis on which the vessel response was determined for the numerical computations and is presented in various text (Tucker (1991) (p106), Lloyd (1989), Lewis (1988a) (p37), Phelps (1997)). Other spectra such as the Jonswap, Ochi 6-parameter are equally useful for particular applications.

Lewis (1988a) (p36) gives the form of the Pierson-Moskowitz spectrum for fully developed seas as,

$$S(\omega) = \alpha g^2 \omega^{-5} \exp\left[-\beta\left(\frac{\omega_0}{\omega}\right)^4\right] \tag{E.1}$$

where

$$\begin{aligned} S(\omega) &= \text{spectral ordinate } [m^2 s] \\ \omega &= \text{frequency [rad/s]} \\ \omega_0 &= g/V_w \\ \alpha &= 0.00810 \\ \beta &= 0.74 \\ g &= \text{acceleration of gravity } [m/s^2] \\ V_w &= \text{wind velocity in } [m/s] \text{ (19.5 m above the surface)} \end{aligned}$$

by setting $\frac{dS(\omega)}{df} = 0$ in equation E.1, the peak or modal frequency ω_m is given as

$$\begin{aligned} \left(\frac{\omega_m}{\omega_0}\right)^4 &= \frac{4}{5}\beta \\ \beta\omega_0^4 &= \frac{5}{4}\omega_m^4 \end{aligned} \tag{E.2}$$

which is equivalent to the $B(\omega)$ (ω in rad/s) term of the Bretschneider spectrum such that

$$B(\omega) = \beta\omega_0^4 = \frac{5}{4}\omega_m^4 \tag{E.3}$$

The parameter A of the Bretschneider spectrum is expressed as

$$A = 4Bm_0, \tag{E.4}$$

thus the Bretschneider spectrum is expressed as (Lewis (1988a) (p37))

$$S(\omega) = A\omega^{-5}\exp(-B\omega^{-4}) \tag{E.5}$$

It is useful to define the Bretschneider spectrum in terms of zero up-crossing period (T_z) and significant wave height H_s. Lewis (1988a) (p37) gives $T_z = 0.710T_0$ for this spectrum such that using E.3

$$B(\omega) = \frac{5}{4}\left(\frac{1.42\pi}{T_z}\right)^4 \tag{E.6}$$

which becomes $B(f) = \left(\frac{0.751}{T_z}\right)^4$ by the use of the relationship $B(\omega) = B(f)(2\pi)^4$. (Parameter A is not a function of frequency so remains unchanged).

Lloyd (1989) gives the significant wave height for the Bretschneider spectrum as

$$\bar{H}_{1/3} = 4.00\sqrt{m_0}\sqrt{1 - \frac{\varepsilon^2}{2}} \tag{E.7}$$

where the band width parameter $\varepsilon = \sqrt{1 - \frac{T_p^2}{T_z^2}} = \sqrt{1 - \frac{m_2^2}{m_0 m_4}}$. Thus for a spectrum of narrow bandwidth ($\varepsilon = 0$), $\bar{H}_{1/3} = 4.00\sqrt{m_0}$ and a wide bandwidth ($\varepsilon = 1$), $\bar{H}_{1/3} = 2.83\sqrt{m_0}$. However, Tucker (1991) prefers to define the significant wave height as $H_s = 4.00\sqrt{m_0}$.

The 15th International Towing Tank Conference (ITTC 1987, see Lewis (1988a)) recommended a form of the Bretschneider spectrum for average conditions less than fully developed seas to be more appropriate in most applications. In this case the two parameters A and B were given as

$$A = \frac{173H_{1/3}^2}{T_1^4} \tag{E.8}$$

$$B = \frac{691}{T_1^4} \tag{E.9}$$

or in terms of zero up-crossing period using the relationship $T_1 = 1.089T_z$ gives

$$A = \frac{123.129H_{1/3}^2}{T_z^4} \tag{E.10}$$

$$B = \frac{491.805}{T_z^4} \tag{E.11}$$

Appendix F

Motion Analysis

F.1 Motion Sickness Incidence

The motion sickness incidence (MSI) or percentage of the population to experience emesis according to O'Hanlon and McCauley (1974) was characterized by distribution curves based on regular sinusoidal motions over a period of 2-hours as a function of average acceleration and frequency expressed as

$$\begin{aligned} MSI &= \int_{-\infty}^{\log \bar{a}} \frac{100}{\sigma\sqrt{2\pi}} e^{-\left[\frac{(x-\mu)^2}{2\sigma^2}\right]} dx \\ &= 50\left[\operatorname{erf}\left(\frac{\log \bar{a} - \mu}{\sqrt{2}\sigma}\right) + 1\right] \end{aligned} \tag{F.1}$$

where

$$\begin{aligned} \sigma &= 0.4 \\ \bar{a} &= \text{mean acceleration } [g] \quad \left(\bar{a} = \frac{2}{\pi} a_{\max} = \frac{\sqrt{8}}{\pi} a_{rms} = \frac{\sqrt{8}}{\pi}\sqrt{m_0}\right) \\ \mu &= 0.654 + 3.697 \log_{10} f_e + 2.320 \left(\log_{10} f_e\right)^2 \\ f_e &= \text{encounter frequency } [Hz] \\ \operatorname{erf}(x) &= \frac{2}{\sqrt{\pi}} \int_0^x e^{-t^2} dt \end{aligned}$$

McCauley et al. (1976) concluded through experiments that the motion sickness incidence (MSI) as a function of frequency, vertical sinusoidal acceleration and time could be described by a two-dimensional normal distribution, which was converted into the products of two univariate normal distributions to give

$$MSI = 100.\Phi_z\left(z_a\right).\Phi_z\left(z_t'\right) : [\%] \tag{F.2}$$

where $\Phi\left(z\right)$ is the standardized cumulative normal distribution function given by

$$\Phi_z\left(z\right) = \frac{1}{2\pi} \int_{-\infty}^{z} \exp\left[-\frac{1}{2}x^2\right] dx \tag{F.3}$$

which was evaluated for z_a and z_t' by

$$z_a = \frac{\log_{10} a - \mu_a(f)}{\sigma_a} \tag{F.4}$$

$$z_t' = \frac{z_t - \rho z_a}{\sqrt{1-\rho^2}} \tag{F.5}$$

where

$$z_t = \frac{\log_{10} t - \mu_t}{\sigma_t} \tag{F.6}$$

and t is the time (minutes), f is the frequency (Hertz), a is the vertical sinusoidal acceleration (g RMS). Also, estimates for the remaining variables that included standard deviations were given as

$$\begin{aligned} \sigma_a &= 0.47 \\ \sigma_t &= 0.76 \end{aligned} \tag{F.7}$$

mean values as

$$\begin{aligned} \mu_a(f) &= 0.87 + 4.36 \log_{10} f + 2.73 (\log_{10} f)^2 \\ \mu_t &= 1.46 \end{aligned} \tag{F.8}$$

and the correlation coefficient as

$$\rho = -0.75 \tag{F.9}$$

This experimental approach based on sine waves essentially precludes the confident prediction of MSI in vessels exposed to broadband motion from irregular sea waves because the adopted RMS acceleration value doesn't necessarily provide an appropriate measure of the acceleration peaks, which may have a significant effect on the human tolerance. The standards of Australian Standard, AS 2670.3 (1990) and International Organisation for Standardisation, ISO 2631/3 (1985) use 1/3 octave frequency analysis of acceleration response to determine MSI values based on their own acceleration distribution. Whilst they provide a standard, more research in this area is needed.

F.2 1/3 Octave Analysis of Acceleration Response

Octave bands are defined as a ratio of an upper (f_2) and a lower bandage frequency (f_1) known as $G = \frac{f_2}{f_1} = 2$ (Australian/New Zealand Standard, AS/NZS 4476 (1997)). As a function of G and the mid-band frequency (f_m) the upper and lower bands are expressed as

$$f_1 = \left(G^{-\frac{1}{2b}}\right)(f_m) \tag{F.10}$$

$$f_2 = \left(G^{+\frac{1}{2b}}\right)(f_m) \tag{F.11}$$

where b is the bandwidth integer designator. For the base-two system this implies $b = 2$. The ratio of f_2 and f_1 is therefore

$$\frac{f_2}{f_1} = \frac{G^{+\frac{1}{2b}}}{G^{-\frac{1}{2b}}} = \frac{2^{+\frac{1}{6}}}{2^{-\frac{1}{6}}} = 2^{\frac{1}{3}} \tag{F.12}$$

On a log scale the ratio of the upper and lower frequency according to equation F.12 is of constant width $\left(\log_2\left(\frac{f_2}{f_1}\right) = \frac{1}{3}\right)$ and the mid-band frequency in terms of the lower frequency f_1 can be determined from equation F.10

$$\begin{aligned} f_m &= \frac{f_1}{2^{-\frac{1}{6}}} = 2^{\frac{1}{6}} f_1 \simeq 1.1225 f_1 \\ \text{therefore } f_1 &= 0.8908 f_m \end{aligned} \tag{F.13}$$

or in terms of the upper frequency f_2 using equation F.11

$$\begin{aligned} f_m &= \frac{f_2}{2^{\frac{1}{6}}} = 2^{-\frac{1}{6}} f_2 \simeq 0.8908 f_2 \\ \text{therefore } f_2 &= 1.1225 f_m \end{aligned} \tag{F.14}$$

Consider the acceleration response energy density spectrum, where the area under the curve represents the total acceleration energy of the ship response to a given wave system. This energy is expressed as

$$\tilde{E} = \rho g \int S_\xi(\omega_e)\, d\omega_e \tag{F.15}$$

The acceleration amplitude in this spectral density function is also given as $\tilde{E} = \frac{1}{2}\rho g \int \bar{\xi}_n^2 d\omega_e$. Equating with F.15 to solve for the n^{th} acceleration amplitude $\bar{\xi}_n$ in some interval $\delta\omega$ gives

$$\bar{\xi}_n = \sqrt{2.\delta\omega_e.S_\xi(\omega_e)} \tag{F.16}$$

where $S(\omega_e)$ is the mean energy density magnitude in the frequency band $\delta\omega$ and is determined by trapezoidal integration such that $S(\omega_e) = \frac{\int_{\omega_1}^{\omega_2} S(\omega_e) d\omega_e}{\omega_2 - \omega_1}$.

Making $\delta\omega_e$ a 1/3 octave, a solution for $\bar{\xi}_n$ may be found for all n discrete frequencies such that $\delta\omega_e = \left(2^{\frac{1}{6}} - 2^{-\frac{1}{6}}\right)(\omega_e)_n$.